Università degli Studi di Palermo

AREA RICERCA E TRASFERIMENTO TECNOLOGICO
SETTORE DOTTORATI E CONTRATTI PER LA RICERCA
U. O. DOTTORATI DI RICERCA

Ph.D. in ADVANCES IN MODELLING, HEALTH-MONITORING, INFRASTRUCTURES, GEOMATICS, GEOTECHNICS, HAZARDS, ENGINEERING STRUCTURES, TRANSPORTATION (AIM HIGHEST)
Dipartimento di Ingegneria
S.S.D. CEAR06

HYBRID FINITE ELEMENTS FOR THE COUPLED PROBLEM OF POROELASTICITY

LA DOTTORESSA
DOTT.SSA SIMONA LO FRANCO

IL COORDINATORE
PROF. PIERO COLAJANNI

IL TUTOR
PROF. FRANCESCO PARRINELLO

I CO TUTOR
PROF. GUIDO BORINO

PROF. GERHARD A. HOLZAPFEL

CICLO XXXVIII
ANNO CONSEGUIMENTO TITOLO 2025

Simona Lo Franco: *Hybrid finite elements for the coupled problem of poroelasticity, ,* © December, 2025

Notation xi

1 FUNDAMENTS OF FINITE POROELASTICITY 4
1.1 Continuum Mechanics and Material Theory 4
1.2 Motions and Configurations 5
1.2.1 Mapping of Volume and Area Elements 7
1.2.2 Strain tensors 8
1.2.3 Stress Tensors and Mass Flux Vectors 10
1.2.4 Balance Laws 12
1.2.5 Thermodynamic consistency 14
1.2.6 The Boundary Conditions for the Coupled Problem 15
1.2.7 Linear poroelasticity 16
1.3 Variational Framework 18
1.3.1 Standard 'u-p' formulation 20
1.3.2 Alternative Variational Formulations 23

2 FINITE ELEMENT FORMULATION FOR POROELASTICITY 27
2.1 Fundamentals of the Finite Element Method 27
2.1.1 Strong and Weak Forms 28
2.2 The Galerkin Approximation Framework 28
2.2.1 Galerkin Discretization 30
2.2.2 Shape Functions and Discrete Spaces 30
2.3 Formulations in the literature for poroelasticity 32
2.3.1 Coupled Finite Element Formulations 32
2.3.2 The u-p formulation 33
2.3.3 The Inf-Sup Condition 35
2.3.4 Alternative Variational Formulations 37

3 A VARIATIONALLY-CONSISTENT HYBRID EQUILIBRIUM ELEMENT FORMULATION FOR LINEAR POROELASTICITY 39
3.1 Introduction 39
3.2 Dual formulation of poroelasticity 41
3.2.1 Primary fields 41
3.2.2 (Strong form of the) Governing equations 42
3.2.3 Thermodynamic consistency 44
3.3 Hybrid formulation of poroelasticity 47
3.3.1 Complementary/Dual poroelastic energy potential 47
3.3.2 Hybrid variational principle for poroelasticity 48
3.4 Numerical simulations 56
3.4.1 Terzaghi's problem 57

3.4.2 Mandel's problem 60
3.4.3 Booker's consolidation problem 63
3.5 Conclusions and future perspectives 68
4 A HYBRID FLUX-PRESERVING FINITE ELEMENT FOR COUPLED FLOW DEFORMATION: LINEAR FORMULATION 70
4.1 Introduction 70
4.2 Canonical form of poroelasticity 71
4.2.1 Primary fields 72
4.2.2 Governing equations 73
4.2.3 Thermodynamic consistency 75
4.3 Hybrid formulation of poroelasticity 78
4.3.1 Canonical minimization principle of poroelasticity 78
4.3.2 Hybrid variational principle of poroelasticity 80
4.4 Numerical simulations 89
4.4.1 Terzaghi's problem 89
4.4.2 Low permeability layer 91
4.4.3 Mandel's problem 93
4.4.4 Consolidation problem 95
4.5 Conclusions and future perspectives 97
5 A HYBRID FLUX-PRESERVING FINITE ELEMENT FOR COUPLED FLOW DEFORMATION: FINITE STRAINS FORMULATION 99
5.1 Introduction 99
5.2 Canonical form of poroelasticity 101
5.2.1 Primary fields 101
5.2.2 Governing equations 102
5.2.3 Thermodynamic consistency 104
5.3 Hybrid formulation of poroelasticity 107
5.3.1 Canonical minimization principle of poroelasticity 107
5.3.2 Canonical minimization principle of poroelasticity 107
5.3.3 Hybrid variational principle of poroelasticity 109
5.4 Discrete form 113
5.5 Numerical simulations 119
5.5.1 Terzaghi's problem 119
5.5.2 Low permeability layer 122
5.6 Conclusions and Future Perspectives 123
BIBLIOGRAPHY 128

Figure 1 The reference and the spatial configuration, $\mathcal{B}_0$ and $\mathcal{B}$. 6
Figure 2 Graphical description for the poroelastic system. 49
Figure 3 Nine-node triangular hybrid equilibrium element(HEE) over which stresses and displacement field are approximated. The pressure field is interpolated over an overlapped six-node quadratic triangular element. 53
Figure 4 Terzaghi's problem. A rectangular column of dimensions a and c, is loaded by a mechanical force q on the top surface. The sided and bottom surfaces of the specimen are impermeable, while the top surface is assumed to be full drained. 57
Figure 5 Terzaghi's problem. Pore pressure contour plot for the hybrid equilibrium element with quadratic stress and pressure fields at the adimensionalised time $t^* = 7.12 \cdot 10^{-6}$. 59
Figure 6 Terzaghi's problem. adimensionalised pore pressure vs. depth trend, for the adimensionalised time $t^* = 7.12 \cdot 10^{-6}$ and $t^* = 1.068 \cdot 10^{-1}$. 60
Figure 7 Mandel's problem. A rectangular plate of dimensions 2a and 2b, is loaded by mechanical force 2F through rigid plates. The top and bottom surfaces of the specimen are impermeable, while the side surfaces are assumed to be pressure-free. 61
Figure 8 Mandel's problem. Comparison of the HEE solution (markers) for fluid pressure p with analytical solution (solid lines) by Cheng and Detounray [33] at non-dimensional times $t^* = 0.01$, $t^* = 0.1$, $t^* = 0.2$, $t^* = 0.5$, $t^* = 1$, for the incompressible (a) and compressible (b) fluid phase. 63
Figure 9 Consolidation problem. A rectangular plate of dimensions B and h, with impermeable bottom and side surfaces and a fully drained top surface, on which a uniformly distributed mechanical load q is placed over length b. 64
Figure 10 Consolidation problem. Pore pressure map plot for the hybrid equilibrium element with quadratic stress and pressure fields at the adimensionalised time $t^* = 2 \cdot 10^{-6}$, with meshes of 10 × 10 (a) and 30 x 30 (b) elements. 65

Figure 11 Consolidation/Footing problem. Contour plot for y-stress for an hybrid equilibrium element with quadratic stress and pressure fields at the adimensionalised time $t^* = 2 \cdot 10^{-6}$, with meshes of 10 × 10 (a) and 30 x 30 (b) elements. 66

Figure 12 Consolidation problem. adimensionalised fluid pore pressure p versus adimensionalised depth y/h of the body at $x = -B/2$ for adimensional times $t^* = 0.0002$, $t^* = 0.004$, $t^* = 0.012$, $t^* = 0.03$, $t^* = 0.08$, $t^* = 0.27$. 67

Figure 13 Consolidation problem. adimensionalised fluid pore pressure p versus adimensionalised depth y/h of the body at $x = -B/2$ for adimensional time $t^* = 2 \cdot 10^{-6}$. Comparison of HEE (in red) and Q9/Q4 with Taylor-Hood interpolation (in blue) results. 68

Figure 14 Sketch of a linear poroelastic body, showing the boundary conditions and the control volume on which the continuity of the fluid phase is imposed. 74

Figure 15 Nine-node triangular hybrid flux element over which the fluid fluxes and the Lagrangian fluid potential variables are approximated. The displacement field is interpolated over an overlapped isoparametric six-node quadratic triangular element. 85

Figure 16 Terzaghi's problem: (a) problem domain ($a = 1\,m, b = 10\,m$) with boundary conditions ($q = 1\,MPa$); (b) fluid pressure p/p_0 as a function of depth y/b, at times $t^* = 7.12 \cdot 10^{-6}$ and $t^* = 1.07 \cdot 10^{-1}$. The Hybrid Flux Element (HFE) solution is compared to the analytical solution; (c) contour plot of fluid pressure p at time $t^* = 7.12 \cdot 10^{-6}$. Material parameters: $G = 1\,MPa$, $\nu = 0.3$, $\alpha = 1$, $M = 100\,000\,MPa$, $k = 1\,m\,s^{-1}$. 91

Figure 17 Low-permeability layer problem: (a) problem domain ($a = 1\,m, b = 1\,m$) with boundary conditions ($q = 30\,MPa$). In the central layer the hydraulic conductivity is equal to $\tilde{k} = k \cdot 10^{-8}$; (b) contour plot of fluid pressure p at time $t^* = 1.63$. Material parameters: $G = 0.81\,MPa$, $\nu = 0.3$, $\alpha = 1$, $M = 20\,000\,MPa$, $k = 2.06991 \cdot 10^{-9}\,m\,s^{-1}$. 92

Figure 18 Low-permeability layer problem. Fluid pressure p/p_0 as a function of depth y/b at time $t^* = 1.63$. The Hybrid Flux Element (HFE) solution is compared to the analytical solution, the Tayor-Hood (TH) solution and the displacement-flux element (Q1-RT0) proposed by Teichtmeister, Mauthe, and Miehe [121]. 93

Figure 19 Mandel's problem: problem domain ($a = 1\,m$, $b = 0.2\,m$) with boundary conditions ($F = 1\,kN$). Material parameters: $G = 1\,MPa$, $\nu = 0.2$, $\alpha = 1$, $M = \{100, 20\,000\}\,MPa$, $k = 1\,m\,s^{-1}$. Taking advantage of symmetry, only the dark gray region is discretized. 94

Figure 20 Mandel's problem: normalized fluid pressure as a function of width x/a, at times $t^* = 0.01$, $t^* = 0.1$, $t^* = 0.2$, $t^* = 0.5$, $t^* = 1$. The Hybrid Flux Element (HFE) solution is compared to the analytical solution; (a) early-incompressible fluid and (b) compressible fluid. 95

Figure 21 Consolidation problem: (a) problem domain ($a = 1\,m$, $b = 1\,m$, $d = a/2$) with boundary conditions ($q = 1\,MPa$); (b) contour plot of fluid pressure p at time $t^* = 2 \cdot 10^{-6}$. Material parameters: $G = 1\,MPa$, $\nu = 0.3$, $\alpha = 1$, $M = 20\,000\,MPa$, $k = 0.1\,m\,s^{-1}$. Taking advantage of symmetry, only the dark gray region is discretized. 96

Figure 22 Consolidation problem: fluid pressure p/p_0 as a function of depth y/b at $x = 0$, for the normalized time $t^* = 2 \cdot 10^{-6}$. The Hybrid Flux Element (HFE) solution is compared to the results from the Tayor-Hood (TH) element [121] and the Hybrid Equilibrium Element (HEE) proposed by Lo Franco, Parrinello, and Borino [72]. 97

Figure 23 Graphical description for the poroelastic system in the reference configuration. 104

Figure 24 Nine-node triangular hybrid flux element, where the fluid fluxes and the Lagrangian fluid potential variables are interpolated. The displacement field is defined over an overlapping six-node quadratic isoparametric triangular element. 114

Figure 25 Terzaghi's problem: comparison of normalized pore pressure vs depth distributions obtained with the analytical solution in [128] and the small and finite deformation HFE. 120

Figure 26 Terzaghi's problem: comparison of displacements at the top layer against time obtained with the analytical solution in [128] and the small and finite deformation HFE, for a load q=0.04 MPa. 121

Figure 27 Terzaghi's problem: displacements at the top layer against time solutions obtained with small and finite deformation formulations, for a load of q=2, 4 and 8 MPa, are compared with the steady state solution [71]. 122

Figure 28 Low permeability problem: pore pressure distributions obtained with small and finite deformation HFE, against the analytical solution in [128]. The solutions coincide, confirming stability and accuracy of the nonlinear framework in the presence of strong hydraulic heterogeneities. 123
Figure 29 Low permeability problem: pore pressure distributions obtained with small and finite deformation HFE, against the Q1-RT0 and TH element solution [121]. 123

In this Section, the adopted mathematical notation is presented. A compact notation is employed, where **bold** letters represent vectors, while **bold capital** and **bold Greek** letters denote tensors of any order. The scalar product between vectors or tensors is indicated by dots corresponding to the number of contracted index pairs.

For example, considering $\mathbf{u} = \{u_i\}$, $\mathbf{j} = \{j_i\}$, $\boldsymbol{\sigma}' = \{\sigma'_{ij}\}$, $\boldsymbol{\sigma} = \{\sigma_{ij}\}$, and $\mathbf{D} = \{D_{ijkh}\}$ as generic vectors and tensors, the following equivalences hold:

$$\mathbf{u} \cdot \mathbf{j} = u_i j_i, \qquad \boldsymbol{\sigma}' : \boldsymbol{\sigma} = \sigma'_{ij}\sigma_{ij}, \qquad \mathbf{D} : \boldsymbol{\sigma} = \{D_{ijkh}\sigma_{kh}\}.$$

The Einstein summation convention is adopted, where repeated indices imply summation. Subscripts refer to components in an orthogonal Cartesian coordinate system, defined by the basis $\{\boldsymbol{e}_1, \boldsymbol{e}_2, \boldsymbol{e}_3\}$. The dyadic product is written as

$$\mathbf{u} \otimes \mathbf{j} = \{u_i j_j\},$$

so that

$$\mathbf{D} : (\mathbf{u} \otimes \mathbf{j}) = \{D_{ijkh} u_k j_h\}.$$

An overdot denotes the (material) time derivative, e.g. $\dot{\mathbf{u}} = d\mathbf{u}/dt$. The symbol ∇ indicates the gradient operator,

$$\nabla \mathbf{u} = \{\partial_j u_i\},$$

with ∇^s representing its symmetric part. The symbol $\nabla\cdot$ indicates the divergence operator, $\nabla \cdot \mathbf{u} = \partial_i u_i$. Finally, the symbol $:=$ is used to indicate definition.

Most frequent symbols:

α	Biot's coefficient
Δt	Time increment
$\boldsymbol{\kappa}$	Permeability tensor
$\widehat{\mathbf{K}}$	spatial permeability tensor
λ	Lagrange multiplier
μ	Fluid potential
ν_d	Drained Poisson coefficient
ν_u	Undrained Poisson coefficient
π	Potential density function

$\psi(\cdot)$	Stored energy function
$\phi(\cdot)$	Dissipation potential function
φ	Effective porosity field
ρ	Density
ρ_f	Density of the fluid phase
ρ_s	Density of the solid phase
m	Variation in fluid mass content
ζ	Variation in fluid volume content
$\boldsymbol{\varepsilon}$	Infinitesimal strain tensor
$\boldsymbol{\sigma}$	Total Cauchy stress tensor
$\boldsymbol{\sigma}'$	Effective Cauchy stress tensor
a_i	Polynomial coefficients for the approximation function
$\mathbf{b}$	Body force per unit mass
$d\mathbf{X}$	infinitesimal line element (in reference configuration)
$d\boldsymbol{x}$	infinitesimal line element (in current configuration)
$d\mathbf{S}$	infinitesimal area element (in reference configuration)
$d\mathbf{s}$	infinitesimal area element (in current configuration)
$d\mathbf{V}$	infinitesimal volume element (in reference configuration)
dv	infinitesimal volume element (in current configuration)
$\mathbf{F}$	Deformation gradient
G	Shear modulus of the solid skeleton
$\mathbf{H}$	Material fluid mass flux vector
$\mathbf{h}$	Spatial fluid mass flux vector
$\mathbf{I}$	Identity tensor
$\mathbf{j}$	Spatial fluid flux vector
$\mathbf{C}$	Elasticity tensor
$\mathbf{D}$	Compliance tensor
J	Jacobian determinant

K	Drained bulk modulus of the solid skeleton
$\mathbf{L}$	Spatial velocity gradient tensor
M	Biot's modulus
$\mathbf{N}$	Outward unit normal on $\partial\mathcal{B}_0$
$\mathbf{n}$	Outward unit normal on $\partial\mathcal{B}$
$\mathbf{P}$	first Piola- kirckoff stress tensor
$\mathbf{P}'$	effective first Piola- kirckoff stress tensor
p	Pore pressure
$\mathbf{q}^u$	Nodal force vector
$\mathbf{q}^\mu$	Nodal flux vector
$\mathbf{r}$	Residual vector
$\mathbf{t}$	Spatial traction vector
$\mathbf{T}$	Material traction vector
t	Time
$\mathbf{u}$	Solid displacement field
$\mathbf{w}$	Seepage velocity
$\mathbf{x}$	Spatial coordinates
$\mathbf{X}$	Material coordinates
$\mathbf{K}^{(\cdot)}_{(\cdot)}$	Stiffness matrix
$\mathcal{B}$	Current configuration of the poroelastic body
$\mathcal{B}_0$	Reference configuration of the poroelastic body
$\partial\mathcal{B}$	Boundary of the current configuration
$\partial\mathcal{B}_0$	Boundary of the reference configuration
$\partial\mathcal{B}_u$	Boundary with prescribed displacements
$\partial\mathcal{B}_t$	Boundary with prescribed tractions
$\partial\mathcal{B}_h$	Boundary with prescribed normal flux
$\partial\mathcal{B}_\mu$	Boundary with prescribed fluid potential
${}^h\mathcal{B}$	Discretized domain of the current configuration
${}^h\mathcal{B}_0$	Discretized domain of the reference configuration
$\mathcal{D}$	Dissipation rate
$\mathcal{E}$	Three-dimensional Euclidean point space
$\Pi^{\Delta t}$	Incremental canonical functional
$\bar{\Pi}^{\Delta t}$	Hybrid incremental functional

$\mathcal{V}_{(\cdot)}$	Space of admissible solutions
$\mathcal{W}_{(\cdot)}$	Space of admissible variations

INTRODUCTION

Among the various challenges involved in modeling multiphysical systems, the numerical simulation of porous media holds a prominent position. A porous medium is defined as a heterogeneous material composed of a solid skeleton interspersed with a network of interconnected pores, which may be saturated by one or more fluid phases [14, 32]. The mass transport of these fluid phases, driven by diffusion, convection, or both, is coupled to the deformation of the solid skeleton, resulting, in the most general case, in a coupled chemo-thermo-mechanical problem. Even when restricting the analysis to small strains and linear elastic behavior of the solid matrix, the overall system remains complex and challenging to model [18, 19]. The theoretical and computational study of such coupled behavior underpins a wide range of applications, including geotechnical engineering [71, 111], energy storage [108], polymer science [62, 74], and biomechanics [7, 10, 12, 47, 51, 67, 69, 84, 85, 115, 116] . The complex mechanical behavior of deformable porous media is typically addressed through two distinct and widely acknowledged theoretical frameworks. The theory of mixtures [25–27, 87, 125, 126], with the related albeit restricted framework of the Theory of Porous Media (TPM) [41, 45] describe the porous medium as a multiphase system, in which distinct continuous constituents coexist and interact through exchange terms governing the transfer of mass, momentum, and energy between the phases. Conversely, poroelastic theories, pioneered by Biot [17, 18], treat the porous medium as a homogenized single-phase continuum. Within this framework, the principles of classical continuum mechanics are formulated directly at the macroscale [38, 39, 128, 129]. Despite significant advances, the study of porous media remains an active field of research. Several fundamental aspects of the fully coupled, nonlinear theory of poroelasticity are still not exhaustively addressed [8, 75]. The governing boundary value problems of poroelasticity are intrinsically complex due to the strong coupling between mechanical and hydraulic fields, thereby often necessitating computational approaches for their practical solution. Over the past decades, an extensive body of literature has emerged on finite element formulations for Biot-type models. Most approaches adopt either a two-field discretization, typically involving solid displacements and pore pressure, or more elaborate formulations involving more than two [3], where the solid displacement field remains however the primary variable of interest. Under critical regimes, standard formulations may fail to satisfy local mass conservation, leading to nonphysical oscillations in the pressure field [132]. This issue becomes particularly severe in undrained or nearly impermeable conditions, where rapid loading generates steep pressure gradients, significantly increasing the stiffness of the coupled problem. The same difficulties arise in the presence of sharp permeability contrasts, where pressure singular-

ities often appear. Standard mixed finite element formulations typically employ the displacement and pore pressure as primary variables, leading to the classical u–p formulation [9, 15, 133, 134]. From a variational perspective, this formulation results in a saddle-point problem, whose well-posedness is governed by the so-called inf-sup (Ladyzhenskaya–Babuška–Brezzi, LBB) condition [28, 29], which ensures the stability of the discrete solution and prevents spurious pressure modes. However, most mixed discretizations satisfy the inf–sup condition only in a global sense, while failing to enforce it at the element level [31]. This limitation often results in the aforementioned non-physical oscillations and numerical instabilities [58, 102]. These issues have motivated extensive research into stabilized finite element formulations for poroelasticity, particularly under nonlinear and finite-deformation conditions. A classical approach employs Taylor–Hood elements [37, 71, 111], where the displacement field is approximated by higher-order (typically quadratic) functions and the pore-pressure field by lower-order (typically linear) interpolations [119]. Alternative approaches include enhanced finite elements, which however may be prone to hourglass instabilities [114]. To reduce computational cost, stabilization techniques for low-order elements, such as pressure-jump stabilization or selective reduced integration, offer practical alternatives to higher-order Taylor-Hood elements. These methods effectively suppress oscillations and alleviate volumetric locking while maintaining computational efficiency. However, under highly nonlinear conditions (e.g., abrupt permeability contrasts, steep pressure gradients, or dynamic processes such as supershear rupture), classical stabilization alone may prove insufficient[49, 58]. In such cases, even when the inf-sup condition is satisfied locally, numerical artifacts such as spurious oscillations may persist, often necessitating adaptive meshing or advanced time-integration schemes to preserve numerical stability. Alternatively, formulations based on different sets of primary variables have been proposed. Notably, the work of Coussy [38] and Miehe, Mauthe, and Teichtmeister [82] introduced variational minimization principles that circumvents the inf–sup condition, yielding inherently stable finite elements [121]. Moreover, finite element formulations based on minimization principles have been proposed for Biot-type problems to address discontinuities in temperature and permeability fields [48]. However, the stability of such formulations critically depends on the choice of functional spaces, particularly for the representation of the conservative field (e.g. fluxes and stresses), which must be conform to the class $H(\mathrm{div})$ [82]. This choice comes at the expense of a significantly increased number of degrees of freedom and a higher computational cost [65]. The hybridization of the variational principle [42, 98–100], involving the introduction of independent complementary fields interpolated along the element boundaries, acting as Lagrange multipliers to weakly enforce inter-element continuity, provides a computationally efficient and intrinsically stable framework for the numerical treatment of coupled and mixed problems. This approach underlies the Hybrid Equilibrium Elements (HEE) [4, 83] and the mixed-hybrid formulations for incompressible materials [11]. Although conceptually related to the Discontinu-

ous Galerkin (DG) and Hybrid Discontinuous Galerkin (HDG) methods [34, 43], the hybridization strategy adopted here yields a distinct global-local family of methods characterized by fewer degrees of freedom and reduced computational complexity. By altering the discrete functional, such approaches provide a flexible setting in which interelement continuity can be relaxed or constraints can be enforced in a weak sense. The resulting formulations are locally conservative, yield better-conditioned element-level problems, avoiding the numerical instabilities typically encountered in conventional formulations, allowing independent selection of approximation orders for trial and test functions. Although hybrid formulations introduce additional degrees of freedom through the Lagrange multipliers, the system can be efficiently reduced, via *static condensation* procedure, to one expressed solely in terms of the generalized unknowns of the primary field [35]. This results in a well-conditioned and compact system particularly amenable to iterative solvers, as the hybrid framework naturally produces symmetric and well-conditioned linear operators [28, 98]. In this thesis, we introduce a novel class of *hybrid-mixed finite element formulations* that combine inherent stability with computational efficiency. By adopting an alternative pair of primary variables, the governing equations are recast as a variational minimization principle, subsequently *hybridized* through the introduction of a third field acting as a Lagrange multiplier. Eliminating the need for globally conforming function spaces, the hybrid approach overcomes the numerical instabilities commonly encountered in conventional mixed formulations, ensuring element-level stability and improving the overall conditioning of the global system, demonstrating enhanced robustness and accuracy in the presence of discontinuities, offering a rigorous and efficient alternative to existing stabilized and mixed formulations.

The insights afforded by this framework, combining a minimization principle with hybridization, may extend beyond poromechanics. The same methodology applies naturally to other coupled systems governed by saddle-point structures, such as fluid-structure interaction, Stokes-Darcy coupling, and problems enforcing strict incompressibility constraints. Moreover, the intrinsic compatibility of the hybrid framework with parallel computing paradigms, including multigrid and GPU-accelerated solvers, may pave the way for scalable, high-performance implementations of emerging multiphysics models.

How did Biot arrive at the partial differential equation? [...]
Perhaps Laplace gave Biot the equation and left him to sink or swim for a few years in trying to derive it. That would have been merely an instance of the way great mathematicians since the very beginnings of mathematical research have effortlessly maintained their superiority over ordinary mortals.

— Clifford Ambrose III Truesdell

1 FUNDAMENTS OF FINITE POROELASTICITY

1.1 CONTINUUM MECHANICS AND MATERIAL THEORY

A porous medium is defined as a heterogeneous material composed of a deformable solid skeleton interspersed with a network of interconnected pores, potentially saturated by one or more fluid phases [14, 32]. The transport of these fluid phases is intrinsically coupled to the mechanical response of the solid matrix, giving rise to a fully coupled problem. Understanding and modeling such interactions is essential across a wide range of fields, spanning from geomechanics [71, 111] to energy storage technologies [108], polymer science [62, 74], and contemporary challenges in biomechanics [7, 10, 47, 69, 84, 115, 116].
Two distinct and widely recognized frameworks are commonly employed to describe the complex mechanics of deformable porous media: the theory of mixtures and the poroelastic theory. The theory of mixtures [25–27, 87, 125, 126], together with its more specialized extension, the Theory of Porous Media (TPM) [41, 45], conceptualizes the porous medium as a multiphase system in which distinct, superimposed continua coexist and interact through exchange terms that govern the transfer of momentum, mass, and energy among the constituent phases. By contrast, poroelastic theories, branching from the seminal work of Biot [17, 18], treat the porous medium as a single-phase, homogenized continuum, wherein the principles of classical continuum mechanics are formulated directly at the macroscale [38, 39, 128, 129]. It is worth recalling that chemo-mechanical models used to describe coupled deformation and diffusive flow in polymeric gels [62, 74] are based on the same framework as poroelastic theory. The two approaches are equivalent under certain simplifying assumptions [5, 40, 110, 118], although mixture theories provide a more rigorous foundation to describe multiphase interactions. In particular, poroelastic theories require the introduction of a macroscale dissipation potential to ensure thermodynamic consistency in

modeling the dissipative interactions between the elastic solid and the interstitial fluid [32, Sec. 4.2].
For the purposes of this work, the focus will be on the poroelastic framework, which provides a robust and tractable methodology for modeling the coupled behavior of the solid skeleton and the interstitial fluids at the macroscale. Within the poroelastic framework, boundary conditions can be conveniently defined at the macroscale level. Consequently, mechanical and hydraulic boundary conditions can be prescribed in terms of experimentally accessible quantities, such as tractions, displacements, pressures, and fluxes, without the need to explicitly account for the phase-specific interactions or interfacial balance relations that are intrinsic to mixture-theoretic descriptions. Within this context, the subsequent sections briefly review and summarize fundamental concepts of continuum mechanics and material theory, drawing on basic principles of continuum mechanics and embedding them within the poroelastic framework to provide a consistent foundation for Chapters 3- 5, where the formulations proposed as novel contributions of this thesis will be further developed.
To describe large deformations of solid bodies and their associated stress states, concepts from tensor calculus on manifolds are employed [61, 77, 90], while the fundamental principles of thermodynamics are grounded in the literature on rational thermodynamics, with reference to seminal works by Coleman and Gurtin [36], Germain, Nguyen, and Suquet [50], Gurtin, Fried, and Anand [56], Šilhavý [113], and Truesdell [126]. For the sake of simplicity, the system is assumed to be isothermal and mass-conservative, implying the absence of internal sources or sinks; furthermore, no chemical interactions between the constituents are considered. The linear case is recalled as a limiting case, performing a linearization around the reference configuration $\mathcal{B}_0$ and characterizing the deformation through the infinitesimal strain tensor $\boldsymbol{\varepsilon} = \nabla^s_{\mathbf{X}}\mathbf{u}$, representing the symmetric part of the displacement gradient [61]. Moreover, for clarity, the connection with the corresponding fields and equations adopted in the classical theory of porous media and related frameworks is presented where deemed necessary.

1.2 MOTIONS AND CONFIGURATIONS

In poroelasticity, kinematics is referred to the solid, implying that motion and related quantities are measured with respect to the configuration of the solid skeleton [40]. To introduce the quantitative and qualitative description of physical phenomena, foundational framework for observation and measurement is required. Such framework is conceptualized through the notion of an observer, which provides the necessary reference to quantify physical properties, specifically the ability to track the evolution of positions in space and the progression of time. Let us suppose that the space for these observations is a three-dimensional Euclidean point space $\mathcal{E}$, and that the occurring times are measured on the real line $\mathbb{R}$. From the perspective of a given observer, any physical event is thus uniquely identified by a location $\mathbf{x} \in \mathcal{E}$ and a time instant $t \in \mathbb{R}^+_0$.

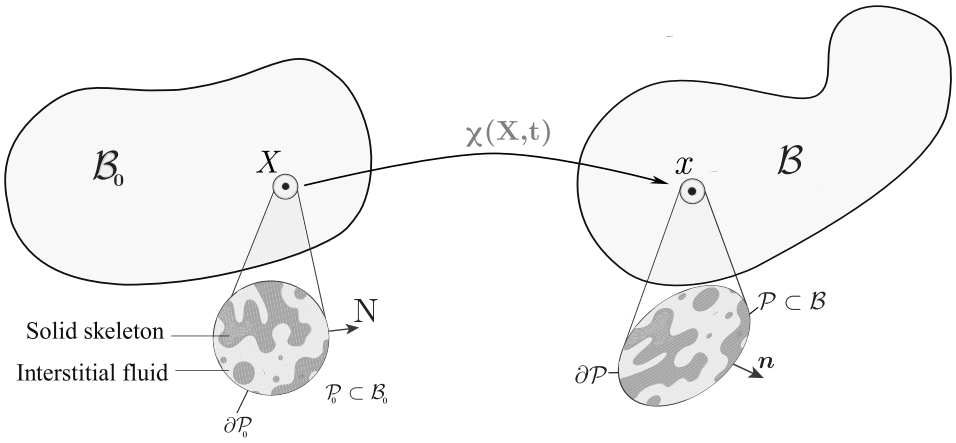

Figure 1: The reference and the spatial configuration, $\mathcal{B}_0$ and $\mathcal{B}$.

" Formally, an observer is a one-to-one mapping which assigns a pair $(\mathbf{x}, t) \in \mathcal{E} \times \mathbb{R}_0^+$ *to an event in the physical world"*[90].

The fundamental object of study is the evolution of a *body* B, formally defined as a set of *material points*. As the body moves through space, the spatial region it occupies, denoted Ω_t, undergoes continuous change over time t. A *configuration* represents a specific placement of the body B in space at a given instant. Formally, it is described by a mapping that assigns to each material point a position in the three-dimensional Euclidean space. This mapping is required to be sufficiently smooth, orientation-preserving, and invertible.

To establish a reference framework for describing the motion, we introduce a fixed *reference configuration* $\mathcal{B}_0$, which provides a means of labeling material points. In contrast, the *current configuration* $\mathcal{B}$ describes the body's placement at time t. Points in the reference configuration are denoted by $\mathbf{X} \in \mathcal{B}_0$ and are called *material coordinates*, while points in the current configuration are denoted by $\mathbf{x} \in \mathcal{B}$ and are called *spatial coordinates* (1).

A motion [1], of the body is described by a time- parameterized family of configurations $\chi : \mathcal{B}_0 \to \mathcal{E}$, where $\mathbf{x} = \chi(\mathbf{X}, t)$ gives the spatial position of material point $\mathbf{X}$ at time t. For a given particle (fixed $\mathbf{X}$) this equation describes a curve in $\mathbb{R}^3$ called the path or trajectory of $\mathbf{X}$ in the motion.

For any fixed time t, the mapping $\chi_t(\mathbf{X}) = \chi(\mathbf{X}, t)$ that relates the reference configuration to the current configuration is called *deformation*. The velocity of material point

1 The formal distinction between the terminology "motion" and "deformation map" is frequently overlooked in the literature, with many authors adopting a unified conceptual framework and notation. For clarity and consistency with prevalent sources, this work follows that convention and treats the two notions as equivalent.

$\mathbf{X}$ is defined as $\mathbf{V}(\mathbf{X}, t) = \dot{\chi}(\mathbf{X}, t)$, representing a vector emanating from point $\mathbf{X}$. When expressed as a function of spatial coordinates $(\mathbf{x}, t)$, takes the name of spatial velocity $\mathbf{v}(\mathbf{x}, t)$, with $\mathbf{V}(\mathbf{X}, t) = \mathbf{v}(\mathbf{x}, t)$ where $\mathbf{x} = \chi(\mathbf{X}, t)$.

The deformation gradient $\mathbf{F}(\mathbf{X}, t)$ is defined as the tangent map of the deformation map:

$$\mathbf{F} = \frac{\partial \chi(\mathbf{X}, t)}{\partial \mathbf{X}}, \tag{1}$$

reminding the reader that the term gradient is appropriate precisely because we have restricted our treatment to Euclidean space. In this setting, the tangent map $D\chi$ coincides exactly with the classical gradient of the vector-valued deformation mapping χ [77].
The inverse of the deformation gradient, denoted as $\mathbf{F}^{-1}$, is mathematically defined as the derivative of the inverse motion function with respect to the position vector $\mathbf{x}$ in the current configuration. This relationship is expressed as:

$$\mathbf{F}^{-1} = \frac{\partial \chi^{-1}(\mathbf{x}, t)}{\partial \mathbf{x}} = \chi^{-1} \otimes \nabla_{\mathbf{x}}. \tag{2}$$

A fundamental requirement for the deformation gradient is its invertibility, which is guaranteed by a strictly positive Jacobian determinant, $J = \det \mathbf{F} > 0$. From a physical perspective, the deformation gradient $\mathbf{F}$ serves as the fundamental linear operator that maps an infinitesimal line element $d\mathbf{X}$ from the reference configuration onto its deformed counterpart $d\mathbf{x}$ in the current configuration via the operation:

$$d\mathbf{x} = \mathbf{F} \cdot d\mathbf{X}. \tag{3}$$

Conversely, the inverse mapping is given by:

$$d\mathbf{X} = \mathbf{F}^{-1} \cdot d\mathbf{x}. \tag{4}$$

1.2.1 *Mapping of Volume and Area Elements*

The deformation gradient $\mathbf{F}$ not only relates the differential line elements in the reference and current configurations, but also governs the transformation of area and volume elements during deformation.
Let us now consider the transformation of material area elements $d\boldsymbol{A} \in \mathcal{B}_0$ to spatial area elements $d\boldsymbol{a} \in \mathcal{B}$. Given two distinct material tangent vectors $\mathbf{dX}_1, \mathbf{dX}_2 \in \mathcal{B}_0$, we define the material area element as $d\boldsymbol{A} = \mathbf{dX}_1 \times \mathbf{dX}_2 = \mathbf{N}\, dA$, where $\mathbf{N} \in \mathcal{B}_0$ is a material unit normal vector. Similarly, the spatial area element is defined as $\mathbf{da} = \mathbf{F}\,\mathbf{dX}_1 \times \mathbf{F}\,\mathbf{dX}_2 = \mathbf{n}\, da$, where $\mathbf{n} \in \mathcal{B}$ is a spatial unit normal vector. The re-

lationship between $d\boldsymbol{A}$ and $d\boldsymbol{a}$ is given by the cofactor of the deformation gradient, $d\boldsymbol{a} = \text{Cof}\,[\mathbf{F}]d\boldsymbol{A} = J\mathbf{F}^{-T}d\boldsymbol{A}$. This relationship is known as *Nanson's formula*.

A material volume element is defined as $V = \langle \mathbf{dX}_1,\ \mathbf{dX}_2 \times \mathbf{dX}_3 \rangle$, where $\mathbf{dX}_1, \mathbf{dX}_2, \mathbf{dX}_3 \in \mathcal{B}_0$ are three linearly independent tangent vectors. The corresponding spatial volume element is

$$dv = \langle \mathbf{FdX}_1,\ \mathbf{FdX}_2 \times \mathbf{FdX}_3 \rangle, \tag{5}$$

and their relationship is governed by the *Jacobian determinant*:

$$dv = J dV, \qquad \text{with } J = \det \mathbf{F}. \tag{6}$$

Finally, according to classical practice in poroelasticity, an homogenization procedure is carried out at the mesoscale, such that at each material point the particles of the solid skeleton and of the interstitial fluid are indistinguishable. The homogenization is based on the definition of an *effective porosity* field $\varphi(\mathbf{X}, t) \in (0, 1]$, which assigns to each volume element dV the reference volume of interconnected pores $dV_f = \varphi\, dV$ filled by fluid [32, Sec. 4.1.1].
In the current configuration, under the assumption of incompressible solid and fluid phases, the total local volume change of the mixture is entirely attributed to the variation of porosity. Consequently, the Eulerian porosity n can be related to its reference counterpart φ and the determinant of the deformation gradient of the solid skeleton J through the kinematic relation [33, 39]

$$n = 1 - \frac{1}{J}(1 - \varphi). \tag{7}$$

This expression follows from the condition of volume additivity,

$$J = \frac{dv}{dV} = \frac{dv_s + dv_f}{dV_s + dV_f}, \tag{8}$$

which reflects the kinematic coupling between the macroscopic deformation of the solid skeleton and the evolution of the pore network. An increase in the local volume ratio J corresponds to an expansion of the pore space, while compression ($J < 1$) leads to a reduction in porosity.

1.2.2 *Strain tensors*

The mapping in (3) encapsulates the combined effects of stretch and rotation inherent in the deformation. This is formally articulated by the polar decomposition theorem, which uniquely decomposes $\mathbf{F}$ into a proper orthogonal rotation tensor $\mathbf{R}$ and a symmetric, positive definite stretch tensor, either $\mathbf{U}$ (right stretch) or $\mathbf{V}$ (left stretch):

$$\mathbf{F} = \mathbf{R} \cdot \mathbf{U} = \mathbf{V} \cdot \mathbf{R}. \tag{9}$$

In addition to the polar decomposition, it is often convenient to introduce a further multiplicative decomposition of the deformation gradient that distinguishes between purely volumetric and isochoric deformations. This separation allows for an independent treatment of the material response associated with volume changes and distortional effects, respectively. The deformation gradient can thus be expressed as

$$\mathbf{F} = J^{1/3}\,\bar{\mathbf{F}}, \tag{10}$$

where $J = \det(\mathbf{F})$ denotes the local volume ratio, and $\bar{\mathbf{F}}$ represents the isochoric (or deviatoric) part of the deformation gradient, which satisfies $\det(\bar{\mathbf{F}}) = 1$. Accordingly, the right and left stretch tensors can be written as

$$\mathbf{U} = J^{1/3}\,\bar{\mathbf{U}}, \qquad \mathbf{V} = J^{1/3}\,\bar{\mathbf{V}}, \tag{11}$$

with $\det(\bar{\mathbf{U}}) = \det(\bar{\mathbf{V}}) = 1$ [81].
To quantify the variation in the squared length of an infinitesimal line element between the reference and current configurations, we consider the expression

$$ds^2 = d\mathbf{x}\cdot d\mathbf{x} = d\mathbf{X}\cdot\mathbf{F}^{T}\cdot\mathbf{F}\cdot d\mathbf{X} = d\mathbf{X}\cdot\mathbf{C}\cdot d\mathbf{X}, \tag{12}$$

which leads to the definition of the right Cauchy-Green tensor:

$$\mathbf{C} = \mathbf{F}^{T}\cdot\mathbf{F}. \tag{13}$$

Analogously, the inverse relation,

$$d\boldsymbol{A}^2 = d\mathbf{X}\cdot d\mathbf{X} = d\mathbf{x}\cdot\mathbf{F}^{-T}\cdot\mathbf{F}^{-1}\cdot d\mathbf{x} = d\mathbf{x}\cdot\mathbf{B}^{-1}\cdot d\mathbf{x}, \tag{14}$$

serves to define the left Cauchy-Green deformation tensor:

$$\mathbf{B} = \mathbf{F}\cdot\mathbf{F}^{T}. \tag{15}$$

While the Cauchy-Green tensors reduce to the identity tensor $\mathbf{I}$ in the undeformed state, strain tensors are designed to vanish when no deformation is present. This is achieved by examining the difference in the squared line elements:

$$d\boldsymbol{a}^2 - d\boldsymbol{A}^2 = d\mathbf{x}\cdot d\mathbf{x} - d\mathbf{X}\cdot d\mathbf{X} = d\mathbf{X}\cdot(\mathbf{C}-\mathbf{I})\cdot d\mathbf{X} = d\mathbf{x}\cdot(\mathbf{I}-\mathbf{B}^{-1})\cdot d\mathbf{x}. \tag{16}$$

The tensors derived from this expression, namely:

$$\mathbf{E} = \frac{1}{2}(\mathbf{C}-\mathbf{I}) \quad \text{and} \quad \mathbf{e} = \frac{1}{2}(\mathbf{I}-\mathbf{B}^{-1}), \tag{17}$$

are recognized as the Green-Lagrange and the Euler-Almansi strain tensors, respectively.

In the geometrically linear theory, the distinction between the reference and current configurations is neglected, and the material and spatial gradients are assumed to coincide, denoted simply by ∇. Under this assumption, the Green-Lagrange strain tensor $\mathbf{E}$ simplifies to the well-known engineering strain tensor:

$$\boldsymbol{\varepsilon} = \mathbf{E}^{\text{lin}} = \frac{1}{2}(\nabla \mathbf{u} + (\nabla \mathbf{u})^{\mathsf{T}}). \tag{18}$$

Finally, the spatial velocity gradient $\mathbf{L}$ is introduced:

$$\mathbf{L} := \nabla_{\mathbf{x}} \mathbf{v} = \dot{\mathbf{F}} \cdot \mathbf{F}^{-1}. \tag{19}$$

It is conventional to decompose this tensor additively into its symmetric and skew-symmetric parts:

$$\mathbf{L} = \mathbf{D} + \mathbf{W}, \tag{20}$$

where

$$\mathbf{D} = \frac{1}{2}(\mathbf{L} + \mathbf{L}^{\mathsf{T}}) \quad \text{and} \quad \mathbf{W} = \frac{1}{2}(\mathbf{L} - \mathbf{L}^{\mathsf{T}}) \tag{21}$$

are defined as the rate of deformation tensor and the spin tensor, respectively.

1.2.3 *Stress Tensors and Mass Flux Vectors*

In this section, we introduce the notion of stress. Different stress tensors are defined via the concept of conjugate variables and are geometrically related to each other. In a way similiar to the concept of stress, fluid flux vectors are defined on the current and reference configurations.

Consider an arbitrary cut-out sub-region $\mathcal{P}_0$ within the reference configuration $\mathcal{B}_0$ of a body and its deformed counterpart $\mathcal{P}_t$ in the current configuration $\mathcal{B}_t$, with boundaries $\partial\mathcal{P}_0$ and $\partial\mathcal{P}_t$, respectively. We assume the existence of a traction vector field $\mathbf{t}(\mathbf{x}, t; \mathbf{n})$ which depends on a spatial unit vector $\mathbf{n}$. The field $\mathbf{t}(\mathbf{x}, t; \mathbf{n})$ represents the reaction force per unit area of a cut surface through the deformed continuum. The orientation of the area element is indicated by the outer normal $\mathbf{n}$. According to Cauchy's fundamental theorem, the traction vector depends linearly on the outward unit normal $\mathbf{n}$ to the surface:

$$\mathbf{t}(\mathbf{x}, t; \mathbf{n}) = \boldsymbol{\sigma}(\mathbf{x}, t)\, \mathbf{n} \tag{22}$$

where $\boldsymbol{\sigma}$ is the total Cauchy stress tensor. The identity $\mathbf{T}\, \mathrm{d}\boldsymbol{A} = \mathbf{t}\, \mathrm{d}a$, which relates the nominal force $\mathbf{t}_0\, \mathrm{d}\boldsymbol{A}$ on the reference area to the true force $\mathbf{t}\, \mathrm{d}a$ on the current area, motivates the definition of the first Piola-Kirchhoff stress tensor (or nominal stress tensor) $\mathbf{P}$ by employing Nanson's formula:

$$\mathbf{P}\, \mathrm{d}\boldsymbol{A} = \boldsymbol{\sigma}\, \mathrm{d}a, \quad \text{which yields} \quad \mathbf{P} = J\boldsymbol{\sigma}\mathbf{F}^{-\mathsf{T}}. \tag{23}$$

The two-point tensor $\mathbf{P}$ takes, at any point $\mathbf{X} \in \mathcal{B}_0$, a unit normal vector $\mathbf{N} \in \mathcal{B}_0$, indicating an undeformed area element's orientation, as input and gives as result the nominal traction vector $\mathbf{T} \in \mathcal{B}$ which represents a reaction force per unit undeformed area, i.e. the nominal traction vector field is:

$$\mathbf{T}(\mathbf{X}, t; \mathbf{N}) = \mathbf{P}(\mathbf{X}, t)\mathbf{N}. \tag{24}$$

Let $\mathfrak{h}$ represent the outward flux of fluid mass across a surface element $d\mathfrak{a}$ of $\partial\mathcal{P}_t$ in the current configuration. This flux is postulated to be a linear function of the surface normal $\mathbf{n}$:

$$h(\mathbf{x}, t; \mathbf{n}) = \mathbf{h}(\mathbf{x}, t) \cdot \mathbf{n} \tag{25}$$

thereby defining the *spatial fluid mass flux vector* $\mathbf{h}$. Scaling this spatial mass efflux by the corresponding reference area element through the identity $\mathbf{H}\, dA = \mathbf{h}\, d\mathfrak{a}$ leads to the definition of the *material fluid mass flux vector* $\mathbf{H}$:

$$\mathbf{H} \cdot d\mathbf{A} = \mathbf{h} \cdot d\mathfrak{a} \quad \text{resulting in} \quad \mathbf{H} = J\mathbf{F}^{-1}\mathbf{h}. \tag{26}$$

To underline the analogy to the different geometric settings of the stress, $\mathbf{H}$ is often called the Piola-Kirchhoff mass flux vector. It can formally be defined by doing a pull-back operation on the spatial mass flux vector $\mathbf{h}$.

Pull-Back, Push-Forward, and the Piola Transformation

In continuum mechanics, the operations of *pull-back* and *push-forward* provide a rigorous framework for transporting tensor fields between the reference (material) configuration $\mathcal{B}_0$ and the current (spatial) configuration $\mathcal{B}$. The **pull-back** operation maps a spatial quantity, defined per unit volume or area in the deformed body, back to the reference configuration. This is achieved using the inverse of the deformation gradient $\mathbf{F}^{-1}$ and its determinant, the Jacobian J. This operation is essential for performing integrations and formulating constitutive equations on a fixed reference domain, as it allows all quantities to be expressed in terms of material coordinates $\mathbf{X}$. Conversely, the **push-forward** operation uses the inverse of the deformation gradient $\mathbf{F}^{-1}$ and J^{-1} to map a material quantity forward to the current configuration.
A canonical example of a pull-back is the **Piola transformation**, which relates a spatial vector field to its referential counterpart through the cofactor of the deformation gradient.This transformation is underpinned by the **Piola identity**, a fundamental result stating that the divergence of the cofactor matrix of $\mathbf{F}$ vanishes:

$$\nabla_{\mathbf{X}}(J\mathbf{F}^{-1}) = 0, \quad \text{or in components,} \quad \frac{\partial}{\partial X_i}\left(J\frac{\partial X_i}{\partial x_j}\right) = 0. \tag{27}$$

Let $\mathbf{H}(\mathbf{x}, t)$ be a spatial vector field, its counterpart in the reference configuration, obtained through the Piola transform, is defined as

$$\mathbf{H}(\mathbf{X}, t) = J\mathbf{F}^{-1}\mathbf{h}(\boldsymbol{\chi}(\mathbf{X}, t), t), \quad \text{with components} \quad H_i = J\frac{\partial X_i}{\partial x_j}h_j, \tag{28}$$

defined such that $\mathbf{H} \cdot \mathbf{N}$ represents the rate of fluid mass crossing a defined boundary per unit reference area and per unit time. A key consequence of this definition and the Piola identity is the transformation rule for the divergence operator:

$$\nabla_X \cdot \mathbf{H} = J\nabla \cdot \mathbf{h}, \quad \text{which reads in coordinates} \quad \frac{\partial H_i}{\partial X_i} = J\frac{\partial h_j}{\partial x_j}. \tag{29}$$

This property is crucial for converting balance laws from their spatial *(Eulerian)* form to their material *(Lagrangian)* form, as it consistently handles the transformation of flux terms across configurations.

1.2.4 *Balance Laws*

1.2.4.1 *Balance of Mass*

Following the classical literature on poroelasticity, let us define the *variation in fluid mass content* $m : \mathcal{B}_0 \times \mathcal{T} \to \mathbb{R}$ introduced by Biot [18], representing the increase of interstitial fluid mass per unit reference volume of the poroelastic solid [82, Eq. $(6)_1$] and [121]. By recasting the principle of fluid mass conservation with respect to the motion of the solid skeleton, we obtain the Lagrangian statement of mass conservation:

$$\frac{dm}{dt} + \nabla_{\mathbf{X}}, \mathbf{H} = 0. \tag{30}$$

Here, m denotes the variation in fluid mass content, so that the quantity $m(\mathbf{X}, t), d\mathcal{B}_0$ measures the net variation of fluid mass—positive in the case of influx and negative in the case of efflux—within the material volume element $d\mathcal{B}_0$ since the initial time $t = 0$. The mass balance formulated with respect to the solid skeleton (see Coussy, Dormieux, and Detournay [40]) indicates that any change in the fluid mass contained in $d\mathcal{B}_0$ is solely due to the net flux of fluid mass across its boundary. Accordingly, we restrict our attention to the balance equation for the fluid phase alone.

1.2.4.2 *Balance of linear momentum*

The balance of linear momentum for the system as a whole, in the quasi-static regime, can be formulated in the spatial setting as:

$$\nabla_{\mathbf{x}} \cdot \boldsymbol{\sigma} + \rho\mathbf{b} = 0, \tag{31}$$

where $\boldsymbol{\sigma}$ denotes the total Cauchy stress tensor and ρ, b denoting respectively the system density and the body forces acting on the system in the reference configuration. Following Terzaghi's theory, the total stress can be decomposed into an effective stress contribution and a pore pressure term $\boldsymbol{\sigma} = \boldsymbol{\sigma}' - p\mathbf{I}$, (Remark 1).
To express the momentum balance in material coordinates, we perform a pull-back operation to the reference configuration $\mathcal{B}_0$, obtaining the first Piola–Kirchhoff stress tensor $\mathbf{P}$, thus obtain the equilibrium statement in the material setting as:

$$\nabla_X \cdot \mathbf{P} + \rho\mathbf{b} = 0. \tag{32}$$

In this framework, the effective part of the stress is denoted by $\mathbf{P}_{\text{eff}}$, corresponding to the pull-back of the effective Cauchy stress:

$$\mathbf{P} = \mathbf{P}' - Jp\mathbf{F}^{-T}, \tag{33}$$

where $J = \det \mathbf{F}$ and $\mathbf{F}$ stands for the deformation gradient.

Remark 1 (Terzaghi's Effective Stress Principle)**.** The notion of effective stress, traces its origin to the seminal work of Karl Terzaghi [122], who introduced it in the context of one-dimensional soil consolidation. Terzaghi's principle asserts that the total stress $\boldsymbol{\sigma}$ can be partitioned into the sum of the effective stress $\boldsymbol{\sigma}'$, carried by the soil skeleton, and the isotropic pore pressure p transmitted by the fluid $\boldsymbol{\sigma} = \boldsymbol{\sigma}' - p\mathbf{I}$. This decomposition emerges as a constitutive assumption that establishes how the macroscopic mechanical response of the composite medium depends on the interaction between the solid and fluid phases.
In the reference (undeformed) configuration, applying the *pull-back* operation to the above expression yields the corresponding relation in terms of the first Piola–Kirchhoff stress tensor $\mathbf{P} = \mathbf{P}' - \alpha Jp\mathbf{F}^{-T}$, where $\mathbf{P}$ is the total first Piola–Kirchhoff stress, $\mathbf{P}'$ denotes the effective contribution, $J = \det(\mathbf{F})$ is the Jacobian of the deformation gradient $\mathbf{F}$, and p is the pore pressure.
This early formulation relies on a series of simplifying assumptions: full saturation of the pore space, incompressibility of both the fluid and the solid grains, a linear elastic and fully reversible mechanical behavior of the skeleton, and the validity of Darcy's law throughout the entire consolidation process. While these assumptions enabled the development of classical consolidation theory, they also impose intrinsic limitations [112]. In particular, the assumption of a purely elastic and reversible skeletal response may lead to unrealistic predictions during unloading, such as negative excess pore pressures and time-dependent unconsolidation. Although originally derived within the framework of small-strain theory, this concept remains fundamental and, in the context of finite deformations, its generalization can be formulated through Biot's theory [20, 32].
Following Biot's formulation, the total Cauchy stress $\boldsymbol{\sigma}$ is commonly expressed through an additive decomposition of the form $\boldsymbol{\sigma} = \boldsymbol{\sigma}' - \alpha p, \mathbf{I}$, where $\boldsymbol{\sigma}'$ denotes the effective

stress tensor responsible for the deformation of the solid matrix, α is Biot's coefficient, and p is the pore fluid pressure. The most general expression of Biot reduces to that of Terzaghi by setting Biot's coefficient to unity.

1.2.5 *Thermodynamic consistency*

In a dissipative system, the dissipation rate, which must be non-negative according to the principle of irreversibility [38, 54, 91]. Denoting with $\psi(\chi, \mu)$ the material Helmholtz free-energy density function of the poroelastic solid, the dissipation rate $\mathcal{D}$ can be formally written as [82, Eq. (14)]

$$\mathcal{D} = \mathbf{P} \cdot \dot{\mathbf{F}} - \dot{\mu}\, m - \dot{\psi} - \nabla\mu \cdot \mathbf{H} \geqslant 0\,, \tag{34}$$

which naturally decomposes into two distinct contributions, i.e., an intrinsic (local) contribution and a transport-related contribution. The intrinsic dissipation rate can be expressed as

$$\mathcal{D}_{\text{int}} = \mathbf{P} \cdot \dot{\mathbf{F}} - \dot{\mu}\, m - \dot{\psi} \geqslant 0\,, \tag{35}$$

depending exclusively on the variables that define the free energy of the elementary system, where the local balance is established. At equilibrium, it characterizes the dissipation rate associated with internal irreversible processes, vanishing in the absence of local dissipative mechanisms. On the other hand, the transport-related dissipation is related to the mass transport of the fluid phase, namely

$$\mathcal{D}_{\text{tr}} = -\nabla\mu \cdot \mathbf{H} \geqslant 0\,. \tag{36}$$

1.2.5.1 *Stored energy and Dissipation Potential function*

Assuming a first-grade local theory, the material Helmholtz free-energy density is posited to be a function of the primary variables, the deformation $\boldsymbol{\chi}$ and the fluid potential μ, and their material gradients: $\psi = \psi(\boldsymbol{\chi}, \nabla\boldsymbol{\chi}, \mu, \nabla\mu)$. Requiring that ψ remain invariant under superposed rigid body motions of the current configuration, for all rotations and translations, and ensuring consistency with the local dissipation inequality (35), the functional dependence reduces to:

$$\psi = \psi(\mathbf{F}, \mu) = \overline{\psi}(\mathbf{C}, \mu) \tag{37}$$

where $\mathbf{C}$ is the right Cauchy-Green deformation tensor (13). Notably, consistency with (35) necessitates that ψ cannot depend on the gradient $\nabla\mu$. From this reduced form, the constitutive equations for the nominal stress $\mathbf{P}$ and the mass increase m are derived, satisfying the demand $\mathcal{D}_{\text{loc}} = 0$ for a non-dissipative elastic response.

The constitutive law governing fluid mass transport is defined through an objective *dissipation potential* function ϕ, which is a function of the material driving force $\nabla_X \mu$ at a *fixed* local state $\mathbf{F}, \mu$:

$$\phi = \phi(\nabla_X \mu; \mathbf{F}, \mu) = \phi(\nabla_X \mu; \mathbf{C}, \mu). \tag{38}$$

The formulation of constitutive equations must be consistent with the Clausius-Duhem inequality (34) and the fundamental principles of frame invariance [56]. Accordingly, the material Helmholtz free-energy density function $\psi = \psi(\chi, \mu)$ stored at a point $\mathbf{X} \in \mathcal{B}$ of the poroelastic solid is defined in terms of the deformation map χ and the fluid potential μ [18, Eq. (2.5)]. From (35), the following constitutive relationships for the total Cauchy stress tensor and the material fluid mass content are derived

$$\mathbf{P} = \partial_\chi \psi(\chi, \mu), \qquad m = -\partial_\mu \psi(\chi, \mu). \tag{39}$$

The inequality in Eq. (36), pertaining to the transport-related dissipation, is satisfied by choosing a convex dissipation potential function $\phi(\nabla_X \mu)$ in the space of the fluid potential gradient $\nabla_X \mu$, such that the material fluid mass flux vector is then given by the constitutive relation [82], which represents a generalized form of Darcy's law:

$$\mathbf{H} = -\partial_{\nabla_X \mu} \phi(\nabla_X \mu). \tag{40}$$

1.2.6 *The Boundary Conditions for the Coupled Problem*

The boundary $\partial\mathcal{B}_0$ of the reference configuration is partitioned to accommodate the two primary global fields, the deformation and the fluid potential. This results in complementary mechanical and fluid-flux boundary sets:

$$\partial\mathcal{B}_0 = \partial\mathcal{B}_0^\varphi \cup \partial\mathcal{B}_0^t \quad \text{and} \quad \partial\mathcal{B}_0 = \partial\mathcal{B}_0^\mu \cup \partial\mathcal{B}_0^h, \tag{41}$$

where $\partial\mathcal{B}_0^\varphi \cap \partial\mathcal{B}_0^t = \emptyset$ and $\partial\mathcal{B}_0^\mu \cap \partial\mathcal{B}_0^h = \emptyset$, as illustrated in Figure 1. We prescribe respectively in Eq. (42) and (43) the Dirichlet and Neumann boundary conditions for the deformation and the fluid potential:

$$\chi = \overline{\chi}(\mathbf{X}, t) \text{ on } \partial\mathcal{B}_0^\chi \quad \text{and} \quad \mu = \overline{\mu}(\mathbf{X}, t) \text{ on } \partial\mathcal{B}_0^\mu, \tag{42}$$

$$\mathbf{P}\mathbf{N} = \bar{\mathbf{t}}(\mathbf{X}, t) \text{ on } \partial\mathcal{B}_0^t \quad \text{and} \quad \mathbf{H} \cdot \mathbf{N} = \overline{H}(\mathbf{X}, t) \text{ on } \partial\mathcal{B}_0^h. \tag{43}$$

Here, $\overline{\chi}$, $\bar{\mathbf{t}}$, $\overline{\mu}$, and $\overline{H}$ are prescribed functions, and $\mathbf{N}$ is the material outward unit normal vector on $\partial\mathcal{B}_0$. The initial condition for the fluid potential is given by:

$$\mu(\mathbf{X}, 0) = 0 \quad \text{in} \quad \mathcal{B}_0. \tag{44}$$

The governing equations of the coupled deformation-fluid-transport problem, formulated in terms of the primary variables $\mathbf{u}$ and m, with the related boundary conditions, are summarized in (262).

$$
\begin{aligned}
&\textit{Compatibility equation} && \boldsymbol{\chi} = \nabla\chi \times (\mathbf{F}) && \text{in } \mathcal{B}_0 \\
&\textit{Balance of mass} && \dot{m} + \nabla_\chi \cdot \mathbf{H} = 0 && \text{in } \mathcal{B}_0 \\
&\textit{Balance of linear momentum} && \nabla \cdot \mathbf{P} + \rho\mathbf{b} = \mathbf{0} && \text{in } \mathcal{B}_0 \\
&\textit{Constitutive total stress} && \mathbf{P} = \partial_\chi \hat{\psi}(\chi, \mu) && \text{in } \mathcal{B}_0 \\
&\textit{Constitutive fluid mass content} && m = \partial_\mu \hat{\psi}(\chi, \mu) && \text{in } \mathcal{B}_0 \\
&\textit{Constitutive material mass flux} && \mathbf{H} = \partial_{\nabla_\chi \mu} \hat{\phi}(\nabla_\chi \mu) && \text{in } \mathcal{B}_0 \\
&\textit{Prescribed deformation map} && \chi = \bar{\chi} && \text{on } \partial\mathcal{B}_0^{\chi} \\
&\textit{Prescribed fluid potential} && \mu = \bar{\mu} && \text{on } \partial\mathcal{B}_0^{\mu} \\
&\textit{Prescribed tractions} && \mathbf{P} \cdot \mathbf{N} = \bar{\mathbf{t}} && \text{on } \partial\mathcal{B}_0^{t} \\
&\textit{Prescribed normal fluxes} && \mathbf{H} \cdot \mathbf{N} = \bar{H} && \text{on } \partial\mathcal{B}_0^{H}
\end{aligned}
\tag{45}
$$

1.2.7 *Linear poroelasticity*

In what follows, we restrict attention to the case of *small deformations*, so that the current and the reference configuration can be regarded as indistinguishable. The deformation of the solid skeleton is then described by the infinitesimal strain tensor

$$\boldsymbol{\varepsilon} = \nabla^s \mathbf{u}, \tag{46}$$

i.e., the symmetric part of the displacement gradient [61]. Consistently with the linearized theory, the configuration of the continuum body is denoted simply by $\mathcal{B}$ and the operator $\nabla(\bullet)$ drops the subscript.
Consider an arbitrary control volume $\mathcal{P} \subset \mathcal{B}$ with boundary $\partial\mathcal{P}$ and outward normal $\mathbf{n}$. Let $\mathbf{h}$ denote the *infinitesimal fluid mass flux*, then the quantity $\mathbf{h} \cdot \mathbf{n}$ measures the mass of fluid leaving $\partial\mathcal{P}$ per unit time and per unit area. The local form of the fluid mass balance in $\mathcal{P}$ can be stated as

$$\dot{m} + \nabla \cdot \mathbf{h} = 0 \qquad \text{on } \mathcal{P}, \tag{47}$$

where m represents the increment of fluid mass per unit volume of porous medium. Throughout this section, we adopt a *volume-based* description, which naturally recovers the classical formulation of linear poroelasticity [17, 39]. Assuming true incompress-

ibility of the fluid (i.e. $\nabla \rho_f = \mathbf{o}$ and $\dot{\rho}_f = 0$), the standard volume-related quantities are introduced as

$$\zeta = \frac{m}{\rho_f}, \qquad \mathbf{j} = \frac{\mathbf{h}}{\rho_f}, \tag{48}$$

where ζ measures the variation of fluid volume per unit volume of porous medium, and $\mathbf{j}$ stands for the volumetric fluid flux. Substituting these definitions into (47) gives the classical form of the continuity equation,

$$\dot{\zeta} + \nabla \cdot \mathbf{j} = 0, \tag{49}$$

which is the standard expression adopted in Biot's linear poroelasticity [17].
Neglecting inertial effects and body forces, and under the assumption of small displacements, the linear momentum balance equation (Eq. (31)) reduces to $\nabla \cdot \boldsymbol{\sigma} = \mathbf{o}$, where the total stress $\boldsymbol{\sigma}$ is additively decomposed in $\boldsymbol{\sigma} = \boldsymbol{\sigma}' - \alpha \mu \mathbf{I}$, following the Biot effective stress principle .
In a similar manner to the formulation of the fluid mass balance equation, the equilibrium equation in Eq. (31), can be recast in terms of volume-related, rather than mass-related, quantities. The variable conjugate to ζ, identified as the fluid pressure p, is derivable from the fluid potential, μ. For a barotropic fluid, a constitutive relation exists between the fluid potential μ, pressure p, and fluid density ρ_f, given by Eq. [121]:

$$p = \rho_f \mu. \tag{50}$$

To complete the system, the thermodynamic structure of the problem must be specified. Let us assume a linear elastic solid skeleton, an ideal barotropic fluid, and normal dissipative mechanisms, then the free-energy density and the dissipation potential are chosen in quadratic form [121], in terms of the infinitesimal strain ε and the fluid mass content m:

$$\psi^*(\varepsilon, \mu) = \tfrac{1}{2}\varepsilon : \mathbb{C} : \varepsilon - \tfrac{1}{2}\frac{\rho_f^2}{M}\mu^2 - \alpha \rho_f \mu \operatorname{tr} \varepsilon, \qquad \hat{\phi}^*(\nabla \mu) = -\tfrac{1}{2}\nabla \mu \cdot \boldsymbol{\kappa} \cdot \nabla \mu, \tag{51}$$

where $\mathbb{C}$ denotes the elasticity tensor of the poroelastic solid, α and M represent Biot's coefficient and modulus, respectively, and $\boldsymbol{\kappa}$ is a constant, symmetric and positive-definite second-order permeability tensor [32]. In the case of isotropy, $\boldsymbol{\kappa} = \kappa \mathbf{I}$. Differentiation yields the dual constitutive relations

$$\begin{aligned} \boldsymbol{\sigma} &= \mathbb{C} : \varepsilon - \alpha \rho_f \mu \\ m &= \rho_f^2 \frac{\mu}{M} + \alpha \rho_f \operatorname{tr} \varepsilon. \end{aligned} \tag{52}$$

Analogous to the procedure applied to the mass balance and equilibrium equations, this constitutive law can also be expressed in terms of volume-related quantities under

the assumption of a truly incompressible fluid. Substituting Eq. (48) and Eq. (50) into the expression Eq. (52) yields:

$$\psi^{**}(\varepsilon,\mu) = \tfrac{1}{2}\varepsilon : \mathbb{C} : \varepsilon - \tfrac{1}{2M}\, p^2 - \alpha\, p\, \mathrm{tr}\,\varepsilon, \qquad \phi^{**}(\nabla\mu) = -\tfrac{1}{2}\,\nabla p \cdot \boldsymbol{\kappa} \cdot \nabla p, \tag{53}$$

being $\boldsymbol{\kappa}$ the permeability tensor. Then, the conjugate variables can be written as

$$\boldsymbol{\sigma} = \mathbb{C} : \varepsilon - \alpha\, p\, \mathbf{I}, \tag{54}$$

$$m = \frac{1}{M}\, p + \alpha\, \mathrm{tr}\,\varepsilon. \tag{55}$$

The linear poroelastic problem in the $(\mathbf{u}, p)$ formulation can be summarized in the following compact form:

Compatibility law	$\varepsilon = \nabla^{s}\mathbf{u}$	in $\mathcal{B}$,	
Momentum balance	$\nabla \cdot \boldsymbol{\sigma} = \mathbf{o}$	in $\mathcal{B}$,	
Fluid mass balance	$\dot{m} + \nabla \cdot \mathbf{h} = 0$	in $\mathcal{B}$,	(56)
Constitutive stress	$\boldsymbol{\sigma} = \mathbb{C} : \varepsilon - \alpha(\rho_f \mu)\mathbf{I}$	in $\mathcal{B}$,	
Constitutive fluid mass content	$m = \frac{1}{M}\,(\rho_f \mu) + \alpha\, \mathrm{tr}\,\varepsilon$	in $\mathcal{B}$,	
Constitutive mass flux	$\mathbf{h} = -\kappa \nabla p,$	in $\mathcal{B}$,	

representing the classical Biot-type model of linear poroelasticity, consistently formulated in terms of the displacement $\mathbf{u}$ and pore pressure p as the primary variables.

1.3 VARIATIONAL FRAMEWORK

This section develops the variational framework underlying the finite element formulations presented in Chapters 3- 5. We begin with a concise overview of the methodological foundations of the variational approach, which provides a rigorous and versatile alternative to the classical differential formulation. For a comprehensive treatment of the subject, the reader is referred to the seminal works of Berdichevsky [16] and Oden and Reddy [88] and Reddy [104]. Building on the theory of Biot's poroelasticity presented in Section 1.1, we then introduce three distinct variational principles, each defined by its own functional and set of primary variables. The first principle, corresponding to the governing differential equations introduced earlier, forms the basis of the standard finite element formulation for poroelasticity. A Legendre transformation, involving a change in one or more primary variables, produces an alternative variational statement in a different functional space. Although the continuous solu-

tions remain equivalent, the corresponding finite element approximations may differ, offering complementary perspectives for the analysis and discretization of deformable porous media. The remainder of the chapter presents two additional alternative principles, which form the foundation of the hybrid-mixed finite element formulations developed in Chapters 3- 5. Finally, we briefly address existence, uniqueness, and stability, motivating the choice of approximation spaces and supporting the adoption of the proposed variational formulations.

In continuum mechanics, the fundamental conservation laws and constitutive relations are naturally expressed through a system of partial differential equations (PDEs). These equations, summarized in (45) and presented in the first part of this chapter, must hold at every point within the domain. This point-wise/local statement is referred to as the strong form of the problem and requires a high degree of regularity in the unknown field functions. The *variational* or *weak form*, on the other hand, operates on a global level.

The variational approach is based on the principle that the equilibrium state of a system is identified as the function ψ that renders the energy functional $\Pi(\psi)$ stationary, being Π a mapping from a function ψ to a scalar quantity. This stationarity condition is expressed formally by requiring that the first variation $\delta\Pi(\psi;\eta)$ vanishes for all admissible variations η in a space $\mathcal{W}$:

$$\delta\Pi(\psi;\eta) \tag{57}$$

vanishes for all admissible variations $\eta \in \mathcal{W}$:

$$\delta\Pi(\psi;\eta) = 0 \quad \forall\, \eta \in \mathcal{V}_0, \tag{58}$$

where $\mathcal{W}$ denotes the space of admissible variations η, typically constrained to satisfy homogeneous essential boundary conditions. This global variational statement is formally equivalent to the strong form of the problem, as it implies the local satisfaction of the governing differential equations and the natural boundary conditions, only under suitable regularity assumptions. The integration-by-parts procedure, inherent in the derivation of the weak form, systematically lowers the order of differentiation by one order relative to the original differential equations. This broadens the space of admissible solutions, allowing the formulation to admit solutions in spaces with reduced regularity requirements. Consequently, while any solution of a strong form (*classical solution*) is invariably the solution of the associated variational problem, the converse is not true. A solution of the variational problem (*weak solution*) constitutes a classical solution only if it possesses the sufficient regularity mandated by the strong form.

1.3.1 *Standard 'u-p' formulation*

A rate-type variational principle, originally developed by Miehe, Mauthe, and Teichtmeister [82] for coupled poroelastic boundary-value problems, can be derived directly from the stored energy and dissipation functionals introduced in Section 1.1. Based on the deformation map field $\boldsymbol{\chi}$ and the fluid potential μ, under the assumption of constant fluid true density, the associated saddle-point structure (see Remark 2) can be recovered in terms of mass-related quantities, while retaining a more general framework [121]. In the final part of this section, the analysis is restricted to the small-strain regime under the assumption of quasi-incompressibility, thereby recovering the classical u–p formulation.

At a given state $\{\boldsymbol{\chi}(\mathbf{X},t),\mu(\mathbf{X},t)\}$, the following *rate potential*[2] is postulated [82, Eq. (79)] through its internal and external contributions:

$$\Pi^*(\boldsymbol{\chi}(\mathbf{X},t),\mu(\mathbf{X},t)) = \int_{B_0} \pi^*(\nabla\boldsymbol{\chi},\mu,\nabla\mu)\,dV \;-\; P^*_{ext}(\boldsymbol{\chi},\mu), \tag{59}$$

where $\pi^*(\nabla\dot{\boldsymbol{\chi}},\mu,\nabla\mu)$ denotes the associated potential density function, defined as in Miehe, Mauthe, and Teichtmeister [82]:

$$\begin{aligned}\pi^*(\nabla\dot{\boldsymbol{\chi}},\mu,\nabla\mu) &= \dot{\psi}(\nabla\boldsymbol{\chi},\mu) - \phi(\nabla\mu)\\ &= \left[\,\partial_{\mathbf{F}}\overline{\psi}_{\text{eff}} - \mu\rho_f J\mathbf{F}^{-T}\right] : \nabla\dot{\boldsymbol{\chi}} \;-\; \phi(\nabla\mu)\,,\end{aligned} \tag{60}$$

where we have assumed the absence of body forces, an assumption that will be maintained hereafter for the sake of simplicity.
The evolution of the total stress and the fluid mass flux vector follows from the mixed *two-field saddle-point principle*:

$$\boxed{\{\dot{\boldsymbol{\chi}},\mu\} = \operatorname{Arg}\left\{\inf_{\dot{\boldsymbol{\chi}}\in\mathcal{V}_{\boldsymbol{\chi}}}\sup_{\mu\in\mathcal{V}_\mu}\Pi^*(\dot{\boldsymbol{\chi}},\mu)\right\}}\,. \tag{61}$$

Starting from the rate potential in Eq . (59):

$$\begin{aligned}\Pi^*(\dot{\boldsymbol{\chi}},\mu) = &\int_{B_0}\left[\,\partial_{\mathbf{F}}\overline{\psi}_{\text{eff}} - \mu\rho_f J\mathbf{F}^{-T}\right] : \nabla\,\delta\dot{\boldsymbol{\chi}}\,dV - \int_{B_0}\nabla\delta\mu\cdot\boldsymbol{\kappa}\cdot\nabla\mu\,dV\\ &-\int_{\partial\mathcal{B}^t}\delta\dot{\boldsymbol{\chi}}\cdot\bar{\mathbf{T}}\,d\Gamma + \int_{\partial\mathcal{B}^h}\delta\mu\bar{H}\,d\Gamma = 0.\end{aligned} \tag{62}$$

2 In (59), we explicitly state the dependence of the primal variables on space and time, while in [73, 82, 121], the expression for the rate potential prescribes that the dependence of Π and π is given directly in terms of the deformation rate $\dot{\boldsymbol{\chi}}$. By applying the chain rule to the time derivative of the deformation map, the same result is obtained. From this point onward, we will follow the notation proposed in [73, 82, 121] for the sake of clarity.

Taking the first variation for admissible virtual rates $\delta\dot{\boldsymbol{\chi}}$ and virtual fluid potentials $\delta\mu$ yields the Euler equations:

$$\begin{aligned}
&\textit{Stress equilibrium:} && -\nabla\cdot\left[\partial_{\mathbf{F}}\overline{\psi}_{\text{eff}} - \mu\rho^{\text{f}}J\mathbf{F}^{-\text{T}}\right] &&= 0 \quad \text{in } B_0,\\
&\textit{Mass balance:} && \rho^{\text{f}}J\mathbf{F}^{-\text{T}} : \nabla\dot{\boldsymbol{\chi}} + \nabla\cdot\left[\partial_{\nabla\mu}\widehat{\phi}^{*}\right] &&= 0 \quad \text{in } B_0,\\
&\textit{Prescribed tractions:} && \left[\partial_{\mathbf{F}}\overline{\psi}_{\text{eff}} - \mu\rho^{\text{f}}J\mathbf{F}^{-\text{T}}\right]\cdot\mathbf{n}_0 - \bar{\mathbf{t}}_0 &&= 0 \quad \text{on } \partial B_0^{\text{t}},\\
&\textit{Prescribed fluid flux:} && \left(\partial_{\nabla\mu}\widehat{\phi}^{*}\right)\cdot\mathbf{n}_0 - \overline{h}_0 &&= 0 \quad \text{on } \partial B_0^{\text{h}}.
\end{aligned} \tag{63}$$

with the admissible variations $\delta\dot{\boldsymbol{\chi}}$ and $\delta\mu$ belonging to the functional spaces

$$\begin{aligned}
\mathcal{V}_{\chi} &= \left\{\boldsymbol{\chi}\in[H^1(B_0)] \,\middle|\, \boldsymbol{\chi} = \bar{\boldsymbol{\chi}} \ \text{ on } \partial B_0^{\chi}\right\},\\
\mathcal{V}_{\mu} &= \left\{\mu\in[L^2(B_0)] \,\middle|\, \mu = \bar{\mu} \ \text{ on } \partial B_0^{\mu}\right\},\\
\mathcal{W}_{\delta\chi} &= \left\{\delta\boldsymbol{\chi}\in[H^1(B_0)] \,\middle|\, \delta\boldsymbol{\chi} = 0 \ \text{ on } \partial B_0^{\chi}\right\},\\
\mathcal{W}_{\delta\mu} &= \left\{\delta\mu\in[L^2(B_0)] \,\middle|\, \delta\mu = 0 \ \text{ on } \partial B_0^{\mu}\right\},
\end{aligned} \tag{64}$$

with $H^1(B_0)$ and $L^2(B_0)$ denoting the standard Sobolev and Lebesgue spaces, respectively.

Remark 2 (On the saddle-point character of the solution)**.** Equation (59) defines a saddle-point problem, corresponding to a minimum with respect to $\boldsymbol{\chi}$ and a maximum with respect to μ. Since the functional $\Pi^*(\boldsymbol{\chi},\mu)$ is strictly convex in $\boldsymbol{\chi}$ and strictly concave in μ, the solution of the continuous rate problem is unique. However, the stability of the discrete solution depends crucially on the choice of the approximation spaces. This issue will be addressed in Ch. 2 in the context of the so-called *inf–sup condition*.

1.3.1.1 *Rate-type variational form of small-strain poroelasticity*

In the small-strain regime, and upon expressing the balance laws in terms of volumetric rather than mass-related quantities (see sec.1.2.7), the variational framework reduces to the classical poroelastic formulation of Coussy [39]. Let us recall the espressions of the quadratic *rate potential* and *dissipation potential*, from sec.1.2.7:

$$\begin{aligned}
\psi^*(\boldsymbol{\varepsilon}, p) &= \tfrac{1}{2}\,\boldsymbol{\varepsilon} : \mathbb{C}_{\text{d}} : \boldsymbol{\varepsilon} - \boldsymbol{\varepsilon} : \mathbf{I}\,p + \tfrac{1}{2M}p^2,\\
\phi^*(\nabla p) &= \tfrac{1}{2}\,\nabla p\cdot\mathbf{k}\cdot\nabla p.
\end{aligned} \tag{65}$$

The extremum condition for the rate global functional in the small strain regime can be thus recovered

$$\delta\Pi(\dot{\mathbf{u}}, p) = 0, \tag{66}$$

where Π collects the rate potential

$$\Pi(\dot{\mathbf{u}}, p) = \int_{B_0} \pi^*(\nabla\dot{\mathbf{u}}, p, \nabla p)\, dv \;-\; P^*_{ext}(\dot{\mathbf{u}}, p), \tag{67}$$

where $\pi^*(\nabla\dot{\mathbf{u}}, p, \nabla p) = \dot{\psi}(\nabla\mathbf{u}, p) - \phi(\nabla p)$ denotes the associated potential density function. For all kinematically admissible virtual displacements $\delta\mathbf{u}$ (vanishing on $\partial\mathcal{B}^u$) and for all the virtual fluid pressure ∂p (vanishing on $\partial\mathcal{B}^p$), the following statement is obtained:

$$\begin{aligned}\int_{\mathcal{B}} \delta\dot{\boldsymbol{\varepsilon}} : \left(\mathbb{C}_d : \boldsymbol{\varepsilon} - \mathbf{I}\, p\right) dv + \int_{\mathcal{B}} \partial p \left(\tfrac{1}{M} p - \mathbf{I} : \dot{\boldsymbol{\varepsilon}}\right)\, dv \\ - \int_{\mathcal{B}} \nabla\delta p \cdot \mathbf{k} \cdot \nabla p\, dv - \int_{\partial\mathcal{B}^t} \bar{\mathbf{t}} \cdot \delta\dot{\mathbf{u}}\, da + \int_{\partial\mathcal{B}^j} \delta p\, \bar{j}\, da = 0.\end{aligned} \tag{68}$$

The statement in Eq. (68) corresponds to the classical variational formulation of poroelasticity, which forms the basis of the standard displacement–pressure finite element schemes [39].

In this standard formulation of poroelasticity, we introduce the *bilinear form*, a functional representation that expresses the variational principle in a compact and mathematically rigorous way. This formulation will prove useful in the development of subsequent concepts. The *bilinear form* [63, 104] is a mapping

$$a : V \times W \to \mathbb{R},$$

which is linear in each argument separately; that is,

$$a(u_1 + u_2, v) = a(u_1, v) + a(u_2, v), \qquad a(u, v_1 + v_2) = a(u, v_1) + a(u, v_2),$$

and

$$a(cu, v) = c\, a(u, v) = a(u, cv),$$

for all $u, u_1, u_2 \in V$, $v, v_1, v_2 \in W$, and scalar $c \in \mathbb{R}$. In the context the variational statement in Eq. , the bilinear form represents the virtual work associated with the Darcy-Biot diffusion process in the deformable solid. The symmetry, continuity, and coercivity of this form determine the well-posedness of the problem (via the Lax–Milgram theorem).

Recalling the governing equations of linear poroelasticity in the displacement–pressure (see box. (1.2.7)), let $\boldsymbol{v}$ and q be the admissible variations δu and δp, associated with $\boldsymbol{u}$ and p, respectively. The weak form of the quasi-static Biot problem is obtained by multiplying the governing equations by these test functions and integrating over the domain $\mathcal{B}$ Eq. (68). This leads to the coupled bilinear form:

$$\mathcal{A}\big((\boldsymbol{u}, p), (\boldsymbol{v}, q)\big) = a(\boldsymbol{u}, \boldsymbol{v}) - b(\boldsymbol{v}, p) + b(\boldsymbol{u}, q) + c(p, q), \tag{69}$$

where

$$
\begin{aligned}
a(\boldsymbol{u},\boldsymbol{v}) &= \int_{\Omega} \big(\mathbb{C} : \boldsymbol{\varepsilon}(\boldsymbol{u})\big) : \boldsymbol{\varepsilon}(\boldsymbol{v})\, d\Omega, \\
b(\boldsymbol{v},p) &= \int_{\Omega} I\, p\, (\nabla \cdot \boldsymbol{v})\, d\Omega, \\
c(p,q) &= \int_{\Omega} \kappa\, \nabla p \cdot \nabla q\, d\Omega.
\end{aligned}
\tag{70}
$$

The bilinear operator $\mathcal{A}\big((\boldsymbol{u},p),(\boldsymbol{v},q)\big)$ couples the elastic response of the solid skeleton and the pressure field of the pore fluid. It is bilinear in the sense that it is linear with respect to each argument $(\boldsymbol{u},p)$ and $(\boldsymbol{v},q)$ independently. The weak formulation seeks $(\boldsymbol{u},p)$ in the functional space $\mathcal{V}_u \times \mathcal{V}_p$ such that

$$
\mathcal{A}\big((\boldsymbol{u},p),(\boldsymbol{v},q)\big) = \mathcal{L}(\boldsymbol{v},q) \quad \forall (\boldsymbol{v},q), \tag{71}
$$

where $\mathcal{L}(\boldsymbol{v},q)$ represents the linear form associated with body forces and external fluxes.

1.3.2 *Alternative Variational Formulations*

1.3.2.1 *Stress–Pressure Variational Formulation*

A rate-type variational principle can also be formulated for the solutions in stress $\boldsymbol{\sigma}$ and fluid potential [3] μ [38], yielding to a minimization type of problem. Restricting the analysis to the small strain hypothesis, the dual the energy functional in Eq., dual dissipation potential function $\breve{\psi}$ and ϕ are obtained as the Legendre transformation with respect to the conjugate couple $(\boldsymbol{\varepsilon},\boldsymbol{\sigma})$ of its dual function ψ and $\widehat{\phi}$.
To this end the functional, for a given state $\{\dot{\boldsymbol{\sigma}},\dot{\mu}\}$, is postulated as:

$$
\begin{aligned}
\dot{\overline{\overline{\Pi}}}(\dot{\boldsymbol{\sigma}},\dot{\mu}) &= \int_{\mathcal{B}} \dot{\overline{\overline{\pi}}}(\dot{\boldsymbol{\sigma}},\dot{\mu})\, dv - \mathcal{P}_{ext}(\dot{\boldsymbol{\sigma}},\dot{\mu}) \\
&= \int_{\mathcal{B}} \dot{\overline{\overline{\pi}}}(\dot{\boldsymbol{\sigma}},\dot{\mu})\, dv - \int_{\partial\mathcal{B}^u} \bar{\boldsymbol{u}} \cdot \dot{\boldsymbol{\sigma}} \cdot \boldsymbol{n}\, da - \int_{\partial\mathcal{B}^h} \mu\, \bar{h}\, da,
\end{aligned}
\tag{72}
$$

where $\dot{\overline{\overline{\pi}}}$ is the internal rate potential per unit volume, taking the form

$$
\dot{\overline{\overline{\pi}}}(\dot{\boldsymbol{\sigma}},\dot{\mu}) = \int_{\mathcal{B}} \Big[\dot{\breve{\psi}}(\boldsymbol{\sigma},\mu) + \phi^*(\nabla\mu)\Big] \tag{73}
$$

3 In Coussy [38], the functional has a dependency on the fluid pressure $p = \rho_f\, \mu$.

being

$$\check{\psi}(\boldsymbol{\sigma}, \mu) = \frac{1}{2}(\boldsymbol{\sigma} + \rho_f \mu \mathbf{I}) : \mathbf{D} : (\boldsymbol{\sigma} + \rho_f \mu \mathbf{I}) + \frac{1}{2}\frac{\varphi}{M}\mu^2. \tag{74}$$

the quadratic expression of the dual stored energy density.

The solution $\{\dot{\boldsymbol{\sigma}}, \dot{\mu}\}$ is the pair of fields that minimizes the functional among all statically admissible stress rate fields and all admissible fluid potential rate fields:

$$\boxed{\{\dot{\boldsymbol{\sigma}}, \dot{\mu}\} = \operatorname{Arg}\left\{\min_{\dot{\boldsymbol{\sigma}} \in \mathcal{V}_\sigma} \min_{\dot{\mu} \in \mathcal{V}_\mu} \Pi(\dot{\boldsymbol{\sigma}}, \dot{\mu})\right\}} \tag{75}$$

with the fields $\boldsymbol{\sigma}, \mu$ and their variations $\delta\boldsymbol{\sigma}, \delta\mu$ belonging to the following functional spaces:

$$\begin{aligned}
&\mathcal{V}_{\boldsymbol{\sigma}} := \{\boldsymbol{\sigma} \in H(\mathrm{Div}, \mathcal{B}) |\, \boldsymbol{\sigma} \cdot n_0 = t \quad \text{on } \partial B^t\},\\
&\mathcal{V}_{\mu} := \{\mu \in L^2(B_0) |\, \mu = \bar{\mu} \quad \text{on } \partial B^\mu,\}\\
&\mathcal{W}_{\boldsymbol{\sigma}} := \{\delta\boldsymbol{\sigma} \in H(\mathrm{Div}, \mathcal{B}) |\, \delta\boldsymbol{\sigma} \cdot n_0 = 0 \quad \text{on } \partial B^t\}\\
&\mathcal{W}_{\mu} := \{\delta\mu \in L^2(B_0) |\, \delta\mu = 0 \quad \text{on } \partial B^\mu,\}.
\end{aligned} \tag{76}$$

Taking variations with respect to admissible virtual stress rate $\delta\dot{\boldsymbol{\sigma}}$ and virtual fluid potential rate $\delta\dot{\mu}$, one obtains the Euler–Lagrange equations:

Compatibility equation	$\nabla^s \mathbf{u} = [\mathbf{D} : (\boldsymbol{\sigma} + \mathbf{I}\,\rho_f \mu)] = 0$	in $\mathcal{B}$
Fluid mass balance	$\mathbf{I} : \mathbf{D} : (\boldsymbol{\sigma} + \rho_f \mu \mathbf{I}) + \frac{\varphi}{M}\mu - \nabla \cdot (\partial_{\nabla\mu} D)$	in $\mathcal{B}$
Prescribed displacements	$\mathbf{u} - \bar{\mathbf{u}} = 0$	on $\partial\mathcal{B}^{\mathbf{u}}$
Prescribed fluid flux	$\partial_{\nabla p}\phi \cdot \mathbf{n} - \bar{h} = 0$	on $\partial\mathcal{B}^h$

(77)

Being a minimization principle rather than a saddle-point formulation, this approach offers significant advantages in terms of the stability of the finite element discretization associated with the variational principle. Nonetheless, a numerical procedure based on the momentum balance equation, which the stress field $\boldsymbol{\sigma}$ must satisfy to be statically admissible, exhibits certain limitations, particularly regarding its generalization to finite deformations. This aspect will be analyzed in detail in the formulation based on this principle, presented in Chapter 3.

1.3.2.2 *Displacement- flux variational Formulation*

A rate-type variational principle developed by Miehe, Mauthe, and Teichtmeister [82], governing the coupled poroelastic boundary-value problem, can be derived directly from the functional expression in Eq. (59). Consider the stored energy density and the dissipation potential function $\widehat{\psi}$ and $\widehat{\phi}$ to be defined by the Legendre transformation with respect to the conjugate couple $(\dot{m}, \mu)$, in terms of its dual function $\widehat{\psi}^*$ and $\widehat{\phi}^*$.

Based on the rate of deformation $\dot{\boldsymbol{\chi}}$, the mass content rate $\dot{m}$ and fluid mass flux $\mathbf{H}$, a canonical minimization principle can be formulated, circumventing the need to explicitly satisfy the inf-sup condition associated with saddle-point formulations [121]. The potential $\Pi(\boldsymbol{\chi}, m, \mathbf{H})$ is postulated at given state $\{\boldsymbol{\chi}, m, \mathbf{H}\}$, with its internal and external contributions

$$\Pi(\dot{\boldsymbol{\chi}}, \dot{m}, \mathbf{H}) = \int_{B_0} \pi(\nabla\dot{\boldsymbol{\chi}}, \dot{m}, \mathbf{H},) \, dV - P_{ext}(\dot{\boldsymbol{\chi}}, \mathbf{H}). \tag{78}$$

where π is the internal rate potential per unit volume, taking the form

$$\pi(\nabla\dot{\boldsymbol{\chi}}, \dot{m}, \mathbf{H}) = \dot{\hat{\psi}}(\nabla\boldsymbol{\chi}, m) + \hat{\phi}(\mathbf{H}) \tag{79}$$

with $\dot{\hat{\psi}} = \partial_{\mathbf{F}}\widehat{\psi} : \nabla\dot{\boldsymbol{\chi}} - \partial_m\widehat{\psi}\,\dot{m}$, and $\mathcal{P}_{ext}$ is the external power. If body forces are neglected, the latter is provided by the surface tractions in the reference configuration $\bar{\mathbf{T}}$ and by the fluid mass transport across the surface related to a prescribed fluid potential $\bar{\mu}$ in the reference configuration [82, Eq. (30)].

At this stage, by enforcing the continuity equation (47), the variable $\dot{m}$ can be eliminated from the statement. Accordingly, the *internal rate potential density* per unit reference volume can be expressed as

$$\pi(\nabla\boldsymbol{\chi}, \mathbf{H}, \nabla_X \cdot [\mathbf{H}]) = \partial_{\mathbf{F}}\widehat{\psi} : \nabla\dot{\boldsymbol{\chi}} - \partial_m\widehat{\psi}\nabla_X \cdot [\mathbf{H}] + \widehat{\phi}(\mathbf{H}). \tag{80}$$

The evolution of the deformation and fluid mass flux vector at a given state $\{\boldsymbol{\chi}, m\}$ is determined by the *two-field minimization principle*

$$\boxed{\{\boldsymbol{\chi}, \mathbf{H}\} = \operatorname{Arg}\{\inf_{\boldsymbol{\chi}\in\mathcal{V}_{\boldsymbol{\chi}}} \inf_{\mathbf{H}\in\mathcal{V}_{\mathbf{H}}} \Pi(\dot{\boldsymbol{\chi}}, \mathbf{H})\}}\,. \tag{81}$$

Note that the minimization structure of this variational principle is governed by the convexity of the dissipation potential function $\widehat{\phi}$. Taking the variation of the rate potential for admissible virtual deformation $\delta\boldsymbol{\chi}$ and $\delta\mathbf{H}$ fluid mass flow, satisfying $\delta\boldsymbol{\chi} = \mathbf{o}$ on ∂B^{φ}_0 and $\delta\mathbf{H}\cdot\mathbf{n} = 0$ on ∂B^{h}_0, one obtains the *Euler equations*

Stress equilibrium	$-\nabla_X \cdot [\partial_{\mathbf{F}}\widehat{\psi}]$	$= 0$	in $\mathcal{B}_0$
Inverse Darcy law	$\nabla[\partial_m\widehat{\psi}] + \partial_{\mathbf{H}}\widehat{\phi}$	$= 0$	in $\mathcal{B}_0$
Prescribed tractions	$(\partial_{\mathbf{F}}\widehat{\psi})\cdot\mathbf{n}_0 - \bar{\mathbf{t}}_0$	$= 0$	on ∂B^{t}_0
Prescribed fluid potential	$-\partial_m\widehat{\psi} + \bar{\mu}$	$= 0$	on ∂B^{μ}_0

Hence, the admissible space for the variation of the deformation and the fluid mass flux are given by

$$\begin{aligned}
&\mathcal{V}_{\boldsymbol{\chi}} := \{\boldsymbol{\chi} \in H^1(B_0) | \, \boldsymbol{\chi} = \varphi \quad \text{on } \partial B^{\varphi}_0\},\\
&\mathcal{V}_{\mathbf{H}} := \{\mathbf{H} \in H(\mathrm{Div}, \mathcal{B}_0) | \, \mathbf{H} \cdot \mathbf{n}_0 = H \quad \text{on } \partial B^{h}_0\},\\
&\mathcal{W}_{\delta\boldsymbol{\chi}} := \{\delta\boldsymbol{\chi} \in H^1(B_0) | \, \delta\dot{\boldsymbol{\chi}} = 0 \quad \text{on } \partial B^{\chi}_0\},\\
&\mathcal{W}_{\delta\mathbf{H}} := \{\delta\mathbf{H} \in H(\mathrm{Div}, \mathcal{B}_0) | \delta\mathbf{H} \cdot \mathbf{n}_0 = 0 \quad \text{on } \partial B^{h}_0\}\,.
\end{aligned} \tag{82}$$

Under the assumption of small strains, for a given state $\{\mathbf{u}, \mathbf{h}, m\}$, the following *rate potential* is postulated [82, Eq. (33)]

$$\Pi(\dot{\mathbf{u}}, \mathbf{h}, \dot{m}) = \int_{\mathcal{B}} \pi(\dot{\boldsymbol{\varepsilon}}, \mathbf{h}, \dot{m}) \, dv - \mathcal{P}_{\mathrm{ext}}(\dot{\mathbf{u}}, \mathbf{h})\,, \tag{83}$$

where π is the internal rate potential per unit volume, taking the form

$$\pi(\dot{\boldsymbol{\varepsilon}}, \mathbf{h}, \dot{m}) = \dot{\hat{\psi}}(\boldsymbol{\varepsilon}, m) + \hat{\phi}(\mathbf{h}) \tag{84}$$

with $\dot{\hat{\psi}} = \partial_{\boldsymbol{\varepsilon}}\hat{\psi} : \dot{\boldsymbol{\varepsilon}} - \partial_m\hat{\psi}\,(\nabla \cdot \mathbf{h})$, and $\mathcal{P}_{\mathrm{ext}}$ is the external power. If body forces are neglected, the latter is provided by the surface tractions $\bar{\mathbf{t}}$ and by the fluid mass transport across the surface related to a prescribed fluid potential $\bar{\mu}$ [82, Eq. (30)]. By imposing the continuity mass equation Eq., the rate-type two-field minimization principle is obtained [121, Eq. (31)]

$$\{\mathbf{u}, \mathbf{h}\} = \mathrm{Arg}\left\{\inf_{\mathbf{u}\in\mathcal{V}_{\mathbf{u}}} \inf_{\mathbf{h}\in\mathcal{V}_{\mathbf{h}}} \Pi^{\Delta t}(\mathbf{u}, \mathbf{h})\right\} \tag{85}$$

determining the displacement vector and fluid mass flux vector at the current time.

Brute-force computer simulations, of course, cannot provide full understanding. But, if carefully calibrated, they can extend the experimental evidence and reveal the essential trend. Thus one can get a clue for an analytical model - the ultimate prize.

— Zdeněk Pavel Bažant

2 FINITE ELEMENT FORMULATION FOR POROELASTICITY

2.1 FUNDAMENTALS OF THE FINITE ELEMENT METHOD

The strong form of the governing equations for poroelasticity, presented in Chapter 1, must hold at every material point $\mathbf{X}$ within the domain $\mathcal{B}$. Closed-form analytical solutions to such systems of partial differential equations are attainable only for problems with highly simplified geometries and boundary conditions. In general applications, numerical discretization is thus required.

The finite element method (FEM) is a powerful computational technique for obtaining approximate solutions to boundary and initial value problems governed by partial differential equations. The fundamental premise of the method involves the discretization of a complex physical domain into a finite number of simpler subdomains, known as elements. Within each element, the variation of the unknown field variable(s) is approximated by piecewise interpolation functions, defined in terms of the nodal values of that variable. This discretization process transforms the governing differential equations into a system of linear algebraic equations where the primary unknowns are the nodal values.

The success of the finite element method can be largely attributed to its capability to accommodate complex geometries by assembling simple, arbitrarily shaped elements and producing sparse, banded system matrices.This property stems from the piecewise-continuous definition of the shape functions N_A. The sparsity results from the compact support of these shape functions, which are associated with nodal degrees of freedom a_i: a given N_i is nonzero only within elements connected to node i.

After a brief review of the fundamental mechanism underlying the finite element method, this chapter addresses the core principles of the u–p **mixed formulation**. Particular attention is devoted to the intrinsic stability difficulties characterizing this approach. Furthermore, we introduce two finite element strategies, developed within alternative variational frameworks, with an emphasis on their mathematical founda-

tions and the challenges associated with their numerical implementation. Their development will be examined in detail in Chapter 4- 5 of this work.

2.1.1 *Strong and Weak Forms*

In contrast to numerical methods based on the direct discretization of differential operators (*strong form*), such as finite difference schemes, the finite element method is founded on the integral statement of the governing equations over the problem domain (*weak form*). The essence of the method lies in approximating the solution of a differential equation by weakening the requirement that the governing relations be satisfied pointwise. Then the solution is sought within a restricted space of admissible functions, thereby reducing the problem from an infinite-dimensional setting to a finite-dimensional one. This procedure is known as the *Galerkin- Ritz method*.

Two distinct procedures are available for deriving such integral statements:

1. the **method of weighted residuals**, which provides the foundation for the Galerkin procedure;
2. the formulation of **variational functionals**, for which a stationary condition is sought (see Chapter 1), Branching the Ritz method.

2.2 THE GALERKIN APPROXIMATION FRAMEWORK

Variational methods, introduced in Chapter 1, seek the admissible function that minimizes a given potential energy functional, leading naturally to the Euler-Lagrange equations. In practice, exact solutions are rarely attainable, and an approximation procedure becomes necessary.
The Ritz method achieves this by restricting the search to a finite-dimensional subspace of admissible variations and determining the linear combination that renders the associated functional stationary, thereby providing a systematic pathway to the weak formulation of the governing equations.

We now turn to the Galerkin approximation method; for a more comprehensive treatment, the reader is referred to Hughes [63] and Reddy [104]. The Galerkin framework constitutes a formal methodology for constructing approximate solutions, but rather than directly minimizing a potential energy functional, this time the procedure is founded upon the **orthogonalization of the residual** with respect to a suitably chosen subspace of weighting functions, which yields the **weak form** of the problem.

In order to define the weak counterpart of the strong-form equations summarized in Box. (45), it is first essential to rigorously characterize two distinct classes of functions, which will serve as the foundation for the subsequent integral statement.

TRIAL FUNCTIONS. The first class consists of *candidate (trial) functions*. From the outset, we require that such admissible functions satisfy the Dirichlet boundary condition

$$u(\bar{x}) = q. \tag{86}$$

Moreover, in order for certain expressions to be well-defined, we impose that the derivatives of the trial solutions be square-integrable(Remark 3).
Accordingly, the set of admissible trial solutions, denoted by $\mathcal{V}$, is defined as all functions with square-integrable derivatives that also satisfy the Dirichlet boundary condition at $x = \bar{x}$:

$$\mathcal{V} = \{u \mid u \in H^1,\ u(\bar{x}) = q\}. \tag{87}$$

where H^1, stands for the Sobolev space.

WEIGHTING FUNCTIONS. The second collection of functions is the set of *weighting (test) functions*. This set is analogous to the trial functions, with the distinction that they must satisfy the homogeneous form of the boundary condition. That is,

$$\mathcal{W} = \{w \mid w \in H^1,\ w(\bar{x}) = 0\}. \tag{88}$$

Remark 3. (On the square integrability requirement.) The square integrability requirement reflects the implicit assumption that all integrals must be finite. Accordingly, restrictions must be placed on the families of functions to which $\mathbf{u}$ and $\mathbf{v}$ belong. Thus, we limit ourselves to bounded functions without loss of generality. Recalling the bilinear form in Ch. 1, the precise degree of smoothness required depends on the order of differentiation appearing in the operators $\mathbf{a}$ or $\mathbf{b}$. Specifically, if n-order derivatives occur in any term of $\mathbf{a}$ or $\mathbf{b}$, then the function must possess $n-1$ continuous derivatives, i.e. be of class C_{n-1}. Functions whose first derivatives are square-integrable (together with the functions themselves) are called H^1 functions, belonging to the Sobolev space.

Multiplying the strong form of the problem by $w \in \mathcal{W}$ and integrating over the domain, followed by integration by parts, yields a weak statement involving derivatives of lower order. This procedure naturally incorporates Neumann and Robin boundary conditions into the integral statement of the problem; such conditions are referred to as *natural boundary conditions*. In contrast, Dirichlet conditions, known as *essential boundary conditions*, must be explicitly enforced on the solution space. The weak statement is generally more permissive than the strong form, as it reduces continuity requirements on the trial functions. *It can be shown that if the weak form holds for all admissible weighting functions w, then the strong form must also hold.*
Indeed, if the residual, corresponding to the bilinear operator $\mathcal{A}$ (Eq. 69) differs from zero at any point, one can select a w such that the weighted integral is nonzero, contradicting the weak statement. Thus, the weak form may be regarded as a **weighted integral of the residuals**. We note that, upon particularization, if the weighting function is

identified with the variation, the approximation equations obtained here are identical to those derived in Section 2 for the same problem using the variational formulation. Indeed, we may now anticipate that *the Galerkin and Ritz (variational) procedures must yield identical results in those cases where natural variational principles exist.*

2.2.1 *Galerkin Discretization*

Starting from the weak form of the problem, we proceed with the Galerkin approximation method, wherein the transition from the continuous variational problem to its discrete counterpart is based on the definition of finite-dimensional trial and test subspaces

$$\mathcal{V}^h \subset \mathcal{V}, \qquad \mathcal{W}^h \subset \mathcal{W}, \tag{89}$$

thus moving from infinite-dimensional spaces to finite-dimensional ones. The superscript h refers to the association of $\mathcal{V}^h$ and $\mathcal{W}^h$ with a partition of the domain ${}^h\mathcal{B}$, parameterized by a characteristic length scale h. We regard $\mathcal{V}^h$ and $\mathcal{W}^h$ as subsets of $\mathcal{V}$ and $\mathcal{W}$, respectively. These collections are commonly called *finite-dimensional function spaces*. This procedure, known as *mesh generation* or *space discretization*, involves partitioning the spatial domain $\mathcal{B}$ into a set of simple, non-overlapping subdomains called *finite elements*. The assembly of these elements forms the *mesh*, which provides the fundamental geometric framework upon which the approximate solution is constructed. Let the discretized domain ${}^h\mathcal{B}$ be partitioned into n_{el} elements such that

$${}^h\mathcal{B} = \bigcup_{e=1}^{n_{el}} \mathcal{B}^e, \qquad \mathcal{B}^e \cap \mathcal{B}^f = \emptyset \quad \text{for} \quad e \neq f, \tag{90}$$

where $\mathcal{B}^e$ denotes the closure of the e-th element.

2.2.2 *Shape Functions and Discrete Spaces*

Let us introduce the explicit form of the functions contained in the discrete trial space ${}^h\mathcal{V}$. Let ${}^h\mathcal{V}$ consist of all linear combinations of given functions $N_A :^h \mathcal{B} \to \mathbb{R}$, where $A = 1, 2, \ldots, n$. By this we mean that if ${}^hw \in {}^h\mathcal{V}$, then there exist constants c_A, $A = 1, 2, \ldots, n$, such that

$${}^h\boldsymbol{w} = \sum_{A=1}^{n} c_A N_A = c_1 N_1 + c_2 N_2 + \cdots + c_n N_n. \tag{91}$$

The functions N_A are called *shape functions*, or equivalently *basis functions* or *interpolation functions*.

Trial functions must also enforce the essential boundary condition; this is achieved by introducing an additional shape function N_{n+1} such that $N_{n+1}(\bar{x}) = 1$, yielding

$$^{h}\mathbf{u} = \sum_{A=1}^{n} d_A N_A + q N_{n+1}. \tag{92}$$

being d_A the nodal displacements. According to the Galerkin method, the trial and test functions are taken from the same functional space. Recalling the bilinear form expressed by (69), and performing the appropriate substitutions, leads to the following discrete system:

$$\sum_{B=1}^{n} a(N_A, N_B) d_B = (N_A, f) + N_A(0)k - a(N_A, N_{n+1})q. \tag{93}$$

This expression represents the algebraic counterpart of the continuous variational problem, where the unknown coefficients d_B correspond to the nodal values of the approximate solution. For convenience and compactness, this system is typically rewritten in matrix form as:

$$\sum_{B=1}^{n} K_{AB} d_B = F_A, \qquad A = 1, \dots, n, \tag{94}$$

where the entries of the stiffness matrix K_{AB} and load vector F_A are explicitly defined as

$$K_{AB} = a(N_A, N_B), \qquad F_A = (N_A, f) + N_A(0)k - a(N_A, N_{n+1})q. \tag{95}$$

Introducing the following matrix notation,

$$\mathbf{K} = [K_{AB}], \quad \mathbf{F} = \{F_A\}, \quad \mathbf{d} = \{d_B\}, \tag{96}$$

the system is the written in its matrix form as

$$\mathbf{K}\mathbf{d} = \mathbf{F}. \tag{97}$$

allowing for the resolution of this algebric system. The discrete system has been introduced in its linear form, where the stiffness matrix $\mathbf{K}$ and the load vector $\mathbf{F}$ depend only on the discretization and prescribed data.
If the assumptions of linear elasticity are no longer valid, the governing system of equations becomes nonlinear. Nonlinearities may be classified into three categories:

1. **material nonlinearities**, where stress increments do not correspond to proportional strain increments;

2. **geometric nonlinearities**, where the hypothesis of infinitesimal displacements is no longer applicable;

3. **constraint nonlinearities**, where boundary or support conditions evolve during loading.

Moreover, nonlinear effects may also emerge from the **coupling** between different physical fields, as in thermo-, electro-, chemo-, or poroelasticity. In such cases, the nonlinear character of the problem does not necessarily originate from the constitutive behavior of the individual phases, but rather from the interdependence between multiple field variables, such as deformation and pore pressure in poroelastic media, which leads to intrinsically coupled and potentially non-proportional responses even under small perturbations.

In this context, the algebraic problem no longer takes the linear form 97, but instead reads

$$R(d) = F_{ext} - F_{int}(d) = 0, \tag{98}$$

where $R(d)$ is the **residual vector**, defined as the difference between the external forces F_{ext} and the internal forces $F_{int}(d)$, the latter depending on the current displacement vector d. The problem is *linearized* at the current configuration by expanding the residual through its **directional derivative**. This operation typically yields the tangent operator, i.e. the Jacobian of the system, which governs the incremental response. The resulting equations are solved within a displacement-controlled incremental scheme, using the classical Newton–Raphson iterative method [22] coupled with a residual-norm convergence criterion.

2.3 FORMULATIONS IN THE LITERATURE FOR POROELASTICITY

2.3.1 *Coupled Finite Element Formulations*

The numerical analysis of fluid diffusion in deformable porous media entails the interaction of multiple physical phenomena. When two or more systems are interdependent in such a way that the independent resolution of any one system is impossible without the simultaneous resolution of the others, the resulting formulation is referred to as a *coupled problem*. The general definition proposed by [13, 15, 22, 63, 134] encompasses both multiphysics problems and their numerical discretizations, characterizing coupled systems as those involving multiple domains and dependent variables where no domain can be solved independently of the others, and no set of dependent variables can be explicitly eliminated at the level of the governing differential equations. The strength of the coupling may vary, ranging from weak to strong, depending on the degree of interaction. Nevertheless, the defining feature of a coupled system lies in the impossibility of a clear separation of the involved physics.

From a structural standpoint, coupled problems may be broadly categorized as follows:

- **Class I**: Systems in which coupling is restricted to domain interfaces and enforced via boundary conditions (e.g., fluid–structure interaction).

- **Class II**: Systems in which coupling is diffuse throughout the computational domain, typically arising from shared source terms or constitutive interdependencies (e.g., multiphase diffusion, poroelasticity).

Poroelasticity, which describes the mechanical response of a fluid-saturated porous medium, provides a canonical example of a **Class II** coupled problem. Here, the deformation of the solid skeleton alters the pore pressure field, while, conversely, the pore pressure exerts an effective load on the solid phase.
The formal definition of a coupled system exhibits important analogies with *mixed formulations* in the finite element method, wherein multiple primary variables are treated as independent unknowns and solved for simultaneously within the system. However, referring to Zienkiewicz, Taylor, and Zhu [134], a crucial distinction must be drawn between the two.
Mixed formulations are typically employed within the context of a single physical phenomenon (e.g., quasi-incompressible elasticity), where the introduction of auxiliary variables serves a primarily numerical purpose, most often to avert stability issues. In such cases, the elimination of certain variables remains feasible (at least in principle), at the level of the governing differential equations. Coupled formulations, by contrast, arise from inherent multiphysics interactions, where the complete elimination of the variables associated with one subsystem is strictly impossible without solving the full set of governing equations.
In a large body of literature, coupled problems are frequently discretized using mixed finite element strategies, thereby contributing to the overlapping of the two terminologies. In accordance with prevailing convention, and without further risk of ambiguity, we shall henceforth refer to the standard finite element discretization of poroelasticity as a *mixed* formulation.

2.3.2 *The u-p formulation*

We now provide a brief description of the mixed u–p formulation (solid displacement – pore pressure), which emerges as the standard discretization strategy for the poroelastic problem described in Chapter 1, from which a wide range of extensions can be found in the literature. Recalling the weak forms of the problem, and associating variations with the respective trial and test functions, the solution of the problem de-

scribed in 1.3.1 consists of the pair $\{\boldsymbol{\chi}, \mu\} \in \mathcal{V}_\chi \times \mathcal{V}_\mu$ that solves, for any admissible pair $\{\delta\boldsymbol{\chi}, \delta\mu\} \in \mathcal{W}_\chi \times \mathcal{W}_\mu$, the following weak form of the problem:

$$\begin{aligned}
&\int_{{}^h\mathcal{B}_0} \left[\partial_{\mathbf{F}}\overline{\psi}_{\text{eff}} - \mu\rho_f J\mathbf{F}^{-T} \right] : \nabla\delta\dot{\boldsymbol{\chi}} dV - \int_{\partial\mathcal{B}^t} \delta\dot{\boldsymbol{\chi}} \cdot \bar{T} dA = 0 \\
&\int_{{}^h\mathcal{B}_0} \delta\mu\rho_f J\mathbf{F}^{-T} : \nabla\dot{\boldsymbol{\chi}} dV - \int_{{}^h\mathcal{B}_0} \nabla\delta\mu \cdot \mathbf{H} dV - \int_{\partial\mathcal{B}^h} \delta\mu\bar{H} dA = 0,
\end{aligned} \tag{99}$$

defining the following spaces for the trial functions $\boldsymbol{\chi}$ and μ and the test functions $\delta\boldsymbol{\chi}$ and $\delta\mu$

$$\begin{aligned}
\mathcal{V}_\chi &= \{\boldsymbol{\chi} \in H^1, |\ \chi = \bar{\chi} \text{ on } \partial^h\mathcal{B}_0^\chi\} \\
\mathcal{V}_\mu &= \{\mu \in L^2, |\ \mu = \bar{\mu} \text{ on } \partial^h\mathcal{B}_0^\mu\} \\
\mathcal{W}_\chi &= \{\delta\boldsymbol{\chi} \in H^1, |\ \delta\chi = 0 \text{ on } \partial^h\mathcal{B}_0^\chi\} \\
\mathcal{W}_\mu &= \{\delta\mu \in L^2, |\ \delta\mu = 0 \text{ on } \partial^h\mathcal{B}_0^\mu\}.
\end{aligned} \tag{100}$$

Starting from this weak form, it is now possible to discretize the problem in time and in space. Under the assumption of quasi-static regime, we can apply the Backward Euler scheme for the time discretization. We denote with $n+1$ and n the quantities at the current and the previous time steps, respectively, with $\Delta t = t_{n+1} - t_n$ the size of the current time step. We obtain the following discrete-time counterpart of:

$$\begin{aligned}
&\int_{{}^h\mathcal{B}_0} \partial_{\mathbf{F}}\left[\partial_{\mathbf{F}}\overline{\psi}_{\text{eff}} - \mu\rho_f J\mathbf{F}^{-T} \right] : \nabla\frac{\boldsymbol{\chi} - \boldsymbol{\chi}_n}{\Delta t} dV - \int_{\partial\mathcal{B}^t} \delta\boldsymbol{\chi} \cdot \bar{T} dA = 0, \\
&\int_{{}^h\mathcal{B}_0} \delta\mu\rho_f J\mathbf{F}^{-T} : \nabla\frac{\boldsymbol{\chi} - \boldsymbol{\chi}_n}{\Delta t} dV - \int_{{}^h\mathcal{B}_0} \nabla\delta\mu \cdot \mathbf{H} dV - \int_{\partial\mathcal{B}^h} \delta\mu\bar{H} dA = 0,
\end{aligned} \tag{101}$$

in which, for clarity of presentation, the subscript $n+1$ is henceforth omitted. It is important to observe that the weak form of the equilibrium equation is inherently rate-independent, since the chosen Helmholtz free energy density does not exhibit any explicit rate dependence.

We now introduce a discretisation in space, for which we refer to [15, 134]. The same shape functions are used to approximate the corresponding trial and weighting functions, recovering the standard Galerkin Method. The approximated trial and weighting functions ${}^h\boldsymbol{\chi}, {}^h\delta\boldsymbol{\chi}, {}^h\mu, {}^h\delta\mu$, can be written as:

$$\begin{aligned}
{}^h\chi &= N_\chi\hat{\chi}, \quad {}^h\delta\chi = N_\chi\hat{\chi} \\
{}^h\mu &= N_\mu\hat{\mu}, \quad {}^h\delta\mu = N_\mu\delta\hat{\mu}
\end{aligned} \tag{102}$$

where $\hat{\cdot}$ are the vectors containing the values of those functions at the mesh nodes, $N_i = \{N_i^1, N_i^2, \ldots, N_i^{n_e}\}$ with $i = \chi, p$ are the vectors containing the shape functions at the n_e nodes of the mesh.

Because the variational statement in Eq. (101) must be satisfied for any arbitrary variation of the nodal material velocity, the discretised equilibrium equation is expressed in terms of the nodal residual, through the *assembly* operation [22], as

$$\mathbf{R} = \mathbf{I} - \mathbf{P} = \mathbf{0}, \tag{103}$$

$$\mathbf{I} = \sum_{e=1, e\in a}^{n_{ae}} \left(\int_{{}^{h}\mathcal{B}_0^{(e)}} \sigma \nabla N_\chi^e \, dV \right),$$

$$\mathbf{P} = \sum_{e=1, e\in a}^{n_{ae}} \left(\int_{\partial {}^{h}\mathcal{B}_0^{(e)}} N_\chi^e \bar{\mathbf{T}} \, dA \right). \tag{104}$$

where the superscript e specifies that the equation is written for a single finite element. Similarly, since the fluid mass balance must be satisfied for an arbitrary variation of the nodal fluid potential, it can be expressed in terms of the pressure residual as

$$\mathbf{R}^p = \mathbf{I}^p - \mathbf{P}^p = \mathbf{0},$$

$$\mathbf{I}^p = \sum_{e=1, e\ni a}^{n_{ae}} \left(\int_{{}^{h}\mathcal{B}_0^{(e)}} N_\mu^e \left[J - J_n \right] \, dV - \Delta t \int_{{}^{h}\mathcal{B}_0^{(e)}} \nabla N_\mu^e \cdot \mathbf{H} \, dV \right),$$

$$\mathbf{P}^p = - \sum_{e=1, e\ni a}^{n_{ae}} \left(\Delta t \int_{\partial {}^{h}\mathcal{B}_0^{(e)}} N_\mu^e \bar{H} \, dA \right),$$

making use of the relation $\dot{J} = \mathbf{F}^{-T} : \nabla \dot{\boldsymbol{\chi}}$ [61], which once integrated in time provides the equality $J - J_n = \mathbf{F}^{-T} : \nabla \boldsymbol{\chi} - \nabla \boldsymbol{\chi}_n$. Nevertheless, the finite element implementation based on the u–p formulation must satisfy the inf–sup (or Ladyzhenskaya–Babuška–Brezzi, LBB) condition. Failure to satisfy this stability criterion leads to non-physical spurious oscillations in the pressure field, as discussed in Section 2.3.3.

2.3.3 *The Inf-Sup Condition*

In Section 1.3, we introduced the variational principle which forms the foundation of the standard u–p formulation. From a variational standpoint, this formulation leads to a saddle-point problem, whose well-posedness critically relies on the satisfaction of the inf–sup condition [28, 29].

The LBB condition provides the fundamental theoretical framework for analyzing the well-posedness of saddle point problems in poroelasticity, ensuring solution existence and uniqueness, and governing the convergence behavior of discrete approximations [21]. Failure to satisfy the inf-sup condition in poroelastic formulations typically leads to spurious pressure oscillations, numerical instabilities, or loss of solution

uniqueness [31]. Consequently, the stability of the discrete problem critically depends on selecting compatible approximation spaces for displacement and pressure that satisfy the discrete inf-sup condition. Numerical symptoms of violation include rank deficiency or near-singularity of the global stiffness matrix, emergence of checkerboard patterns in the pressure field, and lack of convergence under mesh refinement despite using apparently adequate approximation spaces. Formally, for linear poroelasticity, the inf-sup condition reads:

$$\inf_{q \in {}^{h}\mathcal{V}_q} \sup_{\mathbf{v} \in {}^{h}\mathcal{V}_v} \frac{b(\mathbf{v}, q)}{\|\mathbf{v}\|_{\mathcal{V}_v} \, \|q\|_{\mathcal{V}_q}} \quad \geqslant \quad \beta > 0, \tag{105}$$

where $b(\mathbf{v}, q) = \int_{\mathcal{B}} q \, \nabla \cdot \mathbf{v} \, dV$ represents the bilinear form coupling the displacement and pressure fields, $({}^{h}\mathcal{V}_v, {}^{h}\mathcal{V}_q)$ denote the discrete spaces for displacement and pressure respectively, and β is a positive constant independent of the mesh size h [83].

In the nonlinear regime, stability requires that the linearized tangent bilinear form satisfies the inf-sup condition at each Newton-Rhapson iteration. Therefore, the selection of compatible finite element pairs (e.g., Taylor-Hood elements) or the implementation of stabilized multiphase formulations remains essential for ensuring discrete inf-sup stability in finite-strain poroelastic problems [6, 21].

2.3.3.1 *Remedies and Limitations, Other Approaches*

The numerical treatment of coupled problems is governed by strict stability requirements which critically depend on the choice of interpolation spaces and necessitate a careful selection of discretization strategies. This issue becomes particularly evident in poroelasticity, where the interaction between the deformation of the porous skeleton and the flow of the interstitial fluid poses a significant computational challenge. In response, there is considerable interest in developing finite element formulations featuring advanced stabilization techniques, especially for nonlinear and finite-deformation analysis. A cornerstone in this domain is represented by Taylor–Hood elements [119], traditionally employed in mixed $u - p$ formulations. Here, the displacement field is approximated using higher-order (typically quadratic) functions, while the pore-pressure field employs lower-order (generally linear) interpolations. This hierarchical choice fulfills the Ladyzhenskaya–Babuška–Brezzi (inf-sup) condition (Section 2.3.3) and prevents the related spurious pressure oscillations. Extensions of these mixed formulations to finite strains and complex materials have been extensively pursued the framework of TPM, with contributions by De Boer [41], Ehlers [44], and Ehlers and Eipper [45] and later Comellas et al. [37], who introduced nonlinear poro-viscoelastic models. In parallel, the contributions of Li, Borja, and Regueiro [71] and Schrefler [111] addressed dynamic and partially saturated problems under finite strains, highlighting the need for higher order of interpolation order in avoiding volumetric locking un-

der near-incompressibility. To reduce computational cost, stabilization techniques for low-order elements provide alternatives to Taylor–Hood elements. Methods such as pressure-jump stabilization or selective reduced integration effectively suppress oscillations and volumetric locking while retaining efficiency. However, in critical scenarios characterized by pronounced nonlinearities such as abrupt permeability changes, steep gradients, or dynamic regimes e.g., supershear earthquake rupture, stabilization techniques, while effective under moderate circumstances, may prove insufficient. In such cases, residual oscillations or partial locking phenomena may arise, often necessitating the adoption of complementary strategies such as mesh adaptivity or advanced time-stepping algorithms to preserve solution stability. In the most severe instances, numerical oscillations may persist despite these efforts [24, 49, 58, 121]. These challenges will be explored in detail in Chapters 3- 5.

2.3.4 *Alternative Variational Formulations*

2.3.4.1 *Miehe's Variational Framework*

A novel variational approach, already introduced in section 2, has been introduced by Miehe, Mauthe, and Teichtmeister [82] and subsequently refined in Teichtmeister, Mauthe, and Miehe [121], relies on the selection of fluid fluxes and solid deformation as primary variables of the poroelastic problem, leading to a minimization principle that inherently circumvents the classical inf-sup condition, thereby ensuring a more robust numerical framework. The numerical stability of the resulting finite element discretization critically depends on the choice of functional spaces, particularly for the representation of the flux field. The use of Raviart-Thomas (RT0) elements [103] provides a conforming discretization of the fluid flux in the functional space $H(\mathrm{div}, \mathcal{B})$, ensuring inter-element continuity of the normal fluxes. However, this choice comes at the expense of a significantly increased number of degrees of freedom and a higher computational cost. Conversely, a Q1-Q1 discretization, which project the flux on the nodes of the element, while computationally more efficient, is subjected to discontinuities in the normal components of the flux across adjacent elements, leading to non-physical oscillations in pressure and velocity fields, and volumetric locking in nearly-incompressible fluids, which can only be mitigated through reduced integration schemes [121].

2.3.4.2 *Formulations Proposed in this Thesis*

Motivated by the success of hybrid equilibrium formulations [94, 101], Lo Franco et al. have recently developed a Hybrid Equilibrium finite Element (HEE) for linear poroelasticity [72], capable of providing highly accurate solutions in the primary fields of stress and pressure.

STRESS–PRESSURE FORMULATION A novel variationally consistent Hybrid Equilibrium Element formulation, based on a two-field minimization principle, is formulated, with total Cauchy stress and interstitial fluid potential serving as primary variables. The proposed variational principle provides a variationally consistent framework for designing of inherently self-equilibrated Hybrid Equilibrium Elements, where the solid displacement field emerges as Lagrangian variable to enforce stress codiffusivity at element sides. The fulfillment of the inf-sup condition, typically challenging in developing stable and computationally efficient finite element formulations, is locally archived, since the formulation derives from a minimization principle, rather than the classical saddle point principle. The proposed Hybrid Equilibrium Element approach offers a statically admissible solution even in the proximity of singularities or high space gradient stress distribution, providing a more comprehensive assessment of stress distributions and concentrations. The formulation, consisting of 2-D triangular Hybrid Equilibrium Elements, is employed to solve plane strain problems. Among the advantages of the proposed approach, in which accurate stress distributions are obtained, even adopting quite coarse meshes. Remarkably, in the proposed approach no stabilization technique is required.

This formulation is treated in detail in Chapter 3, and it has been published in article [72]:
Lo Franco, S., Parrinello, F. and Borino, G. "A Variationally-constistent Hybrid Equilibrium Element formulation for linear poroelasticity", Computer Methods in Applied Mechanics and Engineering (CMAME), 2024.*
In this chapter, we will draw extensively from the corresponding publication.

DISPLACEMENT–FLUX FORMULATION The approach proposes a novel hybrid flux-preserving finite element formulation, designed to preserve mass flux consistency within each element, by adopting an alternative set of primary variables. An original hybrid variational principle is established, wherein the solid deformation and the mass flux fields are adopted as primary unknowns, while the fluid potential acts as a Lagrange multiplier to enforce weak continuity of mass flow across inter-element boundaries, thus avoiding the necessity of globally conforming function spaces. In particular, the accurate resolution of the fluid pressure field highlights the advantages of the proposed formulation over classical displacement-pressure elements and shows the potential of the proposed method.

This formulation is treated in detail in Chapter 4, and it has been published in article [73]:
Lo Franco, S., Terzano,M., Borino, G., Holzapfel,G.A. and Parrinello, F. "A hybrid flux-preserving finite element for coupled flow deformation: Linear formulation", Computer Methods in Applied Mechanics and Engineering (CMAME), 2025.*
In this chapter, we will draw extensively from the corresponding publication.

Nihil omnino in mundo contingit, in quo non maximi minimive ratio quaepiam eluceat.

— Leonhard Euler

3

A VARIATIONALLY-CONSISTENT HYBRID EQUILIBRIUM ELEMENT FORMULATION FOR LINEAR POROELASTICITY

[1]

The formulation, consisting of 2-D triangular Hybrid Equilibrium Elements, is employed to solve plane strain problems. The element has been implemented in the Open source Finite Element Analysis Program (FEAP) and its performance evaluated against classical benchmark problems for poroelasticity, with emphasis on stress accuracy. The numerical results obtained for the quasi-static analysis of poroelastic systems show the advantages of the proposed approach, in which accurate stress distributions are obtained, even adopting quite coarse meshes. Remarkably, in the proposed approach no stabilization technique is required.

3.1 INTRODUCTION

Despite extensive research conducted on the poromechanical framework and its associated finite element formulations [44, 45, 70, 71], the problem still remains of great scientific interest. Standard Finite Element formulations for poroelasticity typically incorporate solid displacements and fluid pressures as field variables ($u - p$ formulation) [15, 134]. From a variational point of view, this approach leads to a saddle point problem, therefore specific stabilisation procedures are rather needed to achieve accurate solutions [102]. A crucial requirement for well-posedness in such problems is the satisfaction of the inf-sup condition [28]. However, a significant challenge arises as most coupled elements only satisfy the inf-sup condition in a global - rather than local- sense. This deficiency can lead to spurious oscillations and numerical instabilities within the solution [58].
Chapelle and Bathe [31] proposed a numerical “Inf-Sup test" to assess whether a certain combination of functions of the element satisfy the aforementioned condition.

1 Substantial parts of the material presented in this chapter have been extracted and adapted from the paper: Lo Franco, S., Parrinello*, F. and Borino, G. *"A Variationally-constistent Hybrid Equilibrium Element formulation for linear poroelasticity"*, CMAME, 2024. [72]

Among the elements that satisfy the requirement even in local sense, the Taylor-Hood element results to be the most widely used [119]. Other popular choices in poroelasticity include enhanced and stabilised elements. However, enhanced elements are susceptible to hourglass instabilities, while stabilised elements struggle with applicability to complex geometries [114]. Nevertheless, even for elements that satisfy the inf-sup condition locally, numerical fluctuations or oscillations may still arise, especially during the early stages of the consolidation process and for low permeability values [59]. These phenomena constitute a significant challenge in poroelasticity discretization.
By adopting a different set of primary variables, as previously explored by Miehe [82], a minimization principle can be obtained. This approach offers a significant advantage by circumventing the need to satisfy the inf-sup condition, resulting in an inherently more stable element [121]. To the best of our knowledge, no prior study in the literature has already explored a poroelastic Finite Element formulation incorporating both total stress and pore pressure as primary variables.
The present chapter therefore seeks to introduce a novel Hybrid Equilibrium Element for the transient analysis examination of the steady-state behaviour of poroelastic systems. Introducing stress and pressure as primary variables leads to a minimum problem formulation, where the inf-sup condition is satisfied a priori [38]. Moreover, this choice of variables allows for more accurate evaluation of phenomena, e.g. stress concentration, which often occur in nonlinear couplings, even for small deformations. Hybrid Equilibrium Elements (HEEs) are, in fact, able to satisfy a priori the equilibrium equations at any point within the domain [101]. This is achieved by approximating the stress field using functions defined within the class of statically admissible solutions, complementing the conventional displacement-based finite element approach. The term "Hybrid", as introduced by Pian [98] and de Almeida et al. [4], is associated with the employment of a complementary displacement field independently interpolated on the boundary of the element as a Lagrangian variable to enforce co-diffusivity at the boundaries of the element [83, 92].
Consequently, even in the vicinity of singularities, HEEs continue to provide a statically admissible solution, offering a more comprehensive assessment of stress distribution and concentrations, particularly when these phenomena arise due to singularities. In contrast, equilibrium is not imposed locally in the $u-p$ formulation and therefore can be perturbed in the proximity of a mathematical singularity [132]. Despite the well-known drawback of spurious modes associated with the HEE formulation, these can be circumvented using the methodology outlined in [79] and [92], whose work represents a significant contribution, especially in the application of such elements in the study of fracture mechanics and damage [93, 94].

Solving the boundary-value problem for a saturated solid undergoing deformation requires the introduction of a suitable set of variables to establish a coherent theoretical framework. As discussed in Chapter 1, multiple choices are available for the selection of primary variables, each giving rise to distinct formulations and corresponding boundary conditions. In the dual formulation proposed in this chapter, under the assumptions of small strains and inviscid fluid, we recall the variational principle (Eq. (72)) originally introduced by Coussy [38].

3.2.1 *Primary fields*

Within the poroelastic framework, the behavior of both constituent phases is modeled as a homogenized continuum body B and its boundary ∂B, wherein interstitial fluid mass is transported through convective mechanisms. To describe the undeformed configuration of the body, a reference configuration denoted by $\mathcal{B}_0$ is introduced, with each material particle identified by a point $\mathbf{X} \in \mathcal{B}_0$ [61]. This approach is formalized by invoking the concept of the Representative Volume Element (RVE), as introduced by Cheng [32] and Coussy [39], whereby the solid matrix and pore fluid constituents are treated indistinguishably at each material point. In classical poroelasticity, the homogenization process is based on defining an *effective porosity* field $\varphi_0(\mathbf{X}, t) \in (0, 1]$, which assigns to each volume element dv the volume of interconnected pores $dv_f = \varphi\, dv$ [32].

The kinematics of poroelastic media is formulated with respect to the solid, meaning that motion and associated fields are defined relative to the solid skeleton's configuration [40]. The motion of the solid over a time interval $\mathcal{T} = (0, t) \subset \mathbb{R}_+$ is described by the vector-valued *deformation* map $\boldsymbol{\chi} : \mathcal{B}_0 \times \mathcal{T} \to \mathbb{R}^3$, which maps each material point $\mathbf{X} \in \mathcal{B}_0$ at time $t \in \mathcal{T}$ to its spatial position $\mathbf{x} \in \mathcal{B}_t$, where $\mathcal{B}_t = \boldsymbol{\chi}_t(B)$ represents the deformed configuration at time t. The deformation gradient $\mathbf{F} = \nabla_{\mathbf{X}}\boldsymbol{\chi}(\mathbf{X}, t)$ maps material tangent vectors to spatial tangent vectors, with its determinant $J = \det \mathbf{F} > 0$ quantifing the change in volume from the reference element dv to the current element dv. Finally, let us recall the *displacement* field $\mathbf{u} : \mathcal{B}_0 \times \mathcal{T} \to \mathbb{R}^3$, together with its material gradient $\nabla_{\mathbf{X}}\mathbf{u} = \mathbf{F} - \mathbf{I}$, where $\mathbf{I}$ is the identity tensor [61].

For the fluid phase, in accordance with classical poroelastic formulations, we adopt the concept of *variation in fluid mass content* $m : \mathcal{B}_0 \times \mathcal{T} \to \mathbb{R}$, originally introduced by Biot [18]. This scalar field represents the increase in fluid mass per unit reference volume of the porous solid [82, Eq. $(6)_1$].
In this chapter, we assume a linearization around the reference configuration $\mathcal{B}_0$ and characterize the deformation by introducing the *infinitesimal strain tensor* $\boldsymbol{\varepsilon} = \nabla^s_{\mathbf{X}}\mathbf{u}$, representing the symmetric part of the displacement gradient [61]. Consistently with the linearized theory, the configuration of the continuum body and its coordinate are

denoted simply by $\mathcal{B}$ and χ, the effective porosity with φ , and the differential operator $\nabla(\bullet)$ omits the subscript. Finally, the porosity distribution in the saturated porous medium is assumed to be sufficiently smooth, such that $\nabla\rho_f = 0$ and $\nabla\rho_s = 0$. Additionally, the system is free of mass sources and sinks. The solid phase is regarded as incompressible, with $\dot{\rho}_s = 0$ and Biot's coefficient $\alpha = 1$.

3.2.2 *(Strong form of the) Governing equations*

The fundamental governing equations of a linear poroelastic solid include the conservation of mass, momentum, and energy, alongside constitutive laws describing the behavior of the solid matrix and the interstitial fluid [32, Ch. 6]. For the sake of simplicity, the system is assumed to be isothermal and mass-conservative, implying the absence of internal sources or sinks. Furthermore, since no chemical reactions occur between the solid and fluid phases, mass balance can be applied independently to each constituent. Under these assumptions, the mass balance reduces to the continuity equation governing the fluid phase. Considering an arbitrary region of the continuum body $\mathcal{P} \subset \mathcal{B}$ and denoting with $\mathbf{n}$ the outward unit normal to its boundary $\partial\mathcal{P}$, we introduce the fluid mass flux $\mathbf{h} : \mathcal{B} \times \mathcal{T} \to \mathbb{R}^3$, defined such that $\mathbf{h} \cdot \mathbf{n}$ represents the mass of fluid crossing the boundary $\partial\mathcal{P}$ per unit area and per unit time. The continuity equation of the fluid in $\mathcal{P}$ takes then the following local form (see Remark 4)

$$\dot{m} + \nabla \cdot \mathbf{h} = 0\,, \tag{106}$$

where $\dot{m}$ stands for the time derivative of variation in fluid mass content. Under the assumption of small deformations, is related to volumetric strain rate of the system through its volumetric counterpart $\dot{\zeta}$, as $\dot{m} = \rho_f \dot{\zeta} := \rho_f(\dot{\varepsilon} - \varphi\,\dot{\varepsilon}_f)$, where ρ_f is the true mass density of the fluid, $\dot{\varepsilon}$ denotes the volumetric strain rate of the solid skeleton, $\dot{\varepsilon}_f$ the volumetric strain rate of the fluid phase. The former is defined as $\dot{\boldsymbol{\varepsilon}} := \nabla^s \dot{\mathbf{u}}$, with $\dot{\mathbf{u}}$ the solid displacement rate.
Neglecting any inertial effects, the balance of linear momentum for the mixture as a whole can be stated as :

$$\nabla \cdot \boldsymbol{\sigma} + \rho\mathbf{b} = \mathbf{0}\,, \quad \boldsymbol{\sigma} = \boldsymbol{\sigma}^T \quad \text{on } \mathcal{B} \times \mathcal{T}\,, \tag{107}$$

In the framework of Biot's classical theory of poroelasticity [17], the total Cauchy stress tensor $\boldsymbol{\sigma} : \mathcal{B}_0 \times \mathcal{T} \to \mathbb{R}^3$ admits an additive decomposition into two distinct contributions: the Biot stress tensor $\boldsymbol{\sigma}'$, which coincides with the Terzaghi effective stress in the limiting case $\alpha = 1$, and a pressure term accounting for the interstitial fluid pressure $p = \rho_f \mu$, with μ standing for the fluid potential scalar field Chapter 1. This relation is expressed as:

$$\boldsymbol{\sigma} = \boldsymbol{\sigma}' - p\mathbf{I} = \boldsymbol{\sigma}' - \rho_f \mu \mathbf{I}\,, \tag{108}$$

where $\mathbf{I}$ denotes the second-order identity tensor.

Remark 4. The general mass balances in a saturated biphasic mixture, being m_f and m_s, respectively, the mass of fluid and solid phases, can be expressed as in [32]:

$$m_f = \int_{\mathcal{B}} \varphi \rho_f \, dv, \quad m_s = \int_{\mathcal{B}} (1-\varphi) \rho_s \, dv, \tag{109}$$

where ρ_f, ρ_s are the true mass densities of the constituents [39]. The conservation of mass of the fluid phase, written with respect to the motion of the solid skeleton, provides [40, Eq. (57)]

$$\begin{aligned} &\frac{dm_f}{dt} = \frac{d}{dt} \int_{\mathcal{B}} \varphi \rho_f \, dv = 0 \\ &\frac{d(\varphi \rho_f)}{dt} + \varphi \rho_f \nabla \cdot \dot{\mathbf{u}} + \nabla \cdot (\varphi \rho_f \boldsymbol{w}) = 0, \end{aligned} \tag{110}$$

where $\dot{\mathbf{u}} \equiv \dot{\mathbf{u}}_s$ is the velocity of the solid and $\boldsymbol{w} = \dot{\mathbf{u}}_f - \dot{\mathbf{u}}$ is the *discharge velocity*, representing the relative velocity of the fluid with respect to the solid skeleton. At this point, Assuming a constant fluid density, the mass balance simplifies to the continuity equation, which is standard in linear poroelasticity and is expressed in the form given by (106).

The local governing equations (**??**) and (107) must be complemented by suitable boundary and initial conditions. To this end, the boundary $\partial\mathcal{B}$ of the poroelastic domain (see Fig. 2) is partitioned into mutually disjoint subsets corresponding to essential and natural boundary conditions for both mechanical and hydraulic fields:

$$\partial\mathcal{B} = \partial\mathcal{B}^u \cup \partial\mathcal{B}^t = \partial\mathcal{B}^h \cup \partial\mathcal{B}^\mu, \tag{111}$$

with $\partial\mathcal{B}^u \cap \partial\mathcal{B}^t = \emptyset$ and $\partial\mathcal{B}^h \cap \partial\mathcal{B}^\mu = \emptyset$. In accordance with the choice of primary variables introduced in Sec. 4.2.1, the essential (Dirichlet-type) boundary conditions involve the traction vector $\mathbf{t}$ and the fluid potential μ, specified on $\partial\mathcal{B}^t$ and $\partial\mathcal{B}^\mu$:

$$\boldsymbol{\sigma} \cdot \mathbf{n} = \bar{\mathbf{t}} \quad \text{on } \partial\mathcal{B}^t \times \mathcal{T}, \qquad \mu = \bar{\mu} \quad \text{on } \partial\mathcal{B}^\mu \times \mathcal{T}, \tag{112}$$

with $\bar{\mathbf{t}}$ and $\bar{p}$ representing the prescribed traction and the pressure of the fluid phase, respectively. The corresponding natural (Neumann-type) boundary conditions prescribe the displacement field $\mathbf{u}$ on $\partial\mathcal{B}^u$ and the normal component of the fluid mass flux $\mathbf{h} \cdot \mathbf{n}$ on $\partial\mathcal{B}^h$:

$$\mathbf{u} = \bar{\mathbf{u}} \quad \text{on } \partial\mathcal{B}^u \times \mathcal{T}, \qquad \mathbf{h} \cdot \mathbf{n} = \bar{h} \quad \text{on } \partial\mathcal{B}^h \times \mathcal{T}, \tag{113}$$

where $\bar{\mathbf{u}}$ and $\bar{\mathfrak{h}}$ denote the prescribed displacement and fluid flux, respectively. Finally, the initial conditions assume the body to be undeformed and at rest, with no excess pore fluid at the initial time:

$$\boldsymbol{\sigma} \cdot \mathbf{n}(\mathbf{x}, 0) = \mathbf{0}\,, \qquad \mu(\mathbf{x}, 0) = 0 \quad \text{in } \mathcal{B}\,, \tag{114}$$

implying that the medium initially occupies its reference configuration and is in a fluid-saturated equilibrium state.

3.2.3 *Thermodynamic consistency*

It remains essential to ensure consistency with Thermodynamic laws when formulating the state equations of the problem. Indeed, the derivation of constitutive relations for an open thermodynamic system based solely on phenomenological considerations may lead to ambiguity and lack of rigor [38, 123].

In a dissipative system, a finite set of generalised fluxes and their conjugate forces establishes the dissipation rate, characterised by their nonnegative definite inner product [54]. For the system herein considered, these pairs of thermodynamic quantities are represented by the fluxes $\dot{\boldsymbol{\varepsilon}}$ and $\dot{m}$ and the conjugated forces $\boldsymbol{\sigma}$ and μ. Ensuring adherence to the local dissipation inequality [56], the dissipation rate can be formally expressed as follows:

$$\mathcal{D} = -\dot{\psi} + \boldsymbol{\sigma} : \dot{\boldsymbol{\varepsilon}} - \mu\, \dot{m} - \nabla\mu \cdot \mathbf{h} \geqslant 0, \tag{115}$$

where ψ denotes the Helmholtz free energy density per unit volume of the system.
As previously emphasised in [82], the dissipation rate can be subdivided in an intrinsic, or local, contribution, and a transport-related contribution. The intrinsic dissipation rate

$$\mathcal{D}_{\mathrm{int}} = -\dot{\psi} + \boldsymbol{\sigma} : \dot{\boldsymbol{\varepsilon}} - \mu\, \dot{m} = -\dot{\psi} + \boldsymbol{\sigma}' : \dot{\boldsymbol{\varepsilon}} - \varphi\mu\, \dot{\varepsilon}_{\mathrm{f}} \geqslant 0, \tag{116}$$

depends solely on the variables that characterize the free energy of the elementary system where the local balance is defined. At equilibrium states it represents the rate of dissipation due to local actions and consequently vanishes in the absence of local dissipative mechanisms.
In contrast, the transport-related contribution pertains to the fluid mass transport phenomenon:

$$\mathcal{D}_{\mathrm{tr}} = -(\nabla\mu) \cdot \mathbf{h} \geqslant 0. \tag{117}$$

While the fundamental inequality requires some restrictions to the constitutive equations, it does not suffice to ascertain their expressions. Thus, the hypothesis of normality of the dissipation mechanism [38] becomes essential to ensure the identification of the missing equations, inherently satisfying the fundamental inequality. To comprehensively describe the mechanical behaviour of a standard material [38] exhibiting a

normal dissipation mechanism, the expression of the two scalar functions. Namely, the dual stored energy density and the dissipation potential, need to be specified [46].

3.2.3.1 *Dual stored energy density*

Starting from the canonical expression of the free energy function ψ, the expression for the dual form of the energy density is derived as a Legendre transform, in a similar manner to [38]. This results in the expression of dual energy density $\check{\psi}$,

$$\check{\psi}(\boldsymbol{\sigma}, \mu) = -\psi(\varepsilon, m) + \boldsymbol{\sigma} : \varepsilon + m\,\mu, \tag{118}$$

in which $\check{\psi}(\sigma, \mu)$ depends on the primary variables total stress $\boldsymbol{\sigma}$ and fluid potential μ. Consequently, the intrinsic dissipation reads:

$$D^*_{int} = -\dot{\check{\psi}} + \dot{\boldsymbol{\sigma}} : \varepsilon - \dot{p}\, m\dot{\mu} = -\dot{\check{\psi}} + \dot{\boldsymbol{\sigma}}' : \varepsilon - \varphi\, \dot{\mu}\, \epsilon_f \geqslant 0. \tag{119}$$

Under the assumption of absence of local dissipative phenomena, the intrinsic dissipation rate must vanish at equilibrium, implying a cessation of all internal entropy production. Rearranging Eq. (119), by employing the chain rule, yields to:

$$D^*_{int} = \left[\frac{\partial \check{\psi}}{\partial \boldsymbol{\sigma}} - \varepsilon\right] : \dot{\boldsymbol{\sigma}} + \left[-\frac{\partial \check{\psi}}{\partial \mu} - m\right] \dot{\mu} = 0. \tag{120}$$

Following the standard Colemann-Noll procedure [124], the expressions for the two conjugate quantities can be deduced as the partial derivatives of the thermodynamic potential $\check{\psi}(\boldsymbol{\sigma}, \mu)$ with respect to the two primary variables, $\boldsymbol{\sigma}$ and μ:

$$\frac{\partial \check{\psi}}{\partial \boldsymbol{\sigma}} = \varepsilon \qquad \frac{\partial \check{\psi}}{\partial \mu} = -m, \tag{121}$$

therefore,

$$\dot{\varepsilon}(\boldsymbol{\sigma}, \mu) = \frac{\partial^2 \check{\psi}}{\partial \boldsymbol{\sigma} \otimes \partial \boldsymbol{\sigma}} : \dot{\boldsymbol{\sigma}} + \frac{\partial^2 \check{\psi}}{\partial \boldsymbol{\sigma} \partial \mu} \dot{\mu}, \tag{122}$$

$$-\dot{m}(\boldsymbol{\sigma}, \mu) = \frac{\partial^2 \check{\psi}}{\partial \mu \partial \boldsymbol{\sigma}} : \dot{\boldsymbol{\sigma}} + \frac{\partial^2 \check{\psi}}{\partial \mu^2} \dot{\mu}. \tag{123}$$

The two expressions can be related to the dual formulation of the canonical state laws presented in [105] by characterizing the second derivatives of the dual free energy as:

$$\frac{\partial^2 \breve{\psi}}{\partial \boldsymbol{\sigma} \otimes \partial \boldsymbol{\sigma}} = \mathbf{D}, \tag{124}$$

$$\frac{\partial^2 \breve{\psi}}{\partial \boldsymbol{\sigma} \partial \mu} = \frac{\partial^2 \breve{\psi}}{\partial \mu \partial \boldsymbol{\sigma}} = \frac{\rho_f}{K_d} \mathbf{I}, \tag{125}$$

$$\frac{\partial^2 \breve{\psi}}{\partial^2 \mu} = \frac{1}{M}. \tag{126}$$

Finally, substituting Eqs. (124-126) in Eqs. (122-123), the governing equations of solid deformation and content in fluid are obtained:

$$\varepsilon(\boldsymbol{\sigma}, \mu) = \mathbf{D} : \boldsymbol{\sigma} + \frac{\rho_f}{K_d} \mathbf{I}\, \mu, \tag{127}$$

$$-m(\boldsymbol{\sigma}, \mu) = \frac{\rho_f}{K_d} \mathbf{I} : \boldsymbol{\sigma} + \frac{1}{M}\, \mu, \tag{128}$$

where $\frac{1}{M}$ is the Biot modulus, $\mathbf{D}$ is the elastic compliance tensor of the solid phase and K_d is the drained bulk modulus. Additionally, under the hypothesis of true incompressibility of the solid phase the Biot modulus is $1/M = \varphi/K_f$ [33], with K_f the bulk modulus of fluid. The dual form of stored energy function (118) then can be expressed in the following manner:

$$\breve{\psi}\,(\boldsymbol{\sigma}, \mu) = \frac{1}{2}\,(\boldsymbol{\sigma} + \mu \rho_f \mathbf{I}) : \mathbf{D} : (\boldsymbol{\sigma} + \mu \rho_f \mathbf{I}) + \frac{1}{2}\frac{1}{M}\,\rho_f^2\,\mu^2. \tag{129}$$

Under the assumption of perfect elastic behaviour for the solid phase the constitutive behaviour is expressed by Hooke's law $\boldsymbol{\varepsilon}_s = \mathbf{D} : \boldsymbol{\sigma}'$, where the expression for infinitesimal strain of the solid phase reduces to $\boldsymbol{\varepsilon}_s = \nabla^s \mathbf{u}$. Moreover, no local dissipative mechanisms are present and therefore the dissipation rate reduces only to the transport related term.

3.2.3.2 *Dissipation potential function*

The dissipation potential function $\mathcal{D}$ is introduced to account for the dissipation rate associated with fluid diffusion in Eq. (115). Under the hypothesis of normal dissipative mechanisms [38], excluding the dependence of the dissipation potential on the state variables of the system and their gradients, the dissipation potential function is reduced to the following quadratic expression:

$$\phi\,(\nabla \mu) = \frac{1}{2} \nabla \mu \cdot \widehat{\boldsymbol{\kappa}} \cdot \nabla \mu, \tag{130}$$

with $\widehat{\aleph} = \rho_f^2 \aleph$, $\aleph$ being the symmetric and positive definite spatial permeability second-order tensor, leading to the constitutive equation of Darcy's law [19].

3.3 HYBRID FORMULATION OF POROELASTICITY

3.3.1 *Complementary/Dual poroelastic energy potential*

Consider the transient analysis of an elastic porous medium with coupled solid deformation and pore fluid diffusion. Following the framework of Coussy [38] [2], the variational principle for poroelasticity, in terms of the two primary variables $\boldsymbol{\sigma}$ and μ, is given by the following complementary *rate potential*:

$$\begin{aligned} \overline{\overline{\Pi}}(\dot{\boldsymbol{\sigma}}, \dot{\mu}) &:= \int_{\mathcal{B}} \overline{\overline{\pi}}(\dot{\boldsymbol{\sigma}}, \dot{\mu}) \, dv - P_{ext}\,(\dot{\boldsymbol{\sigma}}, \dot{\mu}) \\ \text{where} \quad \overline{\overline{\pi}}(\dot{\boldsymbol{\sigma}}, \dot{\mu}) &= \dot{\check{\psi}}(\boldsymbol{\sigma}, \mu) + \phi\,(\nabla \mu) \end{aligned} \tag{131}$$

with $\dot{\check{\psi}} = \partial_{\boldsymbol{\sigma}} \check{\psi} : \dot{\boldsymbol{\sigma}} - \partial_{\mu} \check{\psi}\, \dot{\mu}$, and $\mathcal{P}_{ext}$ is the external power. Notably, the dependence of $\boldsymbol{\sigma}$ and μ on the time will be implicitly stated through the rest of the paper. Since the problem under consideration is evolutionary, the functional in Eq. (134) must be evaluated over successive configurations of the medium as it evolves in time. A natural way to achieve this is to introduce a time discretization, so that the continuous history of the fields is replaced by a sequence of states at discrete instants t_n. The single time-step recurrence relations are hereafter developed and the solution S_{n+1} at time $t_{n+1} = t_n + \Delta t$ is determined assuming that the solution S_n at the end of the previous time step t_n is known, via:

$$\boldsymbol{\sigma}^{n+1} = \boldsymbol{\sigma}^n + \Delta\boldsymbol{\sigma}, \quad u^{n+1} = u^n + \Delta u. \tag{132}$$

The incremental problem consists of finding $(\Delta\boldsymbol{\sigma}, \Delta\mu)$ within the set of statically admissible fields such that an incremental variational principle is satisfied. Consequently, according to the Crank–Nicolson scheme, the discrete integration in time of the fluid potential field can be evaluated as follow:

$$\int_{t_n}^{t_{n+1}} \mu(\tau)\, d\tau = \frac{\mu^n + \mu^{n+1}}{2} \Delta t = \mu^n \Delta t + \Delta\mu \frac{\Delta t}{2}. \tag{133}$$

For the proposed formulation, the Crank-Nicholson scheme is conditionally stable in time and is preferable to the implicit scheme due to its second-order accuracy. Referring back to the expression of the complementary energy functional Eq. (131) and explicitly detailing the expressions of the stored energy Eq. (129), the dissipation po-

2 The variational principle in [38] is presented in its incremental, rather than rate, form.

tential Eq. (130), and the power term related to external forces, the following complementary energy functional is derived in a similar manner of [38]:

$$\begin{aligned}\overline{\overline{\Pi}} = &\frac{1}{2}\int_{\mathcal{B}} (\Delta\boldsymbol{\sigma} + \rho_f \Delta\mu \mathbf{I}) : \mathbf{D} : (\Delta\boldsymbol{\sigma} + \rho_f \Delta\mu \mathbf{I})\, dv + \frac{1}{2}\int_{\mathcal{B}} \frac{\varphi}{K_f}\, \Delta\mu^2\, dv \\ &+ \frac{1}{2}\int_{\mathcal{B}} \nabla\left(\frac{\mu^n + \mu^{n+1}}{2}\Delta t\right) \cdot \mathbf{K} \cdot \nabla\left(\frac{\mu^n + \mu^{n+1}}{2}\Delta t\right) dv \\ &- \int_{\partial\mathcal{B}^u_e} \mathbf{n} \cdot \Delta\boldsymbol{\sigma} \cdot \Delta\bar{\mathbf{u}}\, ds - \int \partial\mathcal{B}^h_e \left(\frac{\mu^n + \mu^{n+1}}{2}\Delta t\right) \bar{h}\, ds,\end{aligned} \tag{134}$$

where the field of the stress belongs to the class of the statically admissible solutions. The first integral in Eq. (134) gives the complementary strain energy of the solid matrix, which is a quadratic function of effective stress $\boldsymbol{\sigma}' = \boldsymbol{\sigma} + \rho_f \mu \mathbf{I}$. After the spatial discretization, the Crank-Nicholson scheme is non-oscillatory under some conditions on the time and spatial steps [38]. Starting from the previous contributions of Parrinello and Borino [93, 95], a novel Hybrid Equilibrium Element for two-dimensional membrane problems is developed under the framework of Biot's theory, introducing an additional variable designed to account for the fluid potential field.

3.3.2 *Hybrid variational principle for poroelasticity*

The poroelastic domain $\mathcal{B} \subset \mathbb{R}^3$ is discretized by a mesh ${}^h\mathcal{B} = \bigcup_{e=1}^{N_e} \mathcal{B}_e$, consisting of N_e non-overlapping subdomains $\mathcal{B}_e$. Each subdomain is associated with a boundary $\partial\mathcal{B}_e$, which is further divided into S_e sides $\partial\mathcal{B}^s_e$ such that $\partial\mathcal{B}_e = \bigcup_{s=1}^{S_e} \partial\mathcal{B}^s_e$. Every side $\partial\mathcal{B}^s_e$ belongs either to the subset of free boundaries, i.e. $\partial\mathcal{B}^s_e \subset (\partial\mathcal{B}^t \cup \partial\mathcal{B}^h)$, to the subset of constrained boundaries, i.e. $\partial\mathcal{B}^s_e \subset (\partial\mathcal{B}^u \cup \partial\mathcal{B}^\mu)$, or to an internal boundary shared by two distinct subdomains, denoted as $\partial\mathcal{B}^{\text{int}\,s} \equiv \partial\mathcal{B}^s_{e_1} \cap \partial\mathcal{B}^s_{e_2}$ with $e_1 \neq e_2$. Notably, on the same portion of the boundary $\partial\mathcal{B}$, the superimposition of mechanical boundary conditions (i.e., on $\partial\mathcal{B}^t$ or $\partial\mathcal{B}^u$) with hydraulic conditions (i.e., on $\partial\mathcal{B}^\mu$ or $\partial\mathcal{B}^h$) is possible (**??**). Within each Hybrid Equilibrium Element (HEE), the approximating function for the stress field $\boldsymbol{\sigma}_e$ belongs to a finite subspace of statically admissible solutions (neglecting body forces and imposed tractions on its boundary), which satisfy equilibrium *locally* at the element level [4]. Thus, to enforce stress codiffusivity along free element sides, continuum boundaries, and inter-element interfaces, a Lagrange multiplier λ^s_e is introduced at the element edges $s = 1, \ldots, S_e$. From the stationarity conditions, this multiplier naturally emerges as the displacement field $\mathbf{u}_e$, whose approximating functions are chosen as the broken space of the trace of standard isoparametric shape functions. Finally, the fluid potential field μ_e is discretized through an isoparametric mapping, following the same approach typically adopted in

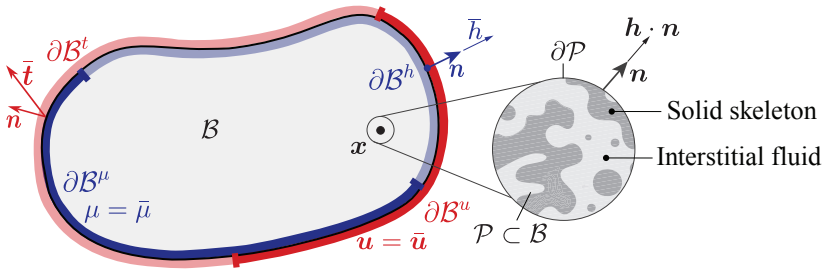

Figure 2: Graphical description for the poroelastic system.

conventional finite element formulations.
Incorporating the imposed constraint into (131), a *hybrid rate* functional is formulated

$$
\begin{aligned}
{}^{h}\dot{\overline{\Pi}}(\boldsymbol{\sigma}, \mu, \lambda) = \sum_{e=1}^{N_e} \Bigg(& \int_{\mathcal{B}_e} \dot{\overline{\pi}}(\boldsymbol{\sigma}_e, \mu_e)\, dv - P_{ext}\,(\boldsymbol{\sigma}_e, \mu_e) + \\
& \sum_{s=1}^{S_e} \left[\int_{\partial\mathcal{B}_e^s / \partial\mathcal{B}_e^u} \lambda_e^s\, (\boldsymbol{\sigma}_e \cdot \mathbf{n}_e^s - \bar{\mathbf{t}})\, ds \right] \Bigg),
\end{aligned}
\tag{135}
$$

with $\bar{\mathbf{t}}$ the prescribed traction vector, being null everywhere except on $\partial\mathcal{B}^t$. The positive sign of the term containing the Lagrange multipliers is adopted to ensure that all terms consistently represent the negative of the external power. This structure ensures a well-posed discretization, provided that the stability conditions outlined by Brezzi [28] are satisfied.
By discretizing the problem in space and time, the incremental form of the functional can be thus stated as follows:

$$
\begin{aligned}
\dot{\overline{\Pi}} = \sum_{e=1}^{N_e} \Bigg[& \frac{1}{2} \int_{\mathcal{B}_e} (\Delta\boldsymbol{\sigma}_e + \Delta\mu_e\, \mathbf{I}) : \mathbf{D} : (\Delta\boldsymbol{\sigma}_e + \Delta\mu_e\, \mathbf{I})\, dv \\
& + \frac{1}{2} \int_{\mathcal{B}_e} \frac{\varphi}{K_f}\, \Delta\mu_e^2 dv + \frac{1}{2} \Delta t^2 \int_{\mathcal{B}_e} \nabla\, (\mu_e^{(n)} + \frac{\Delta\mu_e}{2}) \cdot \mathbf{K} \cdot \nabla (\mu_e^{(n)} + \frac{\Delta\mu_e}{2}) dv \\
& - \Delta t \int_{\partial\mathcal{B}^h} (\mu_e^{(n)} + \frac{\Delta\mu_e}{2}) \bar{h}\, ds \\
& + \sum_{s=1}^{3} \left(\int_{\partial\mathcal{B}_e^s / \partial\mathcal{B}_e^t} (\mathbf{n} \cdot \Delta\boldsymbol{\sigma}_e - \mathbf{t}) \cdot \Delta\lambda_e^s\, ds - \int_{\partial\mathcal{B}^t} t_e^s \cdot \Delta\mathbf{u}_e^s ds \right) \Bigg].
\end{aligned}
\tag{136}
$$

As we have introduced in Chapter 1, the assessment of stationarity conditions of the associated variational principle serves as an essential feature in inferring the variational

consistency to the weak form of the governing equations of the problem. We define the functional spaces to which the field variations ${}^{h}\delta\boldsymbol{\sigma}$, ${}^{h}\delta\mu$, ${}^{h}\delta\lambda$ belong Remark **??**:

$$
\begin{aligned}
{}^{h}\mathcal{W}_{\sigma}^{\text{disc}} &= \left\{ {}^{h}\delta\boldsymbol{\sigma} \in [L^2(\mathcal{B})]^d \,\middle|\, {}^{h}\boldsymbol{\sigma}|_{\mathcal{B}_e} \in \mathbb{P}_k(\mathcal{B}_e;\mathbb{R}^d), \right. \\
&\qquad \left. \nabla\cdot({}^{h}\delta\boldsymbol{\sigma}) = 0 \text{ on } \mathcal{B}_{\gamma},\ {}^{h}\delta\boldsymbol{\sigma}\cdot\mathbf{n} = 0 \text{ on } \partial\mathcal{B}^{t},\ \forall\,\mathcal{B}_e \in {}^{h}\mathcal{B} \right\}, \\
{}^{h}\mathcal{W}_{\mu} &= \left\{ {}^{h}\delta\mu \in L^2(B_0) | \, {}^{h}\delta\mu = 0 \quad \text{on } \partial B^{\mu} \right\}, \\
{}^{h}\mathcal{W}_{\delta\lambda,l} &= \left\{ {}^{h}\delta\lambda \in L^2(\partial\mathcal{B}) \,\middle|\, {}^{h}\delta\lambda|_{\partial\mathcal{B}_e^s} \in \mathbb{P}_l(\partial\mathcal{B}_e^s), \right. \\
&\qquad \left. \delta^{h}\lambda = 0 \text{ on } \partial\mathcal{B},\ \forall\,\partial\mathcal{B}_e^s \subset {}^{h}\partial\mathcal{B}^s \right\},
\end{aligned}
\tag{137}
$$

Taking variations in in Eq. (134) with respect to admissible virtual stress $\delta\boldsymbol{\sigma}$ and virtual fluid potential $\delta\mu$, one obtains the Euler–Lagrange equations:

Compatibility equation	$[\mathbf{D} : (\boldsymbol{\sigma} + \mathbf{I}\,\rho_f\mu)] - \nabla^s\mathbf{u} = 0$	in $\mathcal{B}$
Fluid mass balance	$\mathbf{I} : \mathbf{D} : (\Delta\boldsymbol{\sigma} + \rho_f\Delta\mu\mathbf{I}) + \frac{\varphi}{M}\,\Delta\mu$	
	$+\nabla\cdot(\mathbf{K}\cdot\nabla(\mu_e^{(n)} + \frac{\Delta\mu_e}{2})) = 0$	in $\mathcal{B}$
Prescribed displacements	$\mathbf{u} - \bar{\mathbf{u}} = 0$	on $\partial\mathcal{B}^{u}$
Prescribed fluid flux	$(\mathbf{K}\cdot\nabla(\mu_e^{(n)} + \frac{\Delta\mu_e}{2}))\cdot\mathbf{n} - \bar{h} = 0$	on $\partial\mathcal{B}^{h}$
Prescribed tractions	$\sigma\cdot\mathbf{n} - \bar{t} = 0$	on $\partial\mathcal{B}^{t}$

(138)

where the Lagrange multiplier λ^s can be naturally identified with the displacement field $\mathbf{u}^s$, such that $\mathbf{u}^s = \bar{\mathbf{u}}$ on $\partial\mathcal{B}_e^s \cap \partial\mathcal{B}_e^u$. Once this correspondence between the displacement field and the Lagrange variable is established, the functional space adopted for $\mathbf{u}^s$ coincides with that of the displacement field itself, ensuring kinematic consistency along the element sides.

Remark 5. The space of admissible fluid potential ${}^{h}\boldsymbol{\mu}$ is a finite-dimensional subspace of the Lebesgue space $\mathbf{L}^2(\mathcal{B})$, defined as

$$
{}^{h}\mathcal{V}_{\mu} = \left\{ {}^{h}\mu \in [L^2(\mathcal{B})]^d \,\middle|\, {}^{h}\mu = \bar{\mu} \text{ on } \partial\mathcal{B}^{\mu} \right\}, \tag{139}
$$

where d is the spatial dimension. The local approximation of the stress field ${}^{h}\boldsymbol{\sigma}$ on each element $\mathcal{B}_e$ belongs to a discontinuous finite-dimensional space, i.e.

$$
\begin{aligned}
&{}^{h}\mathcal{V}_{\sigma}^{\text{disc}} = \\
&\left\{ {}^{h}\boldsymbol{\sigma} \in [L^2(\mathcal{B})]^d \,\middle|\, {}^{h}\boldsymbol{\sigma}|_{\mathcal{B}_e} \in \mathbb{P}_k(\mathcal{B}_e;\mathbb{R}^d), \nabla\cdot({}^{h}\boldsymbol{\sigma}) = 0 \text{ on } \mathcal{B}_e, \forall\,\mathcal{B}_e \in {}^{h}\mathcal{B} \right\},
\end{aligned}
\tag{140}
$$

where $\mathbb{P}_k(\mathcal{B}_e;\mathbb{R}^d)$ contains polynomials of total degree $\leqslant k$ on the element ${}^{h}\mathcal{B}_e$. This choice allows the stress to be discontinuous across element interfaces, thus removing the global $H(\text{div})$ conformity requirement [35, 55]. In other words, ${}^{h}\boldsymbol{\sigma}$ does not necessarily belong to $H(\text{div},\mathcal{B})$, which would instead require the continuity of the normal components of the stress across interfaces. To enforce the codiffusivity of the stresses

at the element interfaces, the hybridization procedure introduces an independent set of Lagrange multipliers ${}^{h}\lambda \in {}^{h}\mathcal{V}_{\lambda}$, defined on each element side $\partial\mathcal{B}_e^s \in {}^{h}\partial\mathcal{B}$. The associated finite-dimensional space is

$$\begin{aligned} &{}^{h}\mathcal{V}_{\lambda,l} = \\ &\left\{ {}^{h}\lambda \in L^2(\partial\mathcal{B}) \;\middle|\; {}^{h}\lambda|_{\partial\mathcal{B}_e^s} \in \mathbb{P}_l(\partial\mathcal{B}_e^s),\ {}^{h}\lambda = \bar{\lambda} \text{ on } \partial\mathcal{B}^{\lambda},\ \forall\, \partial\mathcal{B}_e^s \subset {}^{h}\partial\mathcal{B} \right\}, \end{aligned} \tag{141}$$

where $\mathbb{P}_l(\partial\mathcal{B}_e^s)$ denotes the space of polynomials of total degree $\leqslant l$ on the element side $\partial\mathcal{B}_e^s$.

3.3.2.1 *Stationarity of the complementary poroelastic energy funtional*

The stationary condition of the functional Π with respect to the stress tensor $\boldsymbol{\sigma}_e$, on the element $\partial\mathcal{B}_e$, provides a weak form of the compatibility condition between solid strains $\boldsymbol{\varepsilon}_e = \mathbf{D} : (\boldsymbol{\sigma}_e + \rho_F \mu_e \mathbf{I})$ and displacement at the boundary sides $\mathbf{u}_e^s$ with $s = 1, 3$

$$\begin{aligned} &\int_{\mathcal{B}_e} \left(\delta\Delta\sigma_{ij}\right) : D_{ijkl} : (\Delta\sigma_{kl} + I_{kl}\rho_f\Delta\mu)\, dv \\ &- \sum_{s=1}^{3} \left[\int_{\partial\mathcal{B}_e^s/\partial\mathcal{B}_t} n_i^s \cdot \delta\, \Delta\sigma_{ij} \Delta\lambda_j^s\, ds \right] \end{aligned} \tag{142}$$

from which the lagrangian variable λ emerges as the solid displacements, $\mathbf{u}_e$. The stationary condition of the functional $\overline{\overline{\Pi}}$ with respect to the fluid pressure μ_e, on the element $\partial\mathcal{B}_e$, provides and a weak form of the mass balance:

$$\begin{aligned} &\int_{\mathcal{B}_e} \left(\mathbf{I}_{ij}\delta\Delta\mu_e\right) : \mathbf{D}_{ijkl} : (\Delta\boldsymbol{\sigma}_{kl} + \mathbf{I}_{kl}\rho_f\Delta\mu_e)\, dv + \int_{\mathcal{B}_e} (\delta\Delta\mu_e)\, \frac{\varphi}{K_f}\, (\Delta\mu_e)\, dv + \\ &+ \int_{\mathcal{B}_e} (\delta\Delta\mu_e)_{,i}\, \mathbf{K}_{ijkl} \left(\mu_e^{(n)} + \frac{\Delta\mu_e}{2} \right)_{,j} dv + \sum_{s=1}^{3} \left[\int_{\partial\mathcal{B}_e^s} \delta\Delta\mu_e h_s\, ds \right] = 0, \end{aligned} \tag{143}$$

By employing the integration by parts and invoking the divergence theorem, Eq. (**??**) can be decomposed into three distinct statements. The first of the aforementioned statements, within the domain $\mathcal{B}$, leads to the weak form of the mass balance equation:

$$\begin{aligned} &\int_{\mathcal{B}} \delta\Delta\mu\, \mathbf{I}_{ij} : \mathbf{D}_{ijkl} : (\Delta\sigma_{kl} + \mathbf{I}_{kl}\, \rho_f\Delta\mu)\ dv + \int_{\mathcal{B}} \delta\Delta\mu\, \frac{\varphi}{K_f} \rho_f \Delta\mu\, dv \\ &+ \int_{\mathcal{B}} \delta\Delta\mu \left(\mathbf{K}_{ij}\Delta t^2 \left(\mu_e^{(n)} + \frac{\Delta\mu_e}{2} \right)_{,j} \right)_{,i} dv = 0 \end{aligned} \tag{144}$$

finally, can be simplified to:

$$\int_{\mathcal{B}} \delta\Delta\mu \left[\Delta\varepsilon_{ii} - \Delta\varphi\varepsilon_{ii_f} + \Delta t \left(h_j^{(n)} + \frac{\Delta h_j}{2} \right)_{,i} \right] dv = 0 \tag{145}$$

The second and third statements in Eq. (144) on the boundaries, constitute the natural boundary conditions, where the flux associated with the pressures must equal the prescribed flux on the boundary $\partial\mathcal{B}^h$ and vanish on the boundary $\partial\mathcal{B}_e^\mu$

$$\begin{aligned} &\int_{\partial\mathcal{B}^h} \delta\Delta\mu\, n_i\, K_{ij} \Delta t \left(\mu_e^{(n)} + \frac{\Delta\mu_e}{2} \right)_{,j} ds - \int_{\partial\mathcal{B}^h} \delta\Delta\mu\, \bar{h}_n\, ds = 0, \\ &\int_{\partial\mathcal{B}_e^\mu} \delta\Delta\mu\, n_i\, K \cdot \nabla \Delta t \left(\mu_e^{(n)} + \frac{\Delta\mu_e}{2} \right) ds = 0, \end{aligned} \tag{146}$$

$\forall \delta\mu \,|\, \delta\mu = 0$ on $\partial\mathcal{B}_e^\mu$. The stationary condition of the functional $\overline{\overline{\Pi}}$ with respect to the Lagrangian variable λ gives the weak form of the inter-element equilibrium condition for the internal side $\partial\mathcal{B}_{int} = \partial\mathcal{B}_{e_1} \cap \partial\mathcal{B}_{e_2}$:

$$\int_{\partial\mathcal{B}_{int}} \left(n^{e_1}_{\Delta\sigma ij}{}^{e_1} + n_i^{e_2} \cdot \Delta\sigma_{ij}^{e_2} \right) \cdot \delta\Delta\lambda_j^s \, ds = 0 \tag{147}$$

with $\mathbf{n}^{e_1} = -\mathbf{n}^{e_2}$ outward normals of the adjacent elements at the interelement side. The stationary condition of the functional $\overline{\overline{\Pi}}$ with respect to the Lagrangian variable $\mathbf{u}$ gives the weak form of the boundary equilibrium condition for a free boundary side $\partial\mathcal{B}_s^e = \partial\mathcal{B}_e \cap \partial\mathcal{B}_t$

$$\int_{\partial\mathcal{B}_e^s / \partial\mathcal{B}_t} \left(n_i^e \Delta\sigma_{ij}^e - \Delta\bar{t}_j \right) \delta\Delta\lambda_j{}^s \, ds = 0 \tag{148}$$

3.3.2.2 *Discretized form of the functional*

The formulation of Hybrid Equilibrium Elements requires that the stress functions within each element are expressed as a linearly independent set of self-balanced stress fields which forms a complete basis of a vector space capable of embodying all potential statically admissible distribution of a specified polynomial degree [4]. These functions are formulated as polynomials in x and y, representing the coordinates of the element local reference frame. The coefficients of these polynomials, referred to as generalized stresses, have to be determined as the solution. It is noteworthy that these stress fields do not interpolate nodal degrees of freedom; instead, they are defined as functions of the generalized stress parameters.
In this work, the hybrid equilibrium element is developed for two- dimensional plane stress problems, considering a triangular finite element within the domain Ω_e, oriented according to a local Cartesian reference frame (x, y) with its origin at vertex 1,

as depicted in Figure 3. The quadratic stress fields for this two-dimensional element are characterized by the following polynomial functions of second order :

$$\sigma_x(x,y) = a_1 + a_2 y + a_3 y^2 - a_9 x - a_{10} x^2/2 - 2a_{12} xy, \tag{149}$$

$$\sigma_y(x,y) = a_4 + a_5 x + a_6 x^2 - a_8 y - a_{10} y^2/2 - 2a_{11} xy, \tag{150}$$

$$\tau_{xy}(x,y) = a_7 + a_8 x + a_9 y + 2a_{10} xy + a_{11} x^2 + a_{12} y^2, \tag{151}$$

where the coefficients a_n represent the generalised stresses. Such stress fields implicitely verify the homogeneous momentum balance equation, i.e. $\nabla \boldsymbol{\sigma} = 0$.
In accordance to this description, we decide to constrain the representation of the stress field to a sum of polynomial terms, expressed in Voigt notation as:

$$\boldsymbol{\sigma}_e(\mathbf{x}) = \mathbf{S}_e(\mathbf{x})\mathbf{a}_e \tag{152}$$

where $\mathbf{a}_e$ collects all generalised stress variables and $\boldsymbol{\sigma} = [\sigma_x, \sigma_y, \tau_{xy}]^T$.
The proposed HEE incorporates a displacement field as a Lagrangian variable, independently defined for each element side. Within the HEE formulation, nodes can be considered as associated with element sides, allowing two adjacent elements to share the nodes (three in the quadratic formulation) of their common side. As a result, spatial discretization with HEEs leads to several coincident nodes at a common vertex between different elements. Conversely, midside nodes are unique. Consequently, the quadratic polynomial displacement field is discretised on nine nodes for each HEE, with two geometrically coincident nodes for each vertex of the element Figure 3. This choice allows the formulation to effectively satisfy the boundary and the interelement equilibrium conditions [93]. By contrast, in displacement-based formulations, displacement continuity is imposed but tractions at sides are discontinuous between adjacent elements.

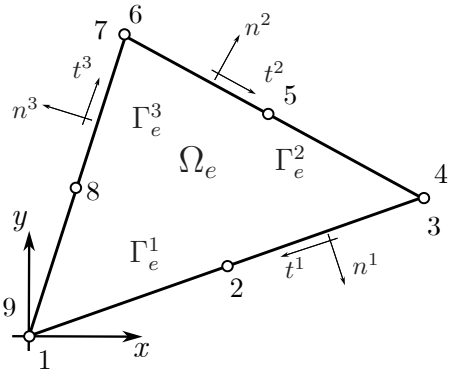

Figure 3: Nine-node triangular hybrid equilibrium element(HEE) over which stresses and displacement field are approximated. The pressure field is interpolated over an overlapped six-node quadratic triangular element.

The displacement components of the element sides $\partial\mathcal{B}_e^s$ with s = 1,...,3 are represented using an isoparametric mapping of the type

$$\mathbf{u}_e^s(\xi) = \bar{\mathbf{N}}(\xi) \cdot \mathbf{u}_e^s, \tag{153}$$

where $\bar{\mathbf{N}}$ collects the shape functions and $\mathbf{u}_e^s$ collects the kinematic degrees of freedom of side $\partial\mathcal{B}_e^s$. Additionally, as a novelty with respect to the existing literature, a quadratic polynomial pressure field is expressed by classical shape functions in the isoparametric space of the element, by constraining the geometrically coincident nodes at vertices:

$$\boldsymbol{\mu}(x, y) = \mathbf{N}_e(\boldsymbol{\eta})\, \boldsymbol{\mu}_e, \tag{154}$$

$$\nabla\boldsymbol{\mu}(x, y) = \nabla\mathbf{N}_e(\boldsymbol{\eta})\, \boldsymbol{\mu}_e = \mathbf{B}_e(\boldsymbol{\eta})\, \boldsymbol{\mu}_e, \tag{155}$$

where $\mathbf{N}_e$ collects the shape functions associated with pore pressure, $\mathbf{B}_e$ matrix collects the relative partial derivative of $\mathbf{N}_e$ and $\boldsymbol{\mu}_e$ collects the element pressure degrees of freedom.
Recalling Eq. (136), by substituting the aforementioned approximating functions, the functional can be expressed in Voigt notation as:

$$\begin{aligned}
\overline{\overline{\Pi}} = \sum_{e=1}^{N_e} \Bigg[& \tfrac{1}{2}\Delta\mathbf{a}_e^T \int_{\mathcal{B}_e} \mathbf{S}_e^T \mathbf{D}\, \rho_f \mathbf{S}_e \, dv\, \Delta\mathbf{a}_e + \tfrac{1}{2}\Delta\mathbf{a}_e^T \int_{\mathcal{B}_e} \rho_f \mathbf{S}_e^T \mathbf{D}\, \mathbf{I}\, \mathbf{N}_e \, dv\, \Delta\boldsymbol{\mu}_e \\
& + \tfrac{1}{2}\Delta\boldsymbol{\mu}_e^T \int_{\mathcal{B}_e} \rho_f \mathbf{S}_e^T \mathbf{D}\, \mathbf{I}\, \mathbf{N}_e \, dv\, \Delta\mathbf{a}_e + \tfrac{1}{2}\Delta\boldsymbol{\mu}_e^T \int_{\mathcal{B}_e} \mathbf{N}_e^T \left(\tfrac{1}{K_s} + \tfrac{\varphi}{K_f}\right) \mathbf{N}_e \, dv\, \Delta\boldsymbol{\mu}_e \\
& - \Delta t \left(\mu_e^{(n)} + \tfrac{\Delta\mu_e}{2}\right)^T \int_{\mathcal{B}_e} \mathbf{B}_e^T \mathbf{K} \mathbf{B}_e \, dv\, \Delta t \left(\mu_e^{(n)} + \tfrac{\Delta\mu_e}{2}\right) \\
& - \Delta\mathbf{a}_e^T \int_{\partial\mathcal{B}_e} \mathbf{S}_e^T \mathbf{n}_e\, \bar{\mathbf{N}}_e \, ds\, \Delta\mathbf{u}_e - \int_{\partial\mathcal{B}_e \cap \partial\mathcal{B}^t} \bar{\mathbf{t}}^T \bar{\mathbf{N}}_e \, ds\, \Delta\mathbf{u}_e \\
& - \int_{\partial\mathcal{B}_e \cap \partial\mathcal{B}^h} \bar{h}\, \mathbf{N}_e^T \, ds\, \Delta t \left(\mu_e^{(n)} + \tfrac{\Delta\mu_e}{2}\right) \Bigg] \\
= \sum_{e=1}^{N_e} \Bigg[& \tfrac{1}{2}\Delta\mathbf{a}_e^T \mathbf{K}_e^{aa} \Delta\mathbf{a}_e + \tfrac{1}{2}\Delta\mathbf{a}_e^T \mathbf{K}_e^{ab} \Delta\boldsymbol{\mu}_e + \tfrac{1}{2}\Delta\boldsymbol{\mu}_e^T \mathbf{K}_e^{ab\,T} \Delta\mathbf{a}_e \\
& + \tfrac{1}{2}\Delta\boldsymbol{\mu}_e^T \mathbf{K}_e^{bb} \Delta\boldsymbol{\mu}_e - \tfrac{1}{2}\Delta t \left(\mu_e^{(n)} + \tfrac{\Delta\mu_e}{2}\right)^T \bar{\mathbf{K}}_e^{bb}\, \Delta t \left(\mu_e^{(n)} + \tfrac{\Delta\mu_e}{2}\right) \\
& - \Delta\mathbf{a}_e^T \mathbf{K}_e^{au} \Delta\mathbf{u}_e - \bar{\mathbf{t}}^T \Delta\mathbf{u}_e - \bar{h}_e^T\, \Delta t \left(\mu_e^{(n)} + \tfrac{\Delta\mu_e}{2}\right) \Bigg].
\end{aligned} \tag{156}$$

where $\partial\mathcal{B}_e = \bigcup_{s=1}^{3} \partial\mathcal{B}_e^s$, and :

$$\mathbf{K}_e^{aa} = \int_{\mathcal{B}_e} \mathbf{S}_e \mathbf{D} \mathbf{S}_e \, dv, \tag{157}$$

$$\mathbf{K}_e^{ab} = \int_{\mathcal{B}_e} \rho_f \mathbf{S}_e \mathbf{D} \mathbf{I} \mathbf{N}_e \, dv, \tag{158}$$

$$\mathbf{K}_e^{bb} = \int_{\mathcal{B}_e} \mathbf{N}_e (\frac{1}{K_s} + \frac{\varphi}{K_f}) \mathbf{N}_e \, dv, \tag{159}$$

$$\bar{\mathbf{K}}_e^{bb} = \int_{\mathcal{B}_e} \mathbf{B}_e \cdot \mathbf{K} \cdot \mathbf{B}_e \, dv, \tag{160}$$

$$\mathbf{K}_e^{au} = \int_{\partial\mathcal{B}_e}^{s} \mathbf{S}_e \mathbf{n}_e \bar{\mathbf{N}}_e \, ds, \tag{161}$$

$$\bar{\mathbf{t}}_e = \int_{\partial\mathcal{B}_e \cap \partial\mathcal{B}^t} \bar{\mathbf{N}}_e \, t_e \, ds, \tag{162}$$

$$\bar{\mathbf{h}}_e = \int_{\partial\mathcal{B}_e \cap \partial\mathcal{B}_h} \mathbf{N}_e^T \, \bar{h} \, ds, \tag{163}$$

$$\mathbf{n}_s^e = \begin{bmatrix} n_x^e & 0 \\ 0 & n_y^e \\ n_y^e & n_x^e \end{bmatrix}, \tag{164}$$

where $\bar{\mathbf{t}}_e$ is the vector of the nodal forces integrating at the element level the traction applied at the free boundary and $\bar{h}_e$ is the vector of the nodal flux at the boundary $\partial\mathcal{B}_e^h = \partial\mathcal{B}_e \cap \partial\mathcal{B}^h$. We introduce now the equations of the single element, the first of which is given as the stationary condition with respect to the incremental vector $\Delta\mathbf{a}_e$ of the energy functional in Eq. (156), the second defines the incremental element nodal vector of the content of fluid $\Delta\mathbf{h}_e$ and the third gives the incremental element nodal force vector $\Delta\mathbf{q}_e$:

$$\partial\Pi_{Poro_{\Delta\mathbf{a}_e}} = \mathbf{K}_e^{aa} \Delta\mathbf{a}_e + \mathbf{K}_e^{ab} \Delta\boldsymbol{\mu}_e - \mathbf{K}_e^{au} \Delta\mathbf{u}_e = 0, \tag{165}$$

$$\Delta\mathbf{h}_e = \mathbf{K}_e^{ab\,T} \Delta\mathbf{a}_e + \mathbf{K}_e^{bb} \Delta\boldsymbol{\mu}_e + \bar{\mathbf{K}}_e^{bb} \, (\boldsymbol{\mu}_e^n + \frac{1}{2}\Delta\boldsymbol{\mu}_e) \, \Delta t \tag{166}$$

$$\Delta\mathbf{q}_e = \mathbf{K}_e^{au\,T} \Delta\mathbf{a}_e. \tag{167}$$

The aforementioned statements represent the element equations of the discretised hybrid equilibrium formulation. Eq. (165) establishes the correlation between nodal displacements and generalised stress variables at the element level, while Eq. (166) establishes the correlation between nodal fluxes and generalised fluid pressure variables at the element level. Therefore, the matrix equation for the single HEE can be stated as follows:

$$\begin{bmatrix} \mathbf{K}_e^{aa} & -\mathbf{K}_e^{au} & \mathbf{K}_e^{ab} \\ -\mathbf{K}_e^{au\,T} & 0 & 0 \\ \mathbf{K}_e^{ab\,T} & 0 & \mathbf{K}_e^{bb} + \bar{\mathbf{K}}_e^{bb}\frac{\Delta t}{2} \end{bmatrix} \begin{bmatrix} \Delta \mathbf{a}_e \\ \Delta \mathbf{u}_e \\ \Delta \boldsymbol{\mu}_e \end{bmatrix} = \begin{bmatrix} 0 \\ -\Delta \mathbf{q}_e \\ \Delta \mathbf{h}_e \end{bmatrix} - \begin{bmatrix} 0 \\ 0 \\ \bar{\mathbf{K}}_e^{bb}\,\Delta t\,\boldsymbol{\mu}_e^n \end{bmatrix}. \quad (168)$$

Considering nodal displacement $\Delta\mathbf{u}$ as the first two degrees of freedom and nodal pressure $\Delta\boldsymbol{\mu}$ as the third one of the same vector of nodal unknowns $\Delta\mathbf{u}^*$, we can rearrange the element equations and rewrite Eq. (168) in the following more compact form:

$$\begin{bmatrix} \mathbf{K}_e^{aa} & \mathbf{K}^{au*} \\ \mathbf{K}^{au*T} & \mathbf{K}_e^{uu} \end{bmatrix} \begin{bmatrix} \Delta \mathbf{a}_e \\ \Delta \mathbf{u}_e^* \end{bmatrix} = \begin{bmatrix} 0 \\ \Delta \mathbf{q}^*{}_e \end{bmatrix} - \begin{bmatrix} 0 \\ \bar{\mathbf{q}}_e^* \end{bmatrix}, \quad (169)$$

where $\Delta\mathbf{q}_e^*$ is the incremental residual vector of the single element. The matrix $\mathbf{K}_e^{aa}$ is symmetric, positive definite and not singular (due to the convexity of the associated functional), the generalised stress vector can be therefore condensed out at the element level, thereby enabling the implementation of the HEE within a conventional displacement-based finite element code.
This allows to derive the expression for the incremental vector of generalised stress and the residual vector as follows:

$$\begin{aligned} \Delta \mathbf{a}_e &= -\mathbf{K}^{aa\,-1}[\mathbf{K}_e^{au\,T}\Delta \mathbf{u}_e^*], \\ \Delta \mathbf{q}_e^* &= [\mathbf{K}_e^{uu} - \mathbf{K}^{au*T}\mathbf{K}_e^{aa\,-1}\mathbf{K}_e^{au*}]\Delta \mathbf{u}_e + \bar{\mathbf{q}}_e^* = \mathbf{K}_e \Delta \mathbf{u}_e + \bar{\mathbf{q}}_e^*, \end{aligned} \quad (170)$$

where $\mathbf{K}_e$ is defined as the incremental stiffness matrix, which can be implemented in a standard displacement based finite element code.

3.4 NUMERICAL SIMULATIONS

The proposed HEE was implemented by introducing a new subroutine in the finite element software FEAP v8.537 [120] and the effectiveness of the proposed stress-based formulation is verified through quasi-static analyses conducted on poroelastic benchmark problems. The obtained results are then compared with those derived from the well established formulation in literature [59, 121]. As previously investigated by [79, 80, 130], the HEE formulation may be prone to Spurious Kinematic Modes (SKM). These modes can be effectively handled by following the methodology, described in [92]. However, all the meshes adopted for the simulations of the benchmark problems presented below relied were not affected by the presence of any spurious modes.

3.4.1 *Terzaghi's problem*

Terzaghi consolidation test [122] stands as a fundamental problem in geotechnical engineering. Provides crucial insights into the behaviour of saturated soils in the process of consolidation, characterised by the progressive reduction in volume of a saturated soil due to the expulsion of pore water under external loading [39, 128]. This problem has been rigorously studied and adopted as a benchmark for assessing the performance of finite element formulations, as detailed in and [59, 121].

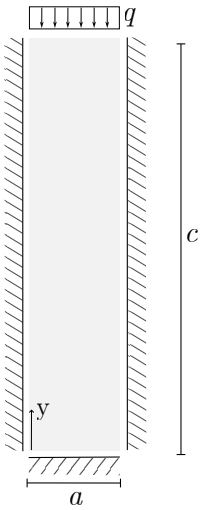

Figure 4: Terzaghi's problem. A rectangular column of dimensions a and c, is loaded by a mechanical force q on the top surface. The sided and bottom surfaces of the specimen are impermeable, while the top surface is assumed to be full drained.

We consider a rectangular specimen (Figure 4) with a height $c = 10\,\mathrm{m}$ and a width $a = 1\,\mathrm{m}$, mechanically constrained in the x-direction on its lateral faces and in the y-direction on its basal surface, with the upper surface being the only permeable boundary. At the initial time $t = 0\,\mathrm{s}$, a sudden vertical load $q = 0.1\,\mathrm{MN\,m^{-2}}$ is applied to the fully drained top boundary and maintained constant throughout the test. The symmetry of the problem implies that the pressure distribution in the horizontal direction remains invariant, consequently, the computational mesh comprises a single column of 30 quadratic triangular elements, with increased density near the top boundary to accurately capture the expected pressure gradient. The material parameters are specified as follows: shear modulus $G = 100\,\mathrm{MN\,m^{-2}}$, fluid density $\rho_f = 1000\,\mathrm{kg\,m^{-3}}$ and spatial permeability $\kappa = 1\,\mathrm{m^3\,s\,kg^{-1}}$. The undrained Poisson's ratio ν_u is assigned values of 0.5 and 0.4, while the drained Poisson's ratio ν_d is fixed at 0.2. The canonical solution to the problem is presented in the pioneering work of Terzaghi [122]. To

facilitate comparison, all parameters have been adimensionalised in accordance with the framework outlined in the aforementioned paper. However, for small values of the non-dimensional time (i.e. $t^* = c_m t/a^2 < 0.01$), the series in Terzaghi's classical solution exhibits extremely slow convergence. It may thus prove more advantageous to employ an approximation specifically tailored for small time steps, as reported in [128]. This approximation yields to:

$$\frac{p}{p_0} = \operatorname{erf}\left(\frac{c-y}{2\sqrt{c_m t}}\right). \tag{171}$$

To assess the robustness and accuracy of the proposed computational approach, the system response under a significantly reduced time step was analysed. This scenario is crucial, as the literature extensively documents that such conditions often lead to numerical oscillations [49, 121]. However, as illustrated in Figure 5, the pressure trend remains free of spurious oscillations. This outcome aligns with theoretical expectations, reinforcing the efficacy of the chosen primary variables.
In Figure 6, the results for pore pressure trend are illustrated at adimensionalised time instants $t^* = 7.12 \cdot 10^{-6}$, and $t^* = 1.068 \cdot 10^{-1}$. The blue lines denote the analytical solution, while the orange dots indicate the values derived from the proposed formulation.
At the moment of loading $t^* = 0$, the pore pressure within the specimen is uniformly homogeneous, reaching its maximum value instantaneously and subsequently decreasing to zero at the top surface. This behaviour is consistent with the analytical solution as delineated in [38]. Given the assumptions of incompressibility for both phases ($\alpha = 1, M \to \infty$), the instantaneous displacement is equal to zero. In fact, since the being instantaneous evolution undrained and the constituents incompressible, the soil layer is unable to undergo any instantaneous deformation.

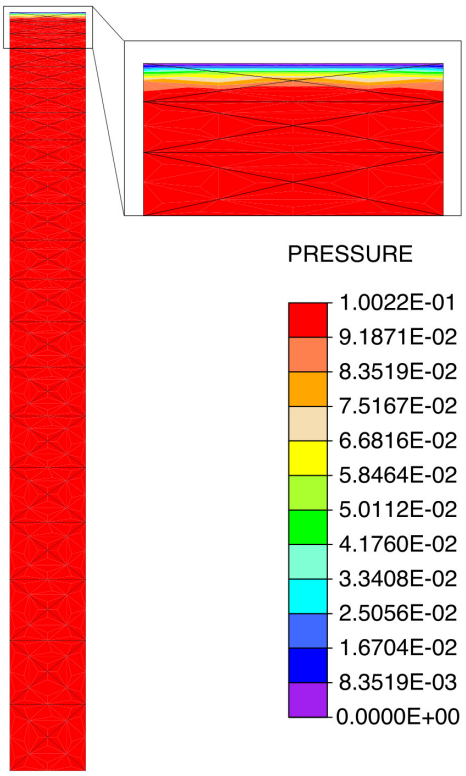

Figure 5: Terzaghi's problem. Pore pressure contour plot for the hybrid equilibrium element with quadratic stress and pressure fields at the adimensionalised time $t^* = 7.12 \cdot 10^{-6}$.

Notably, unlike prior results reported in the literature, these findings exhibit a high degree of correspondence with the analytical solution, even for very early instants of time. This absence of spurious oscillations at very short times, typically present in mixed finite element formulations, is ensured by the specific selection of primary variables and the intrinsic design of the element. Furthermore, for extended time steps, the obtained solution converges with those derived from canonical elements for poroelasticity problems [46, 59, 121].

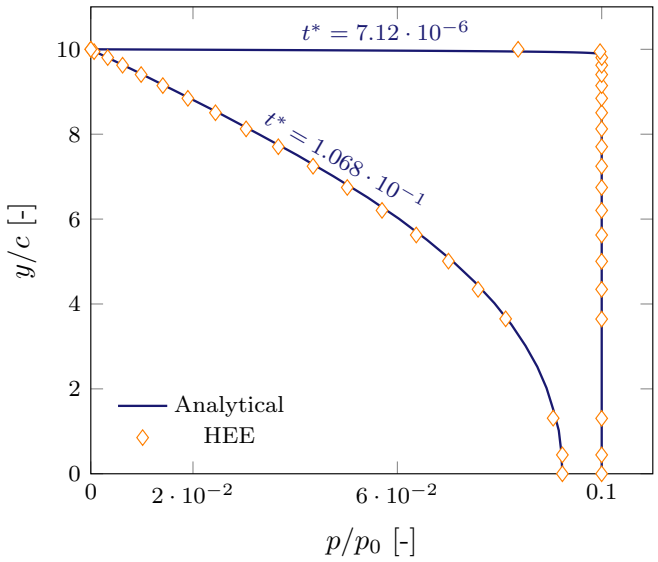

Figure 6: Terzaghi's problem. adimensionalised pore pressure vs. depth trend, for the adimensionalised time $t^* = 7.12 \cdot 10^{-6}$ and $t^* = 1.068 \cdot 10^{-1}$.

3.4.2 *Mandel's problem*

According to the Mandel- Cryler effect [76], experimentally proven by Verruijt [128], the application of a constant load to a soil can cause the pore pressure to initially increase, before decreasing to a final value of zero. The investigation of the aforementioned non-monotonic trend in pore pressure constitutes a classic two-dimensional poroelastic problem. Several authors have subsequently examined the problem as a benchmark for to assess the performance of finite element formulations, as detailed in [1] and [33].
In the first problem among the set presented in [76], a rectangular plate with an infinite length (oriented out of the plane) and a width of $2a$ is placed between two rigid and frictionless plates (Figure 7). The analysis is performed under the plane strain condition by restricting any deformation or flow in the direction perpendicular to the plane. Furthermore, drainage is permitted on the two lateral sides, which are stress-free.

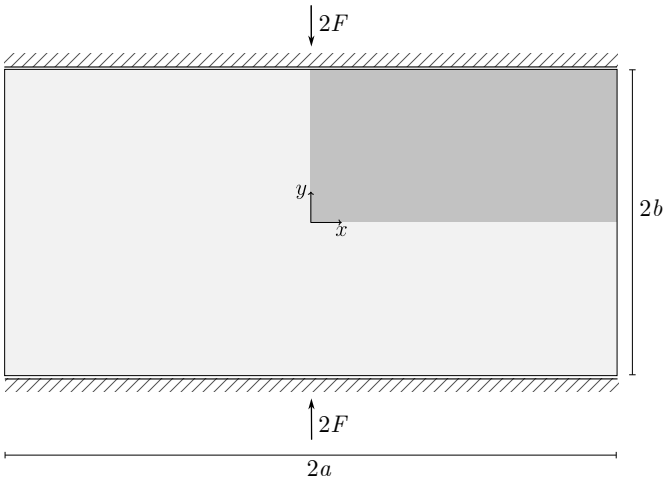

Figure 7: Mandel's problem. A rectangular plate of dimensions 2a and 2b, is loaded by mechanical force 2F through rigid plates. The top and bottom surfaces of the specimen are impermeable, while the side surfaces are assumed to be pressure-free.

A vertical load 2F is applied at time $t^* = 0$, with its value maintained constant during the test. At the moment of loading $t = 0$, the pore pressure is uniform homogeneous, instantaneously diminishing to zero at $|x| = a$. Due to the symmetry property of the problem, we infer that the pressure in the vertical/y direction remains constant.

Cheng and Detournay [33] have previously introduced an analytical solution for the Mandel problem within the framework of Biot's theory. The expression of the non-dimensional pressure, is stated in terms of the imposed load 2F, through the following equation:

$$p = \frac{2FB\,(1+\nu_u)}{3a} \sum_{i=1}^{\infty} \frac{\sin\alpha_i}{\alpha_i - \sin\alpha_i\cos\alpha_i} \left(\cos\frac{\alpha_i x}{a} - \cos\alpha_i\right) \exp\left(-\alpha_i^2 ct/a^2\right), \qquad (172)$$

where

$$\tan\alpha_i = \frac{1-\nu}{\nu_u - \nu}\alpha_i \qquad c = \frac{2\kappa B^2 G(1-\nu)\,(1+\nu_u)^2}{9\,(1-\nu_u)\,(\nu_u-\nu)}.$$

We employ a 10x40 triangular mesh, under a plane strain formulation of the problem. The constitutive parameters are defined by shear modulus $G = 1\,\mathrm{MPa}$, fluid density $\rho_f = 1000\,\mathrm{kg\,m^{-3}}$ and spatial permeability $\kappa = 1\,\mathrm{m^3\,s\,kg^{-1}}$, and Biot's coefficient $\alpha = 1$. As previously stated in **??**, the suggested HEE formulation can be applied to represent both the compressible or incompressible fluid scenarios. Getting advantage of this, the problem is investigated in both of the incompressible and compressible fluid condition, for which the value of ν_u is fixed respectively at 0.5 and 0.4, while the value of ν_d is maintained equal to 0.2. To enable accurate comparisons with the analytical expression of pore pressure, all quantities have been normalised. In Figure 8,

the displayed data corresponds to the adimensional times $t^* = 1$, 0.5, 0.2, 0.1 and 0.01, according to the expression defined in [33]:

$$t^* = t\frac{kG}{a^2}\left[\frac{2}{3}\frac{B}{\alpha}\frac{1+\nu_u}{1-\nu_u}\frac{1-\nu_d}{1-2\nu_d}\right]. \tag{173}$$

The blue line represents the analytical solution, while the orange dots represent the values obtained through the proposed formulation. The results indicate a significant correspondence with the analytical solution. A similar agreement between results and the analytical solution is also observed in the study of the system considering the fluid phase as compressible, as illustrated in Figure 8.

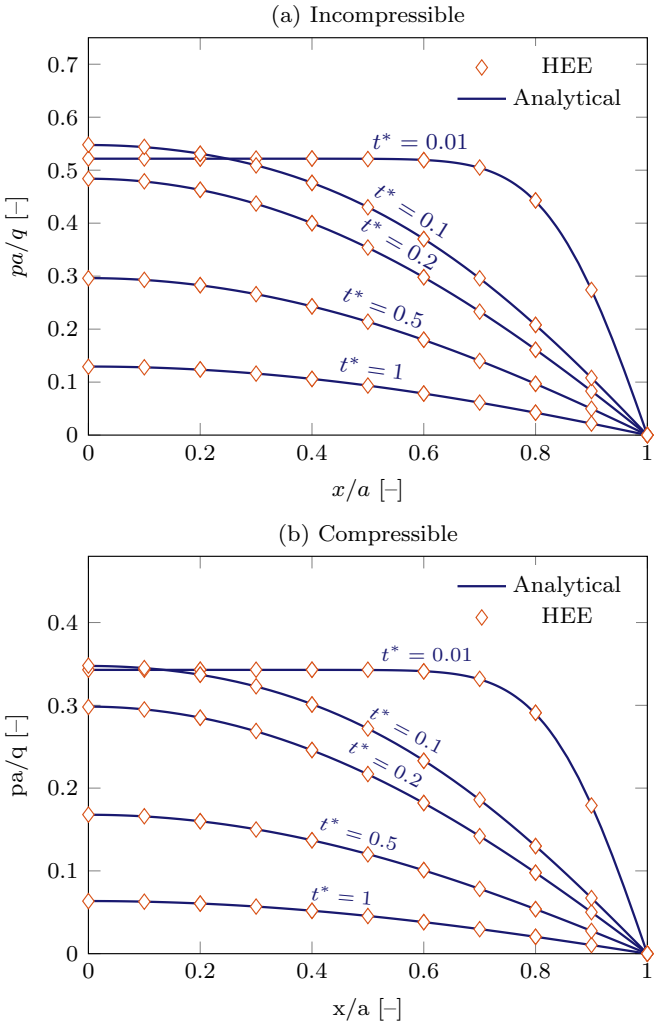

Figure 8: Mandel's problem. Comparison of the HEE solution (markers) for fluid pressure p with analytical solution (solid lines) by Cheng and Detounray [33] at non-dimensional times $t^* = 0.01$, $t^* = 0.1$, $t^* = 0.2$, $t^* = 0.5$, $t^* = 1$, for the incompressible (a) and compressible (b) fluid phase.

3.4.3 *Booker's consolidation problem*

The consolidation problem introduced by Booker and small [23] is formulated to model surface footings situated on horizontally layered soils on a rigid base. As reported in [64], the problem involves an infinite finite depth strip subjected to periodic uniform loading. Due to symmetry of the problem, the region modelled is restricted to the one depicted in Figure 9. As boundary conditions for the system, the horizontal displacement and the shear stress are enforced to be null at the sides,

i.e. $u_x(0,y) = u_x(B,y) = 0$, $\tau_{xy}(0,y) = \tau_{xy}(B,y) = 0$. The bottom is considered fixed, implying that both the horizontal and vertical displacements are constrained $u_x(x,0) = u_y(x,0) = 0$. The top surface is assumed to be permeable by imposing a pressure value $p(x,h) = 0$, with an applied normal traction load of $q = 1\,\mathrm{MN\,s^{-2}}$ for the length $0 < x < b$.

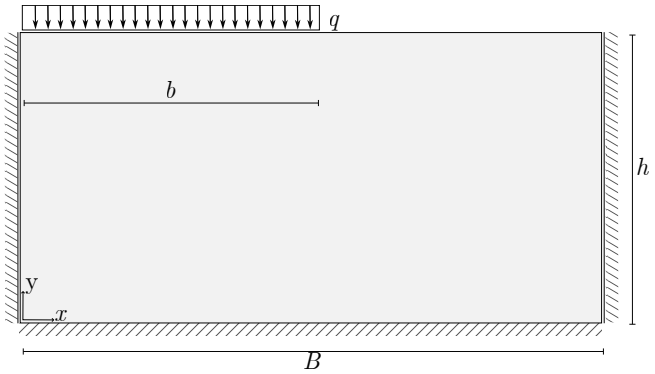

Figure 9: Consolidation problem. A rectangular plate of dimensions B and h, with impermeable bottom and side surfaces and a fully drained top surface, on which a uniformly distributed mechanical load q is placed over length b.

The constitutive parameters are characterised by shear modulus $G = 1\,\mathrm{MPa}$, fluid density $\rho_f = 1000\,\mathrm{kg\,m^{-3}}$ and spatial permeability $\kappa = 1\,\mathrm{m^3\,s\,kg^{-1}}$, drained Poisson's coefficient $\nu_d = 0.3$ and Biot's coefficient $\alpha = 1$. The geometry is modelled using two mesh consisting of a) 10×10 elements and b) 10×10 elements, while the geometric ratio for $(B : b)$ is considered to be 2:1.
To assess the quality of the results through mesh refinement, contour plots for pressure and vertical stress were generated for two meshes with a dimension of 10×10 (a) and 30 x 30 (b) Hybrid equilibrium element with quadratic stress and pressure fields at the adimensionalised time [64] $t^* = 2 \cdot 10^{-6}$.
As depicted in Figure 10 and Figure 11, the pressure and vertical stress trends do not exhibit numerical oscillations, demonstrating the stability and accuracy of the employed method. Notably, even using the coarser mesh, the system's behaviour is captured accurately, without encountering jumps or discontinuities in the results, even at relatively low mesh resolutions.

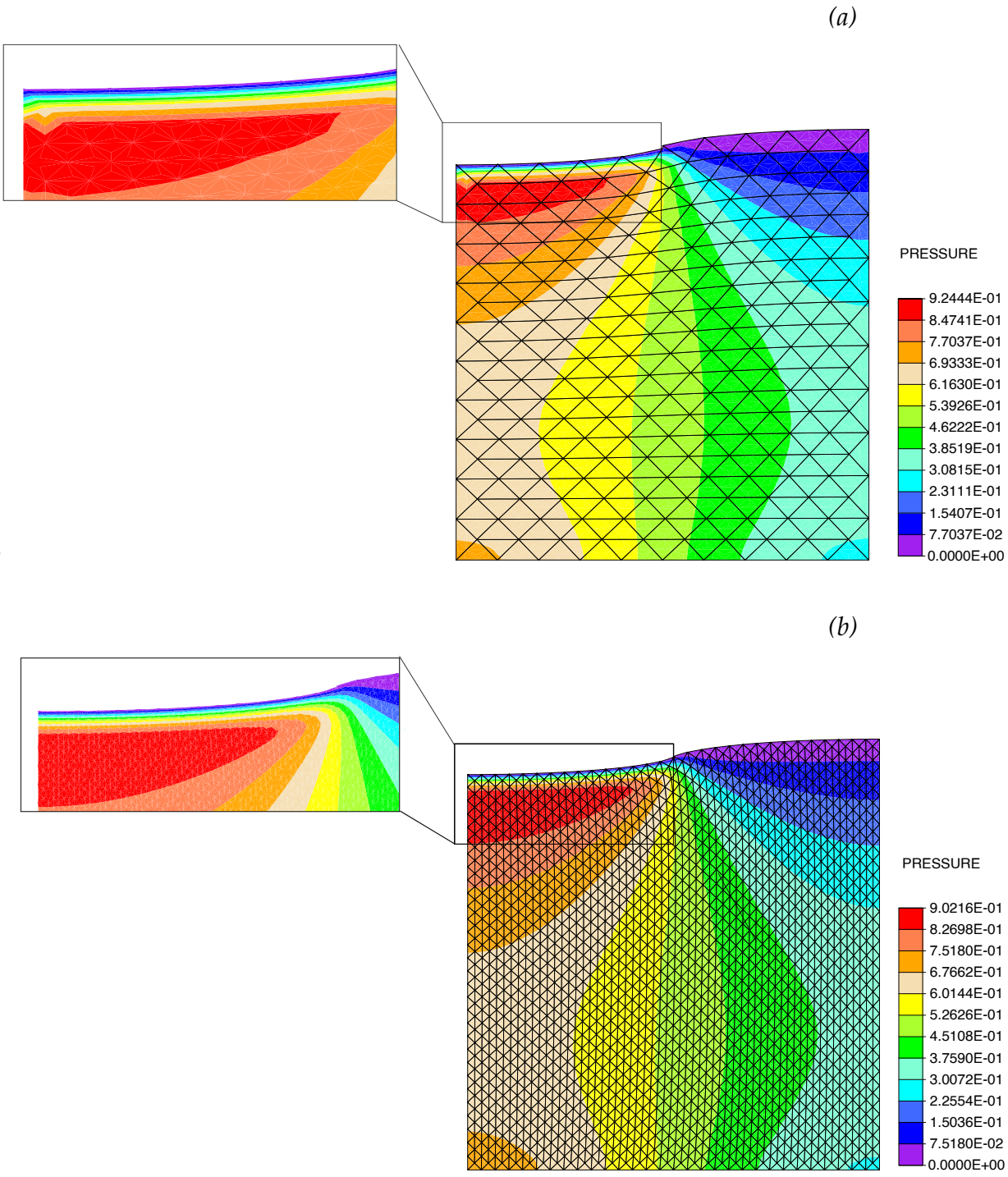

Figure 10: Consolidation problem. Pore pressure map plot for the hybrid equilibrium element with quadratic stress and pressure fields at the adimensionalised time $t^* = 2 \cdot 10^{-6}$, with meshes of 10 × 10 (a) and 30 x 30 (b) elements.

Although, as evident in Figure 10 (a), spurious modes in the displacement field arise for the coarser mesh, an occurrence intrinsic to this formulation, this limitation can be effectively mitigated through h-refinement, as depicted in Figure 10 (b).

(a)

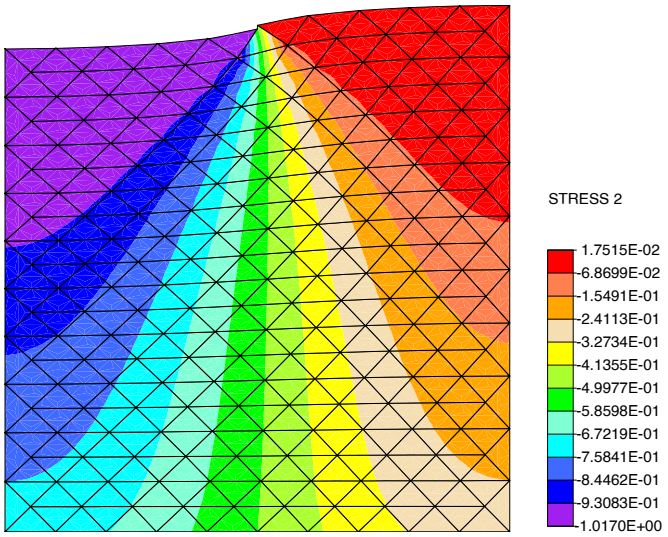

(b)

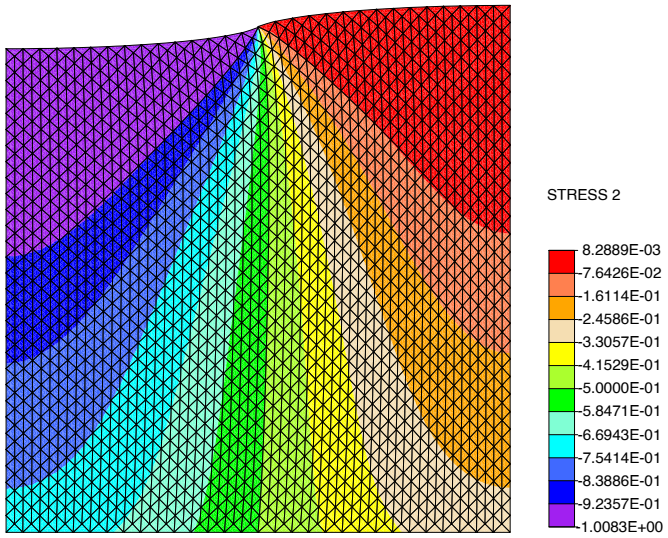

Figure 11: Consolidation/Footing problem. Contour plot for y-stress for an hybrid equilibrium element with quadratic stress and pressure fields at the adimensionalised time $t^* = 2 \cdot 10^{-6}$, with meshes of 10 × 10 (a) and 30 x 30 (b) elements.

The resulting dimensionless pore pressure behaviour at the left line versus depth at adimensional time value is illustrated in fig Figure 12, in which the drained con-

dition is represented by the blue lines, while the undrained condition is shown in red. Notably, for very early time steps, the values of instantaneous pore pressure in the drained condition collapse to — by imposing the same constitutive parameters — with those in the undrained condition. This observation is consistent with the expectations outlined in Terzaghi's problem. Starting from the adimensional time $t^* = 0.012$, a monotonic trend emerges. The Mandel-Cryer effect is evident as the pressure initially increases at the top and subsequently decreases with time, eventually reaching zero.
Numerical oscillations in pore pressure constitute a critical issue for this benchmark problem. In this regard, the pore pressure trend results from the proposed formulation (shown in blue) are compared with the corresponding trend derived by a canonical Q9/Q4 element employing Taylor Hood interpolation for stabilisation (in red), for the adimensionalised time $t^* = 2 \cdot 10^{-6}$ [120]. While notable reductions in comparison to those achieved with the Q9/Q4 element [59] are observed, the Q9/Q4 TH element still manifests spurious oscillations in the pressure trend for a sufficiently adimensionalised time $t^* = 2 \cdot 10^{-6}$. In contrast, the pressure trend obtained through the element introduced in this investigation, based on a minimization formulation, demonstrates an absence of oscillations, even under extremely small time steps. As the process progresses to later time steps, all examined finite element formulations ultimately converge to the same fluid pore pressure trend.

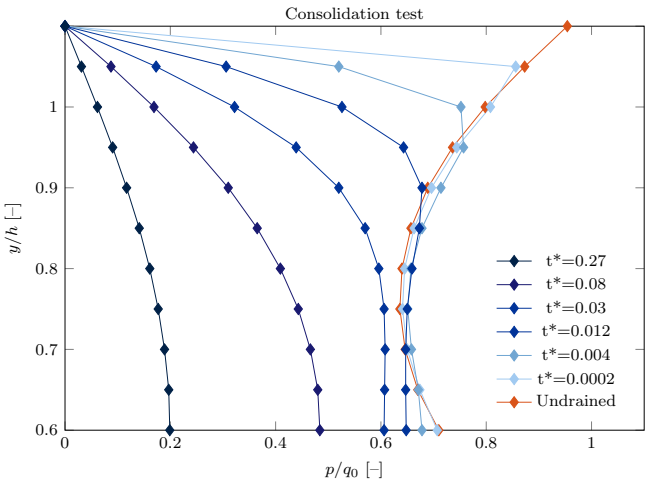

Figure 12: Consolidation problem. adimensionalised fluid pore pressure p versus adimensionalised depth y/h of the body at $x = -B/2$ for adimensional times $t^* = 0.0002$, $t^* = 0.004$, $t^* = 0.012$, $t^* = 0.03$, $t^* = 0.08$, $t^* = 0.27$.

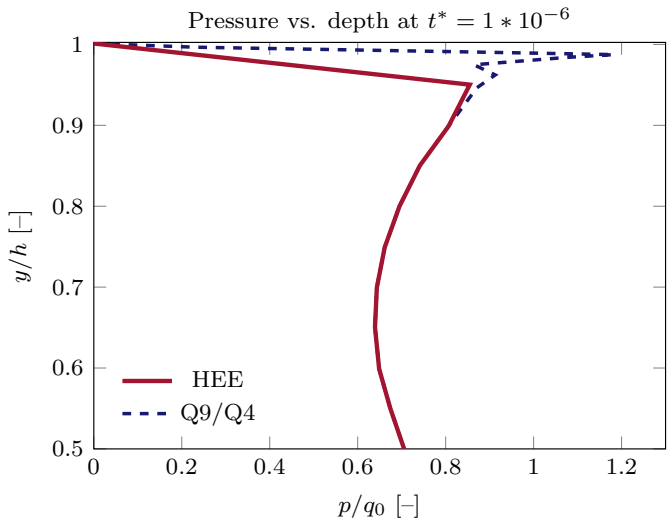

Figure 13: Consolidation problem. adimensionalised fluid pore pressure p versus adimensionalised depth y/h of the body at $x = -B/2$ for adimensional time $t^* = 2 \cdot 10^{-6}$. Comparison of HEE (in red) and Q9/Q4 with Taylor-Hood interpolation (in blue) results.

3.5 CONCLUSIONS AND FUTURE PERSPECTIVES

In this paper, a novel stress/pressure-based Hybrid Equilibrium Element (HEE) for the transient analysis of the of poroelastic materials systems is introduced.

The main result of the present paper is the extension to poroelestic problem of the HEE approaches, which have been already applied to linear elasticity [93, 95] and non linear fracture mechanics problems [94].

As a first step a specific variational principle is introduced and the related stationarity conditions investigated. The adoped continuum variational princple is emploied to derive a variationally consistent finite element discretization. A novel triangulat HEE is deveoped and implemented in FEAP, a open source finite element software [134]. The main drawback is probably the implementation of the proposed HEE formulation, which could be quite difficult in commercial FE programs, compared to the standard displacement based or mixed elements.

The formulation has been validated through a comparative analysis of three classic benchmark problems in poromechanics: the Terzaghi's problem, the Mandel's problem and the footing problem. The obtained results confirmed the validity of the proposed approach. In particular, as expected from the variational derivation and the symmetry of the matrix system in Eq. (169), the responses do not display nonphysical fluctuations in pore pressure trend, which can likely occur in classic $u-p$ formulation. Remarkably, no stabilisation algorithm was necessary for the element development. Moreover, the

proposed formulation offers significant benefits by ensuring the continuity of stresses and pressures, which are critical in engineering applications.

A significant feature emerging from the numerical applications is the high stress accuracy of the proposed HEE approach, even adopting relative coarse meshes. This feature is particularly useful for the analysis of problems where high stress gradient are displayed.

A significant improvement of the proposed formulation would be the non trivial extension to the finite deformation context, opening the proposed approach to applications in biological porous media, where non-linear strains are widely expected. Moreover, in biomechanical problems an accurate stress distribution is of paramount relevance.

Generalising the proposed approach to finite deformations may involve tackling the inversion of the constitutive law, an area that remains relatively unexplored and, where feasible, could introduce theoretical and computational complexities. In fact, inversion of the constitutive law could be not uniquely defined, either globally or locally, and the complementary potential funtional could not always ensure a minimum energy state. Nevertheless, innovative methodologies, such as the one proposed by Ogden [90], could pave the way for overcoming this challenge, without directly inverting the constitutive law.

Ανω κατω παντα.

— ***Ancient Greek saying***

4

A HYBRID FLUX-PRESERVING FINITE ELEMENT FOR COUPLED FLOW DEFORMATION: LINEAR FORMULATION

[1]

4.1 INTRODUCTION

In the previous chapter, the development of an Hybrid Equilibrium finite element (HEE) for linear poroelasticity was thoroughly discussed, demonstrating its capability to deliver highly accurate solutions for the primary fields of stress and pressure. However, one inherent limitation of the HEE formulation lies in the need to invert the constitutive law of the solid, an operation that may be difficult or not straightforward to perform in a finite-strain setting [89]. As an alternative, a novel variational approach, introduced by Miehe, Mauthe, and Teichtmeister [82] and subsequently refined in Teichtmeister, Mauthe, and Miehe [121], relies on the selection of fluid fluxes and solid deformation as primary variables of the poroelastic problem, leading to a minimization principle that inherently circumvents the classical inf-sup condition, thereby ensuring a more robust numerical framework. The numerical stability of the resulting finite element discretization critically depends on the choice of functional spaces, particularly for the representation of the flux field. The use of Raviart-Thomas (RT0) elements [103] provides a conforming discretization of the fluid flux in the functional space $H(\mathrm{div}, \mathcal{B})$, ensuring inter-element continuity of the normal fluxes. However, this choice comes at the expense of a significantly increased number of degrees of freedom and a higher computational cost. Conversely, a Q1-Q1 discretization, while computationally more efficient, is afflicted by discontinuities in the normal components of the flux across adjacent elements, leading to non-physical oscillations in pressure and velocity fields, and volumetric locking in nearly-incompressible fluids, which can only be mitigated through reduced integration schemes [121].

1 Substantial parts of the material presented in this chapter have been extracted and adapted from: Lo Franco, S., Terzano,M., Borino, G., Holzapfel,G.A. and Parrinello*, F. *"A hybrid flux-preserving finite element for coupled flow deformation: Linear formulation"*, CMAME, 2025.[73]

Building upon the paradigm of HEEs and inspired by Miehe's minimization principle [82], the present study introduces a hybrid flux-based formulation for the quasi-static analysis of poroelastic media. The proposed approach departs from classical HEEs (for which we refer to Moitinho de Almeida and Maunder [83]) by adopting the flux field as the primary unknown, with the fluid potential serving as a Lagrange multiplier to ensure continuity of the normal flux across elements and circumvent globally the requirement of defining conforming function spaces. This new formulation retains all the advantages of hybrid approaches, while including the solid deformation field as a primary variable. Notably, the necessity of enforcing inter-element flux continuity, although mathematically rigorous, can become excessively restrictive in the presence of material discontinuities or rapid spatial variations in physical properties [97]. By ensuring weak continuity, the hybrid approach alleviates such limitations, avoiding the numerical instabilities typically encountered in conventional formulations, ensuring stability at the local level and improving the overall numerical conditioning of the system compared to traditional mixed formulations. This strategy is particularly beneficial for problems where permeability discontinuities induce pressure singularities. In such scenarios, conventional mixed formulations based on the displacement-pressure variable pair fail to enforce local continuity, leading to non-physical oscillations [132]. The proper choice of function spaces ensures the well-posedness of the system, preserving the advantages of the hybrid approach [4]. Despite introducing additional degrees of freedom, the method remains computationally efficient by leveraging local condensation of flux variables and reducing globally coupled unknowns. Moreover, it provides a well-conditioned system suitable for iterative solvers, as the hybrid framework naturally leads to symmetric and well-conditioned linear systems [28, 98]. Finally, the structure of the formulation enables an efficient reduction of the global system, ultimately leading to a computationally efficient scheme in which the primary unknowns remain the nodal displacements.

This chapter is organized into the following sections. Section 4.2 provides a detailed description of the flux-based formulation of poroelasticity, summarizing the fundamental equations and thermodynamic background of the theory in a linear setting. After recalling the minimization principle of poroelasticity developed by Miehe, Mauthe, and Teichtmeister [82], Sec. 5.3.1 introduces the novel Hybrid Flux Element (HFE) formulation, whose performance is assessed in Sec. 4.4 for a selection of benchmark problems. Lastly, Sec. 4.5 summarizes the key findings of the study and discusses future extensions.

4.2 CANONICAL FORM OF POROELASTICITY

Addressing the boundary-value problem of a saturated solid undergoing a deformation process requires the introduction of appropriate variables to develop a consistent framework. Several choices are available for selecting the primary variables, each lead-

ing to distinct formulations and corresponding sets of boundary conditions. In the following, the specific choice adopted in this work, leading to the canonical two-field minimization principle developed by Miehe, Mauthe, and Teichtmeister [82], is presented.

4.2.1 *Primary fields*

A poroelastic solid is described as a homogenized continuous body $\mathcal{B}$ in which a flux of interstitial fluid mass can occur through convective transport. As usual in continuum mechanics, it is convenient to introduce a time-independent reference configuration of $\mathcal{B}$, denoted with $\mathcal{B}_0$, such that a particle in the continuous body is represented by a material point $\mathbf{X} \in \mathcal{B}_0$ [61]. A homogenization procedure is carried out at the mesoscale, such that at each material point the particles of the solid skeleton and of the interstitial fluid are indistinguishable. In the classical poroelastic theory, the homogenization is based on the definition of an *effective porosity* field $\phi_0(\mathbf{X}, t) \in (0, 1]$, which assigns to each volume element dV the volume of interconnected pores $dV_f = \phi\, dV$ filled by fluid [32, Sec. 4.1.1].

In poroelasticity, kinematics is referred to the solid, implying that motion and related quantities are measured with respect to the configuration of the solid skeleton [40]. The motion of the solid in a time interval $\mathcal{T} = (0, t) \subset \mathbb{R}_+$ is described by the vector-valued *deformation* field $\boldsymbol{\chi} : \mathcal{B}_0 \times \mathcal{T} \to \mathbb{R}^3$, which assigns to each material point $\mathbf{X} \in \mathcal{B}_0$ and time $t \in \mathcal{T}$ a place $\mathbf{x} \in \mathcal{B}_t$, with $\mathcal{B}_t = \boldsymbol{\chi}_t(\mathcal{B})$ representing the current configuration at time t. The deformation gradient tensor $\mathbf{F} = \nabla_{\mathbf{X}}\boldsymbol{\chi}(\mathbf{X}, t)$, defined as the tangent to the deformation of the solid, transforms material tangent vectors onto spatial tangent vectors. Its determinant $J = \det \mathbf{F} > 0$ measures the transformation of an infinitesimal volume element dV in the reference configuration to dv in the current configuration. The *displacement* field $\mathbf{u} : \mathcal{B}_0 \times \mathcal{T} \to \mathbb{R}^3$ and its material gradient $\nabla_{\mathbf{X}}\mathbf{u} = \mathbf{F} - \mathbf{I}$, where $\mathbf{I}$ is the second-order identity tensor, complete the list of fundamental kinematic quantities [61].

To describe the fluid phase, consistently with the classical literature on poroelasticity, we employ the *variation in fluid mass content* $m : \mathcal{B}_0 \times \mathcal{T} \to \mathbb{R}$ introduced by Biot [18], representing the increase of interstitial fluid mass per unit reference volume of the poroelastic solid [82, Eq. $(6)_1$]. Through the equation of continuity for a control volume of the poroelastic solid, this is related to the *fluid mass flux* $\mathbf{H} : \mathcal{B}_0 \times \mathcal{T} \to \mathbb{R}^3$ (see Sec. 5.2.2).

In the following, the presentation is adapted to the framework of the classical infinitesimal strain theory, for consistency with the subsequent sections of this article. The reader is referred to Miehe, Mauthe, and Teichtmeister [82] and Teichtmeister, Mauthe, and Miehe [121] for a thorough presentation of the poroelastic formulation in the finite deformation setting. Hereafter, we assume a linearization around the reference configuration $\mathcal{B}_0$ and characterize the deformation by introducing the *infinitesimal*

strain tensor $\boldsymbol{\varepsilon} = \nabla^{s}_{\mathbf{x}}\mathbf{u}$, representing the symmetric part of the displacement gradient [61]. Consistently with the linearized theory, the configuration of the continuum body is denoted simply by $\mathcal{B}$ and the operator $\nabla(\bullet)$ drops the subscript.

4.2.2 *Governing equations*

The fundamental governing equations of a linear poroelastic solid are the balances of mass, momentum and energy, in addition to constitutive equations for the solid and the interstitial fluid [32, Ch. 6]. In this section, these are briefly reviewed in order to ensure a consistent use of notation throughout the article. Some aspects of thermodynamical consistency of the poroelastic theory are also recalled. For the sake of clarity, the connection with corresponding fields and equations adopted in the classical theory of porous media and related frameworks is presented, when deemed necessary.

To avoid unnecessary complications, the system is considered to be isothermal and mass-conservative, implying the absence of internal sources or sinks; furthermore, no chemical interaction between the constituents is allowed. Under these assumptions, the balance of mass reduces to the continuity equation of the fluid phase [39]. Considering an arbitrary region of the continuum body $\mathcal{P} \subset \mathcal{B}$ and denoting with $\mathbf{n}$ the outward unit normal to its boundary $\partial\mathcal{P}$, we define the fluid mass flux $\mathbf{h} : \mathcal{B} \times \mathcal{T} \to \mathbb{R}^3$, such that $\mathbf{h} \cdot \mathbf{n}$ measures the mass of fluid leaving $\partial\mathcal{P}$ per unit area and per unit time. The conservation of mass of the fluid in $\mathcal{P}$ takes then the following local form (see Remark 6)

$$\dot{m} + \nabla \cdot \mathbf{h} = 0 \quad \text{on } \mathcal{B} \times \mathcal{T}\,. \tag{174}$$

The balance of linear and angular momentum while neglecting inertial effects results in the relationships

$$\nabla \cdot \boldsymbol{\sigma} + \rho\mathbf{b} = \mathbf{0}\,, \quad \boldsymbol{\sigma} = \boldsymbol{\sigma}^{T} \quad \text{on } \mathcal{B} \times \mathcal{T}\,, \tag{175}$$

where $\mathbf{b}$ is the vector of body forces per unit mass, $\rho = \varphi\rho_f + (1-\varphi)\rho_s$ is the density of the poroelastic solid, and $\boldsymbol{\sigma}$ is the *total* Cauchy stress tensor (see Remark 8).

The local equations (174),(175) must be supplemented by appropriate boundary and initial conditions. In particular, the boundary $\partial\mathcal{B}$ of a poroelastic body (Fig. 14) is partitioned into portions on which essential and natural boundary conditions for the mechanical and hydraulic fields are prescribed, namely

$$\partial\mathcal{B} = \partial\mathcal{B}^{u} \cup \partial\mathcal{B}^{t} = \partial\mathcal{B}^{h} \cup \partial\mathcal{B}^{\mu}\,, \tag{176}$$

where the intersections $\partial\mathcal{B}^{u} \cap \partial\mathcal{B}^{t}$ and $\partial\mathcal{B}^{h} \cap \partial\mathcal{B}^{\mu}$ both consist of empty sets. Consistently with the choice of primary variables presented in Sec. 4.2.1, essential boundary

conditions prescribe values of the displacement field $\mathbf{u}$ on $\partial\mathcal{B}^u$, whereas the normal component of the fluid flux $\mathbf{h}$ is prescribed on $\partial\mathcal{B}^h$, leading to

$$\mathbf{u} = \bar{\mathbf{u}} \quad \text{on } \partial\mathcal{B}^u \times \mathcal{T}, \qquad \mathbf{h}\cdot\mathbf{n} = \bar{h} \quad \text{on } \partial\mathcal{B}^h \times \mathcal{T}, \tag{177}$$

where $\bar{\mathbf{u}}$ and $\bar{h}$ denote the prescribed displacement and normal fluid flux, respectively.

The respective natural boundary conditions refer to the traction vector $\mathbf{t}$ and the fluid potential μ (see Remark 7), which are specified on $\partial\mathcal{B}^t$ and $\partial\mathcal{B}^\mu$, respectively:

$$\boldsymbol{\sigma}\cdot\mathbf{n} = \bar{\mathbf{t}} \quad \text{on } \partial\mathcal{B}^t \times \mathcal{T}, \qquad \mu = \bar{\mu} \quad \text{on } \partial\mathcal{B}^\mu \times \mathcal{T}, \tag{178}$$

with $\bar{\mathbf{t}}$ and $\bar{\mu}$ representing the prescribed traction and fluid potential.

Finally, the initial conditions assign $\mathbf{u}(\mathbf{x},0) = \mathbf{0}$ and $m(\mathbf{x},0) = 0$ in $\mathcal{B}\times\{0\}$, implying that the porous medium is initially in an undeformed reference configuration, with no excess fluid content.

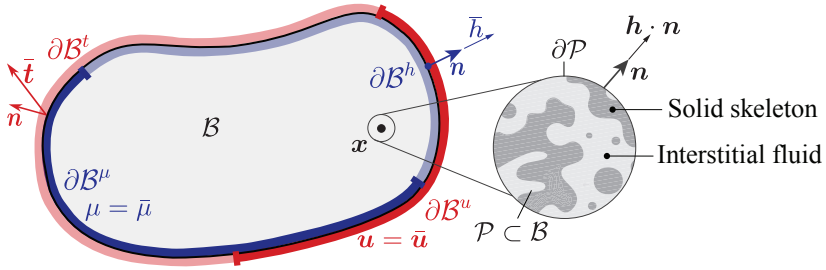

Figure 14: Sketch of a linear poroelastic body, showing the boundary conditions and the control volume on which the continuity of the fluid phase is imposed.

Remark 6. The conservation of mass for the fluid in Eq. (174) is presented in a form which is typical of poroelastic theories, where the elementary volume is treated as an open system [32]. Starting from the general mass balances in a saturated biphasic mixture, let m_f and m_s denote, respectively, the mass of fluid and solid phases, which we can express in the spatial setting as [72],

$$m_f = \int_{\mathcal{B}_t} \varphi\rho_f \, dv, \quad m_s = \int_{\mathcal{B}_t} (1-\varphi)\rho_s \, dv, \tag{179}$$

where ρ_f, ρ_s are the true mass densities of the constituents, i.e., mass of a single phase per unit volume of that phase, and $\varphi = J^{-1}\phi$ is the Eulerian porosity [39]. The conservation of mass of the fluid phase, written with respect to the motion of the solid skeleton, provides [40, Eq. (57)]

$$\frac{dm_f}{dt} = \frac{d}{dt}\int_{\mathcal{B}_t} \varphi\rho_f \, dv = 0 \quad \rightarrow \quad \frac{d(\varphi\rho_f)}{dt} + \varphi\rho_f \nabla\cdot\dot{\mathbf{u}} + \nabla\cdot(\varphi\rho_f \boldsymbol{w}) = 0, \tag{180}$$

where $\dot{\mathbf{u}} \equiv \dot{\mathbf{u}}_s$ is the velocity of the solid and $\boldsymbol{w} = \dot{\mathbf{u}}_f - \dot{\mathbf{u}}$ is the *discharge velocity*, representing the relative velocity of the fluid with respect to the solid skeleton. With $\mathbf{H} = J\mathbf{F}^{-1}\mathbf{h} = J\mathbf{F}^{-1}\varphi\rho_f\boldsymbol{w}$, the continuity equation $(180)_2$ can be expressed in a Lagrangian setting as [40, Eq. (58)]

$$\frac{dm}{dt} + \nabla_X \cdot \mathbf{H} = 0\,, \tag{181}$$

where $m(\mathbf{X}, t) = \phi\rho_f - \phi_0\rho_{f,o}$. This represents the fluid mass variation in the control volume $\mathcal{P}$, starting from time $t = 0$, and is positive if the mass is added. In the linearized setting, Eq. (181) equalizes to Eq. (174), i.e., $\mathbf{H} \equiv \mathbf{h}$.

The continuity equation of linear poroelasticity is expressed as in Biot [17, Eq. (4.3)]

$$\dot{\zeta} + \nabla \cdot \mathbf{j} = 0 \tag{182}$$

where ζ is the variation of the fluid content (amount of fluid volume entering $\mathcal{P}$ per unit volume) and $\mathbf{j}$ is the volumetric fluid flux. These quantities can be related to the corresponding mass-based variables [107] through

$$\zeta = \frac{m}{\rho_f}\,, \quad \mathbf{j} = \frac{\mathbf{h}}{\rho_f} = \varphi\boldsymbol{w}\,. \tag{183}$$

Remark 7. The evolution $\dot{m}$ of the fluid mass content is governed by the fluid chemical potential μ, which, in the case of a barotropic fluid, is related to the pressure p and the fluid density ρ_f through the relation [121]

$$\mu = \frac{p}{\rho_f}\,. \tag{184}$$

4.2.3 *Thermodynamic consistency*

In a dissipative system, a finite set of generalized fluxes $(\dot{\varepsilon}, \dot{m})$, and their conjugate forces (σ, μ) govern the dissipation rate, which must be non-negative according to the principle of irreversibility [38, 54, 91]. Denoting with ψ the Helmholtz free-energy function of the poroelastic solid, the dissipation rate $\mathcal{D}$ can be formally written as [82, Eq. (14)]

$$\mathcal{D} = \boldsymbol{\sigma} : \dot{\boldsymbol{\varepsilon}} + \mu\,\dot{m} - \dot{\psi} - \nabla\mu \cdot \mathbf{h} \geqslant 0\,, \tag{185}$$

which naturally decomposes into two distinct contributions, i.e., an intrinsic (local) contribution and a transport-related contribution. The intrinsic dissipation rate can be expressed as

$$\mathcal{D}_{\text{int}} = \boldsymbol{\sigma} : \dot{\boldsymbol{\varepsilon}} + \mu\,\dot{m} - \dot{\psi} \geqslant 0\,, \tag{186}$$

depending exclusively on the variables that define the free energy of the elementary system, where the local balance is established. At equilibrium, it characterizes the dis-

sipation rate associated with internal irreversible processes, vanishing in the absence of local dissipative mechanisms. On the other hand, the transport-related dissipation is related to the mass transport of the fluid phase, namely

$$\mathcal{D}_{\text{tr}} = -\nabla\mu \cdot \mathbf{h} \geqslant 0\,. \tag{187}$$

The formulation of constitutive equations must be consistent with the Clausius-Duhem inequality (185) and the fundamental principles of frame invariance [56]. Accordingly, the Helmholtz free-energy function $\psi = \hat{\psi}(\boldsymbol{\varepsilon}, m)$ stored at a point $\mathbf{x} \in \mathcal{B}$ of the poroelastic solid is defined in terms of the infinitesimal strain tensor $\boldsymbol{\varepsilon}$ and the variation in fluid mass content m [18, Eq. (2.5)]. From (186), the following constitutive relationships for the total Cauchy stress tensor and the fluid potential are derived

$$\boldsymbol{\sigma} = \partial_{\boldsymbol{\varepsilon}}\hat{\psi}(\boldsymbol{\varepsilon}, m)\,, \quad \mu = \partial_{m}\hat{\psi}(\boldsymbol{\varepsilon}, m)\,. \tag{188}$$

The inequality in Eq. (187), pertaining to the transport-related dissipation, is satisfied by choosing a convex dissipation potential function $\hat{\phi}(\mathbf{h})$ in the space of the fluid mass fluxes $\mathbf{h}$, such that [82]

$$\nabla\mu = -\partial_{\mathbf{h}}\hat{\phi}(\mathbf{h})\,. \tag{189}$$

In the framework of a kinematically linear theory, under the assumption of normal dissipative mechanisms, linear elastic solid skeleton and ideal fluid, the free-energy function and the dissipation potential assume the following quadratic forms [121, Eq. (43)]

$$\hat{\psi}(\boldsymbol{\varepsilon}, m) = \tfrac{1}{2}\,\boldsymbol{\varepsilon} : \mathbb{C} : \boldsymbol{\varepsilon} + \tfrac{M}{2}(\alpha\,\mathrm{tr}\,\boldsymbol{\varepsilon} - \tfrac{m}{\rho_f})^2\,, \quad \hat{\phi}(\mathbf{h}) = \tfrac{1}{2}\mathbf{h} \cdot (\rho_f^2\boldsymbol{\kappa})^{-1}\mathbf{h}\,, \tag{190}$$

where $\mathbb{C}$ denotes the elasticity tensor of the poroelastic solid, α and M represent Biot's coefficient and modulus, respectively, and $\boldsymbol{\kappa}$ is a constant, symmetric and positive-definite second-order *permeability* tensor [32]. In case of isotropy, $\boldsymbol{\kappa} = \kappa\mathbf{I}$.

The governing equations of the coupled deformation-fluid-transport problem, formulated in terms of the primary variables $\mathbf{u}$ and m, with the related boundary conditions, are summarized in (191).

Compatibility equation	$\boldsymbol{\varepsilon} = \nabla^{s}\mathbf{u}$	in $\mathcal{B}$	
Balance of mass	$\dot{m} + \nabla \cdot \mathbf{h} = 0$	in $\mathcal{B}$	
Balance of linear momentum	$\nabla \cdot \boldsymbol{\sigma} + \rho \mathbf{b} = \mathbf{0}$	in $\mathcal{B}$	
Balance of angular momentum	$\boldsymbol{\sigma} = \boldsymbol{\sigma}^{T}$	in $\mathcal{B}$	
Constitutive total stresses	$\boldsymbol{\sigma} = \partial_{\varepsilon}\hat{\psi}(\boldsymbol{\varepsilon}, m)$	in $\mathcal{B}$	
Constitutive fluid potential	$\mu = \partial_{m}\hat{\psi}(\boldsymbol{\varepsilon}, m)$	in $\mathcal{B}$	(191)
Constitutive fluid potential gradient	$\nabla\mu + \partial_{\mathbf{h}}\hat{\phi}(\mathbf{h}) = \mathbf{0}$	in $\mathcal{B}$	
Prescribed displacement	$\mathbf{u} = \bar{\mathbf{u}}$	on $\partial\mathcal{B}^{u}$	
Prescribed fluid potential	$\mu = \bar{\mu}$	on $\partial\mathcal{B}^{\mu}$	
Prescribed tractions	$\boldsymbol{\sigma} \cdot \mathbf{n} = \bar{\mathbf{t}}$	on $\partial\mathcal{B}^{t}$	
Prescribed normal fluxes	$\mathbf{h} \cdot \mathbf{n} = \bar{h}$	on $\partial\mathcal{B}^{h}$	

Remark 8. The stress tensor and fluid potential can be derived explicitly from (188) using the free-energy function provided in $(190)_1$:

$$\boldsymbol{\sigma} = \partial_{\varepsilon}\hat{\psi}(\boldsymbol{\varepsilon}, m) = \mathbb{C} : \boldsymbol{\varepsilon} + \alpha M(\alpha \operatorname{tr}\boldsymbol{\varepsilon} - \tfrac{m}{\rho_f})\mathbf{I}\,, \tag{192}$$

$$\mu = \partial_{m}\hat{\psi}(\boldsymbol{\varepsilon}, m) = -\tfrac{M}{\rho_f}(\alpha \operatorname{tr}\boldsymbol{\varepsilon} - \tfrac{m}{\rho_f})\,. \tag{193}$$

For isotropy and an ideal barotropic fluid, these equations are equivalent to the classical ones proposed by Biot [17]. The free-energy function can be written as

$$\tilde{\psi}(\boldsymbol{\varepsilon}, \zeta) = \tfrac{K}{2}(\operatorname{tr}\boldsymbol{\varepsilon})^2 + G(\boldsymbol{\varepsilon}^{dev} : \boldsymbol{\varepsilon}^{dev}) + \tfrac{M}{2}(\alpha \operatorname{tr}\boldsymbol{\varepsilon} - \zeta)^2\,, \tag{194}$$

where the deviatoric infinitesimal strain tensor is $\boldsymbol{\varepsilon}^{dev} = \mathbb{p} : \boldsymbol{\varepsilon} = \boldsymbol{\varepsilon} - \frac{\operatorname{tr}\boldsymbol{\varepsilon}}{3}\mathbf{I}$ and the elasticity tensor is expressed as $\mathbb{C} = K\mathbb{I}^{sym} + 2G\mathbb{p}$, where $\mathbb{p}$ is the fourth-order projection tensor [61]. The material parameters appearing in (194) are the *drained* bulk modulus of the poroelastic solid K [105] and the shear modulus G, whereas ζ is the variation in fluid content introduced in $(183)_1$. The elastic constants are related through the well-known relationship $K = 2G(1+\nu)/[3(1-2\nu)]$, where ν is the *drained* Poisson's coefficient. Recalling (184) for the pressure p of a barotropic fluid, we obtain

$$\boldsymbol{\sigma} = 2G\boldsymbol{\varepsilon} + (K - \tfrac{2}{3}G)\operatorname{tr}\boldsymbol{\varepsilon}\mathbf{I} + \alpha M(\alpha \operatorname{tr}\boldsymbol{\varepsilon} - \zeta)\,\mathbf{I} = \partial_{\varepsilon}\tilde{\psi}(\boldsymbol{\varepsilon}, \zeta)\,, \tag{195}$$

$$p = -M(\alpha \operatorname{tr}\boldsymbol{\varepsilon} - \zeta) = \partial_{\zeta}\tilde{\psi}(\boldsymbol{\varepsilon}, \zeta)\,. \tag{196}$$

Equation (195) clearly shows that the total stress tensor, appearing in the momentum balance (175), is the sum of an *effective* stress tensor $\boldsymbol{\sigma}'$, associated with the deformation

of the poroelastic solid, and a *pore pressure* term $p\mathbf{I}$, associated with the ideal interstitial fluid [20, 32]. Therefore, we can write

$$\boldsymbol{\sigma} = \boldsymbol{\sigma}' - \alpha p \mathbf{I}\,, \qquad \boldsymbol{\sigma}' = 2G\boldsymbol{\varepsilon} + (K - \tfrac{2}{3}G)\,\mathrm{tr}\,\boldsymbol{\varepsilon}\mathbf{I}\,, \quad p = -M(\alpha\,\mathrm{tr}\,\boldsymbol{\varepsilon} - \tfrac{m}{\rho_f})\,. \tag{197}$$

At this point, it should be clear that this decomposition, empirically introduced by Terzaghi, is by definition a constitutive assumption resulting from an additive form of the free-energy function of the poroelastic solid [82]. The relevant case of $\alpha = 1$ corresponds to true incompressibility of the solid phase, recovering the original effective stress principle by Terzaghi. Biot's modulus simplifies to $M = K_f/\varphi$, where K_f is the bulk modulus of the fluid [32]. The additional constraint $1/M = 0$ enforces incompressibility of the fluid phase, and in such a case the pressure p assumes the meaning of a Lagrange multiplier.

The dissipation potential in $(190)_2$ can be used to obtain the work conjugate force to the fluid mass flux from (257). Then we have

$$\nabla\mu = -\partial_{\mathbf{h}}\hat{\phi}(\mathbf{h}) = -(\rho_f^2\boldsymbol{\kappa})^{-1}\mathbf{h} \quad \rightarrow \quad \mathbf{h} = -\rho_f^2\boldsymbol{\kappa}\nabla\mu\,, \tag{198}$$

which for isotropy and using $(183)_2$ in combination with (184), is equivalent to the classical Darcy law [32]

$$\varphi\boldsymbol{w} = -\kappa\rho_f\nabla p\,. \tag{199}$$

The permeability coefficient in (199) can be related to the *hydraulic conductivity* k through the expression $\kappa = k/(\rho_f|\mathbf{g}|)$, where $|\mathbf{g}|$ is the magnitude of the gravitational acceleration.

4.3 HYBRID FORMULATION OF POROELASTICITY

In this section, we first recall the canonical minimization principle of poroelasticity, derived from a rate-type variational principle formulated for the primary variables introduced in Sec. 4.2.1. Then, the novel hybrid variational principle, developed starting from the same choice of primary fields in the discretized domain, is introduced and elaborated.

4.3.1 *Canonical minimization principle of poroelasticity*

A rate-type variational principle developed by Miehe, Mauthe, and Teichtmeister [82], governing the coupled poroelastic boundary-value problem, can be derived directly from the stored energy and dissipation functionals presented in Sec. 4.2.3. Based on the displacement vector $\mathbf{u}$ and fluid mass flux $\mathbf{h}$, a canonical minimization principle can be formulated, circumventing the need to explicitly satisfy the inf-sup condition associated with saddle-point formulations [121].

At a given state $\{\mathbf{u}, \mathbf{h}, m\}$, the following *rate potential* is postulated [82, Eq. (33)]

$$\dot{\bar{\Pi}}(\dot{\mathbf{u}}, \mathbf{h}, \dot{m}) = \int_{\mathcal{B}} \pi(\dot{\boldsymbol{\varepsilon}}, \mathbf{h}, \dot{m})\, dv - \mathcal{P}_{\text{ext}}(\dot{\mathbf{u}}, \mathbf{h})\,, \tag{200}$$

where π is the internal rate potential per unit volume, taking the form

$$\pi(\dot{\boldsymbol{\varepsilon}}, \mathbf{h}, \dot{m}) = \dot{\hat{\psi}}(\boldsymbol{\varepsilon}, m) + \hat{\phi}(\mathbf{h}) \tag{201}$$

with $\dot{\hat{\psi}} = \partial_{\boldsymbol{\varepsilon}} \hat{\psi} : \dot{\boldsymbol{\varepsilon}} - \partial_m \hat{\psi}\, (\nabla \cdot \mathbf{h})$, and $\mathcal{P}_{\text{ext}}$ is the external power. If body forces are neglected, the latter is provided by the surface tractions $\bar{\mathbf{t}}$ and by the fluid mass transport across the surface related to a prescribed fluid potential $\bar{\mu}$ [82, Eq. (30)].

A time-discrete form of (267) is obtained by considering a finite time interval $[t_n, t_{n+1}]$, with a time step $\Delta t = t_{n+1} - t_n > 0$, and assuming that all field variables are known at time t_n. Accordingly to an implicit scheme, the flux continuity equation (174) is integrated in time as

$$m^{(n+1)} = m^{(n)} - \Delta t\, \nabla \cdot \mathbf{h}^{(n+1)}\,. \tag{202}$$

This approach inherently maintains consistency with the continuous dissipation structure, as established in Miehe, Mauthe, and Teichtmeister [82]. By directly incorporating the continuity equation into the energy functional over the time step Δt, the resulting canonical *incremental variational principle* depends exclusively on the two primary fields, $\mathbf{u}$ and $\mathbf{h}$, as outlined in Teichtmeister, Mauthe, and Miehe [121, Eqs. (28)-(30)]:

$$\begin{aligned}
&\bar{\Pi}^{\Delta t}(\mathbf{u}^{(n+1)}, \mathbf{h}^{(n+1)}) = \\
&\int_{\mathcal{B}} \pi^{\Delta t}(\boldsymbol{\varepsilon}^{n+1}, \mathbf{h}^{(n+1)}, m^{(n+1)})\, dv - \mathcal{P}_{\text{ext}}^{\Delta t}(\mathbf{u}^{(n+1)}, \mathbf{h}^{(n+1)}) \\
&= \int_{\mathcal{B}} \hat{\psi}(\boldsymbol{\varepsilon}^{(n+1)}, m^{(n+1)}) - \underbrace{\hat{\psi}\left(\boldsymbol{\varepsilon}^{(n)}, m^{(n)}\right)}_{\hat{\psi}^{(n)}} + \Delta t\ \hat{\phi}\left(\mathbf{h}^{(n+1)}\right) dv \\
&- \mathcal{P}_{\text{ext}}^{\Delta t}(\mathbf{u}^{(n+1)}, \mathbf{h}^{(n+1)}) \\
&= \int_{\mathcal{B}} \hat{\psi}(\boldsymbol{\varepsilon}^{(n+1)}, \underbrace{m^{(n)} - \Delta t\ \nabla \cdot \mathbf{h}^{(n+1)}}_{m^{(n+1)}}) - \hat{\psi}^{(n)} + \Delta t\, \hat{\phi}\left(\mathbf{h}^{(n+1)}\right) dv \\
&- \int_{\partial \mathcal{B}^t} \bar{\mathbf{t}}^{(n+1)} \cdot \left(\mathbf{u}^{(n+1)} - \mathbf{u}^{(n)}\right) ds + \Delta t \int_{\partial \mathcal{B}^\mu} \bar{\mu}^{(n+1)}\, \mathbf{h}^{(n+1)} \cdot \mathbf{n}\, ds.
\end{aligned} \tag{203}$$

The incremental two-field minimization principle [121, Eq. (31)]

$$\{\mathbf{u}, \mathbf{h}\} = \operatorname{Arg}\left\{ \inf_{\mathbf{u} \in \mathcal{V}_{\mathbf{u}}} \inf_{\mathbf{h} \in \mathcal{V}_{\mathbf{h}}} \bar{\Pi}^{\Delta t}(\mathbf{u}, \mathbf{h}) \right\} \tag{204}$$

determines the displacement vector and fluid mass flux vector at the current time t_{n+1}.

Although the variational principle here summarized provides a rigorous and thermodynamically consistent framework for modeling porous media, some challenges may arise in the discretization of the fluid flux field. The space of admissible displacements $\mathcal{V}_{\mathbf{u}}$ is a subset of the Sobolev space $\mathbf{H}^1(\mathcal{B})$, and therefore can be classically approximated with piecewise C^0 continuous polynomial functions. On the other hand, admissible fluid fluxes are part of the space $\mathcal{V}_{\mathbf{h}} \subset H(\mathrm{div}, \mathcal{B})$, the latter being the space of functions whose divergence is square integrable in $\mathcal{B}$, and requires a piecewise approximation that ensure inter-element continuity of normal traces [29]. The original discretization of the incremental principle (270) employs RTo elements [121], which have polynomial vector functions, ensuring piecewise constant divergence and the continuity of the normal components of the flux across adjacent elements. While this choice ensures mathematical consistency, it entails a large number of degrees of freedom, thereby leading to a high computational cost. Moreover, enforcing strict inter-element continuity conditions, while mathematically appealing, can become overly restrictive when the medium exhibits discontinuities or rapid spatial variations in its physical properties [58]. In the next section, the incremental principle is modified according to the hybrid formulations, which relaxes the continuity constraint on the flux field by introducing independent inter-element Lagrange multipliers [97]. This way, we ensure co-diffusivity, i.e., the resultant flux has continuous normal component between two sides of contiguous elements, while the continuity of the tangential component is not enforced.

4.3.2 *Hybrid variational principle of poroelasticity*

Let us consider a discretization ${}^{h}\mathcal{B} = \bigcup_{e=1}^{N_e} \mathcal{B}_e$ of the two-dimensional domain $\mathcal{B} \subset \mathbb{R}^2$ of a linear poroelastic body with N_e non-overlapping subdomains $\mathcal{B}_e$, each with a boundary $\partial\mathcal{B}_e$. This boundary is partitioned into S_e sides $\partial\mathcal{B}_e^s$, such that $\partial\mathcal{B}_e = \bigcup_{s=1}^{S_e} \partial\mathcal{B}_e^s$. Each element side $\partial\mathcal{B}_e^s$ belongs to either the subset of free boundaries $\partial\mathcal{B}_e^s \subset (\partial\mathcal{B}^t \cup \partial\mathcal{B}^h)$, the subset of constrained boundaries $\partial\mathcal{B}_e^s \subset (\partial\mathcal{B}^u \cup \partial\mathcal{B}^\mu)$, or to the internal boundary shared by two subdomains, denoted by $\partial\mathcal{B}^{\mathrm{int}\,s} \equiv \partial\mathcal{B}_{e_1}^s \cap \partial\mathcal{B}_{e_2}^s$, where $e_1 \neq e_2$.

Within the discretized domain, the displacement field ${}^{h}\mathbf{u}$ is prescribed to be continuous, as customary in classical finite element formulations. In contrast, the flux field ${}^{h}\mathbf{h}$ belongs to a finite-dimensional subspace of mass fluxes that are continuous and satisfy mass conservation *locally* within each subdomain. Therefore, the divergence-conformity must be imposed by introducing a Lagrange multiplier λ_e^s at the element

edges $s = 1, \dots, S_e$. Incorporating the imposed constraint into (267), a *hybrid rate* functional is formulated

$$
\begin{aligned}
{}^{h}\bar{\Pi}(\dot{\mathbf{u}}, \mathbf{h}, \dot{m}, \lambda) = \sum_{e=1}^{N_e} \left(\int_{\mathcal{B}_e} \pi\left(\dot{\boldsymbol{\varepsilon}}_e, \dot{m}_e, \mathbf{h}_e\right) \, dv - \mathcal{P}_{\text{ext}}\left(\dot{\mathbf{u}}_e, \mathbf{h}_e\right) \right. \\
\left. + \sum_{s=1}^{S_e} \left[\int_{\partial \mathcal{B}_e^s / \partial \mathcal{B}_e^\mu} \lambda_e^s \left(\mathbf{h}_e \cdot \mathbf{n}_e^s - \bar{h} \right) \, ds \right] .
\end{aligned}
\tag{205}
$$

with $\bar{\mathbf{h}}$ the prescribed flux vector, being null everywhere except on $\partial \mathcal{B}^h$. The positive sign of the term containing the Lagrange multipliers is adopted to ensure that all terms consistently represent the negative of the external power. This structure ensures a well-posed discretization, provided that the stability conditions outlined by Brezzi [28] are satisfied.

4.3.2.1 *Incremental form*

To derive the variational principle, we consider the time-discrete counterpart of the functional (272) by recalling the implicit update presented in (269). Expressing the internal rate potential $\pi = \hat{\dot{\psi}}(\boldsymbol{\varepsilon}_e, \nabla \cdot \mathbf{h}_e) + \hat{\phi}(\mathbf{h}_e)$ with the specific expressions given in (190) within the functional (272) leads to the following *incremental hybrid* functional:

$$
\begin{aligned}
&{}^{h}\bar{\Pi}^{\Delta t}\left(\boldsymbol{\varepsilon}^{(n+1)}, \mathbf{h}^{(n+1)}, \lambda^{(n+1)}\right) = \\
&\sum_{e=1}^{N_e} \left(\int_{\mathcal{B}_e} \frac{1}{2} \boldsymbol{\varepsilon}_e^{(n+1)} : \mathbb{C}_e : \boldsymbol{\varepsilon}_e^{(n+1)} \, dv - \int_{\mathcal{B}_e} \frac{1}{2} \boldsymbol{\varepsilon}_e^{(n)} : \mathbb{C}_e : \boldsymbol{\varepsilon}_e^{(n)} \, dv \right. \\
&+ \int_{\mathcal{B}_e} \frac{M}{2} \left[\alpha \mathbf{I} : \boldsymbol{\varepsilon}_e^{(n+1)} - \frac{\left(m_e^{(n)} - \Delta t \, \nabla \cdot \mathbf{h}_e^{(n+1)} \right)}{\rho_f} \right]^2 dv - \int_{\mathcal{B}_e} \frac{M}{2} \left[\alpha \mathbf{I} : \boldsymbol{\varepsilon}_e^{(n)} - \frac{m_e^{(n)}}{\rho_f} \right]^2 dv \\
&+ \Delta t \int_{\mathcal{B}_e} \frac{1}{2} \mathbf{h}_e^{(n+1)} \cdot \left(\rho_f^2 \boldsymbol{\kappa} \right)^{-1} \mathbf{h}_e^{(n+1)} \, dv - \int_{\partial \mathcal{B}_e^t} \bar{\mathbf{t}}^{(n+1)} \cdot \left(\mathbf{u}_e^{(n+1)} - \mathbf{u}_e^{(n)} \right) \, ds \\
&+ \Delta t \int_{\partial \mathcal{B}_e^\mu} \bar{\mu}^{(n+1)} \, \mathbf{h}_e^{(n+1)} \cdot \mathbf{n}_e \, ds \\
&\left. + \Delta t \sum_{s=1}^{S_e} \left[\int_{\partial \mathcal{B}_e^s / \partial \mathcal{B}_e^\mu} \lambda_e^{s\,(n+1)} \left(\mathbf{h}_e^{(n+1)} \cdot \mathbf{n}_e^s - \bar{h}^{(n+1)} \right) \, ds \right] .
\end{aligned}
\tag{206}
$$

We define the functional spaces to which the field variations ${}^h\delta\mathbf{u}$, ${}^h\delta\mathbf{h}$, ${}^h\delta\lambda$ belong (see Remark 9):

$$
\begin{aligned}
&{}^h\mathcal{W}_u = \{{}^h\delta u \in H^1(B_0) |\, {}^h\delta u = 0 \quad \text{on } \partial B^u,\} \\
&{}^h\mathcal{W}_{\mathbf{h}}^{\text{disc}} = \left\{ {}^h\delta\mathbf{h} \in [L^2(\mathcal{B})]^d \,\middle|\, {}^h\delta\mathbf{h}|_{\mathcal{B}_e} \in \mathbb{P}_k(\mathcal{B}_e;\mathbb{R}^d),\ {}^h\delta\mathbf{h}\cdot\mathbf{n} = 0 \text{ on } \partial\mathcal{B}^h,\ \forall\, \mathcal{B}_e \in {}^h\mathcal{B} \right\}, \\
&{}^h\mathcal{W}_{\delta\lambda,l} = \left\{ {}^h\delta\lambda \in L^2(\partial\mathcal{B}) \,\middle|\, {}^h\delta\lambda|_{\partial\mathcal{B}_e^s} \in \mathbb{P}_l(\partial\mathcal{B}_e^s),\ {}^h\delta\lambda = 0 \text{ on } \partial\mathcal{B},\ \forall\, \partial\mathcal{B}_e^s \subset {}^h\partial\mathcal{B}^s \right\},
\end{aligned}
\tag{207}
$$

The stationarity of the functional ${}^h\bar{\Pi}^{\Delta t}$ at time t_{n+1}, with respect to primary and Lagrangian variables, leads to the following Euler equations for the subdomain $\mathcal{B}_e$:

Stress equilibrium	$\nabla\cdot(\partial_\varepsilon\hat{\psi}) = 0$	in $\mathcal{B}_e$	
Inverse Darcy law	$\nabla\left(\partial_m\hat{\psi}\right) + \partial_h\hat{\phi} = 0$	in $\mathcal{B}_e$	
Prescribed tractions	$\partial_\varepsilon\hat{\psi}\cdot\mathbf{n} - \bar{\mathbf{t}} = 0$	on $\partial\mathcal{B}_e^t$	
Prescribed fluid potential	$-\partial_m\hat{\psi} + \bar{\mu} = 0$	on $\partial\mathcal{B}_e^\mu$	(208)
Lagrangian variable	$-\partial_m\hat{\psi} + \lambda^s = 0$	on $\partial\mathcal{B}_e^s/\partial\mathcal{B}_e^\mu$	
Prescribed normal fluxes	$\mathbf{h}\cdot\mathbf{n}^s - \bar{h} = 0$	on $\partial\mathcal{B}_e^s \cap \partial\mathcal{B}_e^h$	
Inter-element continuity	$\mathbf{h}_{e_1}\cdot\mathbf{n}_{e_1}^s + \mathbf{h}_{e_2}\cdot\mathbf{n}_{e_2}^s = 0$	on $\partial\mathcal{B}^{\text{int}\,s}$	

Notably, as shown by $(208)_5$, the Lagrange multiplier λ^s emerges as the fluid potential field μ^s, with $\mu^s = \bar{\mu}$ on $\partial\mathcal{B}_e^s \cap \partial\mathcal{B}_e^\mu$. Once this correspondence between the fluid potential field and the Lagrange variable is established, the functional space adopted for λ^s coincides with that of the fluid potential field itself (see Remark 9).

Remark 9. The space of admissible displacements ${}^h\mathbf{u}$ is a finite-dimensional subspace of the Sobolev space $\mathbf{H}^1(\mathcal{B})$, defined as

$$
{}^h\mathcal{V}_\mathbf{u} = \left\{ {}^h\mathbf{u} \in [H^1(\mathcal{B})]^d \,\middle|\, {}^h\mathbf{u} = \bar{\mathbf{u}} \text{ on } \partial\mathcal{B}^u \right\}, \tag{209}
$$

where d is the spatial dimension. The local approximation of the flux field ${}^h\mathbf{h}$ on each element $\mathcal{B}_e$ belongs to a discontinuous finite-dimensional space, i.e.

$$
{}^h\mathcal{H}_k^{\text{disc}} = \left\{ {}^h\mathbf{h} \in [L^2(\mathcal{B})]^d \,\middle|\, {}^h\mathbf{h}|_{\mathcal{B}_e} \in \mathbb{P}_k(\mathcal{B}_e;\mathbb{R}^d),\ \forall\, \mathcal{B}_e \in {}^h\mathcal{B} \right\}, \tag{210}
$$

where $\mathbb{P}_k(\mathcal{B}_e;\mathbb{R}^d)$ contains polynomials of total degree $\leqslant k$ on the element ${}^h\mathcal{B}_e$. This choice allows the flux to be discontinuous across element interfaces, thus removing the global $H(\text{div})$-conformity requirement [35, 55]. In other words, ${}^h\mathbf{h}$ does not neces-

sarily belong to $H(\mathrm{div}, \mathcal{B})$, which would instead require the continuity of the normal components of the flux across interfaces.

To enforce the divergence-conformity of the fluid fluxes at the element interfaces, the hybridization procedure introduces an independent set of Lagrange multipliers ${}^{h}\mu \in {}^{h}\mathcal{V}_{\mu}$, defined on each element side $\partial\mathcal{B}_e^s \in {}^{h}\partial\mathcal{B}$. The associated finite-dimensional space is

$$ {}^{h}\mathcal{V}_{\mu,l} = \left\{ {}^{h}\mu \in L^2(\partial\mathcal{B}) \;\middle|\; {}^{h}\mu|_{\partial\mathcal{B}_e^s} \in \mathbb{P}_l(\partial\mathcal{B}_e^s),\ {}^{h}\mu = \bar{\mu} \text{ on } \partial\mathcal{B}^{\mu},\ \forall\, \partial\mathcal{B}_e^s \subset {}^{h}\partial\mathcal{B} \right\}, \quad (211) $$

where $\mathbb{P}_l(\partial\mathcal{B}_e^s)$ denotes the space of polynomials of total degree $\leqslant l$ on the element side $\partial\mathcal{B}_e^s$.

4.3.2.2 *Stationarity of the hybrid incremental functional*

Following the classical notation of hybrid formulations, we express the functional presented in (206) as ${}^{h}\bar{\Pi}^{\Delta t} = \sum_{e=1}^{N_e} \bar{\Pi}_e^{\Delta t}$. The stationarity of the hybrid incremental functional is computed with respect to the primary variables $\mathbf{u}, \mathbf{h}$ defined in $\mathcal{B}_e$ and the Lagrange multipliers λ_e^s defined over the boundaries $\partial\mathcal{B}_e^s$, at time $t = t_{n+1}$. For better readability, the indices e and $n+1$ are not shown in the following.

$$ \begin{aligned} &\partial_{u_i} {}^{h}\bar{\Pi}^{\Delta t} = 0 \\ &\quad \rightarrow \quad \sum_{e=1}^{N_e} \left[\int_{\mathcal{B}_e} \left[C_{ijkl}\, \varepsilon_{kl} + \alpha M (\alpha \varepsilon_{ii} - \tfrac{m}{\rho_f}) \delta_{ij} \right] \delta\varepsilon_{ij}\, dv - \int_{\partial\mathcal{B}_e^t} \bar{t}_i\, \delta u_i\, ds \right] = 0, \end{aligned} \quad (212) $$

where $\delta\varepsilon_{ij} = \frac{1}{2}(\delta u_{i,j} + \delta u_{j,i})$, with δu_i an admissible virtual displacement satisfying $\delta u_i = 0$ on $\partial\mathcal{B}_e^u$ at time t_{n+1}.

Applying the divergence theorem, we obtain

$$ \begin{aligned} &\sum_{e=1}^{N_e} \left[- \int_{\mathcal{B}_e} \left[C_{ijkl}\, \varepsilon_{kl} + \alpha M (\alpha \varepsilon_{ii} - \tfrac{m}{\rho_f}) \delta_{ij} \right]_{,j} \delta u_i\, dv \right. \\ &\left. + \int_{\partial\mathcal{B}_e} \left[C_{ijkl}\, \varepsilon_{kl} + \alpha M (\alpha \varepsilon_{ii} - \tfrac{m}{\rho_f}) \delta_{ij} \right] n_j \delta u_i\, ds - \int_{\partial\mathcal{B}_e^t} \bar{t}_i\, \delta u_i\, ds \right] = 0, \end{aligned} \quad (213) $$

where the bracketed expressions in the integrals are equal to $\partial\hat{\psi}/\partial\varepsilon_{ij}$, from which we obtain the following Euler equations as

$$ -\left(\frac{\partial\hat{\psi}}{\partial\varepsilon_{ij}} \right)_{,j} = 0 \quad \text{in } \mathcal{B}_e, \qquad \frac{\partial\hat{\psi}}{\partial\varepsilon_{ij}} n_j - \bar{t}_i = 0 \quad \text{on } \partial\mathcal{B}_e^t. $$

As the field $\mathbf{h}_e$ is independently defined within each element domain, the stationarity condition with respect to h_i can be formulated directly at the element level:

$$\begin{aligned}
&\partial_{h_i}\bar{\Pi}_e^{\Delta t} = 0 \\
&\quad\rightarrow\quad \Delta t\int_{\mathcal{B}_e}\frac{M}{\rho_f}\left(\alpha\varepsilon_{ii}-\frac{m^{(n)}-\Delta t\, h_{i,i}}{\rho_f}\right)\delta h_{i,i}\,dv+\Delta t\int_{\mathcal{B}_e}\rho_f^{-2}\kappa_{ij}^{-1}h_j\,\delta h_i\,dv \\
&\qquad +\Delta t\int_{\partial\mathcal{B}_e^{\mu}}\bar{\mu}n_i\,\delta h_i\,ds+\Delta t\sum_{e=1}^{S_e}\int_{\partial\mathcal{B}_e^{s}/\partial\mathcal{B}_e^{\mu}}\lambda^s n_i^s\,\delta h_i\,ds=0\,,
\end{aligned} \tag{214}$$

where δh_i is an admissible virtual fluid flux that satisfies $\delta h_i\, n_i = 0$ on $\partial\mathcal{B}_e^h$ at time t_{n+1}. Applying the divergence theorem, we obtain

$$\begin{aligned}
&-\Delta t\int_{\mathcal{B}_e}\left[\frac{M}{\rho_f}\left(\alpha\varepsilon_{ii}-\frac{m^{(n)}-\Delta t\, h_{i,i}}{\rho_f}\right)\right]_{,i}\delta h_i\,dv+\Delta t\int_{\partial\mathcal{B}_e}\left[\frac{M}{\rho_f}\left(\alpha\varepsilon_{ii}-\frac{m^{(n)}-\Delta t\, h_{i,i}}{\rho_f}\right)\right]n_i\delta h_i\,ds \\
&+\Delta t\int_{\mathcal{B}_e}\underbrace{\rho_f^{-2}\kappa_{ij}^{-1}h_j}_{\partial_{h_i}\hat{\phi}}\,\delta h_i\,dv+\Delta t\int_{\partial\mathcal{B}_e^{\mu}}\bar{\mu}\,n_i\,\delta h_i\,ds+\sum_{e=1}^{S_e}\int_{\partial\mathcal{B}_e^{s}/\partial\mathcal{B}_e^{\mu}}\lambda^s n_i^s\,\delta h_i\,ds=0\,,
\end{aligned} \tag{215}$$

where the expression in brackets is equal to $-\partial\hat{\psi}/\partial m$. Thus, the Euler equations and the natural boundary condition are obtained as

$$\begin{aligned}
\left(\frac{\partial\hat{\psi}}{\partial m}\right)_{,i}+\frac{\partial\hat{\phi}}{\partial h_i}=0 \quad &\text{in } \mathcal{B}_e\,, \\
-\frac{\partial\hat{\psi}}{\partial m}+\bar{\mu}=0 \quad &\text{on } \partial\mathcal{B}_e^{\mu}\,, \\
-\frac{\partial\hat{\psi}}{\partial m}+\lambda^s=0 \quad &\text{on } \partial\mathcal{B}_e^{s}/\partial\mathcal{B}_e^{\mu}\,.
\end{aligned} \tag{216}$$

Finally, by imposing the stationarity with respect to the Lagrange multiplier λ^s we get

$$\begin{aligned}
&\partial_{\lambda^s}{}^h\bar{\Pi}^{\Delta t} = 0 \\
&\quad\rightarrow\quad \sum_{e=1}^{N_e}\left[\Delta t\sum_{s=1}^{S_e}\int_{\partial\mathcal{B}_e^{s}}h_i n_i\,\delta\lambda^s\,ds-\int_{\partial\mathcal{B}_e^{s}}\bar{h}\,\delta\lambda^s\,ds\right]=0\,,
\end{aligned} \tag{217}$$

where $\delta\lambda^s$ is an admissible virtual Lagrange multiplier that satisfies $\delta\lambda^s = 0$ on $\partial\mathcal{B}_e^{\mu}\cap\partial\mathcal{B}_e^{s}$ at time t_{n+1}. The following boundary and inter-element conditions are obtained as

$$\begin{aligned}
h_i n_i-\bar{h}=0 \quad &\text{on } \partial\mathcal{B}_e^{s}\cap\partial\mathcal{B}_e^{h}\,, \\
(h_i n_i)_{e_1}-(h_i n_i)_{e_2}=0 \quad &\text{on } \partial\mathcal{B}_e^{\text{int}\,s}\equiv\partial\mathcal{B}_{e_1}^{s}\cap\partial\mathcal{B}_{e_2}^{s}\,.
\end{aligned} \tag{218}$$

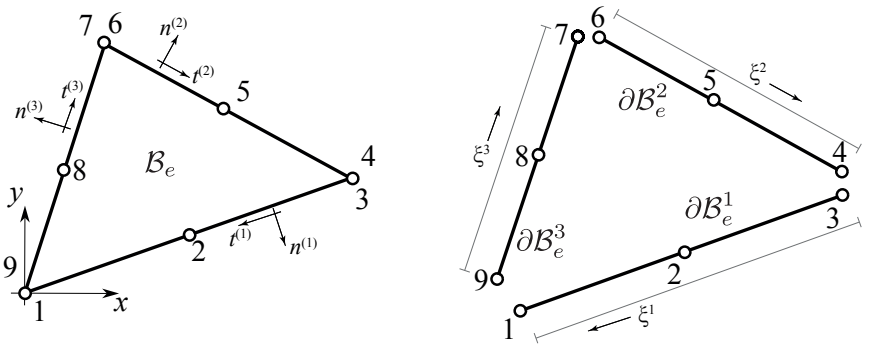

Figure 15: Nine-node triangular hybrid flux element over which the fluid fluxes and the Lagrangian fluid potential variables are approximated. The displacement field is interpolated over an overlapped isoparametric six-node quadratic triangular element.

4.3.2.3 *Discretized form*

We proceed now by introducing the interpolation of the primary variable $\{\mathbf{u}_e, \mathbf{h}_e\}$ and of the Lagrange multipliers μ_e^s. Unlike conventional finite elements, the proposed HFE defines the flux field directly in terms of a set of Cartesian polynomial functions, whose coefficients – denoted as *generalized flux variables* – constitute the fundamental unknowns of the fluid-related problem. In this study, a quadratic triangular finite element, oriented according to a local Cartesian reference frame (x, y) with its origin positioned at vertex 1, is adopted (Fig. 15). The flux fields are thus expressed in terms of second-order polynomial expansions, formally defined as

$$h_{e,x}(x,y) = a_1 + a_2 x + a_3 y + a_4 xy + a_5 x^2 + a_6 y^2 \,, \tag{219}$$

$$h_{e,y}(x,y) = a_7 + a_8 x + a_9 y + a_{10} xy + a_{11} x^2 + a_{12} y^2 \,, \tag{220}$$

$$\nabla \cdot \mathbf{h}_e(x,y) = a_2 + a_4 y + 2a_5 x + a_9 + a_{10} x + 2a_{12} y \,, \tag{221}$$

where the coefficients $a_n, n = 1, \ldots, 12$ represent the generalized flux variables, while $\nabla \cdot \mathbf{h}_e(x,y)$ defines the local divergence of the flux field. In accordance with this description, the representation of the generalized flux field in terms of the polynomial coefficients can be expressed in matrix notation as

$$\mathbf{h}_e(\mathbf{x}) = \mathbf{H}_e(\mathbf{x})\mathbf{h}_e \,, \tag{222}$$

where $\mathbf{H}_e(\mathbf{x})$ is the coefficient matrix and $\mathbf{h}_e$ collects all generalized flux variables.

The fluid potential variables at the element sides $\partial\mathcal{B}_e^s$, with $s = 1, \ldots, 3$, playing the role of Lagrangian variables, are represented using an isoparametric mapping of the form

$$\mu_e^s(\xi^s) = \overline{\mathbf{N}}(\xi^s)\boldsymbol{\mu}_e^s \,, \tag{223}$$

where $\overline{\mathbf{N}}$ collects the quadratic shape functions and $\boldsymbol{\mu}_e^s$ the fluid potential degrees of freedom of side $\partial\mathcal{B}_e^s$.

Finally, the displacement field is expressed by classical quadratic shape functions in the natural coordinates (η_1, η_2). The geometrically coincident nodes at the vertices are constrained through the use of a local connectivity matrix. We obtain the following interpolations

$$\mathbf{u}_e(\boldsymbol{\eta}) = \mathbf{N}_e(\boldsymbol{\eta})\mathbf{u}_e\,, \quad \boldsymbol{\varepsilon}_e(\boldsymbol{\eta}) = \mathbf{B}_e(\boldsymbol{\eta})\mathbf{u}_e\,, \tag{224}$$

where $\mathbf{N}$ collects the shape functions associated with nodal displacements, $\mathbf{u}_e$ the element displacement degrees of freedom, and $\mathbf{B}_e$ is the strain-displacement matrix. It should be noted that, in the framework of the proposed hybrid formulation, nodal degrees of freedom are intrinsically associated with element sides, allowing two adjacent elements to share the nodes along their common edge. As a direct consequence, the spatial discretization induced by HFEs results in multiple coincident nodes at a shared vertex between different elements, whereas mid-side nodes remain distinct. Accordingly, in the adopted quadratic formulation, the fluid potential field is discretized over a total of nine nodes per element, with each vertex hosting two geometrically coincident nodes, as depicted in Fig. 15. This choice allows the formulation to effectively satisfy the boundary and inter-element continuity equations [93].

Inserting the above-mentioned approximating functions into (206) leads to the time- and space-discrete formulation of the incremental hybrid functional in Voigt notation, in which, for the sake of notational clarity, the superscript $n+1$ is omitted and will be consistently dropped hereafter:

$$\begin{aligned}
{}^{h}\bar{\Pi}^{\Delta t} = \sum_{e=1}^{N_e} \Bigg[& \tfrac{1}{2}\mathbf{u}_e^T \int_{\mathcal{B}_e} \mathbf{B}_e^T \mathbf{C}_e \mathbf{B}_e \, dv \, \mathbf{u}_e + \tfrac{1}{2}\mathbf{u}_e^T \int_{\mathcal{B}_e} \mathbf{B}_e^{*T} \alpha^2 M \, \mathbf{B}_e^* \, dv \, \mathbf{u}_e \\
& - \mathbf{u}_e^T \int_{\mathcal{B}_e} \mathbf{B}_e^{*T} \tfrac{\alpha M}{\rho_f} m_e^{(n)} \, dv + \mathbf{u}_e^T \int_{\mathcal{B}_e} \mathbf{B}_e^{*T} \tfrac{\alpha M}{\rho_f} \Delta t \, \mathbf{H}_e^* \, dv \, \mathbf{h}_e \\
& - \mathbf{h}_e^T \int_{\mathcal{B}_e} \mathbf{H}_e^{*T} \tfrac{M}{\rho_f^2} m_e^{(n)} \Delta t \, dv + \frac{1}{2}\mathbf{h}_e^T \int_{\mathcal{B}_e} \mathbf{H}_e^{*T} \frac{M}{\rho_f^2} \Delta t^2 \, \mathbf{H}_e^* \, dv \, \mathbf{h}_e \\
& + \tfrac{1}{2} \int_{\mathcal{B}_e} M \left(\tfrac{m_e^{(n)}}{\rho_f} \right)^2 dv - \tfrac{1}{2}\mathbf{u}_e^{T(n)} \int_{\mathcal{B}_e} \mathbf{B}_e^T \mathbf{C}_e \mathbf{B}_e \, dv \, \mathbf{u}_e^{(n)} \\
& - \tfrac{1}{2} \int_{\mathcal{B}_e} M \left(\alpha \mathbf{B}_e^{*T} \mathbf{u}_e^{(n)} - \tfrac{m_e^{(n)}}{\rho_f} \right)^2 dv \\
& + \tfrac{1}{2}\mathbf{h}_e^T \int_{\mathcal{B}_e} \mathbf{H}_e^T \underline{\kappa}^{-1} \tfrac{\Delta t}{\rho_f^2} \, \mathbf{H}_e \, dv \, \mathbf{h}_e - (\mathbf{u}_e^T - \mathbf{u}_e^{T(n)}) \int_{\partial\mathcal{B}_e^t} \mathbf{N}^T \bar{\mathbf{t}} \, ds \\
& + \Delta t \sum_{s=1}^{S_e} \left[\boldsymbol{\mu}_e^{sT} \int_{\partial\mathcal{B}_e^s} \overline{\mathbf{N}}^T \mathbf{n}_e^{sT} \mathbf{H}_e \, ds \, \mathbf{h}_e - \boldsymbol{\mu}_e^{sT} \int_{\partial\mathcal{B}_e^h} \overline{\mathbf{N}}^T \bar{h} \, ds \right] \Bigg],
\end{aligned} \tag{225}$$

with $\mu^s = \bar{\mu}$ on $\partial\mathcal{B}_e^s \cap \partial\mathcal{B}_e^\mu$.

[2] From (225), the following terms can be collected as

$$
\begin{aligned}
\mathbf{K}_e^{uu} &= \int_{\mathcal{B}_e} \mathbf{B}_e^T \mathbf{C}_e \mathbf{B}_e \, dv + \int_{\mathcal{B}_e} \mathbf{B}_e^{*T} M \alpha^2 \, \mathbf{B}_e^* \, dv \,, \\
\mathbf{K}_e^{uh} &= \int_{\mathcal{B}_e} \mathbf{B}_e^{*T} \frac{\alpha M}{\rho_f} \Delta t \, \mathbf{H}_e^* \, dv \,, \\
\mathbf{K}_e^{hh} &= \int_{\mathcal{B}_e} \mathbf{H}_e^{*T} \frac{M}{\rho_f^2} \Delta t^2 \, \mathbf{H}_e^* \, dv + \int_{\mathcal{B}_e} \mathbf{H}_e^T \kappa^{-1} \frac{\Delta t}{\rho_f^2} \, \mathbf{H}_e \, dv \,, \\
\mathbf{r}_e^u &= \int_{\mathcal{B}_e} \mathbf{B}_e^{*T} \frac{\alpha M}{\rho_f} m_e^{(n)} \, dv \,, \\
\mathbf{r}_e^h &= \int_{\mathcal{B}_e} \mathbf{H}_e^{*T} \frac{M}{\rho_f^2} m_e^{(n)} \Delta t \, dv \,, \\
\mathbf{K}_e^{\mu h} &= \left[\mathbf{K}_e^{\mu h(1)T}, \mathbf{K}_e^{\mu h(2)T}, \mathbf{K}_e^{\mu h(3)T} \right]^T, \quad \text{with} \quad \mathbf{K}_e^{\mu h(s)} = \int_{\partial\mathcal{B}_e^s} \overline{\mathbf{N}}^T \mathbf{n}_e^{sT} \mathbf{H}_e \Delta t \, ds \,, \\
\mathbf{f}_e^t &= \int_{\partial\mathcal{B}_e^T} \mathbf{N}^T \bar{\mathbf{t}} \, ds \,, \\
\mathbf{f}_e^h &= \left[\mathbf{f}_e^{h(1)T}, \mathbf{f}_e^{h(2)T}, \mathbf{f}_e^{h(3)T} \right]^T, \quad \text{with} \quad \mathbf{f}_e^{h(s)} = \int_{\partial\mathcal{B}_e^h} \overline{\mathbf{N}}^T \bar{h} \Delta t \, ds \,.
\end{aligned}
\tag{226}
$$

The stationary conditions for the global system can be derived from the discretized form of the functional in (225) with definitions (226). Namely,

$$
\begin{aligned}
\partial_{\mathbf{u}} \bar{\Pi}^{\Delta t} &= \sum_e \left[\mathbf{K}_e^{uu} \mathbf{u}_e - \mathbf{r}_e^u + \mathbf{K}_e^{uh} \mathbf{h}_e - \mathbf{f}_e^t \right] = \sum_e \left[\mathbf{q}_e^u - \mathbf{f}_e^t \right] = 0 \,, \\
\partial_{\mu} \bar{\Pi}^{\Delta t} &= \sum_e \left[\mathbf{K}_e^{\mu h} \mathbf{h}_e \right] - \mathbf{f}_e^h = \sum_e \left[\mathbf{q}_e^h - \mathbf{f}_e^h \right] = 0 \,, \\
\partial_{\mathbf{h}_e} \bar{\Pi}^{\Delta t} &= \mathbf{K}_e^{uhT} \mathbf{u}_e - \mathbf{r}_e^h + \mathbf{K}_e^{hh} \mathbf{h}_e + \mathbf{K}_e^{\mu hT} \mu_e = 0 \,,
\end{aligned}
\tag{227}
$$

with $\mu_e = \left[\mu_e^{(1)T}, \mu_e^{(2)T}, \mu_e^{(3)T} \right]^T$ and $\mu_e^s = \bar{\mu}$ on $\partial\mathcal{B}_e^s \cap \partial\mathcal{B}_e^\mu$. Notably, as $\mathbf{h}_e$ is independently interpolated within each element, the third equation in (227), representing the weak form of the inverse Darcy's law, is defined at the element level.

The nodal force vector $\mathbf{q}_e^u$, corresponding to the work-equivalent forces transferred to the nodes of the element, and the nodal flux vector $\mathbf{q}_e^h$, associated with fluid transport

2 In Eq. (225), we define the operator $\mathbf{B}_e^* = \mathbf{m}^T \mathbf{B}_e$ to consistently represent volumetric strains within the discrete functional using the matrix notation in two dimensions [134, Ch. 10]. Here, the vector $\mathbf{m} = [1\ 1\ 0]^T$ satisfies the identity $\mathbf{I} : \boldsymbol{\varepsilon}_e = \mathbf{m}^T \mathbf{B}_e \mathbf{u}_e$. The divergence of the discrete fluid flux field is expressed as $\nabla \cdot \mathbf{h}_e = \mathbf{H}_e^* \mathbf{h}_e$, with $\mathbf{H}_e^* = [\frac{\partial}{\partial x} \ \frac{\partial}{\partial y}] \mathbf{H}_e$.

driven by pressure gradients and source terms at the element nodes, are defined as follows:

$$\begin{aligned}
\mathbf{q}_e^u &= \mathbf{K}_e^{uu}\mathbf{u}_e + \mathbf{K}_e^{uh}\mathbf{h}_e - \mathbf{r}_e^u\,, \\
\mathbf{q}_e^h &= \mathbf{K}_e^{\mu h}\mathbf{h}_e\,, \\
\mathbf{K}_e^{uhT}\mathbf{u}_e &+ \mathbf{K}_e^{hh}\mathbf{h}_e + \mathbf{K}_e^{\mu hT}\boldsymbol{\mu}_e - \mathbf{r}_e^h = \mathbf{0}\,.
\end{aligned} \tag{228}$$

The set of linear algebraic equations in (228) defines the element-level relationships within the discretized hybrid formulation at time increment t_{n+1}. Consequently, the corresponding matrix equations governing the individual HFE can be expressed as follows:

$$\begin{bmatrix} \mathbf{q}_e^u \\ \mathbf{q}_e^h \\ \mathbf{0} \end{bmatrix} = \begin{bmatrix} \mathbf{K}_e^{uu} & \mathbf{0} & \mathbf{K}_e^{uh} \\ \mathbf{0} & \mathbf{0} & \mathbf{K}_e^{\mu h} \\ \mathbf{K}_e^{uhT} & \mathbf{K}_e^{\mu hT} & \mathbf{K}_e^{hh} \end{bmatrix} \begin{bmatrix} \mathbf{u}_e \\ \boldsymbol{\mu}_e \\ \mathbf{h}_e \end{bmatrix} - \begin{bmatrix} \mathbf{r}_e^u \\ \mathbf{0} \\ \mathbf{r}_e^h \end{bmatrix}. \tag{229}$$

Combining the nodal displacements $\mathbf{u}_e$ and the nodal fluid potential $\boldsymbol{\mu}_e$ within a single array of unknowns $\mathbf{u}_e^*$ and combining the nodal force vectors $\mathbf{q}_e^u$ and $\mathbf{q}_e^h$ in the vector $\mathbf{q}_e^*$, the element equations can be reformulated in a more compact form:

$$\begin{bmatrix} \mathbf{q}_e^* \\ \mathbf{0} \end{bmatrix} = \begin{bmatrix} \mathbf{K}_e^{uu*} & \mathbf{K}_e^{uh*} \\ \mathbf{K}_e^{uh*T} & \mathbf{K}_e^{hh} \end{bmatrix} \begin{bmatrix} \mathbf{u}_e^* \\ \mathbf{h}_e \end{bmatrix} - \begin{bmatrix} \mathbf{r}_e^{u^*} \\ \mathbf{r}_e^h \end{bmatrix}, \tag{230}$$

where $[\mathbf{r}_e^{u^*}, \mathbf{r}_e^h]^T$ represents the incremental residual array associated with a single element.

The matrix $\mathbf{K}_e^{hh}$ is symmetric, positive definite, and non-singular, owing to the convexity of the associated functional [121], which enables the condensation of the generalized flux vector at the element level. Therefore, in accordance with the hybrid finite element paradigm, the solution procedure is structured upon the condensation of internal variables [57]. The governing system is thus reduced to a formulation expressed exclusively in terms of the primary variables, namely the nodal displacements and nodal fluid potential. Accordingly, the incremental generalized nodal force vector and element flux vector are derived as follows:

$$\mathbf{q}_e^* = \mathbf{K}_e^{uu*}\,\mathbf{u}_e^* + \mathbf{K}_e^{uh*}\,\mathbf{h}_e - \mathbf{r}_e^u\,, \qquad \mathbf{h}_e = \mathbf{K}_e^{hh-1}\left[\mathbf{r}_e^h - \mathbf{K}_e^{uh*T}\,\mathbf{u}_e^*\right], \tag{231}$$

thus resulting in

$$\mathbf{q}_e^* = \underbrace{[\mathbf{K}_e^{uu*} - \mathbf{K}_e^{uh*}\mathbf{K}_e^{hh-1}\mathbf{K}_e^{uh*T}]}_{\mathbf{K}_e}\,\mathbf{u}_e^* - [\mathbf{r}_e^{u*} - \mathbf{K}_e^{uh*}\mathbf{K}_e^{hh-1}\mathbf{r}_e^h]\,, \tag{232}$$

where $\mathbf{K}_e$ denotes the incremental stiffness matrix and the term in square brackets denotes the initial step incremental residual array. Notably, this procedure enables the

seamless integration of the HFE into a conventional displacement-based finite element framework [100].

4.4 NUMERICAL SIMULATIONS

In this section, the accuracy of the HFE formulation is assessed by conducting quasi-static analyses on classical boundary-value problems of poroelasticity. A systematic comparison of the numerical results is performed against analytical solutions and alternative well-established finite element formulations available in the literature [59, 121]. To this purpose, the proposed HFE has been implemented in the finite element software FEAP v8.5 [120] through the development of a dedicated element subroutine. Spurious kinematic modes, usually associated with the Lagrange multiplier fields of hybrid formulation, have not been observed in the benchmark problems considered.

In each boundary-value problem described below, the geometry, boundary conditions and domain discretization are provided. The constitutive laws introduced in (190) depend on a total of $4+2$ independent material parameters, as reported in Table 2.

Parameter	**Description**	**Unit**
G	Shear modulus	MPa
ν	Drained Poisson's ratio	(-)
α	Biot's coefficient	(-)
M	Biot's modulus	MPa
k	Hydraulic conductivity	m/s
ρ_f	Fluid mass density	kg/m^3

Table 2: Material parameters for isotropic linear poroelasticity adopted in the benchmark problems.

The results are presented in terms of normalized fluid pressure $p = \rho_f \mu$ with respect to the normalized time t^*, defined as in [33]

$$t^* = t\frac{kG}{a^2}\left(\frac{2}{3}\frac{B}{\alpha}\frac{1+\nu_u}{1-\nu_u}\frac{1-\nu_d}{1-2\nu_d}\right). \tag{233}$$

4.4.1 *Terzaghi's problem*

Terzaghi's problem describes the consolidation of saturated soils under mechanical loads, a phenomenon characterized by the gradual reduction in volume due to the expulsion of interstitial fluid under external loading [39, 122, 128]. The problem, of primary importance in geotechnical engineering, has been extensively studied and is

widely adopted as a benchmark for evaluating the accuracy and robustness of finite element formulations in poromechanics [59, 121].

The poroelastic body occupies a rectangular domain $\mathcal{B} = (0, a) \times (0, b)$, whose boundary $\partial\mathcal{B}$ is subject to mixed conditions (Fig. 16(a)). The sides and bottom are assumed to be rigid and impermeable, therefore the following essential conditions are prescribed

$$\begin{aligned} u_x = 0\,, \quad h_x = 0 \qquad &\text{on} \quad x = \{0, a\},\, y \in [0, b]\,, \\ u_y = 0\,, \quad h_y = 0 \qquad &\text{on} \quad x \in [0, a],\, y = 0\,. \end{aligned} \tag{234}$$

The top boundary is drained and subject to a uniform compressive traction q, instantaneously applied at $t = 0$ and then held constant, resulting in the following natural conditions

$$\sigma_{yy} = -q\,, \quad \mu = 0 \qquad \text{on} \quad x \in [0, a],\, y = b\,. \tag{235}$$

Owing to the symmetry of the problem, the fluid flow is one-dimensional, hence we expect a uniform fluid pressure along the horizontal direction. Consequently, the computational domain is discretized using a single column of 20 quadratic triangular elements, with a finer mesh near the top boundary to accurately capture pressure gradients expected in the early stages of consolidation.

The analytical solution to the problem was originally derived in the seminal work of Terzaghi [122]. To ensure consistency in the comparison of results, all quantities have been normalized following the procedure previously introduced. However, when approaching significantly reduced values of the non-dimensional time $t^* = ct/a^2 < 0.01$, the classical series representation of Terzaghi's solution exhibits extremely slow convergence. In such cases, it is often preferable to employ an alternative formulation that remains accurate for small time increments. A well-established approximation, reported in [128], is given by

$$\frac{p}{p_0} = \operatorname{erf}\left(\frac{b - y}{2\sqrt{ct}}\right)\,, \tag{236}$$

where $p_0 = q$ and $\operatorname{erf}(\cdot)$ denotes the error function of $(\cdot)$.

Figure 16(b) shows the normalized fluid pressure p/p_0 as a function of normalized depth y/b, at times $t^* = 7.12 \cdot 10^{-6}$ and $t^* = 1.07 \cdot 10^{-1}$. The analytical solution is represented by dark blue lines, while the orange markers refer to the results obtained from the HFE simulation. The short time scenario assumes particular relevance as benchmark, as extensive literature highlights the recurrent emergence of numerical instabilities and oscillatory phenomena [49, 121]. In Lo Franco, Parrinello, and Borino [72], numerical oscillations were already effectively mitigated through the careful selection of primary variables, with both total stress and pressure considered as primary fields. Similarly, the approach adopted in this study, which combines the benefits of

being based on a minimization principle and incorporates the fluid potential field as a Lagrangian variable, ensures that the pressure field remains unaffected by any spurious oscillations.

Initially, the pressure within the specimen is almost uniformly distributed, sharply decreasing to zero at the surface. At short times, most of the domain finds itself in *undrained* conditions, and due to the incompressibility of the skeleton and the nearly-incompressibility of the fluid, the column is unable to undergo any deformation. Notably, the enforcement of the fluid's nearly-incompressibility through the selection of a large Biot modulus did not cause any volumetric locking issues. Moreover, in contrast to classical displacement-pressure formulations [24, 70, 109], the present results exhibit a substantial correspondence with the analytical solution, even at very short time increments. At longer times, the obtained solution converges with that derived from canonical elements for poroelastic problems [46, 59, 121].

A representative contour of the fluid pressure p in the domain, at normalized time $t^* = 7.12 \cdot 10^{-6}$, is illustrated in Fig. 16(c), confirming the absence of spurious oscillations in the fluid pressure field.

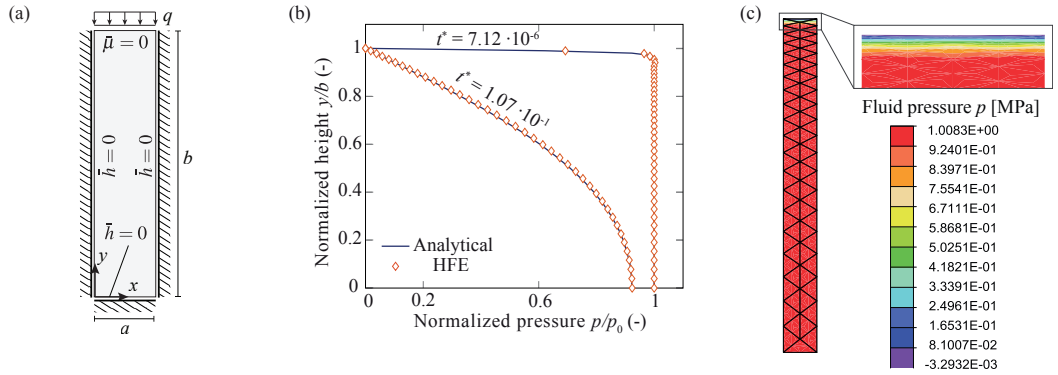

Figure 16: Terzaghi's problem: (a) problem domain ($a = 1\,m, b = 10\,m$) with boundary conditions ($q = 1\,MPa$); (b) fluid pressure p/p_0 as a function of depth y/b, at times $t^* = 7.12 \cdot 10^{-6}$ and $t^* = 1.07 \cdot 10^{-1}$. The Hybrid Flux Element (HFE) solution is compared to the analytical solution; (c) contour plot of fluid pressure p at time $t^* = 7.12 \cdot 10^{-6}$. Material parameters: $G = 1\,MPa$, $\nu = 0.3$, $\alpha = 1$, $M = 100\,000\,MPa$, $k = 1\,m\,s^{-1}$.

4.4.2 *Low permeability layer*

The second benchmark is analogous to the previous one in terms of boundary conditions but involves an inhomogeneous domain. Specifically, the domain $\mathcal{B}$ is divided along the height b into three layers of equal height, with the central layer having hydraulic conductivity $\tilde{k} = k \cdot 10^{-8}$, where k is the reference value of the top and bottom layers (Fig. 17(a)).

It is well established that low-permeability regions can influence the stability of finite element analyses, as highlighted by Haga, Osnes, and Langtangen [58] and Rodrigo [106]. These regions are known to induce spurious oscillations in the calculated fluid pore pressure field [2, 96]. The computational domain is discretized into a 10×15 elements mesh.

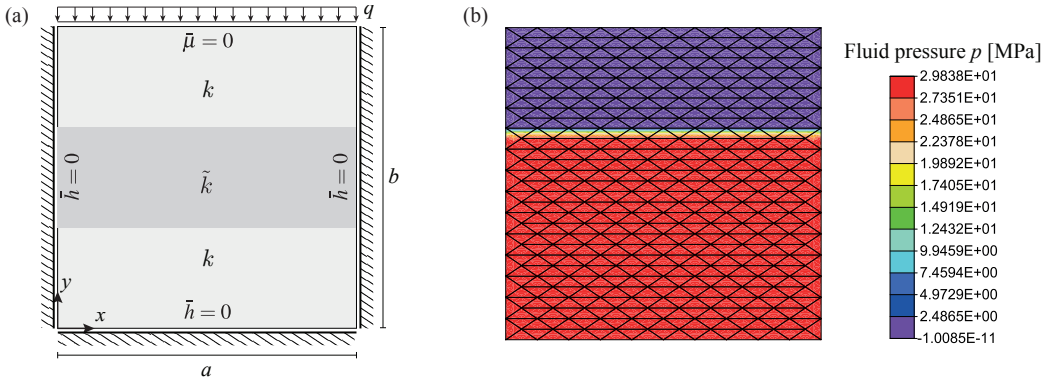

Figure 17: Low-permeability layer problem: (a) problem domain ($a = 1\,m, b = 1\,m$) with boundary conditions ($q = 30\,MPa$). In the central layer the hydraulic conductivity is equal to $\tilde{k} = k \cdot 10^{-8}$; (b) contour plot of fluid pressure p at time $t^* = 1.63$. Material parameters: $G = 0.81\,MPa$, $\nu = 0.3$, $\alpha = 1$, $M = 20\,000\,MPa$, $k = 2.06991 \cdot 10^{-9}\,m\,s^{-1}$.

Figure 18 shows the normalized fluid pressure p/p_0 as a function of normalized height y/b at time $t^* = 1.63$. The numerical solution obtained from the proposed HFE formulation is compared to the analytical two-layer solution proposed by Verruijt [128]. In addition, we included benchmark results from alternative finite element formulations for poroelasticity, including the classical u-p formulation with Taylor-Hood elements (TH) and the displacement-flux minimization-based formulation (Q1-RT0), both reported by Teichtmeister, Mauthe, and Miehe [121]. The analytical solution predicts a localized pressure discontinuity at the interface between the top and the intermediate less permeable layer, whereas the trend is almost uniform in the remaining regions. Due to the brevity of the timescales involved, fluid is unable to flow upwards from the lower layer, resulting in a two-layer configuration, where the lower layer with reduced hydraulic conductivity comprises two-thirds of the total height. The HFE formulation clearly captures the pressure discontinuity, aligning with the ordinate at which the sharp pressure transition is predicted by the analytical curve. The slight underestimation of the fluid pressure near the bottom is attributed to the nearly-incompressibile behavior assumed, in contrast to the perfect incompressibility of the analytical result. In comparison, the TH element seems affected by oscillations at the interfaces between layers, already reported by Haga, Osnes, and Langtangen [58]. Conversely, the minimization-based formulations provides a stable, oscillation-free distribution of the

fluid pore pressure. However, as shown in the figure, while the HFE formulation exhibits an abrupt change in pressure exactly at the interface between the two layers ($y/b = 2/3$), the Q1-RT0 element shifts this transition slightly closer to the surface.

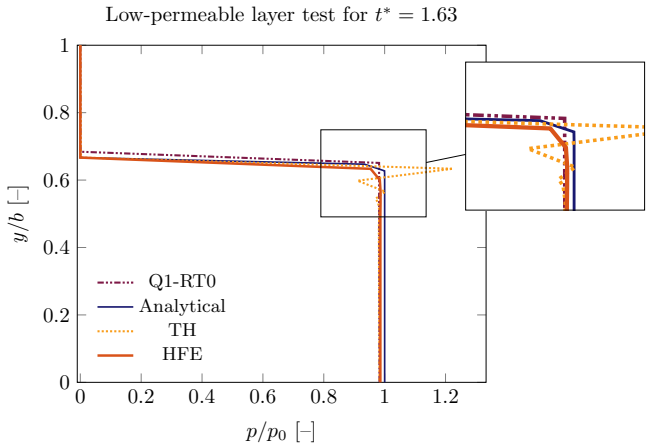

Figure 18: Low-permeability layer problem. Fluid pressure p/p_0 as a function of depth y/b at time $t^* = 1.63$. The Hybrid Flux Element (HFE) solution is compared to the analytical solution, the Tayor-Hood (TH) solution and the displacement-flux element (Q1-RT0) proposed by Teichtmeister, Mauthe, and Miehe [121].

4.4.3 *Mandel's problem*

As third benchmark, we selected another classical solution from the theory of poroelasticity, known as Mandel's problem [76]. A rectangular domain $\mathcal{B} = (-a, a) \times (-b, b)$ is placed between two rigid and frictionless plates and subject to a compressive mechanical load (Fig. 19). The sides are drained and traction-free, resulting in the following natural boundary conditions

$$\sigma_{xx} = \sigma_{xy} = 0\,, \quad \mu = 0 \qquad \text{on} \quad |x| = a,\, y \in [-b, b]\,, \tag{237}$$

whereas the top and bottom plates are frictionless and impermeable, implying

$$\sigma_{xy} = 0\,, \quad h_y = 0 \qquad \text{on} \quad x \in [-a, a],\, |y| = b\,. \tag{238}$$

In addition, a vertical load $2F$ is instantaneously applied to the top and bottom plates load magnitude and maintained constant throughout the test. This loading is enforced by prescribing uniform normal tractions, therefore

$$\sigma_{yy} = -\frac{2F}{2a} \qquad \text{on} \quad x \in [-a, a],\, |y| = b\,. \tag{239}$$

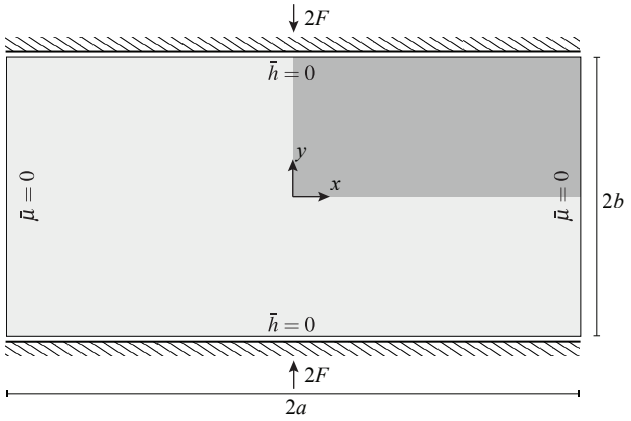

Figure 19: Mandel's problem: problem domain ($a = 1\,\mathrm{m}$, $b = 0.2\,\mathrm{m}$) with boundary conditions ($F = 1\,\mathrm{kN}$). Material parameters: $G = 1\,\mathrm{MPa}$, $\nu = 0.2$, $\alpha = 1$, $M = \{100, 20\,000\}\,\mathrm{MPa}$, $k = 1\,\mathrm{m\,s^{-1}}$. Taking advantage of symmetry, only the dark gray region is discretized.

Due to symmetry and assuming plane strain conditions, flow is restricted to the direction perpendicular to the load, therefore the problem is one-dimensional. Upon loading, the uniform fluid pressure distribution instantaneously drops to zero at the free boundaries in $|x| = a$. Subsequently, the response is non-monotonic, with an initial increase followed by a subsequent decrease that ultimately reaches a steady state of zero pressure, a phenomenon known as Mandel-Cryer effect. This boundary-value problem, whose original solution was revisited by several authors [1], has become a classical benchmark for numerical methods in poroelasticity [33, 121].

The analytical solution for the fluid pressure p, formulated in terms of the applied load $2F$, is given as [33, Eq. (D6)]

$$p = \frac{2FB\,(1+\nu_u)}{3a} \sum_{i=1}^{\infty} \frac{\sin\beta_i}{\beta_i - \sin\beta_i \cos\beta_i} \left(\cos\frac{\beta_i x}{a} - \cos\beta_i \right) \exp\left(-\beta_i^2 c t / a^2\right) , \quad (240)$$

where the *undrained* Poisson's ratio ν_u, the Skempton's coefficient B can be derived from the parameters reported in Table 2 as

$$\nu_u = \frac{2G(1+\nu) + \alpha^2 M(1-2\nu)}{2G} - 1 , \quad B = \frac{3(\nu_u - \nu)}{\alpha(1-2\nu)(1+\nu_u)} ,$$

and consequently, the expressions for $\tan\beta_i$ and c can be evaluated as follows:

$$\tan\beta_i = \frac{1-\nu}{\nu_u - \nu}\beta_i , \quad c = \frac{2\kappa B^2 G(1-\nu)\,(1+\nu_u)^2}{9\,(1-\nu_u)\,(\nu_u - \nu)} .$$

The problem is investigated for both a nearly-incompressible and a compressible fluid, with the Biot modulus M set to 20 000 MPa and 100 MPa, respectively. The numerical results are derived using a 10×40 triangular mesh, taking symmetry into account, allowing only a quarter of the domain to be analyzed.

In Fig. 20, the normalized pressure p/p_0 is plotted as a function of the normalized width x/a, at times $t^* = 1$, 0.5, 0.2, 0.1 and 0.01. The continuous line in the plots represents the analytical solution [33], whereas the orange dots represent the numerical solution derived from the HFE formulation. The curves indicate a significant correspondence of the solutions, for both the nearly-incompressible and compressible fluid scenarios. Notably, good accuracy is achieved when modeling the system with the fluid phase considered nearly-incompressible, without the need for any stabilization techniques or reduced integration procedures.
In addition, volumetric locking, inherent to displacement-based formulations reaching the incompressible limit, was not observed in the benchmark example, owing to the incorporation of the fluid potential as a Lagrangian multiplier variable independently interpolated on each element side.

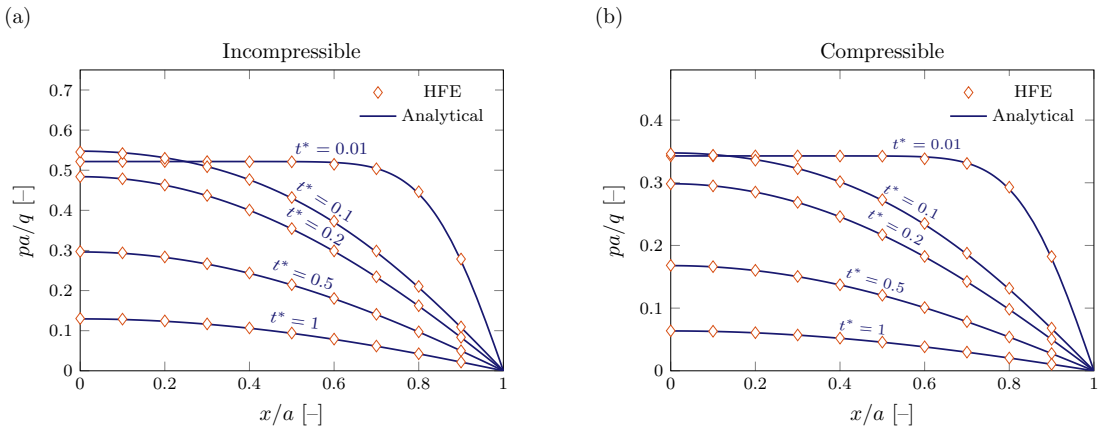

Figure 20: Mandel's problem: normalized fluid pressure as a function of width x/a, at times $t^* = 0.01$, $t^* = 0.1$, $t^* = 0.2$, $t^* = 0.5$, $t^* = 1$. The Hybrid Flux Element (HFE) solution is compared to the analytical solution; (a) early-incompressible fluid and (b) compressible fluid.

4.4.4 *Consolidation problem*

Finally, we consider a two-dimensional boundary-value problem, describing the consolidation induced by a surface footing on a rectangular domain $\mathcal{B} = (-a, a) \times (0, b)$ placed upon a rigid base [23]. A finite width strip $2d < 2a$ is subject to periodic loading q [64]. Due to the problem symmetry, the region modeled can be reduced to a half, as shown in Fig. 21(a).

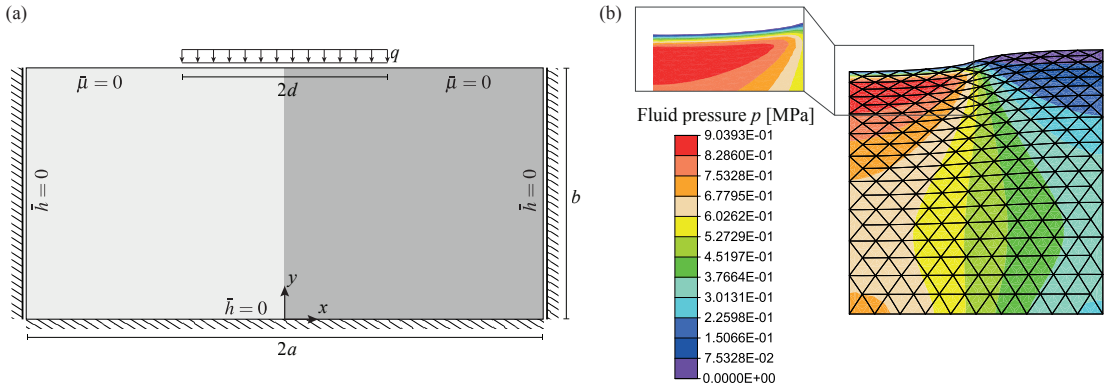

Figure 21: Consolidation problem: (a) problem domain ($a = 1\,m$, $b = 1\,m$, $d = a/2$) with boundary conditions ($q = 1\,MPa$); (b) contour plot of fluid pressure p at time $t^* = 2 \cdot 10^{-6}$. Material parameters: $G = 1\,MPa$, $\nu = 0.3$, $\alpha = 1$, $M = 20\,000\,MPa$, $k = 0.1\,m\,s^{-1}$. Taking advantage of symmetry, only the dark gray region is discretized.

The following boundary conditions are prescribed to the sides

$$u_x = 0\,, \quad \sigma_{xy} = 0\,, \quad h_x = 0 \qquad \text{on} \quad |x| = a,\, y \in [0, b]\,, \tag{241}$$

and to the bottom

$$u_x = u_y = 0\,, \quad h_y = 0 \qquad \text{on} \quad x \in [-a, a],\, y = 0\,. \tag{242}$$

The top surface is drained and subject to a uniform compressive traction q on part of its boundary, instantaneously applied at $t = 0$ and then held constant, resulting in the following natural conditions

$$\begin{aligned} &\sigma_{yy} = -q, \sigma_{xy} = 0\,, \quad \mu = 0 \qquad \text{on} \quad x \leqslant |d|,\, y = b\,, \\ &\sigma_{yy} = \sigma_{xy} = 0\,, \qquad \mu = 0 \qquad \text{on} \quad x > |d|,\, y = b\,. \end{aligned} \tag{243}$$

The geometry is discretized with a mesh composed of 10×10 elements, with a geometric aspect ratio $a : b = 1 : 1$.

Numerical oscillations in the fluid pressure usually constitute a critical issue for this benchmark problem. As illustrated in Fig. 21(b), the fluid pressure contour plot at the normalized time $t^* = 2 \cdot 10^{-6}$ [64] does not contain evidence of these, demonstrating the stability and accuracy of the employed method. Notably, even using a coarse mesh, the system's behavior is captured accurately, without encountering jumps or discontinuities in the results.

In this regard, Fig. 22 shows the fluid pressure curve resulting from the proposed HFE formulation compared with the corresponding plots derived using a classical u-p Taylor-Hood element (TH) and the hybrid equilibrium element (HEE) recently intro-

duced by the author [72]. Although significant improvements over the well-established Q9/Q4 element reported in the literature [59], the TH element still manifests spurious oscillations in the pressure. In contrast, the solution derived from the HFE and HEE formulations, both based on a minimization principle, appears extremely stable. As the process progresses to later time steps, all examined finite element formulations ultimately converge to the same fluid pore pressure trend. Notably, the Mandel-Cryer effect is evident as the pressure initially increases at the top and subsequently decreases with time, eventually reaching zero.

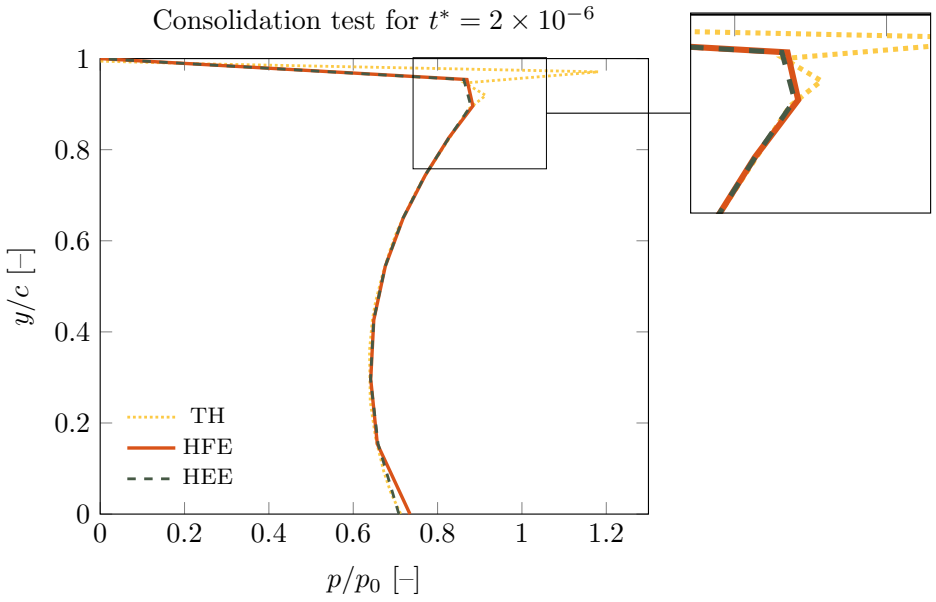

Figure 22: Consolidation problem: fluid pressure p/p_0 as a function of depth y/b at $x = 0$, for the normalized time $t^* = 2 \cdot 10^{-6}$. The Hybrid Flux Element (HFE) solution is compared to the results from the Tayor-Hood (TH) element [121] and the Hybrid Equilibrium Element (HEE) proposed by Lo Franco, Parrinello, and Borino [72].

4.5 CONCLUSIONS AND FUTURE PERSPECTIVES

This chapter introduced a novel hybrid flux-preserving finite element for the transient analysis of poroelastic material systems, based on the choice of displacements and fluid mass fluxes as primary variables. The main contribution of our work is the hybridization of the canonical minimization principle of poroelasticity introduced by Miehe, Mauthe, and Teichtmeister [82], leveraging the hybrid equilibrium formulation, which has been successfully applied to stress-based poroelasticity [72], linear elasticity [93, 95] and nonlinear fracture mechanics [94].

As a first step, a hybrid variational principle is introduced and the related stationarity conditions investigated. A novel triangular HFE is then formulated and implemented in the open-source finite element software FEAP [120]. Through a comparative analysis of several classical benchmark problems in poromechanics, we demonstrated the validity of the proposed approach, as expected from the variational derivation and the symmetry of the matrix system of equations. Notably, the solution does not exhibit nonphysical oscillations in the fluid pressure field, a typical drawback of classical mixed u-p formulation of poroelasticity. Remarkably, no stabilization algorithm was required.

Although the HFE formulation introduces additional complexity by incorporating the fluid potential as a Lagrangian variable, thereby increasing the number of local degrees of freedom per element, the element remains computationally efficient by the static condensation of generalized fluxes at the element level. In contrast to mixed formulations, the hybrid approach allows to reduce the system to a single matrix equation in terms of a generalized nodal variable. As a result, it yields compatible flux fields at the element boundaries while retaining the computational simplicity of an element that can be seamlessly integrated into a displacement-based solution scheme.

A significant feature emerging from the numerical applications is the high accuracy of the solution in terms of fluid potential, even when relatively coarse meshes are employed. This feature is particularly advantageous for problems exhibiting high-pressure gradients. Furthermore, the formulation relaxes the continuity constraints on flux fields across element interfaces, enhancing its robustness in handling complex geometries and multi-field coupling. The resulting fluid flux is co-diffusive at the element level, with continuous normal component between two contiguous elements.

Finally, some open issues remain regarding the enforcement of phase incompressibility constraints in the fluid. The development of enhanced techniques for constraint enforcement, such as augmented Lagrangian formulations, could offer a potential pathway to address these challenges in future research. An additional, significant improvement to the proposed formulation is its extension to the context of finite deformations. This would broaden the applicability of the approach, particularly in soft biological porous media, where nonlinear strains are commonly encountered. In fact, biomechanical simulations of coupled problems can greatly benefit from an accurate solution of fluid pressure distributions, particularly in combination with reduced permeability often encountered. The large strain formulation of the HFE is going to be addressed in a follow-up paper. It is worth recalling that the newly developed flux-based formulation, in contrast to the hybrid equilibrium element recently introduced by the author [72], incorporates deformation as a primary field, therefore enabling seamless integration of more complex nonlinear constitutive models.

Un antico detto, cinese o tibetano, forse arabo-siciliano, dice così:

Caliti junku 'ca passa la China,
caliti junku, da sira 'a matina

— Franco Battiato

5

A HYBRID FLUX-PRESERVING FINITE ELEMENT FOR COUPLED FLOW DEFORMATION: FINITE STRAINS FORMULATION

5.1 INTRODUCTION

In the previous chapter, the development and validation of a *Hybrid Flux-preserving Element* (HFE) for linear poroelasticity were presented, demonstrating its capability to provide accurate and stable solutions for the primary fields of displacements and mass fluid flux. While the linearized framework effectively captured the coupled hydro-mechanical response of porous media under small deformations, its applicability becomes limited when large deformations effects arise. The consideration of large strain effects in modelling the behaviour of saturated geomaterials is essential for accurately describing the consolidation of soft sediments. The seminal work of Gibson, England, and Hussey [52] introduced a Lagrangian formulation of the one-dimensional consolidation problem, highlighting the role of void ratio variations in modifying both the permeability and the deformability of the porous medium. Subsequent studies [30, 53] largely retained a one-dimensional framework, applicable only in the absence of unloading, and thus unable to capture irreversible processes in the soil skeleton under large deformations, a limitation already inherent in Terzaghi's classical theory[112]. A further development was presented by [127], who proposed a FE formulation for finite deformations in poro-hyperelastic soils using a neo-Hookean strain energy function [66]; however, this formulation likewise neglects the irreversible nature of the deformation of the porous skeleton.

The consideration of geometric nonlinearities becomes particularly critical in the formulation of finite element models for biological materialsFranceschini et al. [47], as poroelastic analyses of rapidly loaded, slow-draining tissues are frequently prone to numerical ill-conditioning. For instance, Stokes et al. [117] examines the constraints imposed by this phenomenon on biological tissues representative of the intervertebral disc, subjected to moderate physiological rates of deformation. The emergence of pressure instabilities He, Jing, and Feng [60] and Murad and Loula [86] is shown

to significantly limit the applicability of the finite element method in accurately simulating fluid transport phenomena within soft biological tissues under such loading conditions, with empirical findings further revealing the consequent degradation of accuracy in poroelastic analyses of spinal tissues at physiological strain rates. Although h-refinement, which is frequently effective in mitigating pressure instabilities, could in principle address these challenges, its practical implementation may be severely limited by computational memory requirements and associated costs. This limitation may have similarly profound implications for the modelling of a wide range of biological tissues with analogous mechanical properties, indicating that achieving accurate solutions may require computationally prohibitive compromises between mesh resolution and time step selection, especially in critical scenarios. This assumes particular significance in the context of cerebral tissue, as pathological conditions such as cerebral edema, as well as therapeutic interventions including convection-enhanced drug delivery (CED), may be profoundly affected by the dynamics of fluid perfusion within the tissue [131]. To overcome these limitations, the present chapter extends the hybrid paradigm to the finite-strain regime, introducing a nonlinear *Hybrid Flux-based Element* (HFE) for the quasi-static analysis of large-deformation poroelastic media. This development builds upon the same variational minimization principle presented in Miehe, Mauthe, and Teichtmeister [82] and further refined in Teichtmeister, Mauthe, and Miehe [121], in which the solid deformation and the fluid flux are chosen as the fundamental primary variables of the poromechanical problem. The formulation in [121] yields a variationally consistent minimization principle that inherently circumvents the classical inf–sup condition, thereby ensuring robust accuracy. Nonetheless, the difficulty associated with operating within the $H(\mathrm{div}, \mathcal{B})$ function space for the fluxes becomes even more pronounced in the context of large deformations, where a Piola transformation is required to correctly map the fluxes between the reference and current configurations.

Within the framework proposed in this chapter, as already introduced in Chapter 4, the fluid potential is introduced as a Lagrange multiplier to enforce weak continuity of the normal flux across element boundaries, thereby avoiding the need for globally conforming function spaces. This hybridization strategy preserves the physical consistency of the flux field while substantially improving computational efficiency through local static condensation of internal variables. Consistent with the linear formulation, the resulting system retains symmetry and remains well-conditioned; however, it now accommodates large kinematic transformations and the nonlinear constitutive behaviour of the solid skeleton, offering a robust and efficient approach to model strongly coupled deformation–diffusion phenomena. It is particularly suited for problems characterized by large volumetric changes, nonlinear elasticity, and evolving permeability, such as those encountered in soft tissue mechanics, polymeric gels, and geomechanical processes involving significant compaction or swelling. This chapter is structured as follows. Section 5.2 recalls the finite-strain kinematics and gov-

erning equations of poromechanics, emphasizing the thermodynamic consistency of the large-deformation framework. Section 5.3 introduces the variational principle underlying the proposed Hybrid Finite-Strain Flux Element (HFE-FS) and outlines its finite element implementation. The performance and accuracy of the formulation are demonstrated in Section 5.5, through a series of benchmark problems involving large deformations and nonlinear material response. Finally, Section **??** summarizes the key findings and discusses prospective extensions toward dynamic and fully nonlinear coupled analyses.

5.2 CANONICAL FORM OF POROELASTICITY

5.2.1 *Primary fields*

Consider an homogenized continuous body $\mathcal{B}$ composed by a poroelastic solid in which a flux of interstitial fluid mass can occur through convective transport. Let us define a time-independent reference configuration of $\mathcal{B}$, denoted with $\mathcal{B}_0$, such that a particle in the continuous body is represented by a material point $\mathbf{X} \in \mathcal{B}_0$ relative to a Cartesian material coordinate system [61]. According to classical practice in poroelasticity, an homogenization procedure is carried out at the mesoscale, such that at each material point the particles of the solid skeleton and of the interstitial fluid are indistinguishable. The homogenization is based on the definition of an *effective porosity* field $\varphi_0(\mathbf{X}, t) \in (0, 1]$, which assigns to each volume element dV the volume of interconnected pores $dV_f = \varphi_0\, dV$ filled by fluid [32, Sec. 4.1.1]. In poroelasticity, kinematics is referred to the solid, implying that motion and related quantities are measured with respect to the configuration of the solid skeleton [40]. The motion of the solid in a time interval $\mathcal{T} = (0, t) \subset \mathbb{R}_+$ is given by a (smooth) map $\boldsymbol{\chi} : \mathcal{B}_0 \times \mathcal{T} \to \mathbb{R}^3$, which carries each material point $\mathbf{X} \in \mathcal{B}_0$ into a point $\mathbf{x} := \boldsymbol{\chi}(\mathbf{X}, t) = \mathbf{X} + \mathbf{u}(t), \forall\, \mathbf{X} \in \mathcal{B}_0$, with $\mathbf{u}(\mathbf{X}, t) : \mathcal{B}_0 \times \mathcal{T} \to \mathbb{R}^3$ denoting the displacement field.

The deformation gradient tensor for the motion is defined as

$$\mathbf{F} := \nabla_{\mathbf{X}}\, \boldsymbol{\chi}(\mathbf{X}, t) \equiv \mathbf{I} + \nabla_{\mathbf{X}} \mathbf{u}(\mathbf{X}, t), \tag{244}$$

transforming material tangent vectors onto spatial tangent vectors [61], being $\nabla_{\mathbf{X}}$ the gradient operator with respect to the reference system of coordinates. Its cofactor $cof\,[\mathbf{F}] := \det \mathbf{F}\mathbf{F}^{-T}$ and its Jacobian $J := \det \mathbf{F} > 0$ denote respectively the trasformation of infinitesimal area dA and volume elements dV in the current configuration. For subsequent use (see Sec. 5.2.2), we compute the Fréchet derivative of $J = \det \mathbf{F}$ [90] relative to $\mathbf{F}$ as $\partial_{\mathbf{F}}(\det \mathbf{F}) = cof\,[\mathbf{F}] = \det \mathbf{F}\mathbf{F}^{-T}$. Finally, the right Cauchy-Green tensor $[\mathbf{C}] := \mathbf{F}^T(\mathbf{X}, t)\mathbf{F}(\mathbf{X}, t)$ is defined as a convenient measure of strain, being $J := [\det \mathbf{C}(\mathbf{X}, t)]^{1/2}$.

Following the classical literature on poroelasticity, let us define the *variation in fluid mass content* $m : \mathcal{B}_0 \times \mathcal{T} \to \mathbb{R}$ introduced by Biot [18], representing the increase of interstitial fluid mass per unit reference volume of the poroelastic solid [82, Eq. $(6)_1$] and [121]. The linear case, introduced in Chapter 4, can be recalled as a limited case, performing a linearization around the reference configuration $\mathcal{B}_0$ and characterize the deformation the *infinitesimal strain tensor* $\boldsymbol{\varepsilon} = \nabla^s_{\mathbf{X}}\mathbf{u}$, with $\nabla^s_{\mathbf{X}}\mathbf{u}$ representing the symmetric part of the displacement gradient [61].

5.2.2 *Governing equations*

The fundamental governing equations of a poroelastic solid are the balances of mass, momentum and energy, in addition to constitutive equations for the solid and the interstitial fluid [32, Ch. 6]. In this section, these are briefly reviewed in order to ensure a consistent use of notation throughout the chapter. Some aspects of thermodynamical consistency of the poroelastic theory are also recalled.
To avoid unnecessary complications, the system is considered to be isothermal and mass-conservative, implying the absence of internal sources or sinks; furthermore, no chemical interaction between the constituents is allowed.Under these assumptions, the balance of mass is limited to the continuity equation of the fluid phase [39].

5.2.2.1 *Balance of Mass*

Let $\mathcal{P}_0 \subset \mathcal{B}_0$ denote an arbitrary region of the continuum body in the reference configuration, and let $\mathbf{n}_0$ be the outward unit normal to its boundary $\partial\mathcal{P}_0$. The material fluid mass flux is defined as $\mathbf{H} : \mathcal{B}_0 \times \mathcal{T} \to \mathbb{R}^3$, such that $\mathbf{H} \cdot \mathbf{n}_0$ gives the fluid mass crossing $\partial\mathcal{P}_0$ per unit reference area and unit time. In the material setting, the conservation of mass of the fluid in $\mathcal{P}$ with respect to the motion of the solid skeleton, takes then the following local form:

$$\frac{d_s m}{dt} + \operatorname{Div} \mathbf{H} = 0. \tag{245}$$

As defined, m denotes the variation of fluid mass content, so that $m(\mathbf{X}, t)$ quantifies the net variation of fluid mass, positive for influx, negative for efflux, within the material volume element $d\mathcal{B}_0$ since the initial time $t = 0$. The mass balance formulated with respect to the solid skeleton (see Coussy) shows that any change in the mass of the volume element $d\mathcal{B}_0$ is solely attributable to the net flux of fluid mass across its boundary. Hence, we restrict our attention to the balance for the fluid phase only.

5.2.2.2 *Lagrangian Balance of Momentum*

In absence of body forces, the balance of linear momentum for the mixture as a whole can be formulated in the spatial setting as

$$\nabla_x \cdot \boldsymbol{\sigma} = 0, \tag{246}$$

where $\boldsymbol{\sigma}$ is the total Cauchy stress tensor [18]. Following Terzaghi's principle, the total stress is decomposed into an effective stress contribution and a pore pressure term $\boldsymbol{\sigma} = \boldsymbol{\sigma}_{\text{eff}} - J p \mathbf{F}^{-T}$. To obtain the Lagrangian form of the momentum balance, we pull back (see Section 1.2.3) the spatial statement to the reference configuration $\mathcal{B}_0$, which introduces the first Piola–Kirchhoff stress tensor $\mathbf{P}$:

$$\nabla_X \cdot \mathbf{P} = 0. \tag{247}$$

In this framework, the effective part of the stress is denoted by $\mathbf{P}_{\text{eff}}$, corresponding to the pull-back of the effective Cauchy stress:

$$\mathbf{P} = \mathbf{P}_{\text{eff}} - J \rho_f \mu \mathbf{F}^{-T}, \tag{248}$$

being the pore pressure $p = \rho_f \mu$.

The local balance equations (245) and (247) must be complemented by suitable boundary and initial conditions. The boundary of the poroelastic body, denoted by $\partial\mathcal{B}$ (see Fig. 14), is divided into subsets on which either essential or natural conditions are imposed for both the mechanical and hydraulic fields:

$$\partial\mathcal{B} = \partial\mathcal{B}^{\chi} \cup \partial\mathcal{B}^{t} = \partial\mathcal{B}^{H} \cup \partial\mathcal{B}^{\mu}, \tag{249}$$

with the intersections $\partial\mathcal{B}^{\chi} \cap \partial\mathcal{B}^{t}$ and $\partial\mathcal{B}^{H} \cap \partial\mathcal{B}^{\mu}$ being empty. In accordance with the selection of primary variables introduced in Sec. 5.2.1, the essential (Dirichlet-type) boundary conditions prescribe the deformation mapping $\boldsymbol{\chi}$ on $\partial\mathcal{B}^{\chi}$, and the normal component of the fluid flux $\mathbf{H}$ on $\partial\mathcal{B}^{H}$:

$$\boldsymbol{\chi} = \bar{\boldsymbol{\chi}} \quad \text{on } \partial\mathcal{B}^{\chi} \times \mathcal{T}, \qquad \mathbf{H} \cdot \mathbf{n} = \bar{H} \quad \text{on } \partial\mathcal{B}^{H} \times \mathcal{T}, \tag{250}$$

where $\bar{\boldsymbol{\chi}}$ and $\bar{H}$ denote the prescribed boundary deformation and the imposed normal fluid flux, respectively. The corresponding natural (Neumann-type) boundary conditions are associated with the traction vector $\mathbf{T}$ and the fluid potential μ, which are specified on $\partial\mathcal{B}^{t}$ and $\partial\mathcal{B}^{\mu}$, respectively (Figure 23):

$$\mathbf{P} \cdot \mathbf{N} = \bar{\mathbf{T}} \quad \text{on } \partial\mathcal{B}^{t} \times \mathcal{T}, \qquad \mu = \bar{\mu} \quad \text{on } \partial\mathcal{B}^{\mu} \times \mathcal{T}, \tag{251}$$

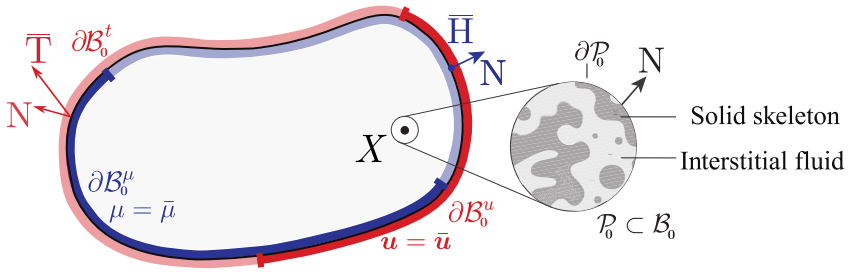

Figure 23: Graphical description for the poroelastic system in the reference configuration.

where $\bar{\mathbf{T}}$ and $\bar{\mu}$ represent the prescribed traction and pore-fluid potential.
Finally, the initial conditions are specified as

$$\chi(\mathbf{X}, 0) = \mathbf{X}, \qquad m(\mathbf{X}, 0) = 0 \quad \text{in } \mathcal{B} \times \{0\}, \tag{252}$$

implying that the porous solid is initially in its undeformed reference configuration and that no excess pore-fluid mass is present.

5.2.3 *Thermodynamic consistency*

In accordance with the principle of irreversibility, the dissipation rate $\mathcal{D}$ is required to be non-negative at every material point [38, 54, 91]. The dissipation inequality is expressed through the duality pairing of the generalized fluxes $(\dot{\chi}, \dot{m})$ with their conjugate forces $(\mathbf{P}, \mu)$ [18, Eq. (2.5)]. The Helmholtz free-energy density stored in the poroelastic medium is assumed to depend on the primary variables χ and m, namely $\psi = \hat{\psi}(\chi, m)$. Within this framework, the dissipation rate admits the representation [82, Eq. (14)]

$$\mathcal{D} = \mathbf{P} \cdot \dot{\chi} + \mu\, \dot{m} - \dot{\hat{\psi}} - \nabla_{\mathbf{X}} \mu \cdot \mathbf{H} \geqslant 0\,, \tag{253}$$

which naturally decomposes into two distinct contributions, i.e., an intrinsic (local) contribution and a transport-related contribution. The intrinsic dissipation rate can be expressed as

$$\mathcal{D}_{\text{int}} = \mathbf{P} \cdot \dot{\chi} + \mu\, \dot{m} - \dot{\hat{\psi}} \geqslant 0\,, \tag{254}$$

depending exclusively on the variables that define the free energy of the elementary system, where the local balance is established. At equilibrium, it characterizes the dissipation rate associated with internal irreversible processes, vanishing in the absence of local dissipative mechanisms. On the other hand, the transport-related dissipation is related to the mass transport of the fluid phase, namely

$$\mathcal{D}_{\text{tr}} = -\nabla_{\mathbf{X}} \mu \cdot \mathbf{H} \geqslant 0\,. \tag{255}$$

The formulation of constitutive equations must be consistent with the Clausius-Duhem inequality (253) and the fundamental principles of frame invariance [56]. From (254), the following constitutive relationships for the total Cauchy stress tensor and the fluid potential are derived in remark 10

$$\mathbf{P} = \partial_{\chi}\hat{\psi}(\chi, m)\,, \quad \mu = \partial_{m}\hat{\psi}(\chi, m)\,. \tag{256}$$

The inequality in Eq. (255), pertaining to the transport-related dissipation, is satisfied by choosing a convex dissipation potential function $\hat{\phi}(\mathbf{H})$ in the space of the material fluid mass fluxes $\mathbf{H}$, such that [82]

$$\nabla_{\chi}\mu = -\partial_{\mathbf{H}}\hat{\phi}(\mathbf{H})\,. \tag{257}$$

Under the assumption of normal dissipative mechanisms, and in absence of intrinsically inelastic behavior of both constituents, the Helmholtz free energy introduced is postulated to possess an additive structure. This potential depends on the deformation gradient $\mathbf{F}$ and the change in fluid mass content m, and is decomposed into an *effective* and a *fluid contribution*:

$$\widehat{\psi}(\mathbf{F}, m) = \widehat{\psi}_{\text{eff}}(\mathbf{F}) + \widehat{\psi}_{\text{fl}}(\mathbf{F}, m), \tag{258}$$

where the first term represents the elastic energy of the dry porous skeleton, and the second accounts for the energy stored by the compressible pore fluid. For the solid skeleton, a compressible Neo-Hookean model [66] of the form

$$\widehat{\psi}_{\text{eff}}(\mathbf{F}) = \frac{G}{2}(\text{tr}(\mathbf{C}) - 3) - G\ln J + \frac{\lambda}{2}(\ln J)^2, \tag{259}$$

is adopted, taking in count for the compressibility of the system due to the pores. In the expression, $\mathbf{C} = \mathbf{F}^{T}\mathbf{F}$ is the right Cauchy–Green deformation tensor, $J = \det(\mathbf{F})$ is the Jacobian, $G > 0$ is the shear modulus, and λ is the Lamé bulk modulus. In the limiting case of small strain regime, such parameters are related to the drained Poisson's ratio ν through the well-known relation $K = 2G(1+\nu)/[3(1-2\nu)]$ and $\lambda =$, where K is the drained bulk modulus [32].
The pore-fluid energy is taken to be quadratic in the fluid content variation:

$$\widehat{\psi}_{\text{fl}}(\mathbf{F}, m) = \frac{M}{2}\left[b(J-1) - \frac{m}{\rho_f}\right]^2, \tag{260}$$

where b denotes Biot's coefficient, M is Biot's modulus, and ρ_f is the fluid density.

The dissipative behavior related to Darcy-type flow is governed by the potential

$$\widehat{\phi}(\mathbf{H}; \mathbf{F}) = \frac{1}{2}\,\mathbf{H} : \widehat{\mathbf{K}}^{-1} : \mathbf{H}, \qquad \widehat{\mathbf{K}} = (\rho_f)^2 K J\,\mathbf{C}^{-1}, \tag{261}$$

where $\mathbf{H}$ is the material mass flux, $\mathbf{C}$ is the right Cauchy–Green tensor, J the Jacobian, and K the spatial permeability tensor, which is related to Darcy's hydraulic conductivity k_h through $K = k_h/(\rho_f g)$. In the isotropic case, the permeability simplifies to $\boldsymbol{\kappa} = \kappa \mathbf{I}$.

The governing equations of the coupled deformation-fluid-transport problem, formulated in terms of the primary variables $\boldsymbol{\chi}, m$ and $\mathbf{H}$, with the related boundary conditions, are summarized in (262).

$$
\begin{aligned}
&\textit{Compatibility equation} && \nabla \times (\mathbf{F}) = \mathbf{0} && \text{in } \mathcal{B}_0 \\
&\textit{Balance of mass} && \dot{m} + \nabla_{\boldsymbol{\chi}} \cdot \mathbf{H} = 0 && \text{in } \mathcal{B}_0 \\
&\textit{Balance of linear momentum} && \nabla_{\boldsymbol{\chi}} \cdot \mathbf{P} + \rho \mathbf{b} = \mathbf{0} && \text{in } \mathcal{B}_0 \\
&\textit{Balance of angular momentum} && \mathbf{F}^{-1}\mathbf{P} = (\mathbf{F}^{-1}\mathbf{P})^{T} && \text{in } \mathcal{B}_0 \\
&\textit{Constitutive total stresses} && \mathbf{P} = \partial_{\boldsymbol{\chi}} \hat{\psi}(\boldsymbol{\chi}, m) && \text{in } \mathcal{B}_0 \\
&\textit{Constitutive fluid potential} && \mu = \partial_m \hat{\psi}(\boldsymbol{\chi}, m) && \text{in } \mathcal{B}_0 \\
&\textit{Constitutive fluid potential gradient} && \nabla_{\boldsymbol{\chi}} \mu + \partial_{\mathbf{H}_0} \hat{\phi}(\mathbf{H}) = \mathbf{0} && \text{in } \mathcal{B}_0 \\
&\textit{Prescribed displacement} && \mathbf{u} = \bar{\mathbf{u}} && \text{on } \partial\mathcal{B}_0^{u} \\
&\textit{Prescribed fluid potential} && \mu = \bar{\mu} && \text{on } \partial\mathcal{B}_0^{\mu} \\
&\textit{Prescribed tractions} && \mathbf{P} \cdot \mathbf{n}_0 = \bar{\mathbf{t}} && \text{on } \partial\mathcal{B}_0^{t} \\
&\textit{Prescribed normal fluxes} && \mathbf{H} \cdot \mathbf{n}_0 = \bar{H} && \text{on } \partial\mathcal{B}_0^{H}
\end{aligned}
\tag{262}
$$

Remark 10 (On the stress tensor and fluid potential.)**.** The first Piola- Kirchhoff stress tensor $\mathbf{P}$ and the fluid potential μ follow from differentiation of the free energy with respect to $\mathbf{F}$ and m, respectively:

$$
\mathbf{P} = \frac{\partial \widehat{\psi}_{fl}}{\partial \mathbf{F}} = G(\mathbf{F} - \mathbf{F}^{-T}) + \lambda \ln J \, \mathbf{F}^{-T} + Mb\left[b(J-1) - \frac{m}{\rho_f}\right] J \, \mathbf{F}^{-T}, \tag{263}
$$

$$
\mu = \frac{\partial \widehat{\psi}}{\partial m} = -\frac{M}{\rho_f}\left[b(J-1) - \frac{m}{\rho_f}\right]. \tag{264}
$$

Equation (263) reveals the additive structure of the total stress, composed of an *effective* stress term associated with the deformation of the solid matrix and a pressure-related contribution generated by the pore fluid. This naturally leads to the classical decomposition

$$
\mathbf{P} = \mathbf{P}' - \alpha p \, \mathbf{I}, \tag{265}
$$

where α is the Biot coefficient and $p = \rho_f \mu$. The special case $\alpha = 1$ corresponds to a perfectly incompressible solid phase, which recovers the original effective stress principle proposed by Terzaghi in the small-strain limit. For a fully incompressible

fluid phase, the constraint $1/M = 0$ applies, and μ acts as a Lagrange multiplier enforcing incompressibility.
Finally, the associated Darcy law in the spatial configuration reads

$$\nabla_{\chi}\mu = -\frac{\partial\widehat{\phi}}{\partial\mathbf{H}} = -(\rho_f^2\widehat{\mathbf{K}})^{-1}\mathbf{H} \quad \Longrightarrow \quad \mathbf{h} = -\rho_f^2\kappa\nabla_{\chi}\mu, \tag{266}$$

showing that the permeability tensor, although isotropic in the reference configuration, can evolve into an anisotropic one under large deformations due to its dependence on both porosity and the deformation gradient.

5.3 HYBRID FORMULATION OF POROELASTICITY

5.3.1 *Canonical minimization principle of poroelasticity*

In this section, following the procedure presented in Ch. (4), we briefly recall the canonical minimization principle of poroelasticity, which is derived from a rate-type variational framework formulated in terms of the primary variables introduced in Sec. 5.2.1. Subsequently, we introduce and discuss the hybrid variational principle, which extends this framework to a discretized setting while relaxing some of the continuity requirements, providing a generalized statement of Eq. 225.

5.3.2 *Canonical minimization principle of poroelasticity*

The coupled boundary-value problem of poroelasticity can be expressed through the rate-type variational formulation proposed by Miehe, Mauthe, and Teichtmeister [82]. This principle is directly derived from the stored energy and dissipation functionals presented in Sec. 5.2.3. Based on the deformation map field $\boldsymbol{\chi}$ and the material fluid mass flux $\mathbf{H}$, a canonical minimization principle can be defined, thus avoiding the explicit enforcement of the inf–sup stability condition typically associated with saddle-point formulations [121].
For a given state $\{\dot{\boldsymbol{\chi}}, \mathbf{H}, \dot{m}\}$, the *rate potential* is introduced as [82, Eq. (33)]:

$$\bar{\Pi}(\dot{\boldsymbol{\chi}}, \mathbf{H}, \dot{m}) = \int_{\mathcal{B}} \pi(\dot{\mathbf{F}}(\dot{\boldsymbol{\chi}}), \mathbf{H}, \dot{m})\, dV - \mathcal{P}_{\text{ext}}(\dot{\boldsymbol{\chi}}, \mathbf{H}), \tag{267}$$

where π denotes the internal rate potential per unit volume, defined as

$$\pi(\dot{\mathbf{F}}, \mathbf{H}, \dot{m}) = \dot{\hat{\psi}}(\mathbf{F}, m) + \hat{\phi}(\mathbf{H}), \tag{268}$$

as in Ch. (4), $\dot{\hat{\psi}} = \partial\hat{\psi} : \dot{\mathbf{F}} - \partial_m\hat{\psi}\,\dot{m}$. The external power $\mathcal{P}_{\text{ext}}$ includes the work of surface tractions $\bar{\mathbf{t}}$ and the contribution due to mass transport across the boundary

associated with a prescribed potential $\bar{\mu}$ [82, Eq. (30)]. Body forces are neglected here for the sake of simplicity.

A time-discrete version of (267) can be obtained by integrating over the time interval $[t_n, t_{n+1}]$ with time step $\Delta t = t_{n+1} - t_n > 0$, assuming that all state variables are known at t_n, under the quasi-static assumption. Following a backward Euler fully implicit time integration scheme, the mass conservation equation (245) can be discretized as

$$m^{(n+1)} = m^{(n)} - \Delta t \, \nabla_X \cdot \mathbf{H}^{(n+1)}. \tag{269}$$

This discretization preserves the consistency of the continuous dissipation structure, as shown by Miehe, Mauthe, and Teichtmeister [82]. By substituting the discrete mass balance directly into the energy functional over the time interval Δt, one obtains the canonical *incremental variational formulation*, which depends only on the deformation map and flux fields, $\boldsymbol{\chi}$ and $\mathbf{H}$ [see 121, Eqs. (28)–(30)]:

$$\begin{aligned} \bar{\Pi}^{\Delta t}(\boldsymbol{\chi}, \mathbf{H}) &= \int_{\mathcal{B}} \pi^{\Delta t}(\mathbf{F}, \mathbf{H}, m) \, dV - \mathcal{P}_{\text{ext}}^{\Delta t}(\boldsymbol{\chi}, \mathbf{H}) \\ &= \int_{\mathcal{B}} \hat{\psi}(\mathbf{F}, m) - \hat{\psi}^{(n)} + \Delta t \, \hat{\phi}(\mathbf{H}) \, dV \\ &\quad - \int_{\partial \mathcal{B}^t} \bar{\mathbf{T}} \cdot (\boldsymbol{\chi} - \boldsymbol{\chi}^{(n)}) \, ds + \Delta t \int_{\partial \mathcal{B}^\mu} \bar{\mu} \, \mathbf{H} \cdot \mathbf{n}_0 \, ds. \end{aligned} \tag{270}$$

in which the superscript $(n+1)$ has been omitted for the sake of readability. The corresponding incremental minimization problem [121, Eq. (31)] reads

$$\{\boldsymbol{\chi}, \mathbf{h}\} = \arg\min_{\boldsymbol{\chi} \in \mathcal{V}_\chi} \min_{\mathbf{H} \in \mathcal{V}_H} \bar{\Pi}^{\Delta t}(\boldsymbol{\chi}, \mathbf{H}), \tag{271}$$

which determines the displacement and material fluid mass flux at the current time step t_{n+1}.

Although this principle provides a robust and thermodynamically consistent foundation for modeling coupled porous media, difficulties may arise when discretizing the flux field. The admissible deformation map space $\mathcal{V}_\chi \subset \mathbf{H}^1(\mathcal{B})$ can be conveniently approximated by piecewise C^0-continuous polynomial functions, as in standard finite element methods. In contrast, the admissible flux space $\mathcal{V}_h \subset H(\text{div}, \mathcal{B})$ consists of functions with square-integrable divergence, which require element-wise continuity of their normal components across interfaces [29]. The original discretization of (270) employed lowest-order Raviart–Thomas (RT) elements [121], ensuring piecewise constant divergence and continuity of the flux normal components between adjacent elements. While this formulation is mathematically consistent, it introduces a substantial number of degrees of freedom, thereby leading to a high computational cost. Moreover, the enforcement of strict inter-element continuity may become overly restrictive when modeling materials with discontinuities or strong spatial heterogeneities [58].

In the following section, this incremental principle is reformulated within a hybrid framework, in which the continuity constraint on the flux field is relaxed through the introduction of inter-element Lagrange multipliers [97]. This hybridization ensures *co-diffusivity*, meaning that the normal component of the resulting flux remains continuous between adjacent elements, while the tangential component is allowed to be discontinuous.

5.3.3 *Hybrid variational principle of poroelasticity*

A discretization of the two-dimensional domain $\mathcal{B} \subset \mathbb{R}^2$ of a the poroelastic medium, denoted as ${}^{h}\mathcal{B} = \bigcup_{e=1}^{N_e} \mathcal{B}_e$, is considered, where N_e represents the total number of non-overlapping subdomains $\mathcal{B}_e$, each bounded by $\partial\mathcal{B}_e$. The boundary of each element is divided into S_e sides $\partial\mathcal{B}_e^s$, such that $\partial\mathcal{B}_e = \bigcup_{s=1}^{S_e} \partial\mathcal{B}_e^s$..Each side $\partial\mathcal{B}_e^s$ can either belong to the set of free boundaries $\partial\mathcal{B}_e^s \subset (\partial\mathcal{B}^t \cup \partial\mathcal{B}^h)$, to the set of constrained boundaries $\partial\mathcal{B}_e^s \subset (\partial\mathcal{B}^u \cup \partial\mathcal{B}^\mu)$, or to an internal interface shared by two adjacent subdomains, denoted as $\partial\mathcal{B}^{\text{int}\,s} \equiv \partial\mathcal{B}_{e_1}^s \cap \partial\mathcal{B}_{e_2}^s, \quad e_1 \neq e_2$.

Within this partitioned domain, the deformation map field ${}^{h}\boldsymbol{\chi}$ is required to satisfy continuity across element interfaces, to ensure the compatibility law. Conversely, the material flux field ${}^{h}\mathbf{H}$ is defined in a finite-dimensional subspace of vector fields that ensure local mass conservation *within each subdomain*. To enforce the inter-element continuity of the normal component of $\mathbf{h}$ (codiffusivty of fluxes), a Lagrange multiplier λ_e^s is introduced along the element sides $s = 1, \dots, S_e$.
By embedding this constraint into the rate potential (267), we obtain the generalized statement of the *hybrid rate functional* introduced in Chapter (4) for small strains assumption:

$$
\begin{aligned}
{}^{h}\bar{\Pi}(\dot{\boldsymbol{\chi}}, \mathbf{h}, \dot{m}, \lambda) = \sum_{e=1}^{N_e} \Bigg[\int_{\mathcal{B}_e} \pi(\dot{\mathbf{F}}_e, \dot{m}_e, \mathbf{H}_e)\, dV - \mathcal{P}_{\text{ext}}(\dot{\boldsymbol{\chi}}_e, \mathbf{h}_e) \\
+ \sum_{s=1}^{S_e} \int_{\partial\mathcal{B}_e^s / \partial\mathcal{B}_e^\mu} \lambda_e^s \left(\mathbf{H}_e \cdot \mathbf{n}_{0e}^s - \bar{H} \right) dS,
\end{aligned}
\tag{272}
$$

with $\bar{\mathbf{H}}$ the prescribed material flux vector, being null everywhere except on $\partial\mathcal{B}^H$. As in Chapter 4, the positive sign in the term associated with the Lagrange multipliers is chosen so that each contribution consistently represents the negative of the external power. This formulation leads to a well-posed discretization, provided that the stability conditions established by Brezzi [28] are fulfilled.

5.3.3.1 *Incremental form of the Hybrid functional*

To derive the variational formulation, we consider the time-discrete counterpart of the functional (272), adopting a fully implicit Backward Euler integration scheme as defined in (269). Making use of the kinematic relation $\mathbf{F} = \nabla_{\boldsymbol{\chi}}\mathbf{u} + \mathbf{I}$, the dependence is reformulated in terms of the displacement field $\mathbf{u}$ rather than the position field $\boldsymbol{\chi}$, to remain consistent with the common convention in the literature.
Accordingly, the Jacobian determinant can be expressed in terms of the nodal displacements as $J = \det(\mathbf{F}) = \det(\nabla_{\boldsymbol{\chi}}\mathbf{u} + \mathbf{I})$. The corresponding variations of $\mathbf{F}$ and J with respect to the virtual displacement $\delta\mathbf{u}$ are given by $\delta\mathbf{F} = \mathbf{B}_e\mathbf{u}_e$ and $\delta J = J\mathbf{F}^{-T}$.
Finally, by substituting the expression of the internal rate potential, $\pi = \dot{\hat{\psi}}(\mathbf{F}_e, \nabla_{\boldsymbol{\chi}} \cdot \mathbf{h}_e) + \hat{\phi}(\mathbf{h}_e)$, together with the constitutive relations provided in (190), into the functional (272), we obtain the corresponding *incremental hybrid functional*:

$$
\begin{aligned}
&\Pi^{\Delta t}(\mathbf{u}, \mathbf{H}, \lambda) = \\
&= \sum_{e=1}^{N_e} \left[\int_{\mathcal{B}_0} \{\hat{\psi}(\mathbf{F}, \nabla_{\boldsymbol{\chi}} \cdot \mathbf{H}) - \hat{\psi}_n + \Delta t\, \hat{\phi}(\mathbf{H}) dV\} - P_{ext} - Hybr = \right. \\
&= \int_{\mathcal{B}_0} \hat{\psi}_{\text{eff}}(\mathbf{F}) dV + \int_{\mathcal{B}_0} \hat{\psi}_{fl}(\mathbf{F}, \nabla_{\boldsymbol{\chi}} \cdot \mathbf{H}) dV - \int_{\mathcal{B}_0} \hat{\psi}_n dV \\
&+ \int_{\mathcal{B}_0} \frac{\Delta t}{2} \hat{\phi}(\mathbf{H}) dV - \int_{\partial \mathcal{B}_0^t} \bar{\mathbf{T}} \left[(\mathbf{u} + \mathbf{X}) - (\mathbf{u} + \mathbf{X})_n \right] dA \\
&+ \sum_s \left[\Delta t \int_{\partial \mathcal{B}_0 / \partial \mathcal{B}_0^{e_\mu}} \lambda \left(\mathbf{H} \cdot N - \bar{H}_n \right) dA \right] + \Delta t \int_{\partial \mathcal{B}_0^\mu} \bar{\mu} \mathbf{H} \cdot \mathbf{N} dA.
\end{aligned}
\tag{273}
$$

As we have introduced in Chapter 1, the assessment of stationarity conditions of the associated variational principle serves as an essential feature in inferring the variational consistency to the weak form of the governing equations of the problem. We define the functional spaces to which the field variations ${}^h\delta\boldsymbol{\chi}, {}^h\delta\mathbf{H}, {}^h\delta\lambda$ belong:

$$
\begin{aligned}
&{}^h\mathcal{W}_{\delta\chi} = \left\{ {}^h\delta\boldsymbol{\chi} \in [H^1(\mathcal{B})]^d \,\middle|\, {}^h\delta\boldsymbol{\chi} = 0 \text{ on } \partial\mathcal{B}^u \right\}, \\
&{}^h\mathcal{W}_{\delta\mathbf{H}}^{\text{disc}} = \\
&\left\{ {}^h\delta\mathbf{H} \in [L^2(\mathcal{B})]^d \,\middle|\, {}^h\delta\mathbf{h}|_{\mathcal{B}_e} \in \mathbb{P}_k(\mathcal{B}_e; \mathbb{R}^d),\ {}^h\delta\mathbf{H} \cdot \mathbf{n} = 0 \text{ on } \partial\mathcal{B}^h,\ \forall\, \mathcal{B}_e \in {}^h\mathcal{B} \right\}, \\
&{}^h\mathcal{W}_{\delta\lambda,l} = \\
&\left\{ {}^h\delta\lambda \in L^2(\partial\mathcal{B}) \,\middle|\, {}^h\delta\lambda|_{\partial\mathcal{B}_e^s} \in \mathbb{P}_l(\partial\mathcal{B}_e^s),\ {}^h\delta\lambda = 0 \text{ on } \partial\mathcal{B},\ \forall\, \partial\mathcal{B}_e^s \subset {}^h\partial\mathcal{B}^s \right\},
\end{aligned}
\tag{274}
$$

For the trial functions, on the other hand, we have (for a more detailed discussion on the choice of the functional space of the field $\mathbf{H}$ the reader is referred to remark 9:

$$
\begin{aligned}
&{}^{h}\mathcal{V}_{\chi} = \left\{ {}^{h}\chi \in [H^{1}(\mathcal{B})]^{d} \,\middle|\, {}^{h}\chi = \bar{\chi} \text{ on } \partial\mathcal{B}^{u} \right\} , \\
&{}^{h}\mathcal{V}_{\mathbf{H}} = \\
&\left\{ {}^{h}\mathbf{H} \in [L^{2}(\mathcal{B})]^{d} \,\middle|\, {}^{h}\mathbf{H}|_{\mathcal{B}_e} \in \mathbb{P}_{k}(\mathcal{B}_e;\mathbb{R}^{d}),\ {}^{h}\mathbf{H}\cdot\mathbf{n} = \bar{H} \text{ on } \partial\mathcal{B}^{t},\ \forall\, \mathcal{B}_e \in {}^{h}\mathcal{B} \right\} , \\
&{}^{h}\mathcal{V}_{\lambda,l} = \\
&\left\{ {}^{h}\lambda \in L^{2}(\partial\mathcal{B}) \,\middle|\, {}^{h}\lambda|_{\partial\mathcal{B}^{s}_{e}} \in \mathbb{P}_{l}(\partial\mathcal{B}^{s}_{e}),\ {}^{h}\lambda = \bar{\lambda} \text{ on } \partial\mathcal{B},\ \forall\, \partial\mathcal{B}^{s}_{e} \subset {}^{h}\partial\mathcal{B}^{s} \right\} ,
\end{aligned}
\tag{275}
$$

The stationarity of the functional ${}^{h}\bar{\Pi}^{\Delta t}$ at time t_{n+1}, with respect to the admissible primary and Lagrangian variables, leads to the following Euler equations for the reference subdomain $\mathcal{B}^{0}_{e}$:

Stress equilibrium	$\nabla_{\mathbf{X}}\cdot(\partial_{\mathbf{F}}\hat{\psi}) = 0$	in $\mathcal{B}_0$
Inverse Darcy law	$\nabla_{\mathbf{X}}\left(\partial_{m}\hat{\psi}\right) + \partial_{\mathbf{H}}\hat{\phi} = 0$	in $\mathcal{B}_0$
Prescribed tractions	$\partial_{\mathbf{F}}\hat{\psi}\cdot\mathbf{N} - \bar{\mathbf{T}} = 0$	on $\partial\mathcal{B}^{t}_{0}$
Prescribed fluid potential	$-\partial_{m}\hat{\psi} + \bar{\mu} = 0$	on $\partial\mathcal{B}^{\mu}_{0}$
Prescribed normal fluxes	$\mathbf{H}\cdot\mathbf{N} - \bar{H} = 0$	on $\partial\mathcal{B}_0 \cap \partial\mathcal{B}^{h}_{0}$
Inter-element continuity	$\mathbf{H}_{e_1}\cdot\mathbf{N}_{e_1} + \mathbf{H}_{e_2}\cdot\mathbf{N}_{e_2} = 0$	on $\partial\mathcal{B}^{\text{int}}$

(276)

Notably, as shown by $(276)_5$, the Lagrange multiplier λ emerges as the fluid potential field $\mu = -\frac{\partial\hat{\psi}_{fl}}{\partial m}$, with $\mu = \bar{\mu}$ on $\partial\mathcal{B}_0 \cap \partial\mathcal{B}^{\mu}_{0}$. Once this correspondence between the fluid potential field and the Lagrange variable is established, the functional space adopted for λ^{s} and its variation coincides with that of the fluid potential field and its variation itself:

$$
\begin{aligned}
&{}^{h}\mathcal{W}_{\mu,l} = \\
&\left\{ {}^{h}\mu \in L^{2}(\partial\mathcal{B}) \,\middle|\, {}^{h}\mu|_{\partial\mathcal{B}^{s}_{e}} \in \mathbb{P}_{l}(\partial\mathcal{B}^{s}_{e}),\ {}^{h}\mu = \bar{\mu} \text{ on } \partial\mathcal{B},\ \forall\, \partial\mathcal{B}^{s}_{e} \subset {}^{h}\partial\mathcal{B}^{s} \right\} , \\
&{}^{h}\mathcal{W}_{\delta\mu,l} = \\
&\left\{ \delta{}^{h}\mu \in L^{2}(\partial\mathcal{B}) \,\middle|\, \delta{}^{h}\mu|_{\partial\mathcal{B}^{s}_{e}} \in \mathbb{P}_{l}(\partial\mathcal{B}^{s}_{e}),\ \delta{}^{h}\mu = 0 \text{ on } \partial\mathcal{B},\ \forall\, \partial\mathcal{B}^{s}_{e} \subset {}^{h}\partial\mathcal{B}^{s} \right\} ,
\end{aligned}
\tag{277}
$$

Remark 11. (On the stationarity of the functional.) The stationarity of the hybrid incremental functional is evaluated with respect to the primary variables $\mathbf{u}$, $\mathbf{H}$ defined in $\mathcal{B}^{e}_{0}$, and the Lagrange multipliers $\boldsymbol{\lambda}^{s}_{e}$ defined over the boundaries $\partial\mathcal{B}^{s}_{e}$, at time $t = t_{n+1}$.

Making use of the identities $dF_{ij}/du_k\,\delta u_k = \delta_{ik}\delta u_k,_j$ and $dJ/dF_{ij} = JF^{-1}_{ji}$, the stationarity with respect to $\mathbf{u}$ gives :

$$\sum_{e=1}^{N_e}\left[\int_{\mathcal{B}_0}\frac{\partial\hat{\psi}_{eff}}{\partial F_{ij}}\frac{\partial F_{ij}}{\partial u_k}\,\delta u_k\,dV+\int_{\mathcal{B}_0}\frac{\partial\hat{\psi}_{fl}}{\partial J}\frac{dJ}{dF_{ij}}\frac{dF_{ij}}{du_k}\delta u_k dA-\int_{\partial\mathcal{B}^t_0}\bar{T}_k\,\delta u_k dA=0\right], \quad (278)$$

with δu_i an admissible virtual displacement satisfying $\delta u_i = 0$ on $\partial\mathcal{B}^u_e$ at time t_{n+1}. Rearranging we obtain:

$$\sum_{e=1}^{N_e}\left[\int_{\mathcal{B}_0}\left[\frac{\partial\hat{\psi}_{eff}}{\partial F_{kj}}-bJ\rho\mu F_{kj}\right]\delta u_k,_j\,dV-\int_{\partial\mathcal{B}^t_0}\bar{T}_k\cdot\delta u_k dA=0\right]. \quad (279)$$

Rearranging terms and applying the divergence theorem yields the Euler equations

$$-\left(\frac{\partial\hat{\psi}}{\partial F_{ij}}\right)_{,j}=0\quad\text{in }\mathcal{B}_e\,,\qquad\frac{\partial\hat{\psi}}{\partial F_{ij}}n_j-\bar{T}_i=0\quad\text{on }\partial\mathcal{B}^t_e\,. \quad (280)$$

As the flux field is independently defined within each element domain, the stationarity condition with respect to $H_{,i}$ can be formulated directly at the element level:

$$\begin{aligned}&\int_{\mathcal{B}_0}\Delta t\frac{\partial\hat{\psi}_{fl}}{\partial m}\frac{\partial H_{i,i}}{\partial H_k}\,\delta H_k\,dV+\int_{\mathcal{B}_0}\Delta t\left(\frac{\partial\hat{\phi}}{\partial H_k}\right)\delta H_k\;d\mathcal{B}_0\\&+\sum_s\int_{\partial\mathcal{B}_0/\partial\mathcal{B}^\mu_0}\lambda\,(\delta H_k N_k)\,dA+\int_{\partial\mathcal{B}^\mu_0}\bar{\mu}\delta H_k N_k dA=0,\end{aligned} \quad (281)$$

where $\delta\mathbf{H}$ is an admissible virtual fluid flux that satisfies $\delta H_k\,N_k = 0$ on $\partial\mathcal{B}^h_0$ at time t_{n+1}. Performing integration by parts, we obtain:

$$\begin{aligned}&\int_{\mathcal{B}_0}\left[\Delta t\left(\frac{\partial\hat{\psi}_{fl}}{\partial m}\right)_{,k}+\left(\frac{\partial\hat{\phi}}{\partial H_k}\right)\right]\delta H_k dV+\int_{\partial\mathcal{B}_0}\Delta t\left(\frac{\partial\hat{\psi}_{fl}}{\partial m}\right)\delta H_k N_k\,dA\\&\sum_s+\int_{\partial\mathcal{B}_0/\partial\mathcal{B}^\mu_0}\lambda\,\delta H_k\,N_k dA+\int_{\partial\mathcal{B}_0\mu}\bar{\mu}\,\delta\mathbf{H}_k N_k dA=0.\end{aligned} \quad (282)$$

We obtain the following Euler equations:

$$\begin{aligned}
&\left(\frac{\partial\hat{\psi}_{fl}}{\partial m}\right)_{,k} + \left(\frac{\partial\hat{\phi}}{\partial H_{0\,k}}\right) = 0 \text{ on } \partial\mathcal{B}_0,\\
&-\left(\frac{\partial\hat{\psi}_{fl}}{\partial m}\right) = \lambda \text{ on } \partial\mathcal{B}_0 \setminus \partial\mathcal{B}_0^{\mu},\\
&-\left(\frac{\partial\hat{\psi}_{fl}}{\partial m}\right) = \bar{\mu} \text{ on } \partial\mathcal{B}_e^{s} \cap \partial\mathcal{B}_0^{\mu}.
\end{aligned} \tag{283}$$

Similarly, stationarity with respect to the Lagrange variable λ gives

$$\sum_s \int_{\partial\mathcal{B}_0/\partial\mathcal{B}_{0\mu}} \Delta t \left(H_k N_k - \bar{H}\right)\, \delta\lambda \, dA = 0, \tag{284}$$

where $\delta\lambda^s$ is an admissible virtual Lagrange multiplier that satisfies $\delta\lambda^s = 0$ on $\partial\mathcal{B}_e^{\mu} \cap \partial\mathcal{B}_e^{s}$ at time t_{n+1}. The following boundary and inter-element conditions are obtained as from which we obtain the Euler equations:

$$\begin{aligned}
&H_k N_k - \bar{H} = 0 \quad \text{ on } \partial\mathcal{B}_e^{s} \cap \partial\mathcal{B}_e^{h},\\
&(H_k N_k)_{e_1} - (H_k N_k)_{e_2} = 0 \quad \text{ on } \partial\mathcal{B}_e^{\text{int}\,s} \equiv \partial\mathcal{B}_{e_1}^{s} \cap \partial\mathcal{B}_{e_2}^{s}.
\end{aligned} \tag{285}$$

5.4 DISCRETE FORM

Let us introduce now the interpolation schemes adopted for the primary variables $\{\mathbf{u}_e, \mathbf{H}_e\}$ and for the Lagrange multipliers $\boldsymbol{\mu}_e^s$, in a total Lagrangian framework. In contrast to standard finite element formulations, the proposed Hybrid Finite Element (HFE) approach defines the flux field directly in terms of Cartesian polynomial functions, whose coefficients, referred to as *generalized flux variables*, constitute the unknowns of the fluid problem. In this work, a quadratic triangular element is employed, oriented with respect to a local Cartesian coordinate system (x, y) whose origin coincides with vertex 1 (see Fig. 15). Accordingly, the flux components are represented by second-order polynomial expansions of the form

$$H_{e,x}(x,y) = a_1 + a_2 x + a_3 y + a_4 xy + a_5 x^2 + a_6 y^2, \tag{286}$$

$$H_{e,y}(x,y) = a_7 + a_8 x + a_9 y + a_{10} xy + a_{11} x^2 + a_{12} y^2, \tag{287}$$

$$\nabla \cdot \mathbf{H}_e(x,y) = a_2 + a_4 y + 2a_5 x + a_9 + a_{10} x + 2a_{12} y, \tag{288}$$

where the coefficients a_n ($n = 1, \ldots, 12$) denote the generalized flux variables, and the last expression gives the local divergence of the flux field, $\nabla \cdot \mathbf{H}_e(x, y)$. Following this notation, the generalized flux field can be written in matrix form as

$$\mathbf{h}_e(\mathbf{x}) = \mathbf{H}_e(\mathbf{x})\, \mathbf{h}_e, \tag{289}$$

where $\mathbf{H}_e(\mathbf{x})$ is the coefficient matrix and $\mathbf{h}_e$ collects all generalized flux degrees of freedom.

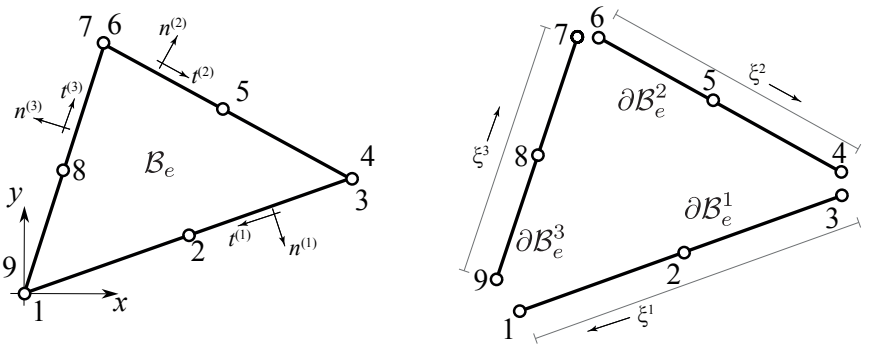

Figure 24: Nine-node triangular hybrid flux element, where the fluid fluxes and the Lagrangian fluid potential variables are interpolated. The displacement field is defined over an overlapping six-node quadratic isoparametric triangular element.

The fluid potential variables defined along the element boundaries $\partial\mathcal{B}_e^s$ ($s = 1, \ldots, 3$), which act as Lagrange multipliers, are interpolated through an isoparametric mapping given by

$$\mu_e^s(\xi^s) = \overline{\mathbf{N}}(\xi^s)\, \boldsymbol{\mu}_e^s, \tag{290}$$

where $\overline{\mathbf{N}}$ contains the quadratic shape functions, and $\boldsymbol{\mu}_e^s$ represents the fluid potential degrees of freedom associated with side $\partial\mathcal{B}_e^s$.

The displacement field, on the other hand, is interpolated using standard quadratic shape functions defined in the natural coordinates (η_1, η_2). The nodes located at element vertices are geometrically coincident and are coupled through a local connectivity matrix. Hence, the displacement and strain fields are expressed as

$$\mathbf{u}_e(\boldsymbol{\eta}) = \mathbf{N}_e(\boldsymbol{\eta})\, \mathbf{u}_e, \quad \mathbf{F}_e(\boldsymbol{\eta}) = \mathbf{B}_e(\boldsymbol{\eta})\, \mathbf{u}_e + \mathbf{I}, \tag{291}$$

where $\mathbf{N}$ is the shape function matrix for nodal displacements, $\mathbf{u}_e$ collects the nodal displacement degrees of freedom, $\mathbf{I}$ stand for the identity matrix and $\mathbf{B}_e$ denotes the strain–displacement operator.

It is worth emphasizing that, within the hybrid framework, the nodal degrees of freedom are intrinsically associated with the element sides, which allows adjacent elements to share nodes along their common edges. As a result, the discretization generated by the HFE contains multiple coincident nodes at element vertices, while

the mid-side nodes remain independent. For the adopted quadratic formulation, the fluid potential field is thus discretized over nine nodes per element, with each vertex containing multiple coincident nodes, as illustrated in Fig. 24. This design ensures that both boundary and inter-element continuity conditions are correctly satisfied [83, 93].

By substituting the interpolation expressions introduced above into the incremental hybrid functional (273), we obtain its time- and space-discrete form in Voigt notation. [1] Substituting the espression of $\hat{\psi}_{fl}$ from 260, and for the sake of clarity, omitting the time index $(n+1)$, the *discrete formulation of the incremental hybrid functional* is given

$$\begin{aligned}\Pi^{\Delta t} = \sum_{e=1}^{N_e} \Bigg[& \int_{\mathcal{B}_0} \widehat{\psi}_{\text{eff}}(\mathbf{F})\, dV + \int_{\mathcal{B}_0} \left[\frac{M}{2} \left(b(J-1) - \frac{m_n}{\rho_f} + \frac{\Delta t\, \mathbf{H}_e^*}{\rho_f} \mathbf{h}_e \right) \right]^2 dV \\ & + \int_{\mathcal{B}_0^e} \frac{1}{2} \Delta t\, \mathbf{h}_e^T \mathbf{H}_e^T \hat{\mathbf{K}}^{-1} \mathbf{H}_e \mathbf{h}_e\, dV - \int_{\partial \mathcal{B}_e^t} \bar{\mathbf{t}}^T \mathbf{N}_e\, dA\, (\mathbf{u} - \mathbf{u}^{(n)}) \\ & + \Delta t \sum_{s=1}^{S_e} \left[\mu_e^s \int_{\partial \mathcal{B}_e^s} \mathbf{M}_e^{s\,T} \mathbf{H}_e \mathbf{n}_e^s\, dA\, \mathbf{h}_e - \mu_e^{s\,T} \int_{\partial \mathcal{B}_e^h} \mathbf{M}_e^{s\,T} \bar{h}_n\, dA \right] \\ & + \Delta t \int_{\partial \mathcal{B}_e^s} \bar{\mu}\, \mathbf{H}_e \mathbf{n}_e^s\, dA\, \mathbf{h}_e \Bigg]\end{aligned} \tag{292}$$

The stationary conditions for the global system can be derived from the discretized form of the functional in Eq.292. Namely,

$$\begin{aligned} \partial_{\mathbf{u}} \Pi^{\Delta t} &= \mathbf{r}^u - \bar{\mathbf{T}} = 0, \\ \partial_{\mathbf{h}_e} \Pi^{\Delta t} &= \mathbf{r}_e^h = 0, \\ \partial_{\mu_s} \Pi^{\Delta t} &= \mathbf{r}^\mu - \bar{\mathbf{H}} = 0, \end{aligned} \tag{293}$$

having introduced the residues $\mathbf{r}^u, \mathbf{r}_e^h, \mathbf{r}^\mu$ at time tn+1:

$$\begin{aligned} \mathbf{r}^u &= \sum_e \mathbf{q}_e^u = \sum_e \left[\int_{\mathcal{B}_e} \left(\mathbf{P}_{\text{eff}}^T - p J \mathbf{F}^{-T} \right) \mathbf{B}_e dV \right] \\ \mathbf{r}_e^h &= \int_{\mathcal{B}_e^0} M \left(b(J-1) - \frac{m_n}{\rho_f} \right) \frac{\Delta t}{\rho_f} \mathbf{H}_e^{*T}\, dV + \int_{\mathcal{B}_e^0} \mathbf{H}_e^{T*} \frac{\Delta t^2}{\rho_f^2} M \mathbf{H}_e^* \mathbf{h}_e dV \\ &\quad + \int_{\mathcal{B}_0^e} \Delta t\, \mathbf{H}_e^T \hat{\mathbf{K}}^{-1} \mathbf{H}_e \mathbf{h}_e dV + \Delta t \int_{\partial \mathcal{B}_e^0} \left(\mu_e^T \mathbf{M}_e^T \mathbf{H}_e \mathbf{n}_e^s \right) dS \\ \mathbf{r}^\mu &= \sum_e \mathbf{q}_e^\mu = \sum_e \sum_s \left[\int_{\partial \mathcal{B}_e^0} \mathbf{M}_e^T \mathbf{H}_e \mathbf{n}_e^s dS \mathbf{h}_e \right] \end{aligned} \tag{294}$$

1 In Eq. (225), the operator $\mathbf{B}_e^* = \mathbf{m}^T \mathbf{B}_e$ is defined to represent volumetric strains in two dimensions, following Zienkiewicz, Taylor, and Zhu [134, Ch. 10]. Here, $\mathbf{m} = [1\ 1\ 0]^T$ satisfies $\mathbf{I} : \boldsymbol{\varepsilon}_e = \mathbf{m}^T \mathbf{B}_e \mathbf{u}_e$. The divergence of the discrete flux field is written as $\nabla \cdot \mathbf{h}_e = \mathbf{H}_e^* \mathbf{h}_e$, where $\mathbf{H}_e^* = [\frac{\partial}{\partial x} \ \frac{\partial}{\partial y}] \mathbf{H}_e$. The discrete material normal vector is denoted as $\mathbf{n}_e$, to prevent any ambiguity with the displacement shape function.

through the following definitions:

$$
\begin{aligned}
p &= -M\left(b(J-1) - \frac{m_n}{\rho_f} + \frac{\Delta t\, \mathbf{H}^*_e}{\rho_f}\mathbf{h}_e\right) \\
\bar{\mathbf{T}} &= \sum_e \mathbf{f}^t_{e,s} = \sum_e \left[\int_{\partial\mathcal{B}^t_0} \bar{\mathbf{t}}^T \mathbf{N}_e dA\right] \\
\bar{\mathbf{H}} &= \sum_e \mathbf{f}^h_{e,s} = \sum_e \left[\int_{\Gamma_s \cup \Gamma^0_h} \mathbf{M}^{s\,T}_e \bar{h}_n \, dA\right].
\end{aligned}
\tag{295}
$$

The vector $\mathbf{h}$ is independently defined for each element, therefore, the residual $\mathbf{r}^e_h$ is expressed for the single element. The second equation in Eq.293 can be thus formulated directly on the individual finite element, representing the weak form of the inverse Darcy's law. Notably, the relations derived from the residual formulation are inherently nonlinear. Consequently, a computable approximation of the solution requires the linearization of the residual equations, which is carried out through the concept of the directional derivative, as discussed in Bonet and Wood [22]. This procedure enables the implementation of an iterative Newton-Raphson method for solving the resulting system of equations.

Residual vector $\mathbf{r}_u$

For the residual vector $\mathbf{r}_u(\mathbf{u}, \mathbf{h})$ at the timestep $(i+1)$ we have:

$$
\begin{aligned}
\mathbf{r}^u &= \mathbf{r}^{u,(i)} + \frac{d\mathbf{r}^u}{d\mathbf{u}}\Delta\mathbf{u} + \frac{d\mathbf{r}^u}{d\mathbf{h}}\Delta\mathbf{h} = ru,(i) + \sum_e \left[\frac{d\mathbf{q}^u_e}{d\mathbf{u}_e}\Delta\mathbf{u}_e + \frac{d\mathbf{q}^u_e}{d\mathbf{h}_e}\Delta\mathbf{h}_e\right] = 0, \\
\mathbf{r}_u &= \mathbf{r}^{(i)}_u + \sum_e \left[(\bar{\mathbf{K}}^{uu}_e + \bar{\bar{\mathbf{K}}}^{uu}_e)\Delta\mathbf{u}_e + \mathbf{K}^{uh}_e\Delta\mathbf{h}_e\right] = 0.
\end{aligned}
\tag{296}
$$

being the derivative of the residual $\mathbf{r}_u$, with respect to the variables $\mathbf{u}$ and $\mathbf{H}$

$$
\begin{aligned}
\frac{d\mathbf{r}_u}{d\mathbf{u}} &= \sum_e \int_{\mathcal{B}^e_0} \left[\frac{d\mathbf{P}}{dF}\mathbf{B}_e\right]^T \mathbf{B}_e dV - \int_{\mathcal{B}^e_0} \mathbf{B}^T_e \mathbf{F}^{-1} J \frac{dp}{dJ} J\mathbf{F}^T \mathbf{B}_e dV \\
&\quad - \int_{\mathcal{B}^e_0} p_i \frac{dJ}{dF}\mathbf{B}^T_e \mathbf{F}^T \mathbf{B}_e dV - \int_{\mathcal{B}^e_0} p_i J \frac{d\mathbf{F}^{-T}}{d\mathbf{u}}\mathbf{B}_e dV = \\
&\quad = \sum_e \int_{\mathcal{B}^e_0} \mathbf{B}^T_e \mathbf{C}^{PF}\mathbf{B}_e dV + \int \mathbf{B}^T_e \mathbf{F}^{-1} JMbJ\mathbf{F}^{-T}\mathbf{B}_e dV = \sum_e \left[\overline{\mathbf{K}}^{uu}_e + \overline{\overline{\mathbf{K}}}^{uu}_e\right] \\
\frac{d\mathbf{r}_u}{d\mathbf{h}_e} &= -\int_{\mathcal{B}^0_e} \frac{\partial}{\partial\mathbf{h}}\left[pbJ\mathbf{F}^{-T}\right]\mathbf{B}_e dV = +\int_{\mathcal{B}^0_e} bJ\mathbf{B}^T_e \mathbf{F}^{-1}\frac{M\Delta t}{\rho_F}\mathbf{H}^*_e dV = \mathbf{K}^{uh}_e.
\end{aligned}
\tag{297}
$$

with

$$\bar{\mathbf{r}}_e^{u(i)} = \int_{\Omega_0^e} \left(\mathbf{P}_{\text{eff}}^T + JM \left(b(J-1) - \frac{m_n}{\rho_f} \right) \mathbf{F}^{-T} \right) \mathbf{B}_e \, dV. \tag{298}$$

Residual vector $\mathbf{r}_h$

For the element residual vector $\mathbf{r}_h^{(i+1)}(\mathbf{u}, \mathbf{h}, \boldsymbol{\mu})$ at the timestep $(i+1)$ we can write:

$$\begin{aligned} \mathbf{r}_e^{h(i+1)} &= \mathbf{r}_e^{h(i)} + \frac{d\mathbf{r}_e^h}{d\mathbf{u}_e}\Delta\mathbf{u}_e + \frac{d\mathbf{r}_e^h}{d\mathbf{h}_e}\Delta\mathbf{h}_e + \frac{d\mathbf{r}_e^h}{d\boldsymbol{\mu}_e}\Delta\boldsymbol{\mu}_e = \\ &= \bar{\mathbf{r}}_e^{h(i)} + \mathbf{K}_e^{uh^T}\Delta\mathbf{u}_e + \mathbf{K}_e^{hh}\mathbf{h}_e + \mathbf{K}_e^{\mu h^T}\Delta\boldsymbol{\mu}_e = 0 \end{aligned} \tag{299}$$

being the derivative of the residual rh, with respect to the variables u, H and mu

$$\begin{aligned} \frac{d\mathbf{r}_e^h}{d\mathbf{u}_e} &= \int_{\mathcal{B}_e^0} \mathbf{H}_e^{*T} \frac{Mb\Delta t}{\rho_f} J\mathbf{F}^{-T}\mathbf{B}_e dV = \int_{\mathcal{B}_0^e} \mathbf{H}_e^{*T} \frac{Mb\Delta t}{\rho_f} \mathbf{F}^{-T}\mathbf{B}_e dV = \mathbf{K}_e^{hu} = \mathbf{K}_e^{uhT}, \\ \frac{d\mathbf{r}_e^h}{d\mathbf{h}_e} &= \int_{\mathcal{B}_e^0} \mathbf{H}_e^{T*} \frac{\Delta t^2}{\rho_f^2} M\mathbf{H}_e^* dV + \int_{\mathcal{B}_0^e} \Delta t \mathbf{H}_e^T \hat{\mathbf{K}}^{-1} \mathbf{H}_e dV = \overline{\overline{\mathbf{K}}}_e^{hh} + \overline{\overline{\mathbf{K}}}_e^{hh} = \mathbf{K}_e^{hh}, \\ \frac{d\mathbf{r}_e^h}{d\boldsymbol{\mu}_e} &= \sum_s \left[\Delta t \int_{\partial\mathcal{B}_e^0} \left(\mathbf{M}_e^T \mathbf{H}_e \mathbf{n}_e^s \right)^T dS \right] = \mathbf{K}_e^{\mu h T}, \end{aligned} \tag{300}$$

where the matrix $\mathbf{K}_e^{\mu h} = \left[\mathbf{K}_{e,1}^{\mu h}, \mathbf{K}_{e,2}^{\mu h}, \mathbf{K}_{e,3}^{\mu h} \right]^T$ collects the relevant side element matrices, and

$$\bar{\mathbf{r}}_e^{h(i)} = \int_{\mathcal{B}_e^0} M \left(b(J^{(i)} - 1) - \frac{m_n}{\rho_f} \right) \frac{\Delta t}{\rho_f} M\mathbf{H}_e^{*T} \, dV, \tag{301}$$

Residual vector $\mathbf{r}_\mu$

The third stationarity condition yields a linear equation, and therefore no linearization is required. Therefore, the third equation of the expression is recalled Eq.297:

$$\mathbf{r}^\mu = \sum_e \mathbf{q}_e^\mu = \sum_e \mathbf{K}_e^{\mu h} \mathbf{h}_e, \tag{302}$$

with

$$\mathbf{K}_e^{\mu h} = \Delta t \sum_s \left[\int_{\partial\mathcal{B}_e^0} \mathbf{M}_e^T \mathbf{H}_e \mathbf{n}_e^s dS \right], \tag{303}$$

where $\mathbf{q}_e^\mu = \left[\mathbf{q}_{e,1}^\mu, \mathbf{q}_{e,2}^\mu, \mathbf{q}_{e,3}^\mu \right]^T$ collects the nodal flux vectors of the three sides of the element.

To summarize, the stationary conditions governing the global system 293 may be equivalently expressed by incorporating the definitions provided in Eq.296-303:

$$\begin{aligned}
\partial_{\mathbf{u}}\Pi &:= \mathbf{r}_e^{(u} = \sum_e \left[(\overline{\mathbf{K}}_e^{uu} + \overline{\overline{\mathbf{K}}}_e^{uu})\Delta\mathbf{u}_e + \mathbf{K}_e^{uh}\mathbf{h}_e \right] + \sum_e \mathbf{q}_e^{u\,(i)} - \bar{\mathbf{T}} = 0. \\
\partial_{\mathbf{h}}\Pi &:= \mathbf{r}_e^{h} = \mathbf{K}_e^{uh^T}\Delta\mathbf{u}_e + \mathbf{K}_e^{hh}\mathbf{h}_e + \mathbf{K}_e^{\mu h^T}\boldsymbol{\mu}_e + \bar{\mathbf{r}}_e^{h(i)} = 0. \\
\partial_{\mu}\Pi &:= \sum_e \mathbf{q}_e^{\mu} - \bar{\mathbf{H}} = \sum_e \left[\mathbf{K}_e^{\mu h}\mathbf{h}_e \right] - \bar{\mathbf{H}}
\end{aligned} \tag{304}$$

Since the generalized flux vector $\mathbf{h}_e$ is independently interpolated within each element, the second equation in Eq.304, which represents the weak form of the inverse Darcy's law, is formulated at the element level. The nodal force vector $\mathbf{q}_e^u$, corresponding to the work-equivalent forces transmitted to the element nodes, and the nodal flux vector $\mathbf{q}_e^{\mu}$, associated with fluid transport induced by pressure gradients and source terms, are defined then as follows:

$$\begin{aligned}
\mathbf{q}_e^u &= (\bar{\mathbf{K}}_e^{uu} + \bar{\bar{\mathbf{K}}}_e^{uu})\Delta\mathbf{u}_e + \mathbf{K}_e^{uh}\mathbf{h}_e - \bar{\mathbf{r}}_e^{u(i)}, \\
\mathbf{q}_e^h &= \mathbf{K}_e^{uh^T}\Delta\mathbf{u}_e + \mathbf{K}_e^{hh}\mathbf{h}_e + \mathbf{K}_e^{\mu h^T}\boldsymbol{\mu}_e - \mathbf{r}_e^{h(i)} = 0, \\
\mathbf{q}_e^{\mu} &= \mathbf{K}_e^{\mu h}\mathbf{h}_e,
\end{aligned} \tag{305}$$

keeping in mind that the superscript $(i+1)$ has been omitted here for the sake of clarity. Denoting the sum $(\overline{\mathbf{K}}_{uu}^e + \overline{\overline{\mathbf{K}}}_{uu}^e)$ as $\mathbf{K}_e^{uu}$, the iterative element equations (305) can be written in the matrix notation as

$$\begin{bmatrix} \mathbf{q}_e^u \\ \mathbf{q}_e^{\mu} \\ 0 \end{bmatrix} = \begin{bmatrix} \mathbf{K}_e^{uu*} & 0 & \mathbf{K}_e^{uh} \\ 0 & 0 & \mathbf{K}_e^{\mu h} \\ \mathbf{K}_e^{uh^T} & \mathbf{K}_e^{\mu h^T} & \mathbf{K}_e^{hh} \end{bmatrix} \begin{bmatrix} \Delta\mathbf{u}_e \\ \boldsymbol{\mu}_e \\ \mathbf{h}_e \end{bmatrix} - \begin{bmatrix} \bar{\mathbf{r}}_u^{e(i)} \\ 0 \\ \mathbf{r}_h^{e(i)} \end{bmatrix}. \tag{306}$$

By assembling the nodal displacement vector $\Delta\mathbf{u}_e$ and the nodal fluid potential vector $\boldsymbol{\mu}_e$ into a unified array of unknowns, denoted by $\Delta\mathbf{u}_e^*$, and similarly grouping the nodal force vectors $\mathbf{q}_e^u$ and $\mathbf{q}_e^{\mu}$ into the composite vector $\mathbf{q}_e^*$, the element-level equations can be expressed in a compact matrix form as:

$$\begin{bmatrix} \mathbf{q}_e^* \\ 0 \end{bmatrix} = \begin{bmatrix} \mathbf{K}_e^{uu*} & \mathbf{K}_e^{uh*} \\ \mathbf{K}_e^{uh*T} & \mathbf{K}_e^{hh} \end{bmatrix} \begin{bmatrix} \Delta\mathbf{u}_e^* \\ \mathbf{h}_e \end{bmatrix} - \begin{bmatrix} \bar{\mathbf{r}}_e^{u(i)} \\ \mathbf{r}_e^{h(i)} \end{bmatrix}, \tag{307}$$

where the column vector $[\bar{\mathbf{r}}_e^{u(i)}, \bar{\mathbf{r}}_e^{h(i)}]^T$ denotes the incremental residual associated with the element under consideration. The matrix $\mathbf{K}_e^{uu}$ is symmetric, positive definite, and non-singular due to the convex nature of the underlying variational functional [121], enabling the condensation of the generalized flux variables at the element level. Following the standard hybrid finite element methodology [57], the computational

procedure is thus formulated in terms of the elimination of internal variables. Consequently, the resulting system of equations is expressed solely in terms of the primary nodal quantities, namely the displacement and fluid potential degrees of freedom. Then, the generalized flux vector $\mathbf{h}_e$ is condensed out from the second equation in Eq.(305)

$$\mathbf{h}_e = \mathbf{K}_e^{hh^{-1}} \left[\mathbf{r}_e^{h(i)} - \mathbf{K}_e^{uh^T} \Delta \mathbf{u}_e^* \right]. \tag{308}$$

The corresponding nodal force vector $\mathbf{q}_e^*$ can therefore be written as:

$$\mathbf{q}_e^* = \mathbf{K}_e^{uu} \, \Delta \mathbf{u}_e^* + \mathbf{K}_e^{uh*} \, \mathbf{h}_e - \bar{\mathbf{r}}_u^{e(i)}, \tag{309}$$

which yields

$$\mathbf{q}_e^* = \underbrace{\left[\mathbf{K}_e^{uu} - \mathbf{K}_e^{uh*} \mathbf{K}_e^{hh-1} \mathbf{K}_e^{uh*T} \right]}_{\mathbf{K}_e} \mathbf{u}_e^* - \left[\bar{\mathbf{r}}_e^{u(i)} - \mathbf{K}_e^{uh*} \mathbf{K}_e^{hh-1} \bar{\mathbf{r}}_h^{h(i)} \right], \tag{310}$$

where $\mathbf{K}_e$, the incremental stiffness matrix, corresponds to the Schur complement of the first matrix in Eq. (308) [78]. Consequently, it is symmetric and positive definite, since the $\mathbf{K}_e^{hh}$ matrix is itself symmetric and positive definite by construction. The term enclosed in brackets on the right-hand side represents the incremental residual vector evaluated at the initial iteration. This structure enables the hybrid finite element scheme to be seamlessly integrated into a standard displacement-based finite element framework [83].

5.5 NUMERICAL SIMULATIONS

In this chapter we revisit two of the benchmark problems already discussed in Chapter 4, but reformulated within the finite deformation framework introduced in Section 5.3. The purpose is not to reintroduce the problems in detail, but rather to assess the consistency of the nonlinear framework when applied to canonical tests whose analytical solutions are derived under small deformation assumptions. In these cases, the finite deformation formulation is expected to reproduce the linear solution, thus providing a stringent verification of the implementation. At the same time, we show that when finite strains develop, the small deformation formulation is no longer able to provide an accurate description, whereas the large deformation framework continues to deliver physically consistent results.

5.5.1 *Terzaghi's problem*

The classical consolidation problem of Terzaghi, already presented in Section 5.5.1, is here re-examined with the finite deformation formulation. The problem setup, bound-

ary conditions, and material parameters are identical to those in Chapter 4 and will not be repeated here. Figure 25 shows the comparison between the pore pressure profiles obtained with the finite deformation formulation, the small deformation solution, and the analytical solution. As expected, the results show that the curve in large deformations perfectly overlaps with that from the small deformation formulation and analytical solution, as reported in Fig. 25, thus confirming the consistency of the nonlinear code when applied to a benchmark in which small strains are involved. While in this benchmark the two formulations yield indistinguishable results, the large deformation framework becomes essential when addressing scenarios characterized by significant strains or nonlinear material responses .This observation is in line with the considerations of Larsson and Larsson [68], who showed that the two formulations coincide in the limit of small strains, while appreciable differences emerge when finite deformations are involved. To illustrate this point, we have repeated the same benchmark under a modified set of parameters chosen to induce larger strains, following the approach of Li, Borja, and Regueiro [71]. For comparison, the numerical solution is evaluated against the analytical one reported in Cheng and Detournay [33]. First, the displacement field is plotted for an applied load of $q = 0.04\,\text{MPa}$, corresponding to a small-strain analysis (Fig. 26). The solution obtained from the large-strain formulation, which coincides with that of the small-strain case, shows an excellent agreement with the analytical solution, thus confirming the steady-state value reported in Li, Borja, and Regueiro [71].

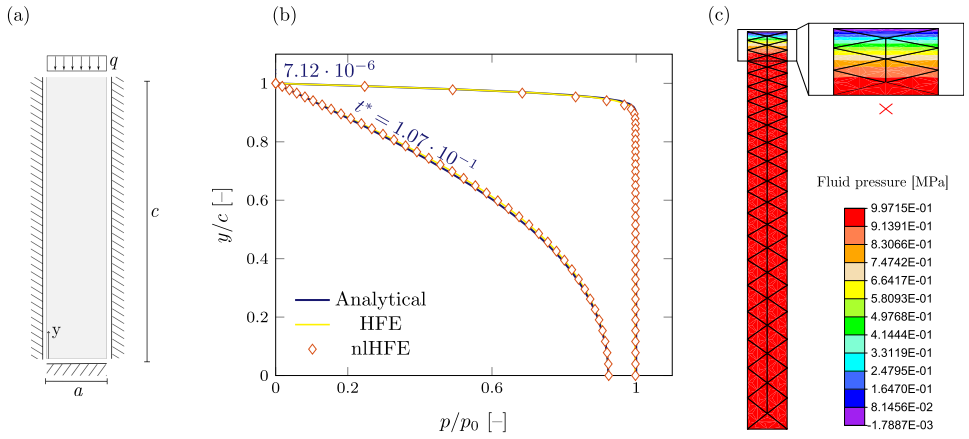

Figure 25: Terzaghi's problem: comparison of normalized pore pressure vs depth distributions obtained with the analytical solution in [128] and the small and finite deformation HFE.

Subsequently, the analysis is extended to the large-deformation regime (Fig. 27) by applying external loads of $q = 2$, 4, and 8 MPa. In this case, the small deformation formulation departs significantly from the expected physical response, whereas the

finite deformation framework continues to provide a consistent solution. To validate this observation, the two numerical solutions are compared against the steady-state response obtained from the purely elastic solution of the system, accounting for both geometric and constitutive nonlinearities. The results confirm that the finite deformation formulation is required to capture the correct behaviour once the problem departs from the linearized kinematic regime.

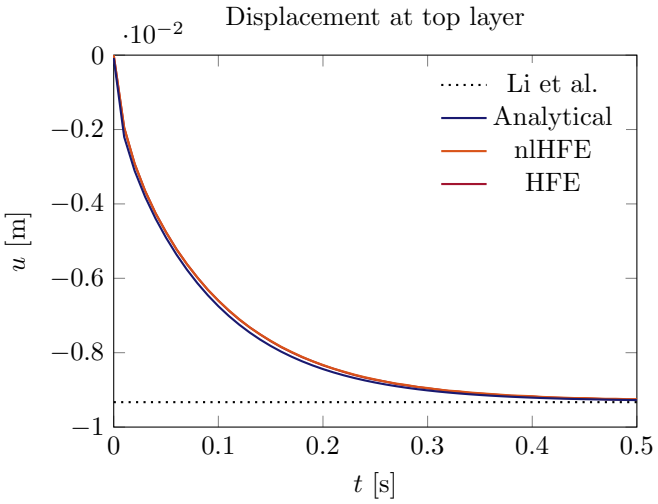

Figure 26: Terzaghi's problem: comparison of displacements at the top layer against time obtained with the analytical solution in [128] and the small and finite deformation HFE, for a load q=0.04 MPa.

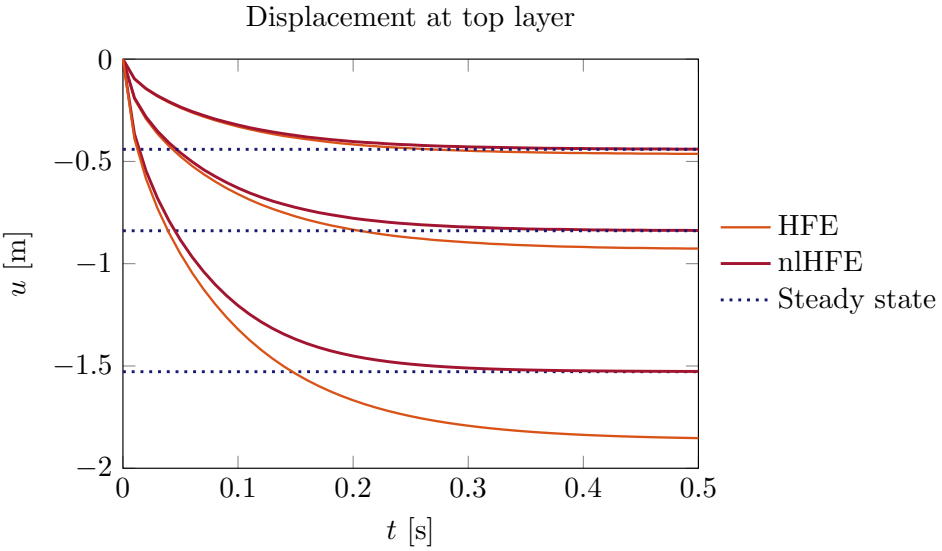

Figure 27: Terzaghi's problem: displacements at the top layer against time solutions obtained with small and finite deformation formulations, for a load of q=2, 4 and 8 MPa, are compared with the steady state solution [71].

5.5.2 *Low permeability layer*

The second benchmark, consisting of a stratified medium with a central layer of reduced permeability, was already introduced in Chapter 4. The same configuration is here reconsidered within the finite deformation framework. Geometry, boundary conditions, and material parameters are unchanged and are not repeated for brevity. Figure 28 presents the pore pressure distribution obtained with the nonlinear formulation, together with the corresponding small deformation solution, from both HFE and analytical solution. The two results are indistinguishable, and no spurious oscillations are observed, despite the severe hydraulic heterogeneity introduced by the low-permeability layer. In Figure 29 the the nonlinear framework is compared with the results from [121] as expected, it reproduces physical behaviour and confirms its robustness even in the presence of strong permeability discontinuities. This outcome, combined with the Terzaghi benchmark, shows that the finite deformation formulation remains consistent with the linear theory when strains are small, while offering the necessary generality to address more demanding scenarios. As an immediate extension of the present work, more detailed analyses of geometric nonlinearities, together with the investigation of complex geometries and boundary conditions, will be required to further assess the capability of the formulation to deliver accurate and computationally efficient results in large deformation poromechanics.

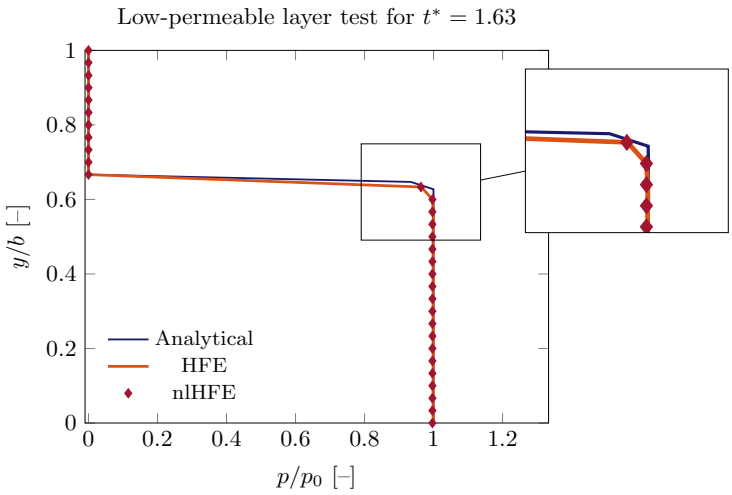

Figure 28: Low permeability problem: pore pressure distributions obtained with small and finite deformation HFE, against the analytical solution in [128]. The solutions coincide, confirming stability and accuracy of the nonlinear framework in the presence of strong hydraulic heterogeneities.

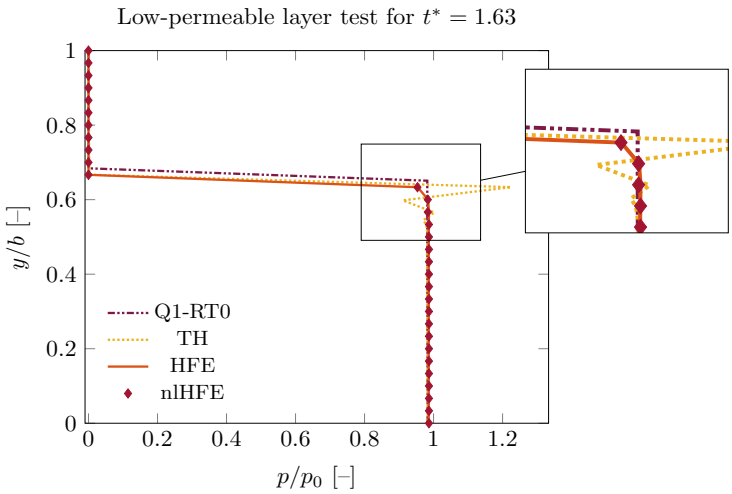

Figure 29: Low permeability problem: pore pressure distributions obtained with small and finite deformation HFE, against the Q1-RT0 and TH element solution [121].

5.6 CONCLUSIONS AND FUTURE PERSPECTIVES

This study extends to the finite-deformation regime the hybrid finite element formulation introduced in Chapter 4, adopting a total Lagrangian framework that preserves

fluxes for the transient analysis of poroelastic media. The method is developed by selecting the deformation map and the material fluid mass fluxes as the primary variables. The principal advancement lies in the hybridization of the canonical minimization framework for poroelasticity proposed by Miehe, Mauthe, and Teichtmeister [82], here reinterpreted within a hybrid equilibrium setting, an approach previously demonstrated to be effective in stress-based poroelasticity [72], linear elasticity [93, 95], and nonlinear fracture mechanics [94].

As a preliminary step, a hybrid variational principle was formulated, and the corresponding stationarity conditions were systematically derived. Based on this theoretical foundation, a triangular hybrid finite element was implemented within the open-source finite element software FEAP [120]. Some preliminary comparative analyses of classical benchmark tests in poromechanics confirmed the accuracy and stability of the proposed methodology, consistent with its variational derivation and the symmetry of the resulting system matrix. In agreement with the results obtained for the small-deformation formulation, the computed fluid pressure fields were free from spurious oscillations, commonly observed in conventional mixed u–p formulations, without requiring any stabilization procedure. Moreover, for benchmark simulations involving small displacements, the results were in perfect agreement with those produced by the corresponding small-strain formulation.

As for the hybrid formulations introduced in Chapter 3 and 4, although the inclusion of the fluid potential as a Lagrange multiplier increases the number of elemental degrees of freedom, the proposed scheme remains computationally efficient through static condensation of generalized fluxes at the element level. Unlike standard mixed methods, the hybrid framework reduces the global system to a single matrix equation expressed in terms of generalized nodal variables. As a result, it ensures flux compatibility across element interfaces while preserving the implementation simplicity of a displacement-based approach.

A noteworthy outcome of the numerical experiments is the high accuracy achieved in the evaluation of the fluid potential, even on relatively coarse meshes. This characteristic proves especially beneficial in problems exhibiting steep pressure gradients. Additionally, the relaxation of flux continuity constraints across element boundaries enhances the robustness of the formulation when applied to geometrically complex and strongly coupled multiphysics problems. The resulting flux fields display co-diffusive behavior at the element level, with continuity of the normal component across adjacent elements.

Despite these encouraging results, several aspects merit further investigation, particularly the rigorous enforcement of phase incompressibility in the fluid phase. Future developments may explore augmented Lagrangian or related techniques to address this challenge effectively. Further studies are also required to evaluate the convergence rates of the proposed formulation and to perform direct comparisons with existing numerical solutions to assess its performance quantitatively. Upcoming research will

focus on examining the efficiency and accuracy of the method in simulations involving complex geometries and boundary conditions, where nonlinear coupling effects become dominant. Finally, particular attention will be devoted to problems where permeability highly depends on the deformation gradient, allowing for meaningful comparisons with alternative formulations available in the literature.

CONCLUSIONS

In this thesis, a new class of hybrid–mixed finite element formulations for the diffusion deformation coupled problem in porous media has been developed, designed to combine inherent stability with computational efficiency. The proposed approach is based on the introduction of an alternative set of primary variables, through which the governing equations can be recast in the form of a variational minimization, rather that saddle, principle. This principle is subsequently hybridized by incorporating an additional field acting as a Lagrange multiplier, which enforces weak continuity of one of the primary fields across element boundaries. Such a formulation removes the need for globally conforming function spaces for one of the primal variables, thereby enhancing flexibility in the numerical discretization. By enforcing only weak continuity conditions for one of the primary variables, the hybrid framework successfully alleviates some of the classical limitations of traditional mixed methods for poroelasticity. This strategy is particularly beneficial in avoiding the numerical instabilities that typically arise from incompatible function spaces, ensuring stability at the local level and improving the global conditioning of the algebraic system. This aspect becomes especially relevant in problems characterized by discontinuities in permeability, where the pressure field often exhibits singular behavior. In such scenarios, conventional mixed formulations based on the displacement-pressure variable pair fail to enforce local continuity, leading to non-physical oscillations. Several methodologies have been proposed in the literature to mitigate these issues, among them, four-field approaches and a wide range of stable or stabilized finite element schemes. While these methods have proven effective in many contexts, the formulation presented in this work offers distinct advantages that, to the best of the author's knowledge, are not typically shared by existing approaches. Four-field formulations, for example, are intrinsically stable but require the introduction of a considerably larger number of primary variables, which inevitably increases computational cost and implementation complexity. By contrast, the method proposed, although it introduces additional degrees of freedom through the Lagrange multiplier method, can be efficiently reduced, via static condensation, to a system expressed solely in terms of generalized displacement degrees of freedom. This process reduces the global system to a compact form expressed solely in terms of generalized displacement variables, thus ensuring both computational efficiency and compatibility with standard finite element solvers. With respect to stabilized formulations, it is widely recognized that they can provide accurate and robust results across a broad spectrum of applications. However, they still encounter significant challenges in scenarios involving sharp permeability contrasts or material discontinuities, which are frequently observed in the modeling of biological or geological porous me-

dia. As highlighted by Teichtmeister, Mauthe, and Miehe [121], such discontinuities can compromise the stability and convergence properties even of advanced stabilized schemes. The approach developed in this thesis directly addresses these shortcomings, exhibiting enhanced robustness and accuracy in the presence of strong heterogeneities, and thus represents a reliable and rigorous alternative to traditional mixed and stabilized formulations. It should nevertheless be noted that the implementation of the proposed method may require the use of dedicated meshing procedures and customized post-processing tools, particularly for the visualization of condensed variables such as fluid fluxes and potentials. Despite these additional requirements, the method remains highly flexible and computationally efficient, offering significant advantages for a wide range of applications in poroelasticity and multiphysics modeling. Future developments will focus on a deeper assessment of the convergence behavior of the formulation and on its application to more complex nonlinear and coupled problems. These extensions are expected to open new perspectives in the computational analysis of saddle-type variational systems, which have traditionally posed significant numerical challenges. Overall, the proposed framework establishes a solid and versatile foundation for the next generation of hybrid variational formulations, with potential implications extending well beyond the field of poromechanics.

[1] Y. Abousleiman, A. H.-D. Cheng, L. Cui, E. Detournay, and J.-C. Roegiers. "Mandel's problem revisited." In: *Géotechnique* 46.2 (1996), pp. 187–195. ISSN: 0016-8505, 1751-7656. DOI: 10.1680/geot.1996.46.2.187.

[2] G. Aguilar, F. Gaspar, F. Lisbona, and C. Rodrigo. "Numerical stabilization of Biot's consolidation model by a perturbation on the flow equation." In: *International Journal for Numerical Methods in Engineering* 75.11 (2008), pp. 1282–1300. DOI: 10.1002/nme.2295.

[3] E. Ahmed, F. A. Radu, and J. M. Nordbotten. "Adaptive poromechanics computations based on a posteriori error estimates for fully mixed formulations of Biot's consolidation model." In: *Computer Methods in Applied Mechanics and Engineering* 347 (2019), pp. 264–294. ISSN: 0045-7825. DOI: https://doi.org/10.1016/j.cma.2018.12.016.

[4] J. P. Moitinho de Almeida and J. A. T. de Freitas. "Alternative approach to the formulation of hybrid equilibrium finite elements." In: *Computers & Structures* 40.4 (Jan. 1991), pp. 1043–1047. ISSN: 0045-7949. DOI: 10.1016/0045-7949(91)90336-K. (Visited on 11/04/2023).

[5] L. Anand. "2014 Drucker Medal Paper: A derivation of the theory of linear poroelasticity from chemoelasticity." In: *Journal of Applied Mechanics* 82.11 (2015), p. 111005. ISSN: 0021-8936, 1528-9036. DOI: https://doi.org/10.1115/1.4031049.

[6] R. M. Aronson, N. Castelletto, F. P. Hamon, J. A. White, and H. A. Tchelepi. "Pressure-stabilized fixed-stress iterative solutions of compositional poromechanics." In: *Computer Methods in Applied Mechanics and Engineering* 427 (2024), p. 117008. ISSN: 0045-7825. DOI: https://doi.org/10.1016/j.cma.2024.117008.

[7] G. A. Ateshian. "Mixture theory for modeling biological tissues: illustrations from articular cartilage." In: *Biomechanics: Trends in Modeling and Simulation*. Ed. by G. A. Holzapfel and R. W. Ogden. Vol. 20. Cham: Springer International Publishing, 2017, pp. 1–51. ISBN: 978-3-319-41473-7 978-3-319-41475-1. DOI: https://doi.org/10.1007/978-3-319-41475-1_1.

[8] G. A. Ateshian and J. A. Weiss. "Anisotropic hydraulic permeability under finite deformation." In: *Journal of Biomechanical Engineering* 132.11 (2010), pp. 1–7. DOI: 10.1115/1.4002588.

[9] F. Auricchio, L. B. Da Veiga, F. Brezzi, and C. Lovadina. "Mixed finite element methods." In: *Encyclopedia of Computational Mechanics*. Ed. by E. Stein, R. Borst, and T. J. R. Hughes. 2nd. Wiley, 2017, pp. 1–53. ISBN: 978-1-119-00379-3 978-1-119-17681-7. DOI: 10.1002/9781119176817.ecm2004.

[10] L. C. Auton and C. W. MacMinn. "From arteries to boreholes: Steady-state response of a poroelastic cylinder to fluid injection." In: *Proceedings of the Royal Society A: Mathematical, Physical and Engineering Sciences* 473.2201 (May 2017). ISSN: 1364-5021, 1471-2946. DOI: 10.1098/rspa.2016.0753.

[11] G. Avancini, N. Shauer, H. Luiz Oliveira, and P. R. Devloo. "A primal double-hybrid FEM for 3D compressible and incompressible elasticity using H(div)-L2 spaces." In: *Computer Methods in Applied Mechanics and Engineering* 446 (2025), p. 118295. ISSN: 0045-7825. DOI: https://doi.org/10.1016/j.cma.2025.118295.

[12] N. A. Barnafi, B. Gómez-Vargas, W. J. Lourenço, R. F. Reis, B. M. Rocha, M. Lobosco, R. Ruiz-Baier, and R. W. dos Santos. "Finite Element Methods for Large-Strain Poroelasticity/Chemotaxis Models Simulating the Formation of Myocardial Oedema." In: *Journal of Scientific Computing* 92.3 (2022), p. 92.

[13] K. Bathe. *Finite Element Procedures*. Prentice Hall, 2006. ISBN: 9780979004902. URL: https://books.google.it/books?id=rWvefGICfO8C.

[14] J. Bear. *Dynamics of Fluids in Porous Media*. New York: Elsevier, 1972.

[15] T. Belytschko, W. K. Liu, B. Moran, and K. I. Elkhodary. *Nonlinear finite elements for continua and structures*. 2nd. Chichester: Wiley, 2014.

[16] V. L. Berdichevsky. *Variational Principles of Continuum Mechanics. II. Applications*. 1st ed. Interaction of Mechanics and Mathematics. Springer Berlin Heidelberg, 2009, pp. X, 430. ISBN: 978-3-540-88468-2. DOI: 10.1007/978-3-540-88469-9.

[17] M. A. Biot. "General theory of three-dimensional consolidation." In: *Journal of Applied Physics* 12.2 (1941), pp. 155–164. DOI: 10.1063/1.1712886.

[18] M. A. Biot. "Theory of Finite Deformations of Porous Solids." In: *Indiana University Mathematics Journal* 21.7 (1972), pp. 597–620.

[19] R de Boer. "Theory of Porous Media: Highlights in Historical Development and Current State." In: *Applied Mechanics Reviews* 55.2 (Apr. 2002), B32–B33. ISSN: 0003-6900. DOI: 10.1115/1.1451169.

[20] R. de Boer and W. Ehlers. "The development of the concept of effective stresses." In: *Acta Mechanica* 83.1 (1990), pp. 77–92. ISSN: 1619-6937. DOI: 10.1007/BF01174734.

[21] D. Boffi, F. Brezzi, and M. Fortin. *Mixed Finite Element Methods and Applications*. 1st ed. Vol. 44. Springer Series in Computational Mathematics. Berlin, Heidelberg: Springer, 2013, pp. XIV + 685. ISBN: 978-3-642-36518-8. DOI: 10.1007/978-3-642-36519-5.

[22] J Bonet and R. D. Wood. *Nonlinear Continuum Mechanics for Finite Element Analysis*. Cambridge: Cambridge University Press, 2008. ISBN: 978-1-139-46754-4. DOI: https://doi.org/10.1017/CBO9780511755446.

[23] J. R. Booker and J. C. Small. "Finite layer analysis of consolidation. I." In: *International Journal for Numerical and Analytical Methods in Geomechanics* 6.2 (1982), pp. 151–171. DOI: 10.1002/nag.1610060204.

[24] J. Booker and J. Small. "An investigation of the stability of numerical solutions of Biot's equations of consolidation." In: *International Journal of Solids and Structures* 11.7 (1975), pp. 907–917. ISSN: 0020-7683. DOI: https://doi.org/10.1016/0020-7683(75)90013-X.

[25] R. M. Bowen. "Theory of mixtures." In: *Continuum Physics*. Elsevier, 1976, pp. 1–127. ISBN: 978-0-12-240803-8. DOI: 10.1016/B978-0-12-240803-8.50017-7.

[26] R. M. Bowen. "Incompressible porous media models by use of the theory of mixtures." In: *International Journal of Engineering Science* 18.9 (1980), pp. 1129–1148. ISSN: 0020-7225. DOI: https://doi.org/10.1016/0020-7225(80)90114-7.

[27] R. M. Bowen. "Compressible porous media models by use of the theory of mixtures." In: *International Journal of Engineering Science* 20.6 (Jan. 1982), pp. 697–735. ISSN: 0020-7225. DOI: https://doi.org/10.1016/0020-7225(82)90082-9.

[28] F. Brezzi. "On the existence, uniqueness and approximation of saddle-point problems arising from lagrangian multipliers." In: *Revue française d'automatique, informatique, recherche opérationnelle. Analyse numérique* 8.R2 (1974), pp. 129–151. ISSN: 0397-9342, 2777-3493. DOI: 10.1051/m2an/197408R201291.

[29] F. Brezzi and M. Fortin. *Mixed and Hybrid Finite Element Methods*. Springer Series in Computational Mathematics. New York: Springer-Verlag, 1991. ISBN: 978-0-387-97582-5. DOI: 10.1007/978-1-4612-3172-1.

[30] K. W. Cargill. "Prediction of consolidation of very soft soil." In: 110.6 (1984), 775 – 795. DOI: 10.1061/(ASCE)0733-9410(1984)110:6(775).

[31] D. Chapelle and K. J. Bathe. "The inf-sup test." In: *Computers & Structures* 47.4 (June 1993), pp. 537–545. ISSN: 0045-7949. DOI: https://doi.org/10.1016/0045-7949(93)90340-J.

[32] A. Cheng. *Poroelasticity*. New York: Springer International Publishing, 2016.

[33] A. H. Cheng and E. Detournay. "A direct boundary element method for plane strain poroelasticity." en. In: *International Journal for Numerical and Analytical Methods in Geomechanics* 12.5 (1988), pp. 551–572. ISSN: 0363-9061, 1096-9853. DOI: 10.1002/nag.1610120508.

[34] B. Cockburn. "An introduction to the Discontinuous Galerkin method for convection-dominated problems." In: *Advanced Numerical Approximation of Nonlinear Hyperbolic Equations: Lectures given at the 2nd Session of the Centro Internazionale Matematico Estivo (C.I.M.E.) held in Cetraro, Italy, June 23–28, 1997*. Ed. by A. Quarteroni. Berlin, Heidelberg: Springer Berlin Heidelberg, 1998. DOI: 10.1007/BFb0096353.

[35] B. Cockburn and J. Gopalakrishnan. "A Characterization of Hybridized Mixed Methods for Second Order Elliptic Problems." In: *SIAM Journal on Numerical Analysis* 42.1 (2004), pp. 283–301. DOI: 10.1137/S0036142902417893.

[36] B. D. Coleman and M. E. Gurtin. "Thermodynamics with Internal State Variables." In: *The Journal of Chemical Physics* 47.2 (July 1967), pp. 597–613. ISSN: 0021-9606. DOI: 10.1063/1.1711937.

[37] E. Comellas, S. Budday, J.-P. Pelteret, G. A. Holzapfel, and P. Steinmann. "Modeling the porous and viscous responses of human brain tissue behavior." In: *Computer Methods in Applied Mechanics and Engineering* 369 (Sept. 2020), p. 113128. ISSN: 0045-7825. DOI: 10.1016/j.cma.2020.113128. (Visited on 11/04/2023).

[38] O. Coussy. *Mechanics of Porous Continua*. Wiley, 1995. ISBN: 978-0-471-95267-1. URL: https://books.google.it/books?id=iZNsQgAACAAJ.

[39] O. Coussy. *Poromechanics*. 2nd. Chichester: Wiley, 2004. ISBN: 978-0-470-84920-0.

[40] O. Coussy, L. Dormieux, and E. Detournay. "From mixture theory to Biot's approach for porous media." In: *International Journal of Solids and Structures* 35.34 (1998), pp. 4619–4635. ISSN: 0020-7683. DOI: 10.1016/S0020-7683(98)00087-0.

[41] R. De Boer. *Theory of Porous Media*. Heidelberg: Springer, 2000. ISBN: 978-3-642-64062-9 978-3-642-59637-7. DOI: 10.1007/978-3-642-59637-7.

[42] V. Dobrev, T. Kolev, C. S. Lee, V. Tomov, and P. S. Vassilevski. "Algebraic Hybridization and Static Condensation with Application to Scalable H(div) Preconditioning." In: *SIAM Journal on Scientific Computing* 41.3 (2019), B425–B447. DOI: 10.1137/17M1132562.

[43] H. Egger and J. Schöberl. "A hybrid mixed discontinuous Galerkin finite-element method for convection–diffusion problems." In: *IMA Journal of Numerical Analysis* 30.4 (July 2009), pp. 1206–1234. ISSN: 0272-4979. DOI: 10.1093/imanum/drn083.

[44] W. Ehlers. "Foundations of multiphasic and porous materials." In: *Porous Media: Theory, Experiments and Numerical Applications*. Ed. by W. Ehlers and J. Bluhm. Berlin, Heidelberg: Springer Berlin Heidelberg, 2002, pp. 3–86. ISBN: 978-3-662-04999-0. DOI: 10.1007/978-3-662-04999-0_1.

[45] W. Ehlers and G Eipper. "Finite elastic deformations in liquid-saturated and empty porous solids." In: *Porous Media: Theory and Experiments*. Vol. 34. Dordrecht: Springer Netherlands, 1999, pp. 179–191.

[46] M. Flaschel, S. Kumar, and L. De Lorenzis. "Automated discovery of generalized standard material models with EUCLID." In: *Computer Methods in Applied Mechanics and Engineering* 405 (2023), p. 115867. ISSN: 0045-7825. DOI: 10.1016/j.cma.2022.115867.

[47] G. Franceschini, D Bigoni, P Regitnig, and G. A. Holzapfel. "Brain tissue deforms similarly to filled elastomers and follows consolidation theory." In: *Journal of the Mechanics and Physics of Solids* 54.12 (2006), pp. 2592–2620. DOI: 10.1016/j.jmps.2006.05.004.

[48] L. Galuppi, A. Haydar, and G. Royer-Carfagni. "Specialization of a new flux-based approach to thermal problems. Numerical study of glass façades of buildings with cast shadows." In: *Journal of Building Engineering* 98 (2024), p. 110949. ISSN: 2352-7102. DOI: https://doi.org/10.1016/j.jobe.2024.110949.

[49] C. Gavagnin, L. Sanavia, and L. De Lorenzis. "Stabilized mixed formulation for phase-field computation of deviatoric fracture in elastic and poroelastic materials." In: *Computational Mechanics* 65.6 (2020), pp. 1447–1465. ISSN: 0178-7675, 1432-0924. DOI: 10.1007/s00466-020-01829-x.

[50] P. Germain, Q. S. Nguyen, and P. Suquet. "Continuum Thermodynamics." In: *Journal of Applied Mechanics* 50.4b (Dec. 1983), pp. 1010–1020. ISSN: 0021-8936. DOI: 10.1115/1.3167184.

[51] A. Giammarini and A. Pandolfi. *A model of the human cornea as a hydrated, fluid-saturated medium*. 2025. DOI: https://doi.org/10.48550/arXiv.2510.07072.

[52] R. Gibson, G. England, and M. Hussey. "The theory of one-dimensional consolidation of saturated clays." In: *Geotechnique* 17.3 (1967), 261 – 273. DOI: 10.1680/geot.1967.17.3.261.

[53] R. Gibson, R. Schiffman, and K. Cargill. "The theory of one-dimensional consolidation of saturated clays. II. Finite nonlinear consolidation of thick homogeneous layers." In: *Canadian Geotechnical Journal* 18.2 (1981), 280 – 293. DOI: 10.1139/t81-030.

[54] J. D. Goddard. "Dissipation potentials for reaction-diffusion systems." In: *Industrial & Engineering Chemistry Research* 54.16 (2015), pp. 4078–4083. ISSN: 0888-5885. DOI: 10.1021/ie503661b.

[55] J. Gopalakrishnan and J. Guzmán. "Symmetric Nonconforming Mixed Finite Elements for Linear Elasticity." In: *SIAM Journal on Numerical Analysis* 49.4 (2011), pp. 1504–1520. DOI: 10.1137/10080018X.

[56] M. E. Gurtin, E. Fried, and L. Anand. *The Mechanics and Thermodynamics of Continua*. Cambridge: Cambridge University Press, 2010. ISBN: 978-0-521-40598-0. DOI: 10.1017/CBO9780511762956.

[57] R. J. Guyan. "Reduction of stiffness and mass matrices." In: *AIAA Journal* 3.2 (1965), pp. 380–380. DOI: doi.org/10.2514/3.2874.

[58] J. B. Haga, H. Osnes, and H. P. Langtangen. "On the causes of pressure oscillations in low-permeable and low-compressible porous media." In: *International Journal for Numerical and Analytical Methods in Geomechanics* 36.12 (2012), pp. 1507–1522. ISSN: 1096-9853. DOI: 10.1002/nag.1062.

[59] A. B. Harish, R. L. Taylor, and S. Govindjee. "A poroelastic element for FEAP using AceGen." English. In: *Current Trends and Open Problems in Computational Mechanics*. Springer Nature, Jan. 2022, pp. 161–169. DOI: 10.1007/978-3-030-87312-7_17.

[60] L. He, L. Jing, and M. Feng. "New stabilized mixed finite element methods for two-field poroelasticity with low permeability." In: *Applied Mathematics and Computation* 494 (2025), p. 129285. ISSN: 0096-3003. DOI: https://doi.org/10.1016/j.amc.2025.129285.

[61] G. A. Holzapfel. *Nonlinear Solid Mechanics: A Continuum Approach for Engineering Science*. Chichester: Wiley, 2000. DOI: 10.1023/A:1020843529530.

[62] W. Hong, X. Zhao, J. Zhou, and Z. Suo. "A theory of coupled diffusion and large deformation in polymeric gels." In: *Journal of the Mechanics and Physics of Solids* 56.5 (2008), pp. 1779–1793. DOI: 10.1016/j.jmps.2007.11.010.

[63] T. Hughes. *The Finite Element Method: Linear Static and Dynamic Finite Element Analysis*. Dover Civil and Mechanical Engineering. Dover Publications, 2012. ISBN: 9780486135021. URL: https://books.google.it/books?id=cHH2n_qBK0IC.

[64] C. T. Hwang, N. R. Morgenstern, and D. W. Murray. "On solutions of plane strain consolidation problems by finite element methods." In: *Canadian Geotechnical Journal* 8.1 (1971), pp. 109–118. ISSN: 0008-3674, 1208-6010. DOI: 10.1139/t71-009.

[65] A. B. Jeeja, B. Kiefer, S. Prüger, O. Rheinbach, and F. Röver. "Comparison of a Minimization and a Saddle Point Formulation of a Coupled Mechanics-Diffusion Problem Implemented in deal.II." In: *PAMM* 25.1 (2025), e202400188. DOI: https://doi.org/10.1002/pamm.202400188.

[66] A. Kossa, M. T. Valentine, and R. M. McMeeking. "Analysis of the compressible, isotropic, neo-Hookean hyperelastic model." In: *Meccanica* 58.1 (2023), pp. 217–232.

[67] D. Kucherenko and A. Korneva. "A poroelastic model of the optic nerve shows a significant effect of fluid pressure on the nerve fibers." In: *Mechanics of Materials* 204 (2025), p. 105299. ISSN: 0167-6636. DOI: https://doi.org/10.1016/j.mechmat.2025.105299.

[68] J. Larsson and R. Larsson. "Non-linear analysis of nearly saturated porous media: theoretical and numerical formulation." In: *Computer Methods in Applied Mechanics and Engineering* 191.36 (2002), pp. 3885–3907. ISSN: 0045-7825. DOI: https://doi.org/10.1016/S0045-7825(02)00333-X.

[69] Y. Leng, M. de Lucio, and H. Gomez. "Using poro-elasticity to model the large deformation of tissue during subcutaneous injection." In: *Computer Methods in Applied Mechanics and Engineering* 384 (Oct. 2021). ISSN: 0045-7825. DOI: https://doi.org/10.1016/j.cma.2021.113919.

[70] R. W. Lewis. *The finite element method in the static and dynamic deformation and consolidation of porous media*. John Wiley & Sons, 1999.

[71] C. Li, R. I. Borja, and R. A. Regueiro. "Dynamics of porous media at finite strain." In: *Computer Methods in Applied Mechanics and Engineering* 193.36-38 (2004), pp. 3837–3870. DOI: 10.1016/j.cma.2004.02.014.

[72] S. Lo Franco, F. Parrinello, and G. Borino. "A variationally-consistent hybrid equilibrium element formulation for linear poroelasticity." In: *Computer Methods in Applied Mechanics and Engineering* 434 (2025), p. 117576. DOI: 10.1016/j.cma.2024.117576.

[73] S. Lo Franco, M. Terzano, G. Borino, G. A. Holzapfel, and F. Parrinello. "A hybrid flux-preserving finite element for coupled flow deformation: Linear formulation." In: *Computer Methods in Applied Mechanics and Engineering* 447 (2025), p. 118351. ISSN: 0045-7825. DOI: https://doi.org/10.1016/j.cma.2025.118351.

[74] A. Lucantonio, P. Nardinocchi, and L. Teresi. "Transient analysis of swelling-induced large deformations in polymer gels." In: *Journal of the Mechanics and Physics of Solids* 61.1 (2013), pp. 205–218. DOI: 10.1016/j.jmps.2012.07.010.

[75] C. W. MacMinn, E. R. Dufresne, and J. S. Wettlaufer. "Large deformations of a soft porous material." In: *Physical Review Applied* 5 (2016), p. 044020. DOI: 10.1103/PhysRevApplied.5.044020.

[76] J. Mandel. "Consolidation des sols (étude mathématique)." In: *Géotechnique* 3.7 (1953), pp. 287–299. ISSN: 0016-8505. DOI: 10.1680/geot.1953.3.7.287.

[77] J. Marsden and T. Hughes. *Mathematical Foundations of Elasticity*. Dover Civil and Mechanical Engineering. Dover Publications, 2012. ISBN: 9780486142272. URL: https://books.google.it/books?id=-STEAgAAQBAJ.

[78] J. Maryska, M. Rozložník, and M. Tuma. "Schur Complement Systems in the Mixed-Hybrid Finite Element Approximation of the Potential Fluid Flow Problem." In: *SIAM Journal on Scientific Computing* 22.2 (2000), pp. 704–723. DOI: 10.1137/S1064827598339608.

[79] E. A. W. Maunder, J. P. Moitinho de Almeida, and A. C. A. Ramsay. "A GENERAL FORMULATION OF EQUILIBRIUM MACRO-ELEMENTS WITH CONTROL OF SPURIOUS KINEMATIC MODES: THE EXORCISM OF AN OLD CURSE." en. In: *International Journal for Numerical Methods in Engineering* 18 (Sept. 1996), pp. 3175–3194. DOI: https://doi.org/10.1002/(SICI)1097-0207(19960930)39:18<3175::AID-NME978>3.0.CO;2-3. (Visited on 03/25/2024).

[80] E. a. W. Maunder and J. P. Moitinho de Almeida. "The stability of stars of triangular equilibrium plate elements." en. In: *International Journal for Numerical Methods in Engineering* 77.7 (2009), pp. 922–968. ISSN: 1097-0207. DOI: 10.1002/nme.2441.

[81] C. Miehe. "Aspects of the formulation and finite element implementation of large strain isotropic elasticity." In: *International Journal for Numerical Methods in Engineering* 37.12 (1994), pp. 1981–2004. DOI: https://doi.org/10.1002/nme.1620371202.

[82] C. Miehe, S. Mauthe, and S. Teichtmeister. "Minimization principles for the coupled problem of Darcy–Biot-type fluid transport in porous media linked to phase field modeling of fracture." In: *Journal of the Mechanics and Physics of Solids* 82 (2015), pp. 186–217. ISSN: 0022-5096. DOI: 10.1016/j.jmps.2015.04.006.

[83] J. P. Moitinho de Almeida and E. A. W. Maunder. "Equilibrium Finite Element Formulations." In: John Wiley Sons, Ltd, 2017. ISBN: 9781118925782. DOI: https://doi.org/10.1002/9781118925782.ch3.

[84] V. C. Mow, M. H. Holmes, and W. M. Lai. "Fluid transport and mechanical properties of articular cartilage: A review." In: *Journal of Biomechanics* 17.5 (1984), pp. 377–394. DOI: 10.1016/0021-9290(84)90031-9.

[85] V. C. Mow, S. C. Kuei, W. M. Lai, and C. G. Armstrong. "Biphasic creep and stress relaxation of articular cartilage in compression? Theory and experiments." In: *Journal of Biomechanical Engineering* 102.1 (Feb. 1980), pp. 73–84. DOI: 10.1115/1.3138202.

[86] M. A. Murad and A. F. D. Loula. "On stability and convergence of finite element approximations of Biot's consolidation problem." In: *International Journal for Numerical Methods in Engineering* 37.4 (1994), pp. 645–667. DOI: https://doi.org/10.1002/nme.1620370407.

[87] I. Müller. "A thermodynamic theory of mixtures of fluids." In: *Archive for Rational Mechanics and Analysis* 28.1 (1968), pp. 1–39. DOI: 10.1007/BF00281561.

[88] J. T. Oden and J. N. Reddy. *Variational Methods in Theoretical Mechanics*. 2nd ed. Universitext. Springer Berlin Heidelberg, 1983. ISBN: 978-3-642-68811-9. DOI: 10.1007/978-3-642-68811-9.

[89] R. W. Ogden. "Inequalities associated with the inversion of elastic stress-deformation relations and their implications." In: *Mathematical Proceedings of the Cambridge Philosophical Society* 81.2 (1977), 313–324. DOI: 10.1017/S030500410005338X.

[90] R. Ogden. *Non-linear Elastic Deformations*. Ellis Horwood series in mathematics and its applications. E. Horwood, 1984. ISBN: 978-0-85312-273-9.

[91] L. Onsager. "Reciprocal Relations in Irreversible Processes. I." In: *Physical Review* 37.4 (Feb. 1931). Publisher: American Physical Society, pp. 405–426. DOI: https://doi.org/10.1103/PhysRev.37.405.

[92] F. Parrinello. "Restraining approach for the spurious kinematic modes in hybrid equilibrium element." In: *Computational Mechanics* 52.4 (2013), pp. 885–901. ISSN: 0178-7675. DOI: 10.1007/s00466-013-0851-x.

[93] F. Parrinello. "Hybrid equilibrium element with interelement interface for the analysis of delamination and crack propagation problems." en. In: *International Journal for Numerical Methods in Engineering* 122.1 (2021), pp. 190–218. ISSN: 1097-0207. DOI: https://doi.org/10.1002/nme.6531.

[94] F. Parrinello. "Hybrid equilibrium formulation with adaptive element side orientation for cohesive crack prediction." In: *International Journal for Numerical Methods in Engineering* 125.17 (2024), e7543. DOI: 10.1002/nme.7543.

[95] F. Parrinello and G. Borino. "Hybrid equilibrium element with high-order stress fields for accurate elastic dynamic analysis." In: *International Journal for Numerical Methods in Engineering* 122.21 (2021). DOI: https://doi.org/10.1002/nme.6793.

[96] P. J. Phillips and M. F. Wheeler. "A coupling of mixed and discontinuous Galerkin finite-element methods for poroelasticity." In: *Computational Geosciences* 12.4 (2008), pp. 417–435. DOI: 10.1007/s10596-008-9082-1.

[97] T. H. H. Pian. "Finite element formulation by variational principles with relaxed continuity requirements." In: *The Mathematical Foundations of the Finite Element Method with Applications to Partial Differential Equations*. Ed. by A. K. Aziz. Academic Press, 1972, pp. 671–687. ISBN: 978-0-12-068650-6. DOI: https://doi.org/10.1016/B978-0-12-068650-6.50029-0.

[98] T. H. H. Pian. "A historical note about 'hybrid elements'." In: *International Journal for Numerical Methods in Engineering* 12.5 (1978), pp. 891–892. ISSN: 1097-0207. DOI: 10.1002/nme.1620120514.

[99] T. H. H. Pian. "Overview of hybrid finite element methods for solid mechanics." In: *Computational Mechanics '88*. Ed. by S. N. Atluri and G. Yagawa. Berlin: Springer, 1988, pp. 1039–1042. ISBN: 978-3-642-64818-2 978-3-642-61381-4. DOI: 10.1007/978-3-642-61381-4_273.

[100] T. H. H. Pian. "State-of-the-art development of hybrid/mixed finite element method." In: *Finite Elements in Analysis and Design* 21.1-2 (1995), pp. 5–20. DOI: 10.1016/0168-874X(95)00024-2.

[101] T. H. H. Pian and C.-C. Wu. *Hybrid and incompatible finite element methods*. Modern Mechanics and Mathematics 4. Boca Raton: Chapman & Hall/CRC, 2006. ISBN: 978-1-58488-276-3. DOI: 10.1201/9780203487693.

[102] M. Preisig and J. H. Prévost. "Stabilization procedures in coupled poromechanics problems: A critical assessment." In: *International Journal for Numerical and Analytical Methods in Geomechanics* 35.11 (2011), pp. 1207–1225. ISSN: 1096-9853. DOI: 10.1002/nag.951.

[103] P. A. Raviart and J. M. Thomas. "Primal hybrid finite element methods for 2nd order elliptic equations." In: *Mathematics of Computation* 31.138 (1977), p. 391. DOI: 10.2307/2006423.

[104] J. Reddy. *Energy Principles and Variational Methods in Applied Mechanics*. Wiley, 2002. ISBN: 9780471179856. URL: https://books.google.it/books?id=3gw5rxLQdaQC.

[105] J. R. Rice and M. P. Cleary. "Some basic stress diffusion solutions for fluid-saturated elastic porous media with compressible constituents." en. In: *Reviews of Geophysics* 14.2 (May 1976), pp. 227–241. ISSN: 8755-1209, 1944-9208. DOI: https://doi.org/10.1029/RG014i002p00227.

[106] C. Rodrigo. "Poroelasticity problem: numerical difficulties and efficient multigrid solution." In: *SeMA Journal* 73.1 (2016), pp. 31–57. ISSN: 2281-7875. DOI: 10.1007/s40324-015-0054-9.

[107] J. W. Rudnicki. "Linear poroelasticity." In: *Handbook of Materials Behavior Models*. Elsevier, 2001, pp. 1118–1125. ISBN: 978-0-12-443341-0. DOI: 10.1016/B978-012443341-0/50113-7.

[108] A. Salvadori, R. McMeeking, D. Grazioli, and M. Magri. "A coupled model of transport-reaction-mechanics with trapping. Part I – Small strain analysis." In: *Journal of the Mechanics and Physics of Solids* 114 (2018), pp. 1–30. DOI: 10.1016/j.jmps.2018.02.006.

[109] R. S. Sandhu, H. Liu, and K. J. Singh. "Numerical performance of some finite element schemes for analysis of seepage in porous elastic media." In: *International Journal for Numerical and Analytical Methods in Geomechanics* 1.2 (1977), pp. 177–194. DOI: https://doi.org/10.1002/nag.1610010205.

[110] M. Schanz and S. Diebels. "A comparative study of Biot's theory and the linear Theory of Porous Media for wave propagation problems." In: *Acta Mechanica* 161.3 (2003), pp. 213–235. DOI: https://doi.org/10.1007/s00707-002-0999-5.

[111] B. Schrefler. "Computer modelling in environmental geomechanics." In: *Computers & Structures* 79.22 (2001), pp. 2209–2223. ISSN: 0045-7949. DOI: https://doi.org/10.1016/S0045-7949(01)00076-1.

[112] A. Selvadurai. "Irreversibility of soil skeletal deformations: The Pedagogical Limitations of Terzaghi's celebrated model for soil consolidation." In: *Computers and Geotechnics* 135 (2021), p. 104137. ISSN: 0266-352X. DOI: https://doi.org/10.1016/j.compgeo.2021.104137.

[113] M. Šilhavý. *The Mechanics and Thermodynamics of Continuous Media*. 1st ed. Theoretical and Mathematical Physics. Springer Berlin, Heidelberg, 1997. DOI: https://doi.org/10.1007/978-3-662-03389-0.

[114] J. C. Simo and M. S. Rifai. "A class of mixed assumed strain methods and the method of incompatible modes." In: *International Journal for Numerical Methods in Engineering* 29.8 (1990), pp. 1595–1638. ISSN: 1097-0207. DOI: 10.1002/nme.1620290802.

[115] B. R. Simon. "Multiphase poroelastic finite element models for soft tissue structures." In: *Applied Mechanics Reviews* 45.6 (1992), pp. 191–218. DOI: https://doi.org/10.1115/1.3121397.

[116] B. R. Simon, M. V. Kaufmann, M. A. McAfee, A. L. Baldwin, and L. M. Wilson. "Identification and determination of material properties for porohyperelastic analysis of large arteries." In: *Journal of Biomechanical Engineering* 120.2 (1998), pp. 188–194. DOI: 10.1115/1.2798301.

[117] I. A. Stokes, S. Chegini, S. J. Ferguson, M. G. Gardner-Morse, J. C. Iatridis, and J. P. Laible. "Limitation of Finite Element Analysis of Poroelastic Behavior of Biological Tissues Undergoing Rapid Loading." In: *Annals of Biomedical Engineering* 38.5 (2010), pp. 1780–1788.

[118] A. Stracuzzi, E. Mazza, and A. E. Ehret. "Chemomechanical models for soft tissues based on the reconciliation of porous media and swelling polymer theories." In: *ZAMM - Journal of Applied Mathematics and Mechanics / Zeitschrift für Angewandte Mathematik und Mechanik* 98.12 (2018), pp. 2135–2154. DOI: https://doi.org/10.1002/zamm.201700344.

[119] C. Taylor and P. Hood. "A numerical solution of the Navier-Stokes equations using the finite element technique." In: *Computers & Fluids* 1.1 (1973), pp. 73–100. DOI: 10.1016/0045-7930(73)90027-3.

[120] R. L. Taylor. *FEAP – Finite Element Analysis Program*. 2014. URL: http://www.ce.berkeley/feap.

[121] S. Teichtmeister, S. Mauthe, and C. Miehe. "Aspects of finite element formulations for the coupled problem of poroelasticity based on a canonical minimization principle." In: *Computational Mechanics* 64.3 (2019), pp. 685–716. ISSN: 1432-0924. DOI: 10.1007/s00466-019-01677-4.

[122] K. Terzaghi. "Theory of Consolidation." en. In: *Theoretical Soil Mechanics*. John Wiley & Sons, Ltd, 1943, pp. 265–296. ISBN: 978-0-470-17276-6. DOI: https://doi.org/10.1002/9780470172766.ch13.

[123] C Truesdell. "Sulle basi della termodinamica delle miscele." In: *Rend. Accad. Naz. Lincei* 44.8 (1968), pp. 381–383.

[124] C. Truesdell and W. Noll. *The Non-Linear Field Theories of Mechanics*. Berlin, Heidelberg: Springer, 2004, pp. 1–579. ISBN: 978-3-662-10388-3. DOI: 10.1007/978-3-662-10388-3_1.

[125] C. Truesdell. "Sulle basi della termomeccanica I." In: *Atti della Accademia Nazionale dei Lincei. Classe di Scienze Fisiche, Matematiche e Naturali. Rendiconti.* 22.8 (1957), pp. 33–38.

[126] C. Truesdell. *Rational Thermodynamics*. New York: McGraw Hill, 1969. DOI: 10.1007/978-1-4612-5206-1.

[127] R. Uzuoka and R. I. Borja. "Dynamics of unsaturated poroelastic solids at finite strain." In: *International Journal for Numerical and Analytical Methods in Geomechanics* 36.13 (2012), pp. 1535–1573. DOI: https://doi.org/10.1002/nag.1061.

[128] A. Verruijt. *Theory of Consolidation*. Dordrecht: Springer Netherlands, 2010, pp. 65–90. DOI: 10.1007/978-90-481-3441-0_4.

[129] H. Wang. *Theory of Linear Poroelasticity with Applications to Geomechanics and Hydrogeology*. Princeton Series in Geophysics. Princeton: Princeton University Press, 2000. ISBN: 978-0-691-03746-2. DOI: 10.1515/9781400885688.

[130] L. Wang and H. Zhong. "A traction-based equilibrium finite element free from spurious kinematic modes for linear elasticity problems." en. In: *International Journal for Numerical Methods in Engineering* 99.10 (2014), pp. 763–788. ISSN: 1097-0207. DOI: 10.1002/nme.4701. URL: https://onlinelibrary.wiley.com/doi/abs/10.1002/nme.4701 (visited on 07/26/2024).

[131] T. Yuan, W. Zhan, M. Terzano, G. A. Holzapfel, and D. Dini. "A comprehensive review on modeling aspects of infusion-based drug delivery in the brain." In: *Acta Biomaterialia* 185 (2024), pp. 1–23. ISSN: 1742-7061. DOI: https://doi.org/10.1016/j.actbio.2024.07.015.

[132] O. C. Zienkiewicz. "Displacement and equilibrium models in the finite element method by B. Fraeijs de Veubeke, Chapter 9, Pages 145–197 of Stress Analysis, Edited by O. C. Zienkiewicz and G. S. Holister, Published by John Wiley & Sons, 1965." In: *International Journal for Numerical Methods in Engineering* 52.3 (2001), pp. 287–342. DOI: 10.1002/nme.339.

[133] O. C. Zienkiewicz and T. Shiomi. "Dynamic behaviour of saturated porous media; The generalized Biot formulation and its numerical solution." In: *International Journal for Numerical and Analytical Methods in Geomechanics* 8.1 (1984), pp. 71–96. DOI: 10.1002/nag.1610080106.

[134] O. C. Zienkiewicz, R. L. Taylor, and J. Z. Zhu. *The Finite Element Method: Its Basis and Fundamentals*. 7th. Elsevier Science, 2013. ISBN: 978-0-08-095135-5.

Le savant n'étudie pas la nature parce que cela est utile; il l'étudie parce qu'il y prend plaisir et il y prend plaisir parce qu'elle est belle.

— Henri Poincarè

RINGRAZIAMENTI

Νενικηκαμεν, *abbiamo vinto*, questa è la frase attribuita a Fidippide, il messaggero che nel 490 a.C. corse fino ad Atene per portarvi la notizia della vittoria nella battaglia di Maratona.
Ed è così che questa corsa, faticosa ma vittoriosa, arriva a compimento. Questi tre anni, rapidi e densi insieme, sono solcati da tutti quelli che, per una stagione o per la vita, mi hanno sostenuta. Mi prendo questo spazio per lasciare loro solo un breve pensiero, convinta che conoscano già tutto l'affetto che io provi per loro.

Ringrazio innanzitutto il mio supervisore, il prof. Parrinello, colui che mi ha insegnato a leggere quelle che banalmente chiamiamo "mappe colorate", per aver speso insieme ore davanti a codici Fortran e per aver condiviso con me la gioia di vederli compilare. Per tutta la pazienza che mi ha riservato in questi anni, specie quando, nel caldo torrenziale dell'estate panormitana, abbiamo ricalcolato decine di volte la stazionarietà del funzionale di Coussy.
Ringrazio il prof. Borino, per sopportarmi sin dal mio lavoro di tesi magistrale, per tutte le ore passate a chiaccherare in corridoio su cosa significhi termodinamicamente consistente e per tutte quelle passate ad ascoltarmi mentre filosofeggiavo sulla "inf-sup condition", sulla democraticizzazione della conoscenza e su quanto la cipollina sia il pezzo di rosticceria supremo. Idea stranamente condivisa da entrambi.
Ringrazio il prof. Holzapfel, che ha scommesso su di me ancor prima di conoscermi, che si è preso cura di me, non solo durante il mio visiting period a Graz, ma anche in tutto il periodo successivo, fino a prendere un volo da Trondheim a Palermo per poter assistere alla mia difesa.
Un ringraziamento va alla commissione della difesa e ai revisori di quest'eleborato, primo di tutti il prof. Spada, al quale tante volte mi sono ritrovata a chieder consigli sugli elementi finiti, ai prof. Larsson e Marino, con cui ho l'onore di difendere questo lavoro e ai prof. De Almeida e Lebon, le cui preziose revisioni sono state cruciali nel processo di *labor limae* di quest'elaborato. Ringrazio tutti voi per aver creduto in questo progetto, fuori dai sentieri battuti.
Ringrazio la prof. Pirrotta, che ha avuto cura di me in questi anni, che fosse con un pensierino da una delle tante mete visitate o con un abbraccio in corridoio, il suo sostegno è stato determinante. Ringrazio il prof. Di Paola, i suoi consigli sono di guida per tutto

il corridoio di Scienza. Ricordo bene quando, nel momento di massima confusione del mio turbolento primo anno, mi disse "tu hai l'ossessione negli occhi". Adesso, forse, ho capito.

Ringrazio tutti i componenti della mia famiglia, Mamma e Papà, Franci e Samu, che mi hanno sostenuto, ciascuno secondo le proprie peculiarità eppure in egual misura nell'amore che mi hanno riservato. In tutte le mie brutture e in tutti i miei silenzi. Sono certa che qualunque cosa la vita ci riservi, sarete sempre con me.

Ringrazio Creep, mia compagna di avventura da sempre. Tu riesci a credere nelle mie idee perfino quando neacnhe io riesco a farlo. Grazie per ogni suggerimento, per ogni abbraccio e per ogni parola che in questi anni mi hai concesso. Sei preziosa.
Ringrazio il mio figlioccio, per continuare a essere una presenza fondamentale nella mia vita da tanti anni, ormai. Il bene che ci unisce è grande. Ringrazio Maria, legata a me da un filo, tanto invisibile quanto indelebile.
Ringrazio Veronica per il suo esser dolce e MariP per ogni parola buona, sei un'amica preziosa e un'anima gentile. Ringrazio Elisa, perchè non le manca mai il sorriso, perchè mi contagia sempre con il suo entusiasmo. Ringrazio Vinc, perchè è stata la mia certezza a cui chiedere aiuto, sempre pronta ad aiutarmi nel momento del bisogno. Ringrazio infine Giammi, la storia dei velociraptor al primo anno di dottorato è stata quantomeno illuminante. Dovresti brevettarla.

Ringrazio i colleghi e gli amici che ho avuto la fortuna di conoscere a Graz, siete stati la mia casa.
In particolare, un grazie va *alla diva* Franci, poterti conoscere è stato un incredibile privilegio e una delle circostanze più fortuite della mia vita. Una parte di me rimarrà per sempre in quella casa verde dalle pareti costellate di puzzle, nelle nostre colazioni a base di toast e nei nostri riti domenicali. Non sarai mai troppo lontana, neanche a miglia di distanza.
Grazie Capitano Maxi, per avermi redarguito sull'*uomo in vestaglia*, per ogni conflitto verbale e verboso, sei arrogante quasi quanto me.
Grazie Michele, per avermi sostenuta in questo viaggio, tra un *povera Italia* e un *figghiu miu*, e per il tuo contributo al nostro (figlio) paper.
Ringrazio le mie compagne di stanza, la mia personalissima solleva panche del segno della vergine, la mia compagna di abbuffate e di playlist, nonchè la mia *radical-chic* preferita. Siete riuscite a rendere un ambiente familiare l'ufficio, anche solo grazie al nostro appuntamento-caffè di ogni pomeriggio. Per non parlare dei *"momenti-torta"*.
Non mi scordo del prof. Giambanco, al quale credo di aver riservato in questi anni le mie migliori battute. Vedremo di organizzarci per tener pieno di barattolo di caramelle.

Ringrazio infine ogni collega con cui ho scambiato anche solo quattro chiacchere al bar, sono sicura di aver imparato qualcosa da ciscuno di voi. O magari, vi ho solo *scroccato* un caffè.

Ho giocato a far finta di controllare la natura delle cose, pur consapevole che ciò che inseguiamo rimane, e rimarrà sempre, un passo oltre il nostro sguardo, misterioso e indomabile. Eppure la tentazione di carpirne un frammento è forte, perchè, come amava dire *il filosofo della paseggiata delle cinque*, mi piace stare *con i piedi ben radicati a terra, ma con lo sguardo rivolto alle stelle*. Sarà sempre così.